

**MOLECULAR AND FUNCTIONAL ASPECTS OF  
HYDROLYASES / INHIBITORS WITH EMPHASIS  
ON ASPARTIC PROTEASE INHIBITOR**

*Thesis submitted to University of Pune  
For the degree of*

**DOCTOR OF PHILOSOPHY  
IN  
BIOTECHNOLOGY**

By  
**Vishnu Menon**

Division of Biochemical Sciences  
National Chemical Laboratory  
Pune – 411008  
India

**January 2012**

*Dedicated to my mentor  
&  
my family*

*'The whole of science is nothing more than a  
refinement of everyday thinking'*

**Albert Einstein**

## TABLE OF CONTENTS

ACKNOWLEDGMENTS	(i)
CERTIFICATE	(iii)
DECLARATION BY THE RESEARCH SCHOLAR	(iv)
ABBREVIATIONS	(v)
ABSTRACT	(vii)
LIST OF PUBLICATIONS	(xv)
CONFERENCES /POSTERS/ ABSTRACTS	(xvii)
Chapter 1	<p><b>General Introduction</b> <span style="float: right;">1-72</span></p> <p>Introduction <span style="float: right;">3</span></p> <p style="padding-left: 20px;">Enzyme classification <span style="float: right;">3</span></p> <p style="padding-left: 20px;">Significance of proteases <span style="float: right;">4</span></p> <p style="padding-left: 20px;">Occurrence of proteases <span style="float: right;">8</span></p> <p style="padding-left: 20px;">Classification of proteases <span style="float: right;">8-13</span></p> <p style="padding-left: 40px;">Serine proteases <span style="float: right;">10</span></p> <p style="padding-left: 40px;">Thiol/ Cysteine proteases <span style="float: right;">10-11</span></p> <p style="padding-left: 40px;">Metalloproteases <span style="float: right;">11</span></p> <p style="padding-left: 40px;">Glutamic acid proteases <span style="float: right;">11-12</span></p> <p style="padding-left: 40px;">Threonine proteases <span style="float: right;">12</span></p> <p style="padding-left: 40px;">Aspartic proteases <span style="float: right;">13</span></p> <p style="padding-left: 60px;">Occurrence <span style="float: right;">13-14</span></p> <p style="padding-left: 60px;">Crystallographic studies <span style="float: right;">15</span></p> <p style="padding-left: 60px;">Mechanism of action <span style="float: right;">16</span></p> <p style="padding-left: 60px;">Classification <span style="float: right;">17-24</span></p> <p style="padding-left: 80px;"><i>Pepsin family</i> <span style="float: right;">17-18</span></p> <p style="padding-left: 80px;"><i>Retropepsin family</i> <span style="float: right;">18-19</span></p> <p style="padding-left: 80px;"><i>Cauliflower mosaic virus proteases family</i> <span style="float: right;">19-20</span></p> <p style="padding-left: 80px;"><i>Membrane bound aspartic proteases</i> <span style="float: right;">20-21</span></p> <p style="padding-left: 80px;"><i>GxGD aspartic proteases</i> <span style="float: right;">20-21</span></p> <p style="padding-left: 80px;"><i>Putative aspartic proteases</i> <span style="float: right;">22-23</span></p> <p style="padding-left: 80px;"><i>Plant aspartic proteases</i> <span style="float: right;">23-24</span></p> <p style="padding-left: 20px;">Proteases inhibitors <span style="float: right;">24-25</span></p> <p style="padding-left: 20px;">Classification of Proteases inhibitors <span style="float: right;">25-29</span></p> <p style="padding-left: 40px;"><i>Based on mechanism of inhibition</i> <span style="float: right;">27</span></p> <p style="padding-left: 40px;"><i>Based on physiological relevance</i> <span style="float: right;">27-28</span></p> <p style="padding-left: 20px;">Aspartic protease inhibitor <span style="float: right;">30-54</span></p> <p style="padding-left: 40px;">Mechanism of inhibition <span style="float: right;">30-31</span></p> <p style="padding-left: 40px;">Classification <span style="float: right;">31-32</span></p> <p style="padding-left: 60px;"><i>Proteinaceous Inhibitor</i> <span style="float: right;">31-32</span></p>

	<i>Low-Molecular-Weight Inhibitors</i>	32-34
	<i>Inhibitors of pepsin</i>	34-36
	<i>Inhibitors of cathepsin D</i>	36-39
	<i>Inhibitors of HIV protease</i>	40-43
	<i>Inhibitors of renin</i>	43-46
	<i>Inhibitors of BACE</i>	46-48
	<i>Inhibitors of <math>\gamma</math>-secretase</i>	48-50
	<i>Inhibitors of Plasmepsins</i>	50-52
	<i>Inhibitors of secretory aspartic proteases (SAPs)</i>	52-54
	Future perspective for inhibitor design	54-57
	Bibliography	59-72
<b>Chapter 2</b>	<b>Isolation and identification of microbes for the production of aspartic protease inhibitor</b>	<b>73-103</b>
	Summary	75
	Introduction	76-77
	Experimental procedures	78-87
	Results	88-100
	Isolation and identification of actinomycetes	88-89
	<i>Morphological and biochemical identification</i>	90-91
	<i>Identification of isolate by 16S rDNA sequencing</i>	90-91
	Production of aspartic protease inhibitor from <i>Streptomyces</i> sp MBR04	91-95
	Isolation and identification of the fungal isolate	96-98
	<i>Morphological characteristics</i>	96
	<i>Identification of isolate by ITS sequencing</i>	97-98
	Production of aspartic protease inhibitor from <i>Penicillium</i> sp VM24	98-100
	Discussion	101
	Bibliography	102-103
<b>Chapter 3</b>	<b>Purification and characterization of aspartic protease inhibitors from <i>Streptomyces</i> sp MBR04 and <i>Penicillium</i> sp VM24</b>	<b>104-126</b>
	Summary	106
	Introduction	107
	Experimental procedures	108-113
	Results	114-124
	Purification of inhibitor from <i>Streptomyces</i> sp MBR04	114-115
	Biochemical characterization	115-118
	Purification of inhibitor from <i>Penicillium</i> sp VM24	119-120
	Biochemical characterization	120-124
	Discussion	125
	Bibliography	126

<b>Chapter 4</b>	<b>Mechanistic and structural insights into the inhibition of therapeutically significant aspartic protease by inhibitor from <i>Streptomyces</i> sp MBR04</b>	<b>127-190</b>
<b>Part A</b>	<b><i>Kinetic interactions of pepsin with the inhibitor: Correlation to inhibitor induced conformational changes</i></b>	<b>129-157</b>
	Summary	130
	Introduction	131-135
	Experimental procedures	136-140
	Results	141-153
	Kinetic analysis of the inhibition of pepsin	141-146
	Thermodynamics of inhibitor binding to pepsin	147-148
	Fluorescence analysis of pepsin-inhibitor interactions	148-151
	Circular dichroism analysis of pepsin-APD-inhibitor complex	151-152
	Chemical modification of inhibitor	152-153
	Discussion	154-157
<b>Part B</b>	<b><i>Slow-tight binding inhibition of Cathepsin D: Implications in mechanism of inactivation</i></b>	<b>158-190</b>
	Summary	159
	Introduction	160-163
	Experimental procedures	164-168
	Results	169-178
	Inhibitor progress curve analysis	169-172
	Thermodynamics of inhibitor binding to human cathepsin D	172-173
	Fluorometric analysis of cathepsin D-inhibitor interactions	174-177
	Circular dichroism analysis	177-178
	Discussion	179-185
	Bibliography	186-190
<b>Chapter 5</b>	<b>Aspartic protease inhibitor from <i>Penicillium</i> sp VM24 as antifungal peptide: Implications in combating mycotic infections</b>	<b>191-222</b>
	Summary	193
	Introduction	194-200
	Experimental procedures	201-203
	Results	204-215
	Antifungal activity of the inhibitor from <i>Penicillium</i> sp VM24	204-210
	Aspartic protease and xyloglucanase in growth inhibition	211-212
	Chemical modification of the inhibitor and assessment of its antifungal potency	212-215
	Discussion	216-218
	Bibliography	219-222

<b>Chapter 6</b>	<b>Bifunctional role of aspartic protease inhibitor from <i>Penicillium</i> sp VM24: inactivation of aspartic protease and xyloglucanase</b>	<b>223-285</b>
<b>Part A</b>	<b><i>Interactions of a protease inhibitor with an aspartic protease from <i>Aspergillus</i> sp</i></b>	<b>225-245</b>
	Summary	226
	Introduction	227-228
	Experimental procedures	229-232
	Results	233-242
	Kinetic analysis of the inhibition of fungal aspartic protease	233-234
	Substrate kinetics	235
	Progress curve analysis	235-240
	Fluoremetric analysis	240-241
	Circular dichroism analysis	241-242
	Discussion	243-245
<b>Part B</b>	<b><i>Slow-tight binding inhibition of xyloglucanase from <i>Thermomonospora</i> sp by an aspartic protease inhibitor</i></b>	<b>246-285</b>
	Summary	247
	Introduction	248-250
	Experimental procedures	251-257
	Results	258-274
	Purification of xyloglucanase	258
	Kinetic analysis of the inhibition of xyloglucanase	259-265
	Fluorescence studies on enzyme-inhibitor interactions	265-269
	Circular dichroism analysis of enzyme-substrate-inhibitor	269-270
	Inactivation of xyloglucanase by TNBS, PHMB and DEP	270-273
	Effect of inhibitor on the isoindole fluorescence	273-274
	Discussion	275-281
	Bibliography	282-285
<b>Chapter 7</b>	<b>Functional aspects of hydrolyases</b>	<b>286-308</b>
	Summary	288
	Introduction	289-290
	Experimental procedures	291-294
	Results	295-304
	Acid hydrolysis of TKP	295-296
	Enzymatic hydrolysis	297-300
	Effect of surfactants on GXG hydrolysis	301-302
	Fermentation of acid and enzymatic hydrolysates	302-303
	Immobilization and reuse of <i>D hansenii</i>	304
	Discussion	305-306
	Bibliography	307-308

## ACKNOWLEDGEMENTS

गुरुर्ब्रह्म गुरुर्विष्णु गुरुर्देवो महेश्वरः ।  
गुरुः साक्षात् परब्रह्मा तस्मै श्री गुरवे नमः ॥

*I would like to connote my whole-hearted gratitude and indebtedness to my mentor **Dr Mala Rao**, for introducing me to the mesmerizing dominion of Biochemistry and Microbial Biotechnology. I consider myself extremely fortunate to have her as my mentor who gave me the freedom to explore on my own, and owe her lots of gratitude for guidance to recover when my steps faltered. I sincerely thank her for her excellent guidance, teaching, encouragement, benign attention, and for helping me out in most stressful times, both scientific and personal, which helped me to think positively and remain optimistic. Her scientific temperament, innovative approach, dedication towards her profession and down to earth nature has inspired me the most. I hope that I could be as lively, enthusiastic and energetic as her and to someday be able to command an audience as well as she can. Although this exaltation is insufficient, I preserve an everlasting gratitude for her.*

*With much appreciation, I would like to mention the role of **Dr Yogesh Souche** and **Girish Kulkarni** for their help in my research works on DNA sequencing and molecular identification of the microbes. I am also grateful to **Dr's Sushama Gaikwad** and **Mahesh Kulkarni** for their support in HPLC and fluorescence studies. Special thanks to **Dr Asmita Prabhune** for introducing me to NCL family. I profoundly thank **Dr Barry MacCleary** (Megazyme International Ireland Ltd) and **Mr A. Agarwal** (Simosis International Ltd.) for kindly providing xyloglucan from tamarind seeds and tamarind kernel powder respectively during my research. I also thank **Mrs Snehal More** for her help and support.*

*I would like to thank **Dipali** for her encouragement, valuable and timely help and the lighter moments shared. I am indeed thankful to her for helping me in the purification of xyloglucanase and gel electrophoresis. I find words inadequate to express the appreciation of my seniors **Dr's Vinod** and **Ajit** for their constructive comments and suggestions, ceaseless inspiration, advice and timely help throughout my work. Special thanks are to*



*my seniors Dr's Anish, Sharmili, Aarohi, CV, Shiv, Ashwini, Sachin, Sharath, Sridevi, Atul for their help and inspiration.*

*I fall short of words to express my feelings towards my all time friends, Rupesh and Pramod. They have made an outstanding impact on my outlook towards life and science. They have been there all the time with me in my ups and downs.*

*Thanks are due to my labmates Gyan, Vaibhav, Harish, Jaysbree, Siddharth, Malathi, Ishwar, Dhananjay, Suresh, Avinash, Yashwant, Pushpa, Raj, Padma, Aparna, Nupur, Asmita, Nilesb, Tanaji, Mebraj, for the cordial and friendly atmosphere in the lab. Special thanks to all my FB and Orkut friends. Will always cherish the moments shared with you all.*

*I thank Mrs. Indira Mobandas and Mr. Ramakant Lambbar for their ready and unpretentious help whenever required, even in times of need. I am thankful to Mr. Trehan and Mr. Jagtap for their technical assistance for instrumentation and other chores.*

*I thank the Director, National Chemical Laboratory for making the facilities available for my work. I acknowledge the financial assistance by CSIR, New Delhi in the form of Junior and Senior research fellowship during the tenure of my work.*

*I owe my deepest gratitude to my parents, brothers, sisters, BIL's, SIL's, my lovable nephews and nieces for their eternal support and understanding of my goals and aspirations. Without them, I would not have been able to complete much of what I have done and become who I am. Special indebtedness to my Mom for what I have achieved today. They are the light that shines my way and the drive for my ever-persistent determination. Without their enduring support and encouragement, it would not have been possible to embark upon this journey in life. I acknowledge several friends and well wishers, whom I have not mentioned above and whose best wishes have always boosted me. I am grateful to God Almighty for providing me all the blessings for making this effort a success.*

**VISHNU MENON**

## CERTIFICATE

Certified that the work incorporated in the thesis entitled “**Molecular and functional aspects of hydrolyases / inhibitors with emphasis on aspartic protease inhibitor**” submitted by **Mr. Vishnu Menon** for the Degree of *Doctor of Philosophy*, was carried out by the candidate under my supervision at Division of Biochemical Sciences, National Chemical Laboratory, Pune - 411 008, Maharashtra, India. Material obtained from other sources is duly acknowledged in the thesis.

**Dr. Mala Rao**  
(Research Supervisor)

## DECLARATION BY RESEARCH SCHOLAR

I hereby declare that the thesis entitled “**Molecular and functional aspects of hydrolyases / inhibitors with emphasis on aspartic protease inhibitor**” submitted for the Degree of Doctor of Philosophy to the University of Pune, has been carried out by me at Division of Biochemical Sciences, National Chemical Laboratory, Pune - 411 008, Maharashtra, India, under the supervision of **Dr. Mala Rao**. The work is original and has not been submitted in part or full by me for any other degree or diploma to any other University.

**Vishnu Menon**  
(Research Scholar)

## ABBREVIATIONS

°C	Degree Celsius
μl	Micro liter
Å	Angstrom
APD	N-acetyl-L-phenylalanyl-L-3, 5-diodotyrosine
BBTI	Bowman-Birk trypsin inhibitor
BLAST	Basic local alignment search tool
BSA	Bovine serum albumin
CD	Circular dichroism
CH <sub>3</sub> CN	Acetonitrile
Da	Dalton
DANLME	diazoacetylnorleucine methyl ester
DEP	Diethylpyrocarbonate
DMAB	p-dimethyl amino benzaldehyde
DNA	Deoxyribonucleic acid
dNTP	Deoxy nucleotide triphosphate
E	Enzyme
EC	Enzymes classification
EDTA	Ethylene diamine tetra acetic acid
EI*	Enzyme inhibitor complex
EPNE	1, 2-epox-3-(p-nitrophenoxy) propane
E <sub>t</sub>	Total enzyme
g	Gram
h	Hours
HIV	Human immunodeficiency virus
I	Inhibitor
I <sub>t</sub>	Total inhibitor
kDa	Kilo dalton
<i>K<sub>i</sub></i>	Inhibition constant
<i>K<sub>m</sub></i>	Michaelis Menton constant
L	Liter
LB	Luria Bertani
M	Molar
Min	Minutes
ml	Milliliter
mM	Milli molar
Nbs <sub>2</sub>	5,5'-dithiobis(2-nitrobenzoic acid)
NCBI	National center for biotechnology information
nm	Nanometers
OD	Optical density
OPTA	o-phthalaldehyde
PAGE	Polyacrylamide gel electrophoresis
PCR	Polymerase chain reaction
pHMB	p-hydroxymercutybenzoic acid
pI	Isoelectric point

rDNA	Ribosomal deoxyribonucleic acid
REA	Relative Enzyme Activity
RNAase	Ribonuclease
rp-HPLC	Reverse phase high performance liquid chromatography
rpm	Revolutions per minute
SDS	Sodium dodecyl sulphate
SDS-PAGE	Sodium dodecyl sulfate polyacrylamide gel electrophoresis
TCA	Trichloric acid
TE	Tris-ethylene diamine tetra acetic acid
TFA	Trifluoroacetate
TLCK	Na-p-tosyl-L-lysine chloromethyl ketone
TNBS	2,4,6-trinitrobenzenesulfonic acid
TPCK	N-tosyl-L-phenyl alanine
TPCK	N-tosyl-L-phenyl alanine chloromethyl ketone
$V_{max}$	Maximum velocity

## ABSTRACT

The diversity and specificity of proteases constitute the basis for their serendipitous nature and multifaceted physiological activities. Proteases participate in most aspects of cell nutrition, physiology, signaling cascades and microbial pathogenesis. Their activity, if uncontrolled, would be destructive to the cell or organisms and therefore must be precisely regulated. The most significant aspect of protease action is the control of protease activity to limit cleavage to intended substrates without destruction of functional proteins. Many proteases are also essential for propagation of diseases, and hence inhibition of proteases is emerging as a promising approach in medicinal application for cancer, obesity, hepatitis, herpes, cardiovascular, inflammatory, neurodegenerative diseases, and various infectious and parasitic diseases. Aspartic proteases (3.4.23) are relatively a small group of proteolytic enzyme that has received enormous interest because of their significant roles in human diseases like involvement of renin in hypertension, cathepsin D in metastasis of breast cancer,  $\beta$ -secretase in Alzheimer's disease, plasmepsins in malaria, HIV-1 peptidase in acquired immune deficiency syndrome, and secreted aspartic peptidases in candidal infections. There have been developments on clinically active inhibitors of HIV-1 peptidase, which have been licensed for the treatment of AIDS. The inhibitors of plasmepsins and renin are considered a viable therapeutic strategy for the treatment of malaria and hypertension. Cathepsin D inhibitors have broadened the knowledge of structure, mechanism and contribution of cathepsin D in therapy of diseases. These inhibitors are mainly synthetic molecules; however there is paucity on biologic inhibitors from microbes. The application of biologic inhibitors will stimulate renewed interest in the therapeutic targeting of aspartic proteases. Currently the research strategies are focusing on the need for improved comprehension of protease-regulated cascades, along with precise selection of targets and improved inhibitor specificity. The objectives of the present work are:

- (A) Isolation and identification of microbes producing aspartic protease inhibitor
- (B) Purification and characterization of inhibitor
- (C) Interaction studies of the inhibitor with therapeutically significant aspartic proteases.
- (D) Role of aspartic protease inhibitor as an antifungal agent

The summary of the findings has been presented in the following chapters

### **Chapter 1: General introduction**

This chapter covers the literature survey on the occurrence and classification of proteases, the mechanism of catalysis with emphasis to aspartic proteases and the role of aspartic proteases as drug targets. In addition, the chapter also describes the structure and significance of biologic and synthetic inhibitors of aspartic proteases in therapeutic interventions.

### **Chapter 2: Isolation and identification of microbes for the production of aspartic protease inhibitor**

The involvement of aspartic proteases in various human diseases has spurred stupendous research interest in isolating new inhibitors from different sources. Exploiting the soil biodiversity, we have isolated two potent cultures producing aspartic protease inhibitor. Preliminary morphological characteristics revealed one to be an actinomycetes and the other belonging to the kingdom fungi. Further the biochemical studies and 16S rDNA sequence homology affirmed that the actinomycetes isolate belong to the genus *Streptomyces*. The 16S rDNA was sequenced and the BLAST search analysis showed 99% homology to *Streptomyces cinerochromogenes*. The sequence was submitted to GenBank and accession number JN627518 was obtained. The optimum temperature and pH for growth of *Streptomyces* sp MBR04 were 28°C and 6.0 respectively. *Streptomyces* sp MBR04 produced 92 IU/ml of inhibitor in a medium containing soya meal (SBM) as inducer at 28°C in 48h. The optimized process and nutritional parameters increased the inhibitor yield to 11.39 folds as compared to the basal medium. The fungal isolate was identified as a *Penicillium* sp on the basis of ITS sequence homology. The ITS sequence of *Penicillium* sp VM24 was deposited to GenBank and an accession number of JN673378 was obtained. The optimum temperature and pH for growth of *Penicillium* sp VM24 were 28°C and 5.0 respectively. *Penicillium* sp VM24 produced 154 IU/ml of inhibitor in a medium supplemented with soy meal as inducer in 96h under submerged fermentation (SmF). The culture also produced inhibitor units of 1148 IU/g in a media containing wheat bran and soy meal in 6

days under solid state fermentation (SSF) conditions. This is the first report of a fungal isolate producing aspartic protease inhibitor.

### **Chapter 3: Purification and characterization of aspartic protease inhibitors from *Streptomyces* sp MBR04 and *Penicillium* sp VM24**

The extracellular culture filtrates of *Streptomyces* sp MBR04 and *Penicillium* sp VM24 were subjected to activated charcoal treatment, ultrafiltration and gel filtration to remove high molecular weight impurities and salts. The inhibitors were concentrated by lyophilization and were further purified to homogeneity by rp-HPLC. The purified inhibitor showed a specific activity of 429 U/mg and a 59 fold increase in purification with a yield of 15% from *Streptomyces* sp MBR04. The inhibitor was stable in a broad range of pH (2-6) and temperatures (25-40°C). The molecular mass of the inhibitor was 1078 as determined by mass spectrometry (MALDI-TOF) and revealed a single homogenous band with a Mr of 1072 on Tricine-SDS-PAGE. Amino acid composition of inhibitor showed the presence of D, D G, A, K, L, Y, W residues and CD spectrum conceded the absence of any periodic structure in the secondary structure of the inhibitor. The purified inhibitor from *Penicillium* sp VM24 showed a specific activity of 350 U/mg and a 52 fold increase in purification with a yield of 18%. The inhibitor showed stability in a broad range of pH (2-6) and temperatures (25-40°C). The molecular mass of the inhibitor was 1585 Da as determined by mass spectrometry (MALDI-TOF) and revealed a single homogenous band with Mr of 1580 on Tricine-SDS-PAGE. Amino acid composition of inhibitor showed D, D, D, E, A, H, K, L, I, Y, W residues. The secondary structure determination by CD analysis revealed the presence of 6.5%  $\alpha$ -helix, 49%  $\beta$ -sheet, and 45% aperiodic structures. The inhibitor from *Streptomyces* sp was found to inhibit pepsin and cathepsin D and the inhibitor from *Penicillium* sp inhibited fungal aspartic protease. The inhibitors exhibited no inhibitory activity against other classes of proteases like trypsin, chymotrypsin, papain and subtilisin.



## Chapter 4: Mechanistic and structural insights into the inhibition of therapeutically significant aspartic protease by inhibitor from *Streptomyces* sp MBR04

### *Part A- Kinetic interactions of pepsin with the inhibitor: Correlation to inhibitor induced conformational changes*

A low molecular weight aspartic protease inhibitor from *Streptomyces* sp MBR04 exhibiting a two-step inhibition mechanism against pepsin is reported. The kinetic interactions revealed a reversible, competitive, time-dependent slow-tight binding inhibition with an  $IC_{50}$  and  $K_i$  values of 4.5 nM and 4 nM respectively. The inhibition followed a rapid equilibrium step to form a reversible enzyme-inhibitor complex (EI), which isomerizes to the second enzyme inhibitor complex (EI\*), which dissociated at a very slow rate. The rate constants determined for the isomerization of EI to EI\* and for the dissociation of EI\* were  $2.65 \pm 0.32 \text{ s}^{-1}$  and  $0.070 \pm 0.01 \text{ s}^{-1}$ , respectively. The overall inhibition constant  $K_i^*$  was 0.12nM. The binding of the inhibitor with the enzyme and the subsequent conformational changes induced were monitored by exploiting the intrinsic tryptophanyl fluorescence. The rate constants derived from fluorescence studies were in agreement with the kinetic data correlating the conformational alterations to isomerization of EI to EI\*. The conformational changes induced upon inhibitor binding to pepsin were monitored by far and near UV analysis. A comparative analysis in the fluorescence spectra of pepsin upon binding of APD or the classical known active site directed inhibitor, pepstatin was found to be similar to that of inhibitor, suggesting that the inhibitor binds in the active site of the enzyme. To evaluate the effects of the inhibitor on the secondary structure of the enzyme, we have analyzed the CD spectra of pepsin-inhibitor complex. Interestingly, the pepsin-inhibitor complex, pepsin-APD complex and pepsin-pepstatin complex exhibited a similar pattern of negative ellipticity in the far-UV region, suggesting that the inhibitor causes similar structural changes in the enzyme as that of the substrate. These studies revealed that the inhibitor binds to the active site and causes inactivation of pepsin. Chemical modification of the inhibitor with group specific reagents WRK and TNBS abolished the antiproteolytic activity of the inhibitor due to the involvement of Asp and Lys residues.

***Part B- Slow-tight binding inhibition of Cathepsin D: Implications in mechanism of inactivation***

Cathepsin D, a lysosomal aspartic protease is of potential interest as a target for drug design due to its implication in the pathology of breast and ovarian cancer. The active site cleft of cathepsin D is bound by a conformationally mobile loop known as flap, which is important in substrate binding and catalysis. Investigations of the steady-state kinetic interactions of cathepsin D and the *Streptomyces* sp inhibitor revealed reversible, competitive, time-dependent slow-tight binding nature of the inhibitor with an  $IC_{50}$  and  $K_i$  values of 3.2 nM and 2.5 nM respectively. The binding of the inhibitor with the enzyme and the subsequent conformational changes in the flap region were monitored by exploiting the intrinsic fluorescence of the surface exposed Trp-54 residue, which is present at the proximity of the flap. We have demonstrated by fluorescence and circular dichroism studies that the inhibitor binds in the active site of cathepsin D. The localized conformational changes induced in cathepsin D due to the interaction with the inhibitor were investigated by fluorescence spectroscopic studies. The titration of the enzyme with increasing concentrations of the inhibitor resulted in a concentration dependent quenching of the tryptophan fluorescence. A comparative analysis in the fluorescence spectra of cathepsin D upon binding of the synthetic substrate or the known active site directed inhibitor, pepstatin was found to be similar to that of the inhibitor, suggesting that the inhibitor binds in the active site of the enzyme. To evaluate the effects of the inhibitor on the secondary structure of the enzyme, we have analyzed the CD spectra of cathepsin D-inhibitor complex. Interestingly, the cathepsin D-inhibitor complex, cathepsin D-substrate complex and the cathepsin D-pepstatin complex exhibited a similar pattern of negative ellipticity in the far-UV region, suggesting that the inhibitor causes similar structural changes in the enzyme. Based on our results, we propose that the inactivation is due to the reorganization of the flaps impairing its flexibility leading towards inaccessibility of the substrate to the active site of the enzyme. The inhibitor will be significant as a potential lead molecule for the development of drugs targeted towards overactive and/or deregulated expression of cathepsin D in cancers and Alzheimers.

## **Chapter 5: Aspartic protease inhibitor from *Penicillium* sp VM24 as antifungal peptide: Implications in combating mycotic infections**

A low molecular weight inhibitor from *Penicillium* sp VM24 was found to exhibit inhibitory activity against phytopathogenic fungi, including *Aspergillus fumigatus*, *Aspergillus niger*, *Aspergillus oryzae*, *Claviceps purpurea*, *Colletotrichum* sp., *Curvularia fallax*, *Fusarium oxysporum*, *Fusarium moniliforme*, *Fusarium udum*, *Fusarium solani* and *Rhizopus* sp. The 50% inhibitory concentrations of the peptidic inhibitor ranged from 0.58 to 4.5 µg/ml, whereas the MIC varied from 0.30 to 2.8 µg/ml for the fungal growth inhibition. Microscopic observation of the fungal cultures treated with the inhibitor revealed a reduction in mycelial growth or retardation of spore germination. Growth of representative phytopathogenic fungi on synthetic selective media containing specified carbon source produced xyloglucanase and aspartic protease. The fungal growth inhibition in the presence of inhibitor revealed the role of these enzymes in fungal growth. The chemical modification of Asp/Glu or Lys residues of the inhibitor by 2,4,6-trinitrobenzenesulfonic acid and Woodward's reagent K respectively, abolished the antifungal activity. The kinetic analysis of the TNBS and WRK modified inhibitor abolished its antixyloglucanolytic and antiproteolytic activity. In addition, the inhibitor inhibited xyloglucanase and aspartic protease with  $K_i$  values of 500 nM and 0.85 µM respectively. Our investigations led us to envisage a paradigm shift in the concept of fungal growth inhibition for the role of antixyloglucanolytic and antiproteolytic activity.

## **Chapter 6: Bifunctional role of aspartic protease inhibitor from *Penicillium* sp VM24: inactivation of aspartic protease and xyloglucanase**

### ***Part A- Interactions of a protease inhibitor with an aspartic protease from *Aspergillus* sp***

Aspartic proteases from *Aspergillus* sp are significant targets for therapeutic interventions as they are reported as virulence factor in invasive aspergillosis. The present chapter describes the inactivation of an aspartic protease from *Aspergillus saitoi* by a low molecular weight peptidic inhibitor from *Penicillium* sp VM24. The steady-state kinetic interactions of the fungal aspartic protease with the inhibitor

exhibited reversible, competitive, time-dependent tight binding nature of the inhibitor with  $IC_{50}$  and  $K_i$  values of 1.8  $\mu\text{M}$  and 0.85  $\mu\text{M}$  respectively. The rate constants determined for the formation and dissociation of EI were  $6.25 \times 10^{-3} \text{ s}^{-1}$  and  $11.84 \times 10^{-3} \text{ s}^{-1}$  respectively. The binding of the inhibitor with the fungal aspartic protease and the subsequent conformational changes induced were monitored by intrinsic tryptophanyl fluorescence. To investigate the effects of the inhibitor on the secondary structure of the fungal aspartic protease, we have analyzed the CD spectra of the enzyme-inhibitor complex. Interestingly, the aspartic protease-inhibitor complex and aspartic protease-pepstatin complex exhibited a similar pattern of negative ellipticity in the far-UV region. These studies deciphered that the inactivation of the enzyme is due to the binding of the inhibitor to the active site of aspartic protease. The new inhibitor will be a potential lead compound for the development of molecules to combat human fungal infections.

***Part B- Slow-tight binding inhibition of xyloglucanase from Thermomonospora sp by an aspartic protease inhibitor***

This section of the chapter describes the evaluation of kinetic parameters of the inhibition of xyloglucanase by a peptidic inhibitor from *Penicillium* sp VM24. The inhibitor also inactivated an aspartic protease from *Aspergillus saitoi* (Part A) establishing the bifunctional nature of the inhibitor. Xyloglucanase was secreted by an alkalothermophilic *Thermomonospora* sp and was purified to homogeneity. SDS-PAGE revealed a single homogenous band of xyloglucanase with a molecular weight of 144 KDa and exhibited specificity towards xyloglucan. The steady state kinetic interactions of xyloglucanase with the inhibitor affirmed irreversible, non-competitive, two-step inhibition mechanism with  $IC_{50}$  and  $K_i$  values of 780 nM and 500 nM respectively. CD-spectra and tryptophanyl fluorescence analysis of xyloglucanase incubated with increasing inhibitor concentrations concede the conformational changes in enzyme structure due to irreversible denaturation of enzyme upon inhibitor binding. Further to elucidate the inhibition mechanism, xyloglucanase was probed with a fluorescent chemoaffinity label o-phthalaldehyde (OPTA), which revealed that complete inactivation occurred due to binding of one mole of OPTA to the active site of xyloglucanase. OPTA has been known to form a fluorescent isoindole derivative by crosslinking the proximal thiol and amino groups

of cysteine and lysine. The chemical modification of xyloglucanase using trinitrobenzenesulphonic acid (TNBS) showed the presence of a single lysine residue in the active site of xyloglucanase. The inactivation studies of diethylpyrocarbonate (DEP)-modified xyloglucanase established the presence of an essential histidine at or near the catalytic site of xyloglucanase. The involvement of cysteine in the formation of a xyloglucanase-isoindole derivative has been negated by fluorometric and chemical modification studies on xyloglucanase with group-specific reagents. Modification of histidine and lysine residues by DEP and TNBS respectively, abolished the ability of the enzyme to form an isoindole derivative with OPTA, indicating that histidine and lysine participate in the formation of the isoindole complex. The abolished isoindole fluorescence of o-phthalaldehyde (OPTA)-labeled xyloglucanase revealed that the inhibitor binds to the active site of the enzyme and disrupts the native interactions between the lysine and histidine residues.

## **Chapter 7: Functional aspects of hydrolyases**

Glycosyl hydrolases are a widespread group of enzymes that hydrolyse the glycosidic bond between two or more carbohydrates, or between a carbohydrate and a non-carbohydrate moiety. They are increasingly being utilized for the bioconversion of lignocellulose for potential application in biofuel sector. Lignocellulose consists of cellulose, hemicellulose and lignin. The effective utilization of hemicellulose would play a significant role in the economic viability of second generation biofuel. The present chapter reports the hydrolysis and ethanol production from tamarind kernel powder, a rich source of galactoxyloglucan using xyloglucanase and thermotolerant *Debaromyces hansenii*. The acid hydrolysis of tamarind kernel powder with 2 N H<sub>2</sub>SO<sub>4</sub> yielded an overall saccharification of 94% based on the total available carbohydrate content and further fermentation at 40°C with thermotolerant *D hansenii* produced an ethanol yield of 0.35 g/g. A maximum hydrolysis of 55% and 78% for galactoxyloglucan was obtained in 48 h at 50°C using *Thermomonospora* xyloglucanase and a commercial enzyme, Accellerase<sup>TM</sup>1000 respectively. The synergistic effect of β-galactosidase and xyloglucanase was demonstrated by the exogenous addition of β-galactosidase to *Thermomonospora* xyloglucanase which improved the overall hydrolysis of galactoxyloglucan by 30%. The rate of hydrolysis of galactoxyloglucan with xyloglucanase and accellerase was

increased by 15-20% in the presence of chemical surfactants (tween 80 and toluene) or protein additive (BSA). The fermentation of enzymatic hydrolysates of galactoxyloglucan by xyloglucanase or accellerase with *D. hansenii* at 40°C produced an ethanol yield of 0.39 g/g and 0.41 g/g respectively. The enzymatic hydrolysates of galactoxyloglucan by xyloglucanase or accellerase when fermented with Ca-alginate immobilized *D. hansenii* produced an ethanol yield of 0.45 g/g and 0.43 g/g respectively with theoretical conversion efficiencies of 78% - 88%. The immobilized yeast cells were reused six cycles at 40°C with 100% fermentation efficiency.

## PUBLICATIONS

**Vishnu Menon**, Gyan Prakash and Mala Rao (2010) Enzymatic hydrolysis and ethanol production using xyloglucanase and *Debaromyces hansenii* from tamarind kernel powder: galactoxyloglucan predominant hemicellulose. **J Biotechnol.** 48(4):233-9.

**Vishnu Menon**, Gyan Prakash, Asmita Prabhune and Mala Rao (2010) Biocatalytic approach for the utilization of hemicellulose for ethanol production from agricultural residue using thermostable xylanase and thermotolerant yeast. **Bioresour Technol**, 101 (14): 5366 – 5373.

**Vishnu Menon**, Gyan Prakash, Mala Rao (2010) Value added products from hemicelluloses: Biotechnological perspective. **Global Journal of Biochemistry** 1 (1): 36-67.

**Vishnu Menon**, Rupesh Divate and Mala Rao (2011) Bioethanol production from renewable polymer lichenan using lichenase from an alkalothermophilic *Thermomonospora* sp. and thermotolerant yeast. **Fuel processing technology** 92: 401-406.

Dipali Pol, **Vishnu Menon** and Mala Rao (2012) Biochemical characterization of a novel thermostable xyloglucanase from an alkalothermophilic *Thermomonospora* sp. **Extremophiles** 16: 135-146.

**Vishnu Menon** and Mala Rao (2012). Protease inhibitors: Emphasizing functional aspects of aspartic protease inhibitors. **Functional plant science and biotechnology: special issue on protease inhibitors**. (In press)

**Vishnu Menon** and Mala Rao. Slow-tight binding inhibition of cathepsin D by a low molecular weight inhibitor from *Streptomyces* sp MBR04: Implications in mechanism of inactivation (Communicated)

**Vishnu Menon** and Mala Rao. Biochemical characterization of a peptidic aspartic protease inhibitor from a novel *Penicillium* sp: Kinetic interactions with fungal aspartic protease (Communicated)

**Vishnu Menon** and Mala Rao. Kinetic and mechanistic insights into the inhibition of pepsin with a slow-tight binding inhibitor from *Streptomyces* sp MBR04: Inhibitor induced conformational changes (manuscript under preparation)

**Vishnu Menon** and Mala Rao. Interactions of xyloglucanase by a bifunctional aspartic protease inhibitor: Implications as a biocontrol agent (manuscript under preparation)

## CHPATERS IN BOOK

**Vishnu Menon** and Mala Rao Recent trends in valorization of lignocellulose to biofuel. In **Microorganisms in sustainable agriculture and biotechnology**. Chapter 18, T Satyanarayana et al (Eds), Springer (In press)

**Vishnu Menon** and Mala Rao. Microbial aspartic protease inhibitors (In press)

## CONFERENCES / ABSTRACTS / POSTERS

**Vishnu Menon**, Gyan Prakash and Mala Rao. Poster presented in the International conference in Bioprocesses in food industries (ICBF) held in Osmania University, Hyderabad, November 6<sup>th</sup> – 8<sup>th</sup>, 2008.

**Vishnu Menon**, Gyan Prakash, Asmita Prabhune and Mala Rao Poster presented in the 50<sup>th</sup> Annual Conference in Microbiology (AMI) held in National Chemical Laboratory, Pune, December 15<sup>th</sup> – 18<sup>th</sup> 2009.

**Vishnu Menon** and Mala Rao. Poster presented in the International conference of genomic studies (ICGS) and Indo-Italian workshop on industrial and pharmaceutical biotechnology (IIWIPB), held in Madurai Kamaraj University, Madurai, November 12 – 14, 2010.

**Vishnu Menon**, Rupesh Divate, and Mala Rao. Poster presented in the International conference of genomic studies (ICGS), and Indo-Italian workshop on industrial and pharmaceutical biotechnology (IIWIPB), held in Madurai Kamaraj University, Madurai, November 12 – 14, 2010.



# Chapter 1

*'If you knew what you were doing it wouldn't be called  
research'*

Albert Einstein



**General introduction**

## INTRODUCTION

The biochemical reactions necessary to support life are catalyzed by enzymes representing a remarkable diversity of substrate and reaction specificities. The enzymes carry out highly complex chemical conversions under physiological conditions and retain their stereospecificity and regiospecificity in comparison to many organic chemical reactions. They vary in size and can have molecular weights of several thousands to several million daltons, and still can catalyse reactions involving molecules as small as carbon dioxide or nitrogen, or as large as a complete chromosome. Although enzymes are large molecules, the actual catalysis takes place in the active site where a small number of amino acid residues contribute to catalytic function. With the advent of structural determination of proteins and by designing chemical/biochemical experiments, several catalytic mechanisms for enzymes have been proposed. The past few decades have witnessed spectacular advances and betterment of living standards due to the beneficial integration of enzyme technology with scientific progress and rapid translation of laboratory findings into practical technologies and commercial scale manufacturing processes.

## ENZYME CLASSIFICATION

The International Union of Biochemistry and Molecular Biology (IUBMB) developed a system of enzyme nomenclature, in which enzymes are divided into six major classes, each with numerous subgroups, based on the nature of the chemical reaction they catalyze.

- [1] Oxidoreductases: Catalyze oxidation or reduction of their substrates
- [2] Transferases: These enzymes catalyze group transfer of their substrates
- [3] Hydrolases: Catalyse bond breakage with the addition of water
- [4] Lyases: Lyases remove groups from their substrates
- [5] Isomerases: These enzymes catalyze intramolecular rearrangements
- [6] Ligases: Catalyze the joining of two molecules at the expense of chemical energy

Hydrolases catalyze the hydrolysis of a chemical bond and are classified as EC 3 in the EC number classification of enzymes. Based on the bonds they act they can be further classified into several subclasses. Although a vast array of literature is available for enzymes, including their structures, gene sequences, mechanisms, metabolic pathways and kinetic data, it tends to be spread between many different databases and throughout the literature. Most web resources relating to enzymes [such as BRENDA (Schomburg et al., 2004), KEGG (Kanehisa et al., 2004), the IUBMB Enzyme Nomenclature website (IUBMB 2005) and IntEnz (Fleischmann et al., 2004)] focus on the overall reaction, accompanied in some cases by a textual or graphical description of the mechanism. However, this does not allow for detailed *in silico* searching of the chemical steps which take place in the reaction. MACiE (Holliday et al., 2005) combines detailed stepwise mechanistic information [including 2-D animations (Holliday et al., 2006)], a wide coverage of both chemical space and the protein structure universe, and the chemical intelligence of the Chemical Markup Language for Reactions (CMLReact) (Holliday et al., 2005). This usefully complements both the mechanistic detail of the Structure-Function Linkage Database (SFLD) for a small number of rather 'promiscuous' enzyme superfamilies (Pegg et al., 2006) and the wider coverage with less chemical detail provided by EzCatDB (Nagano 2005), which also contains a limited number of 3D animations.

## SIGNIFICANCE OF PROTEASES

At the earliest stages of protein evolution in primitive organisms, proteases are evolved as simple destructive enzymes necessary for protein catabolism and generation of amino acids. For many years, studies on proteases focused on their original roles as blunt aggressors associated with protein demolition. However, the realization that, beyond these nonspecific degradative functions, proteases act as sharp scissors and catalyze highly specific reactions of proteolytic processing, producing new protein products, inaugurated a new era in protease research (Neurath and Walsh 1976). The current success of research in this group of ancient enzymes derives mainly from the large collection of findings demonstrating their relevance in the control of multiple biological processes in all living organisms (Sauer et al., 2004; Siegel 2006; Page-McCaw et al., 2007). Thus, proteases regulate the fate,

localization, and activity of many proteins, modulate protein-protein interactions, create new bioactive molecules, contribute to the processing of cellular information, and generate, transduce, and amplify molecular signals. As a direct result of these multiple actions, proteases influence DNA replication and transcription, cell proliferation and differentiation, tissue morphogenesis and remodeling, heat shock and unfolded protein responses, angiogenesis, neurogenesis, ovulation, fertilization, wound repair, tissue remodeling, stem cell mobilization, hemostasis, blood coagulation, inflammation, immunity, autophagy, senescence, necrosis, and apoptosis. Consistent with these essential roles of proteases in cell behavior and survival and death of all organisms, alterations in proteolytic systems underlie multiple pathological conditions such as cancer, neurodegenerative disorders, inflammatory, cardiovascular, bacterial, viral and parasitic diseases. Accordingly, many proteases are a major focus of attention for the pharmaceutical industry as potential drug targets or as diagnostic and prognostic biomarkers (Turk 2006). Table 1 summarizes the proteases widely used as therapeutic drug targets. Many infectious microorganisms require proteases for replication or use proteases as virulence factors, which have facilitated the development of protease-targeted therapies for diseases of great relevance to human life such as AIDS (Turk 2006). Proteases also play key roles in plants and contribute to the processing, maturation, or destruction of specific sets of proteins in response to developmental cues or to variations in environmental conditions (Garcia-Lorenzo et al., 2006). Finally, proteases are also important tools of the biotechnological industry because of their usefulness as biochemical reagents or in the manufacture of numerous products (Saeki et al., 2007; Lopez-Otin and Bond 2008).

<b>Table 1</b> Proteases commonly used as therapeutic drug targets			
<b>Class</b>	<b>Protease</b>	<b>Disease indication</b>	<b>References</b>
<b>Aspartic proteases</b>	Pepsin	Acidity	Dash et al., 2003 Eder et al., 2007 Gosh 2010
	HIV Protease	HIV infection	
	Cathepsin D	Cancer	
	Cathepsin E	Cancer	
	Protease A or Saccharopepsin	Yeast infections	
	Renin	Hypertension	
	Plasmeprin	Malaria	
	Secretory aspartic proteases	Candidial infections	
	$\beta$ -secretase	Alzheimer's diseases	
	Neutrophil elastase	Cystic fibrosis, emphysema	
<b>Serine proteases</b>	Plasma Kallikrein	Chronic inflammation and asthma	Rosenblum and Kozarich 2003 Turk 2006 Chien et al., 2009
	Tissue Kallikrein	Hypertension, Cardiac ischemia,	
	Corin	Hypertension	
	Chymases	Cardiac hypertrophy, heart failure,	
	Urokinase	Myocardial infarction and heart failure,	
	Cathepsin B and L	Cancer invasion, growth and angiogenesis	
	Cathepsin S	Cancer invasion, growth and angiogenesis	
	Cathepsin K	Tumour bone metastases, osteoporosis	
	Cathepsin F	Atherosclerosis	
	Cathepsin C	Papillon-Lefevre syndrome	
<b>Cysteine proteases</b>	Cathepsin V	Autoimmune disease	Broemme D 1999 Turk and Guncar 2003 Leung-Toung et al., 2006 Fricker 2010
	Facilipains	Malaria	

<b>Metallo-proteases</b>	Angiotensin converting enzymes (ACE)	Hypertension	Overall and Kleifeld 2006 Vanlaere and Libert 2009 Morrison et al., 2009 Dejonckheere et al., 2011
	Matrix metalloproteases (MMP-2, 9, 14)	Myocardial infarction, cancer progression, angiogenesis	
	Tumour necrosis factor alpha activating enzyme (TACE)	Cancer growth and development	
<b>Threonine proteases</b>	Proteasome	Cancer growth and progression, Malaria	Elliot et al., 2003 Adams 2004 Tschan et al., 2011

## OCCURRENCE OF PROTEASES

Proteases are physiologically necessary for living organisms and are ubiquitous, being found in a wide diversity of sources such as plants, animals, and microorganisms (Rao et al., 1998). The most familiar proteases of animal origin are pancreatic trypsin, chymotrypsin, pepsin and renins. Their production in pure form is depended on the availability of livestock for slaughter, which in turn is governed by political and agricultural policies. The use of plants as a source of proteases is governed by several factors such as availability of land for cultivation and suitability of climatic conditions for growth. Moreover, production of proteases from plants is a time-consuming process. Papain, bromelain, keratinases and ficin represents some of the well known proteases of plant origin (Rao et al., 1998). The inability of the plant and animal proteases to meet current world demands has led to an increased interest in microbial proteases. Proteases from microbial origin are preferred to the enzymes from plant and animal sources since they possess almost all the characteristics desired for their biotechnological applications. Microbial proteases account for approximately 40% of the total worldwide enzyme sales (Ward et al., 2009). Proteases have been identified in a wide range of viruses, with no correlation to capsid complexity, presence of lipid envelope, or nature of their genomes. They are found in enveloped and nonenveloped ssRNA and dsDNA viruses (Babe and Craik 1997).

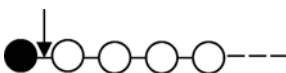
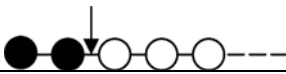

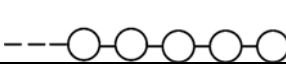

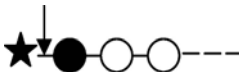
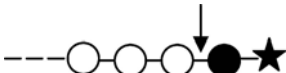
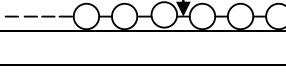
## CLASSIFICATION OF PROTEASES

Currently, proteases are classified on the basis of three major criteria: (i) type of reaction catalyzed, (ii) nature of the catalytic site and (iii) evolutionary relationship with reference to structure. Depending on their site of action, proteases are categorized into two major groups, i.e., exopeptidases and endopeptidases (Table 2). Exoproteases act only near the ends of the N or C termini of the polypeptide chains and are classified accordingly as amino- and carboxyproteases, respectively. Endoproteases attack peptide bonds in more central locations of the polypeptide chain more remote from the N and C termini and indeed free amino or carboxyl groups are known to inhibit or retard enzyme action (Ward et al., 2009). Based on



the functional group present at the active site, proteases are further classified into four prominent groups, i.e., serine proteases, aspartic proteases, cysteine proteases, and metalloproteases and two newly established families, i.e. glutamic acid proteases and threonine proteases. There are a few miscellaneous proteases which do not precisely fit into the standard classification, e.g., ATP-dependent proteases which require ATP for activity (Dash et al., 2003).

**Table 2** Proteases and their mechanism of action

Proteases	Mode of action	Common active site substituents /metal
<b>Exopeptidases</b>		
3.4.11 Aminopeptidases		Free N-terminus
3.4.14 Dipeptidyl peptidases		Not applicable
3.4.14 Tripeptidyl peptidases		Not applicable
3.4.16–3.4.18 Carboxypeptidase		Free C-terminus
3.4.16 Serine type protease		Xaa-Ser-Yaa
3.4.17 Metalloprotease		HEXXH-H/HEXXH-E, zinc or cobalt ions
3.4.18 Cysteine-type protease		Cys-His/His-Cys
3.4.15 Peptidyl dipeptidase		Not applicable
3.4.13 Dipeptidases		Not applicable
3.4.19 Omega peptidases		Blocked N-terminus
		Blocked C-terminus
<b>3.4.21–3.4.34 Endopeptidases</b>		
3.4.21 Serine protease		Xaa-Ser-Yaa
3.4.22 Cysteine		Cis-His/His-Cys
3.4.23 Aspartic protease		Asp-Xaa-Gly
3.4.23.19 Glutamic acid protease		Glu-Gln
3.4.24 Metalloproteases		HEXXH-H/ HEXXH-E
3.4.25 Threonine proteases		Thr

*Open circles represent the amino acid residues in the polypeptide chain. Solid circles indicate the terminal amino acids, and stars signify the blocked termini. Arrows show the sites of action of the enzyme (Ward et al., 2009).*

## SERINE PROTEASES

Serine proteases contain a serine group in their active site, which is essential for substrate binding and cleavage. Generally, serine proteases are characterized by their broad substrate specificity, and their activity extends beyond purely peptidase to include esterase and amidase activities (Rao et al., 1998). Serine proteases exist among exoprotease, endoprotease, oligoprotease, and omega protease groups. Important representative enzyme groups include the chymotrypsins (SA), subtilisins (SB), carboxyprotease C (SC), and *Escherichia* D-Ala-D-Ala protease A (SE), and these have primary structures that are totally unrelated (Ward et al., 2009). Serine proteases are characterized by having a conserved glycine-containing peptide, Gly-Xaa-Ser-Yaa-Gly, associated with the catalytic serine. A common reaction mechanism in the form of a catalytic center containing serine as a nucleophile, aspartate as an electrophile, and histidine as a base, is exhibited by groups SA, SB and SC, respectively. Interestingly, distinctive protein folding strategies among these groups accomplish similar geometric orientations of these residues, suggesting a convergent evolutionary background. Some groups may be differentiated from the latter groups in that they lack the serine-aspartate-histidine catalytic center (Kraut 1977).

## THIOL/ CYSTEINE PROTEASES

Cysteine proteases generally may be assigned to one of the following four groups according to their side chain specificities: (1) papain-like (includes clostripain and streptopain), (2) trypsin-like with preference for cleavage at the arginine residue, (3) specific to glutamic acid and (4) others. Most have neutral pH optima. All cysteine proteases have cysteine/histidine catalytic dyad, although the order of these residues (Cys-His or His-Cys) may vary (McGrath 1999). They generally need reducing agents such as sodium bisulfite, hydrogen cyanide, or cysteine for retaining their activity (Chapman et al., 1997). Biocatalysis is mediated by a double-displacement pathway involving general acid-base formation and hydrolysis of an acyl-thiol intermediate. The enzyme initially binds noncovalently to the substrate, after which acylation of the enzyme occurs together with release of the first product. Water reacts with the acyl enzyme releasing the second product through deacylation. These

enzymes have broad specificity and also attack amide ester, thiol ester, and thiono ester bonds.

## METALLOPROTEASES

The divalent metal-requiring metalloproteases are a very diverse group of proteases, which include both endoproteases and exoproteases. They are inhibited by chelating agents such as ethylenediaminetetraacetic acid, but not by sulfhydryl agents or diisopropyl fluorophosphate (DFP) (Holmes and Matthews 1981). Thermolysin, a neutral zinc protease produced by *B. stearothermophilus*, is one of the most thoroughly characterized metalloproteases where a histidine and glutamine residues participate in the active site providing a ligand for zinc and for catalytic function, respectively. Generally the metal-binding site includes the motif His-Glu-Xaa-Xaa-His. Biocatalysis requires bound divalent cations, and the removal of metal through dialysis or with chelating agents causes inactivation. Metalloproteases are important in many aspects of biology, ranging from cell proliferation, differentiation and remodeling of the extracellular matrix (ECM) to vascularization and cell migration (Chang and Werb 2001).

## GLUTAMIC ACID PROTEASES

Glutamic acid protease was derived from a former pepstatin-insensitive carboxyl protease. Glutamic acid proteases have been discovered from *Styloidium lignicola* (Fujinaga et al., 2004) and *Aspergillus niger var. macrosporus* (Sims et al., 2004). Although absent from the Saccharomycetales class, glutamic acid proteases appear to be present in all other ascomycetes species examined. A large number of coding regions for glutamic proteases were also found clustered together in the *Phanerochaete chrysosporium* genome, despite apparently being absent from three other species of Basidiomycota (Sims et al., 2004). The catalytic mechanism is based on the two enzymes from the aspergilloglutamic and scytalidoglutamic proteases. The active site diad glutamic acid and glutamine play a critical role in substrate binding and catalysis. These amino acids along with their associated water molecules act as nucleophiles to exhibit an acid-base mechanism distinct from that of the

aspartic proteases. The glutamic acid acts as a general acid in the first phase of catalysis, donating a proton to the carbonyl oxygen of the scissile peptide bond of the substrate (Sims et al., 2004). Simultaneously, an OH<sup>-</sup> is donated by water associated with the active site of the enzyme to the carbonyl oxygen of the peptide bond of the substrate. Sometimes, two water molecules are involved in the reaction. The transition state of the substrate is thought to be stabilized by hydrogen bonding with the two catalytic residues. Then, glutamic acid donates a proton to the amide nitrogen atom of the scissile peptide bond triggering the breakdown of the tetrahedral intermediate and thus effecting peptide bond cleavage (Fujinaga et al., 2004).

### **THREONINE PROTEASES**

Threonine protease was discovered in 1995 as a part of a multicomponent proteasome complex in microbial cells. It assembles into a multimeric complex in order to position its substrates, and uses a Thr-Glu/Asp-Lys triad (Lowe et al., 1995; Baumeister and Lupas 1997). The archaeobacterial proteasome has 14 active sites in the inner channel, one on each  $\beta$  subunit. The hydrolytic sites are spatially separated from the intracellular components. Reports have indicated that the active site nucleophile is the hydroxyl group on the threonine at the N-terminus of the  $\beta$  subunit. The replacements of the terminal threonine by serine in archaeobacterial proteasomes allows complete proteolytic activity (Baird et al., 2006). Therefore, the conservation of the threonines in the active sites of all threonine proteases from bacteria to eukaryotes is unclear. Looking at the diverse functions of the threonine proteases in bacteria and mammals, it is evident that the phylogenetically ancient proteasome has undergone adaptations that favor different functions in different physiological situations (Ward et al., 2009).

### **ASPARTIC PROTEASES**

Aspartic proteases commonly known as acidic proteases are the endopeptidases that depend on aspartic acid residues for their catalytic activity. According to the MEROPS database, aspartic proteases are now grouped, on the basis of amino acid sequence similarity, into 14 different families, which are assembled into six clans

based on their evolutionary relationship and tertiary structure. The families of aspartic proteases in the MEROPS database (A1, A2, A3, A9, A11, and A33) all belong to only one clan (AA), with their members being readily identified by the presence of characteristic hallmark sequence motifs (Rawlings et al., 2010). These 'archetypal' aspartic proteases include eukaryotic enzymes such as pepsin and viral retropepsins, including HIV-1 retropepsin (Dunn 2002). The members of families A1 and A2 are known to be related to each other, while those of family A3 show some relatedness to A1 and A2. Seven of these families (A8, A22, A24, A25, A31, A26, and A5) are organized into distinct clans in which, although Asp residues are known to be critical for enzymatic activity, they appear in diverse sequence motifs (Rawlings et al., 2010). This set of families contains the only aspartic proteases of bacterial origin that have so far been characterized: these include signal peptidase II from *Escherichia coli*, which is the type peptidase of family A8 (Sankaran 2004), the prepilin peptidases of family A24 (Dupuy et al., 2004), GPR endopeptidase from *Bacillus megaterium* in family A25 (Carroll and Setlow 2005), omptin from *E. coli*, which is the type peptidase of family A26 (Vandeputte-Rutten et al., 2001), and HybD peptidases of family A31 (Theodoratou et al., 2005). Most aspartic proteases show maximal activity at low pH (pH 3 to 4) and have isoelectric points in the range of pH 3 to 4.5. Their molecular masses are in the range of 30 to 45 KDa.

### **OCCURENCE**

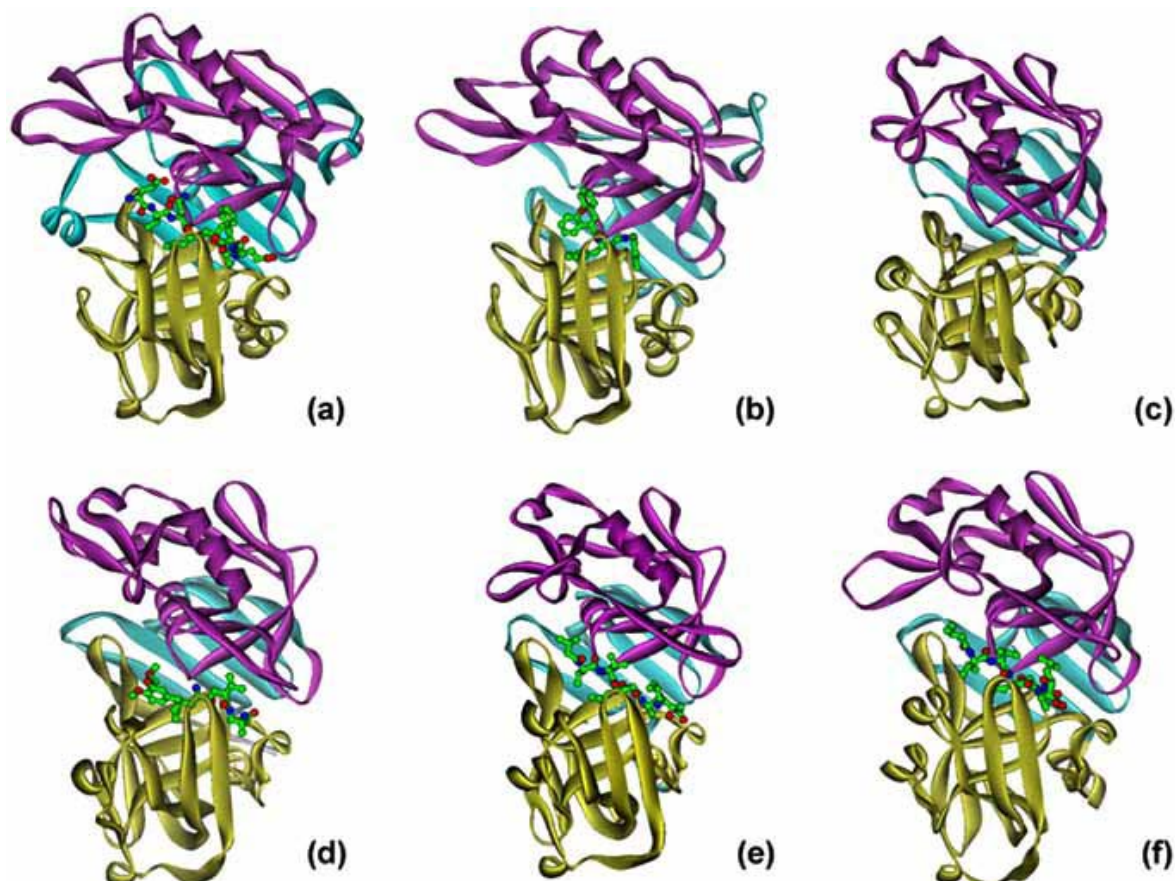
Aspartic proteases have been isolated and studied from a wide range of organisms such as vertebrates, plants, fungi, parasites, retroviruses and bacteria (Hill and Phylip 1997; James et al., 1998). Aspartic proteases from microbial origin are typically sorted into two groups, (i) pepsin-like enzymes produced by *Aspergillus*, *Penicillium*, *Rhizopus* and *Neurospora* and (ii) rennin-like enzymes produced by *Endothia* and *Mucor* sp. (Rao et al., 1998). Fungal aspartic proteases are distributed among families A1, A2 and A11 of clan AA and family A22 of clan AD, the majority belonging to the A1 family, together with pepsin-like enzymes from many different origins (Sabotic et al., 2009). Although many aspartic proteases have been described from ascomycetes, only a few have been described in basidiomycetes, including basidiomycetous yeasts *Cryptococcus neoformans* (Loftus et al., 2005; Pinti et al.,

2007) and *Phaffia rhodozyma* (Bang et al., 1999) and three mushrooms: *Amanita muscaria* (Nehls et al., 2001), *Pleurotus ostreatus* (Park et al., 2006) and *Polyporus tulipiferae* (formerly *Irpex lacteus*) (Kobayashi et al., 1989). Apart from a *Cryptococcus neoformans* aspartic protease that belongs to the A22 family, all other aspartic proteases described from basidiomycetes belong to the A1 family. Some aspartic proteases for which no sequence data is available have been described from other basidiomycetes, and are not listed in the MEROPS database. These are 25, 35, 50 and 36 KDa pepstatin A sensitive aspartic protease from *Phanerochaete chrysosporium* (Dass et al., 1995), *Russula decolorans* (Rudenskaia et al., 1980), *Laetiporus sulphureus* (Kobayashi et al., 2003) and *Ustilago maydis* (Mercado-Flores et al., 2005) respectively. Microbial acid proteases exhibit specificity against aromatic or bulky amino acid residues on both sides of the peptide bond, which is similar to pepsin, but their action is less stringent than that of pepsin. Aspartic proteases are also important virulence factors and are involved in the pathogenicity of many viruses, including immunodeficiency viruses, and also in pathogenic fungi, *Candida albicans*, whose secreted aspartyl proteinases have been most studied (Eder et al., 2007).

In the human genome aspartic proteases are the smallest class with only 15 members, however, this class has proven to be a rich source for drug targets for the pharmaceutical industry. Human aspartic proteases are found in 2 clans, clan AA and clan AD, reflecting their different tertiary structures. Clan AA has two families, family A1 containing the classical aspartic proteases (renin, pepsin A, pepsin C, cathepsin D, cathepsin E, BACE1, BACE2, and napsin A) and family A2 including proteases which are integrated by retroviruses into the human genome like HIV protease. Clan AD contains intramembrane cleaving proteases such as the presenilins and signal peptide peptidase (Eder et al., 2007). Aspartic proteases like pepsin, gastricsin, and renin from human body are secretory and have well-defined physiological roles. Cathepsin D, is found ubiquitously in the lysosomes of most cells (Saftig et al., 1995), while Cathepsin E is located within the endoplasmic reticulum/trans-Golgi network/endosomal compartments of cells (Kageyama 1998).

### *CRYSTALLOGRAPHIC STUDIES OF ASPARTIC PROTEASES*

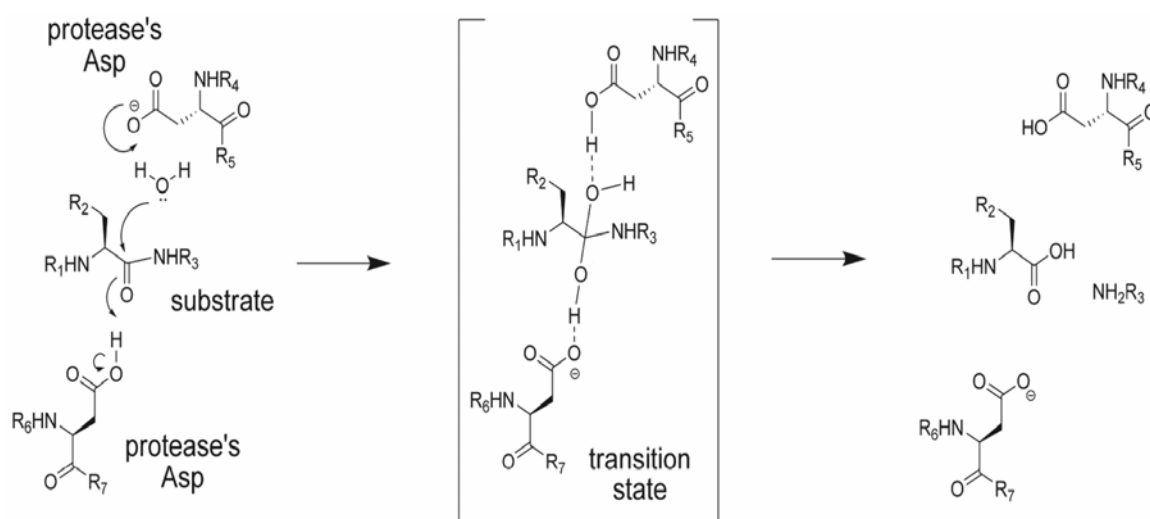
Aspartic proteases have been studied extensively for their structure and functional relationships and have been the topics of several reviews or monographs (Rao et al., 1998; Dunn, 2002; Simoes and Faro 2004; Eder et al., 2007; Minarowska et al., 2008; Bhaumik et al., 2009; Chen et al., 2009; Fengwu et al., 2010). The crystal structures of most A1 human aspartic proteases have been solved. They follow a general fold with three topologically distinct regions, a N-terminal domain, a C-terminal domain and a six-stranded anti-parallel  $\beta$ -sheet interdomain connecting the two other domains (Figure 1).



**Figure 1** Crystal structures for human aspartic proteases. The crystal structures for (a) BACE-1 (b) BACE-2 (c) Cathepsin E (d) Renin (e) Pepsin A (f) Cathepsin D.

*MECHANISM OF ACTION*

The specificity of the catalysis has been explained on the basis of available crystal structures. The structural and kinetic studies also have suggested that the mechanism involves general acid-base catalysis with lytic water molecule that directly participates in the reaction (Figure 2). In contrast to serine and cysteine proteases, catalysis by aspartic proteases does not involve a covalent intermediate though a tetrahedral intermediate exists. The nucleophilic attack is achieved by two simultaneous proton transfers, one from a water molecule to the diad of the two-carboxyl groups and a second one from the diad to the carbonyl oxygen of the substrate with the concurrent CO-NH bond cleavage. This general acid-base catalysis, which may be called a “push-pull” mechanism, leads to the formation of a noncovalent neutral tetrahedral intermediate (Northrop 2001; Dunn 2002). This is supported by the crystal structures of various aspartic protease-inhibitor complexes and by the thiol inhibitors mimicking a tetrahedral intermediate formed after the attack by the lytic water molecule (Rao et al., 1998; Eder et al., 2007).



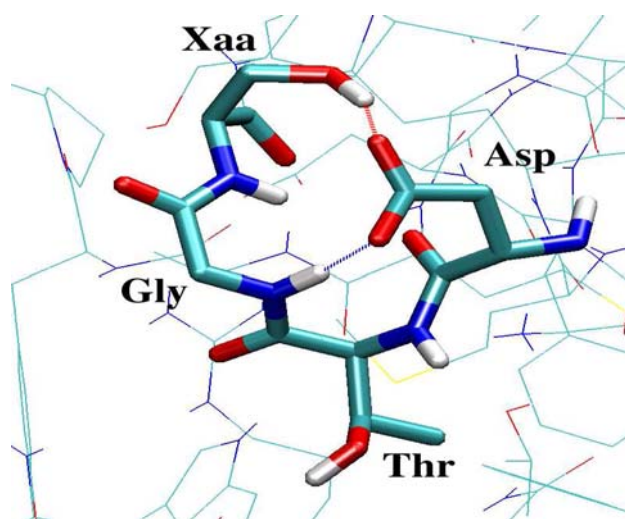
**Figure 2** Mechanism of action of aspartic proteases



## CLASSIFICATION OF ASPARTIC PROTEASES

### *Pepsin family*

All members of the pepsin family have been found in eukaryotes. The family includes animal enzymes from the digestive tract, such as pepsin and chymosin, lysosomal enzymes, such as cathepsin D, and enzymes involved in post-translational processing, such as renin and yeast aspartic protease 3. Members from protozoa, fungi and plants are also known. Most of the pepsin members have a molecular weight of  $\sim 35$  KDa. The enzymes are approximately 330 amino acids long, with only  $\sim 5\%$  of sequence identity between all members of the family. The zymogens feature a N-terminal pro-peptide of up to 50 amino acids long, which is cleaved upon activation. Pepsin-like aspartic proteases characteristically consist of two internally homologous domains, each of which provides a catalytic Asp to the active site. Each Asp is present in the hallmark motif Asp-Thr / Ser-Gly, followed further downstream by a hydrophobic-hydrophobic-Gly sequence (Figure 3). Together, these motifs form a structural feature known as a psi loop, which serves to locate the two Asp residues necessary for operation of the catalytic machinery (Dunn 2002).



**Figure 3** Conserved active site loop in aspartic proteases. The Xaa residue, in pepsin is a Ser, typical of the N-terminal lobe of pepsins.

In contrast, retroviral-type aspartic proteases are obligate homodimers, in which each monomer contributes one catalytic motif to one psi loop. Enzymes with a pepsin-like ‘archetypal’ organization are by far the most numerous and well-characterized aspartic proteases, and have been thought to be confined to

eukaryotes. This has been supported by structural evidence suggesting that pepsin-like enzymes evolved through a gene duplication and fusion event from a retropepsin-type of ancestral gene (Tang et al., 1978). However, the absolute requirement for the psi loop structural feature described above provides four landmark motifs (two Asp-Thr / Ser-Gly and two hydrophobic-hydrophobic- Gly) that are required to be present in conserved locations, and so can be searched for during data mining operations to identify putative pepsin-like aspartic proteases in any newly sequenced genome. In such an endeavor, contrary to long-held beliefs, pepsin-like aspartic proteases were detected within the genomes of a few bacteria (Rawlings and Bateman 2009). All of the currently sequenced bacterial genomes (~1000) were examined, and putative aspartic protease encoding genes were identified in seven species. Of these, two pairs of Asp-Thr / Ser-Gly + hydrophobic-hydrophobic- Gly motifs were present in the predicted polypeptides from five species, all marine psychrophiles, including *Shewanella amazonensis* (Simoes et al., 2011).

### *Retropepsin family*

Retropepsins are smaller than pepsins (each domain contains ~100-130 amino acids), whereas the fold of each of their domains resembles that of the N-terminal lobe of pepsins. In particular, each domain has a  $\beta$ -structure, and the external flap is clearly present. Dimerization of the two subunits occurs by molecular recognition, while the N- and C- terminal residues fold in a 4 strands wide anti-parallel  $\beta$ -sheet, where each chain alternates one strand. Like in pepsins, this structural motif is the only one that cross-links the two subunits (Figure 4). The active site region of retropepsins is very similar to that of pepsins. In particular the already discussed Asp-Thr-Gly-Ala motif is present in the cleavage loops. The two subunits are separated by a cavity that resembles the groove of pepsins, where the substrate is binding. For effective catalysis, the retroviral aspartic proteases seem to require at least a seven residues long peptide (Darke et al., 1988). These show unusual specificity in their ability to cleave a peptide bond of polyprotein substrates containing a proline in P1' (Pearl and Taylor 1987). Their action is optimal on oligopeptides containing the Tyr-Pro sequence, although they show some activity against peptides with other amino acid

residues in P1 and P1'; among all, the Met-Met sequence has been found particularly effective (Darke et al., 1988).

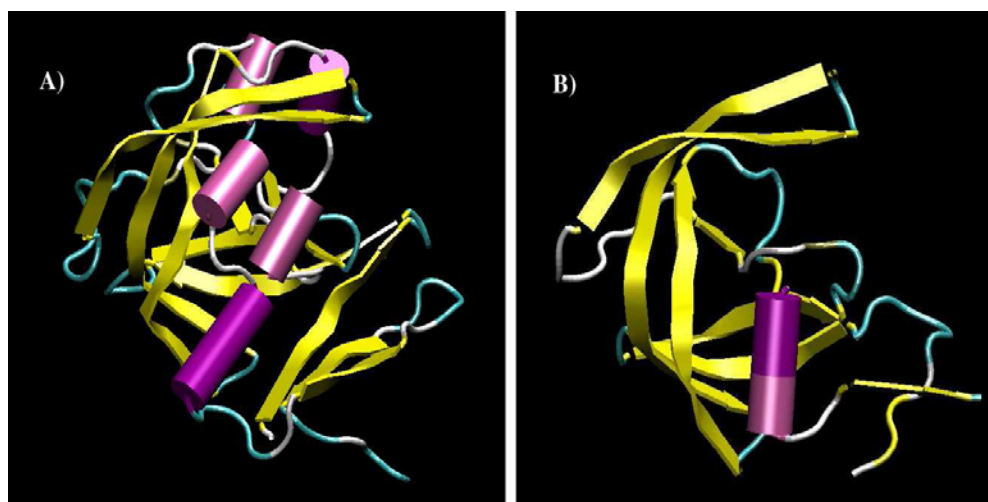


Figure 4 Comparison of the N-terminal lobe of a pepsin (A) and a monomeric unit of a retropepsin (B).  $\alpha$ -helices are coloured in magenta,  $\beta$ -sheets in yellow.

Retropepsin is required for processing of all three viral polyproteins, although cellular enzymes perform initial stages of envelope polyprotein cleavage. Processing occurs at a very late stage in virion assembly, usually after budding of virus particles from the cell membrane; inactive virions containing only gag polyprotein can be formed. Processing seems to be essential for RNA dimerization within the virion, and hence for infectivity. Therefore, there have been intense research interests in the development of inhibitors of retropepsins as antiretroviral agents (Hellen and Wimmer 1992). A subset of the retropepsins from oncoviruses and avian retroviruses are larger proteins with N terminal domain homologous to dUTPases. Li et al (2011) have reported a reteroviral protease (XMVR) showing more close resemblance to the monomeric pepsin-like enzymes.

#### *Cauliflower mosaic virus proteases family*

Cauliflower mosaic virus belongs to a group of plant viruses known as pararetroviruses. Although the viral genome is double-stranded DNA, it contains an open reading frame (ORF V) analogous to the pol gene of retroviruses. ORF V encodes a polyprotein, including a reverse transcriptase that is homologous to that of retroviruses and based on an Asp-Thr-Gly triplet near the N terminus, it was suggested to be included as an aspartic proteases as well (Fuetterer and Hohn 1987).

The existence of an endoproteases was confirmed by mutational studies that implicated the involvement of Asp 45 in catalysis. There was also weak inhibition by pepstatin. The proteases are larger than retropepsin, however, because it contains only one Asp-Thr-Gly sequence, it is assumed to be active only as a dimer (Torruella et al., 1989). Other pararetroviruses contain sequences homologous to the cauliflower mosaic virus proteases.

### *Membrane bound aspartic proteases*

#### *BACE-1 and BACE-2*

BACE-1 ( $\beta$ -amyloid precursor protein cleaving enzyme- 1, Asp2, memapsin-2) is a membrane bound aspartic protease expressed in the brain and other tissues (Vassar et al., 1999; Yan et al., 1999). BACE-1 activity in the brain is responsible for the proteolytic truncation of amyloid precursor protein (APP) to C99, which is further processed by presenilins to generate amyloidogenic peptides A $\beta$ 40 and A $\beta$ 42. The latter peptides constitute the major components of amyloid plaques accumulating in the brain of Alzheimer's disease (AD) patients. As plaque formation is believed to be directly linked to the progression of the disease, BACE-1 represents an attractive target for therapeutic intervention of AD (Hardy and Selkoe 2002). The X-ray structure of a variant of BACE-1 lacking the transmembrane part of the protease revealed that BACE-1 is similar to other human A1 proteases such as pepsin A, renin and cathepsin D (Hong et al., 2000; Hong et al., 2002). BACE2 is a close homologue of BACE1 sharing 51% identity at the amino acid level (Yan et al., 1999). It is expressed in the central nervous system and many peripheral tissues, but its expression level in neurons is substantially lower than that of BACE1 (Bennett et al., 2000). Since BACE2 cleaves  $\beta$ - secretase substrates similar to BACE1 (Hussain et al., 2000) it was speculated that BACE2 might also act as a  $\beta$ -secretase to cleave APP. However, the role of BACE2 in A $\beta$  generation is controversial and recent data rather argue against BACE2 being involved in the formation of neuritic plaques in Alzheimer's disease (Basi et al., 2003; Sun et al., 2005; Vassar 2005). In addition to its potential role in the central nervous system, BACE2 has also been implicated in two closely related muscle diseases, sporadic inclusion-body myositis (Vattemi et al.,

2003) and hereditary inclusion body-myopathies, and it is upregulated in breast and colon cancers (Xin et al., 2000).

### *GxGD aspartic proteases*

Presenilins (PS1 and PS2) and signal peptide peptidase (SPP) are members of the GxGD aspartic protease family of integral membrane proteins (clan AD) (Steiner et al., 2000; Martoglio and Golde 2003). The unique feature of this group of enzymes is their ability to promote so-called intramembrane proteolysis and to cleave substrate polypeptides within a transmembrane region. The most prominent and best studied members of the GxGD protease family are the two presenilins (Hardy 1997). They form the catalytic subunits of  $\gamma$ -secretase, a multiprotein complex which plays a crucial role in Alzheimer's disease (De Strooper 2003). Together with BACE1,  $\gamma$ -secretase is responsible for the generation of the amyloidogenic A $\beta$  peptides out of APP (Selkoe and Kopan 2003). Driven by the hypothesis that reduction of the synthesis of A $\beta$  peptides might slow down disease progression in patients with Alzheimer's disease,  $\gamma$ -secretase and particularly its proteolytic subunit, PS1 and PS2, are considered as therapeutic targets (Hardy and Higgins 1992; Wolfe 2002). The second GxGD protease with proven proteolytic activity is SPP (Weihofen et al., 2002). Despite limited sequence homology, the sequences of SPP and the presenilins can be aligned almost throughout their entire length. This structural similarity and the identical active site motifs within the transmembrane regions argue for a common catalytic mechanism. Accordingly, a number of  $\gamma$ -secretase inhibitors were found to inhibit SPP (Weihofen et al., 2003). There are, however, major differences between PSs and SPP. PSs require endoproteolysis for activation and act as proteolytic subunits of a multiprotein complex. SPP, in contrast, does not undergo endoproteolysis and functions independent of additional components. The most striking difference is the opposite orientation of the catalytic domains within the plane of the membrane. Presenilin is integrated into the membrane such that it can cleave type I anchored transmembrane proteins (Laudon et al., 2005), whereas SPP is embedded in opposite orientation predisposed to cleave type II anchored substrates (Friedmann et al., 2004).

### *Putative aspartic proteases*

Families of proteases are strictly categorized as of unknown catalytic type, but they exhibit certain indications of aspartic type of proteases. These include putative transposition endopeptidases, thermopsin, scytalidopepsin B, Leader peptidase II. They also include pseudomonapepsin and sporulation sigma factor processing peptidase (Dash et al., 2003). Several putative aspartic proteases with different relative molecular masses and N-termini are expressed in the basidiocarps of basidiomycete *Clitocybe nebularis* (Sabotica et al., 2009). A putative aspartic protease is expressed in the infective larvae, young adults, and adult worms of *Angiostrongylus cantonensis*, a blood feeding helminth. The expression level of aspartic protease gene changes with development but also has a sexual difference in individual developmental stages of *A. cantonensis* (Hwang et al., 2010). There are a number of incompletely characterized peptidases that cannot be assigned to any catalytic type and show no homology to peptidases of known family. These are listed in Table 3.

**Table 3** Members of families of aspartic proteases<sup>a</sup>

Family	Database code
<b>Family U7: Endopeptidase IV</b>	
Endopeptidase IV ( <i>Escherichia coli</i> )	SPA_ECOLI, LICA_HAEIN
Minor capsid protein precursor C (bacteriophage $\lambda$ )	VCAC_LAMBD
Soh B gene product ( <i>E. coli</i> )	(M73320)
<b>Family U2: Aminopeptidase iap</b>	
Alkaline phosphatase enzyme conversion protein ( <i>E.coli</i> )	IAP_ECOLI
<b>Family U5: Tail-specific protease</b>	
Tail-specific protease ( <i>E. coli</i> )	(M75634)
OrfX ( <i>Agmenellum</i> )	(X63049)
<b>Family U5: Murein endopeptidase</b>	
Penicillin-insensitive endopeptidase ( <i>E.coli</i> )	MEPA_ECOLI
<b>Family U8: Bacteriophage Murein endopeptidase</b>	
Murein endopeptidase (bacteriophage)	ENPP_
<b>Family U9: Prohead endopeptidase</b>	
Prohead endopeptidase (bacteriophage T4)	PCCP_BPT4
<b>Family U3: Spore endopeptidase</b>	
Spore Endopeptidase ( <i>Bacillus</i> ) (9124)	(M55262)
<b>Family U20: <math>\gamma</math>-D-Glutamyl-l-diamino acid opeptidase II</b>	
$\gamma$ -D-Glutamyl-l-diamino acid opeptidase II ( <i>B.spaericus</i> )	(X64809)
<b>Family U26: Enterococcus D-Ala-D-Ala carboxypeptidase</b>	
D-Ala-D-Ala carboxypeptidase ( <i>Enterococcus</i> )	(M90647)
<b>Family U29: Encephalomyelitis virus proeinase 2A</b>	
Proteinase 2A (Theiler's mureine encephalomyelitis virus)	POLG_TMEVD
Proteinase 2A (Encephalomyocarditis virus)	POLG_EMCV
<b>Family U27: Lactococcus ATP-dependent proteinase</b>	
ATP-dependent proteinases ( <i>Lactococcus</i> )	(X67821)
<b>Family U28: Aspartyl dipeptidase</b>	
Aspartyl dipeptidase ( <i>Salmonella</i> )	<i>b</i>

<sup>a</sup> EC is the enzyme nomenclature number (Nomenclature Committee of the International Union of Biochemistry and Molecular Biology, "Enzyme Nomenclature 1992," Academic Press, Orlando, Florida, 1992, and supplement); - indicate that no EC number has been assigned. Literature references to the individual proteins are generally to be found in the database entries for which the codes are given. (b- Conlin et al., 1994)

### *Plant aspartic proteases*

Plant aspartic proteases have been distributed among families A1, A3, A11 and A12 of clan AA, and family A22 of clan AD. The majority of plant aspartic proteases belong to the A1 family, together with pepsin-like enzymes from many different origins. In common with other members of the A1 family, plant aspartic proteases are active at acidic pH, are specifically inhibited by pepstatin and have two aspartic acid residues responsible for the catalytic activity. However, there are several

structural and functional features that make plant aspartic proteases unique among aspartic proteinases. (van der Hoorn 2008).

Many plant aspartic proteases are synthesized as the pre-proform. cDNA cloning of plant aspartic proteases has demonstrated the presence of an insert of approximately 100 amino acids at the C terminal region that is not found in animal or microbial aspartic proteases. This plant aspartic proteases-specific insert (PSI) may thus characterize aspartic proteases of plant origin (Runeberg-Roos et al., 1994; Faro et al., 1999). Investigations of the crystal structures of phytepsin (Kervinen et al., 1999) and cardosin A (Frazao et al., 1999) also showed that the PSI should be located in the surface of the molecule, as each of these pro aspartic proteases binds to the plasma membrane at the PSI site prior to being transported into the vacuole, where the PSI is eventually removed by processing (Kervinen et al., 1999; Törmäkangas et al., 2001; Vieira et al., 2001). The function of the PSI for vacuolar targeting in plant aspartic proteases is not common to all plant aspartic proteases but varies depending on the kind of aspartic protease (Terauchi et al., 2006).

## PROTEASE INHIBITORS

Many biological functions rely on proteases. Since the hydrolysis of the peptide bond catalyzed by proteases is essentially irreversible, an extensive regulatory network of protease inhibitors has evolved to ensure targeted spatial and temporal control of their activity. The action of proteases is tightly controlled to prevent improper cleavage of signalling molecules. Protease activities are regulated at the transcriptional level by differential expression and at the protein level by activation of inactive zymogens and by the binding of inhibitors and cofactors. Activation can be either autocatalytic or catalysed by other proteases. Alternatively, proteases are sometimes activated with the assistance of an activation complex, such as the death-inducing signalling complex (DISC), which is involved in the activation of various caspases (Medema et al., 1997). As such, preventing protease activation could be an attractive area for potential new therapeutics, and is particularly amenable to RNAi approaches (Reed 2002). Protease activity is also regulated by cofactors, proteins that



reversibly bind to proteases and/or inhibitors and affect their final activity, often in an allosteric manner (Turk 2006)

The other major regulators of protease activity are their endogenous or exogenous inhibitors. In this regard, nature has been economical because the number of endogenous human inhibitors identified is substantially smaller than the number of proteases identified (only 105 in humans), with only a slightly higher number identified in mice (Gomis-Ruth et al., 1997). This might be explained by the low specificity of the inhibitors for their target proteases. Multicellular organisms possess endogenous protease inhibitors to control proteolytic activity. Most of these inhibitory proteins are directed against serine protease, although some are known to target cysteine, aspartyl, or metalloproteases. Indeed, inhibitors of serine, cysteine, and metalloproteases are distributed throughout the biological world. Protein inhibitors of aspartic proteases are relatively uncommon and are found in specialized locations.

### *CLASSIFICATION OF PROTEASE INHIBITORS*

Protease inhibitors can be broadly separated into two general categories based upon their spectrum of activity: the nonspecific protease inhibitors and the class-specific protease inhibitors.

- A) Nonspecific protease inhibitors are capable of inhibiting members of all 4 classes of proteases. This class of inhibitors consists solely of the alpha macroglobulins, including human  $\alpha_2$ -macroglobulin ( $\alpha_2$ -M). Alpha macroglobulins are very large proteins that comprise as much as 8-10% of total serum protein. The alpha macroglobulins are able to exert their effects on a variety of proteases because of a unique mechanism of action, referred to as the trap mechanism. The protease binds to a generic bait region on the alpha macroglobulin molecule, resulting in a conformational change in the alpha macroglobulin. This conformational change exposes a receptor-binding domain, causing rapid removal of the alpha macroglobulin-protease complex from circulation by receptor-mediated endocytosis in the reticuloendothelial

system (Hibbetts et al., 1999). Even when contacting a protease in a non-living system (e.g., foodstuffs), accessibility of the bound protease to extraneous protein substrates is severely hampered due to steric hindrance by the enveloping  $\alpha_2$ -M molecule. One alpha macroglobulin molecule can bind to one or two molecules of protease. Although no single specific role for the alpha macroglobulins has been identified, their major function seems to be the rapid inhibition of excess proteolytic activity due to either endogenous or exogenous proteases. Though alpha macroglobulins may be the primary inhibitor of some proteolytic enzymes, they seem to play a supportive role in the modulation of many other proteases. In addition to inhibiting proteolysis, alpha macroglobulins also can bind many nonproteolytic enzymes (Borth 1992).

- B)** Class-specific protease inhibitors are each capable of inhibiting proteases from only 1 of the 6 classes of proteases listed above (Laskowski and Kato 1980). These have lower molecular weights and higher specificity for target enzymes when compared to the alpha macroglobulins. Their higher specificity is due to specific binding sites located within the active site of the enzyme. Thus the class-specific protease inhibitors can be divided into 6 superfamilies (serine, threonine, glutamine, cysteine, aspartyl and metalloprotease inhibitors) according to the mechanism employed at the active site of proteases they inhibit. Most of these inhibitors abolish all enzymatic activity toward all substrates, have strictly competitive inhibitory activity, and have inhibitory sites that can each inhibit proteases belonging to only 1 of the 6 classes of proteolytic enzymes. All of these protease inhibitors prevent access of substrates to the proteases' active sites through steric hindrance (Figure 5).

Many act in a substrate like manner by binding directly to the active site of the protease, whereas others bind to surface sites adjacent to the actual active site. Both methods prevent interaction between the protease and substrate, and both may be reversible (Bode and Huber 1992). Some protease inhibitors interfere with more than one type of protease. For example, the serine family of protease inhibitors (serpins) is generally thought to be active against serine

proteases, yet contains several important inhibitors of cysteine proteases as well.

Class specific protease inhibitors can be classified according to their mechanism of inhibition or by the physiological outcome or relevance of the inhibition (Figure 5).

### *Based on mechanism of inhibition*

Four different mechanisms for protease inhibition have been described :-

- A) Canonical inhibitors (lock-and-key) bind to their targets in a substrate-like manner to form an almost Michaelis-type complex, a principle used by serine protease inhibitors (serpins) (Silverman et al., 2001)
- B) Exosite-binding inhibitors directly block the active site by binding adjacent to it and covering it partially in a substrate-like manner. This principle was observed initially with cystatins and cysteine cathepsins (Stubbs et al., 1990)
- C) Inhibitors might also bind in a quasi-substrate-like manner that is a combination of the canonical and exosite-binding mechanisms (for example, as with tissue inhibitor of metalloproteinases) (Gomis-Ruth et al., 1997)
- D) Allosteric inhibitors - such as X-linked inhibitor of apoptosis protein, which inhibits caspase 9 - prevent dimerization by binding in the interdomain region away from the active site (Shiozaki et al., 2003)

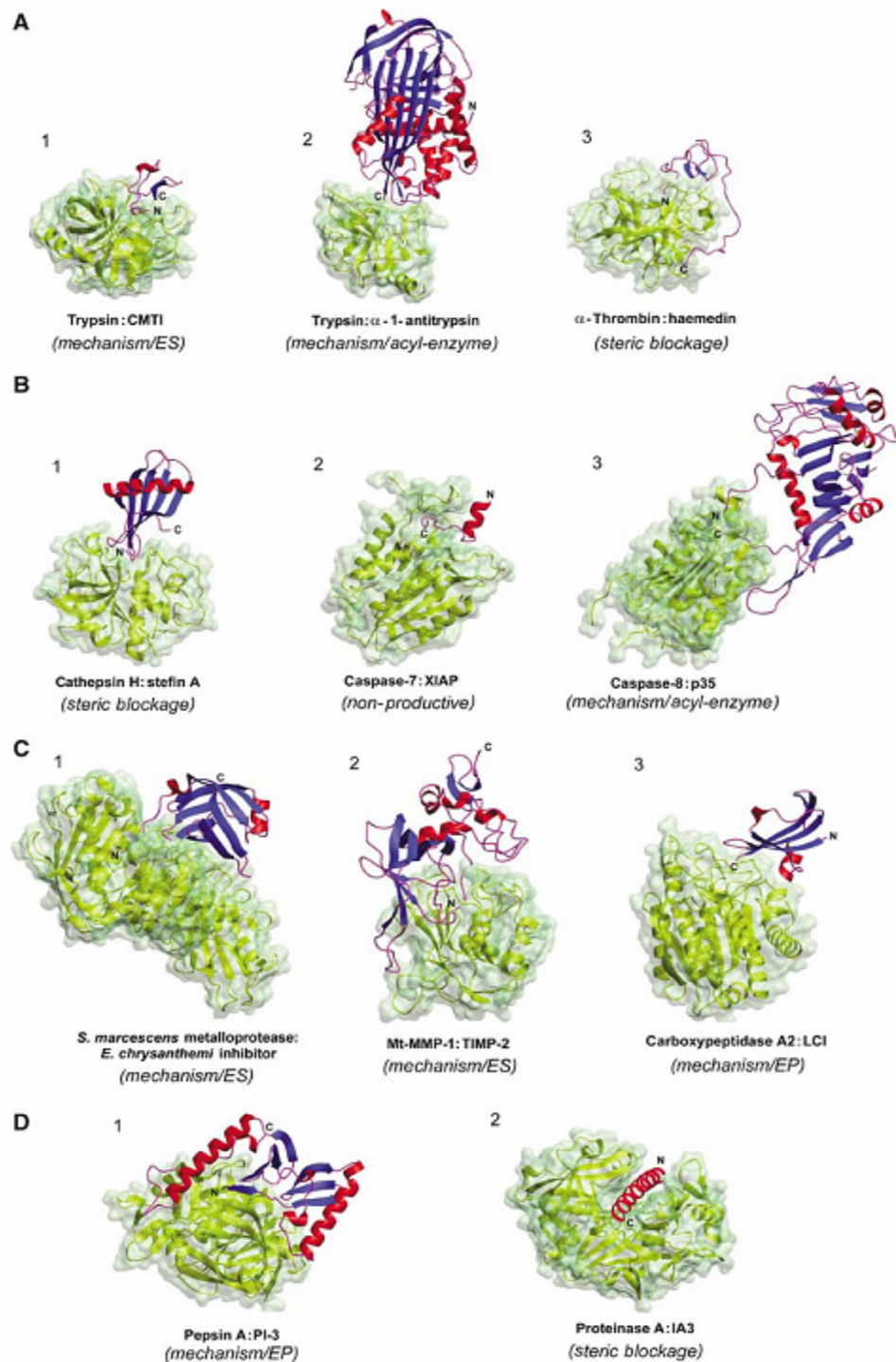
With the exception of allosteric inhibitors all other endogenous protein inhibitors are mostly competitive.

### *Based on physiological relevance*

The physiological inhibition of proteases depends on temporal and spatial co-localization of the protease and its inhibitor, their relative concentrations and binding kinetics; this leads to two major categories of physiological inhibitors (Turk et al., 2002) [1] Emergency type inhibitors (characterized by a large excess concentration of inhibitor, rapid binding and no co-localization with proteases) with the major function to block any protease activity in an inappropriate compartment (for example, cystatins) (Turk et al., 2002). [2] Regulatory type inhibitors (often co-

localized with proteases) which are responsible for the fine regulation of protease activity. Regulatory type inhibitors can be subdivided into the following categories:

- A) **Threshold inhibitors:** low concentration and rapid binding, their major function is to neutralize accidental protease activation (for example, inhibitors of apoptosis) (Deveraux et al., 1997)
- B) **Buffer-type inhibitors:** weak binders, these temporarily block proteases to prevent inappropriate activity and can be easily displaced from the complex (for example, propeptides of cathepsins) (Turk et al., 2000)
- C) **Delay-type inhibitors:** often irreversible, slow binders that enable protease activity for a limited amount of time (for example, antithrombin) (Olson et al., 2002)
- D) **Pro-inhibitors:** synthesized as inactive, and require proteolytic processing to become active (for example, invariant chain p41 fragment resulting from the proteolytic processing of major histocompatibility class II molecules) (Bevec et al., 1996)



**Figure 5** Examples of protease–inhibitor complexes. (A) Serine protease–inhibitor complexes: (1) canonical: trypsin–CMTI (PDB: 1PPE), (2) serpin: trypsin– $\alpha$ -1-antitrypsin (1EZS), (3) noncanonical:  $\alpha$ -thrombin–haemedin (1EOF). (B) Cysteine protease–inhibitor complexes: (1) cathepsin H–stefin A (1NB5), (2) caspase-7–XIAP (1I51), (3) caspase-8–p35 (1I4E). (C) Metalloprotease–inhibitor complexes: (1) *Serratia marcescens* metalloprotease–*Erwinia chrysanthemi* inhibitor (1SMP), (2) membrane-type MMP-1–TIMP-2 (1BQQ), (3) human carboxypeptidase A2–LCI (1DTD). (D) Aspartic protease–inhibitor complexes: (1) porcine pepsin–PI-3 (1F34), (2) proteinase A–IA3 (1DPJ). 3D structures of proteases are represented by yellow ribbons with water accessibility surface colored in pale green. Secondary structure elements of inhibitors are marked in blue ( $\beta$ -sheets), red ( $\alpha$ -helices) and magenta (coils). The inhibition types of particular enzyme:inhibitor pairs are given in parentheses (Otlewski et al., 2005).

## ASPARTIC PROTEASE INHIBITOR

Aspartic proteases are relatively a small group of proteolytic enzymes. Over the last decade, they have received tremendous research interest as potential targets for pharmaceutical intervention as many have been shown to play significant roles in physiological and pathological processes. Despite numerous efforts, however, the only inhibitors for aspartic proteases currently in the market are directed against the HIV protease of viral origin. Nevertheless, several inhibitors including those targeting renin-angiotensin system and  $\beta$ -secretase are in clinical or preclinical developments and few other aspartic proteases are discussed as potential drug targets. Currently the research strategies are focusing on the need for improved comprehension of protease-regulated cascades, along with precise selection of targets and improved inhibitor specificity. There are many hundreds of crystal structures now deposited in the pdb database for inhibitor-bound and uncomplexed aspartic proteases including viral proteases (HIV-1, HIV-2, SIV, FIV), cathepsin D, renin, rennin/chymosin, penicillopepsin, secreted aspartic protease, pepsin, mucoropepsin, retropepsin, saccharopepsin, rhizopuspepsin, and plasmepsin II.

### *MECHANISM OF INHIBITION*

A strong inhibition of an active protease by a protein appears to be a paradox. Inhibitor structures, modes of inhibition, kinetic and thermodynamic parameters, and the nature of the enzyme-inhibitor complexes are surprisingly diversified. On the other hand, in many cases, convergence of structure and/or function can be observed, pointing to the fact that there are a limited number of inhibition modes (Otlewski et al., 2005).

Proteolytic inhibition by protease inhibitors can occur via 2 mechanisms: irreversible trapping reactions and reversible tight binding reactions. In tight-binding reactions, the inhibitor binds directly to the active site of the protease; these reactions are reversible and the inhibitor can dissociate from the enzyme in either the virgin state, or after modification by the protease (Fear et al., 2007). Aspartic proteases generally bind 6 to 10 amino acid regions of their polypeptide substrates, which are typically processed, with the aid of two catalytic aspartic acid residues in

the active site (James and Sielecki 1987). Thus, there is usually considerable scope for building inhibitor specificity for a particular aspartic protease by taking advantage of the collective interactions between a putative inhibitor, on both sides of its scissile amide bond, and a substantial portion of the substrate-binding groove of the enzyme. Some aspartic protease also have one or more flaps that close down on top of the inhibitor, further adding to inhibitor protease interactions and increasing the basis for selectivity. The scissile amide bond undergoes nucleophilic attack by a water molecule, which is itself partially activated by deprotonated catalytic aspartic acid residue. The protonated aspartic acid donates a proton to the amide bond nitrogen, generating a zwitterionic intermediate, which collapses to the cleaved products. The water molecule that binds between the enzyme and inhibitor is thought to position a peptide substrate, stretching the peptide bond out of planarity toward a tetrahedral transition state that is stabilized by a second water molecule (Chatfield and Brooks 1995).

### *CLASSIFICATION OF ASPARTIC PROTEASE INHIBITORS*

The aspartic acid protease inhibitors are grouped into 7 families: the potato plant Kunitz inhibitors (Mares et al., 1989), the *Ascaris* inhibitors (Martzen et al., 1990), the yeast inhibitor IA3 (Schu et al., 1991), a domain of the sea anemone thyroglobulin type-1 inhibitor (Lenarcic and Turk 1999; Galesa et al., 2003), the pig serpin inhibitor (Mathialagan and Hansen 1996), the *Bacillus* sp peptide, ATBI (Dash and Rao 2001) and the squash aspartic acid proteinase inhibitor (SQAPI) (Christeller et al., 1998; Farley et al., 2002). The structures for some of these proteins have been solved and are to date, very different from each other and exhibit distinct, and in some cases, novel inhibitory mechanisms. Depending on their molecular nature, aspartic protease inhibitors can be classified in two categories, (1) proteinaceous inhibitors, and (2) low-molecular-weight inhibitors.

#### *Proteinaceous Inhibitor*

In a sharp contrast to the ubiquitous presence of multiple forms of proteinaceous inhibitors of other classes of proteases from different sources of plants, animals, and microorganisms, there is a paucity of proteinaceous inhibitors of aspartic proteases.

Protein inhibitors of aspartic proteases are relatively uncommon and are found in only a few specialized locations (Bennet et al., 2000). Few of the examples include renin-binding protein in mammalian kidney, which, intriguingly, has now been identified to be the enzyme, N-acetyl-D-glucosamine-2-epimerase (Kay et al., 1983; Phylip et al., 2001), a 17-kDa inhibitor of pepsin and cathepsin E from the parasite *Ascaris lumbricoides* (Kageyama, 1998; Ng et al., 2000), proteins from plants such as potato, tomato, and squash (Kreft et al., 1997; Christeller et al., 1998), and a pluripotent inhibitor from sea anemone of cysteine proteases as well as cathepsin D (Lenarcic and Turk, 1999). There is a report of an 8-kDa polypeptide inhibitor from yeast, which inhibits the vacuolar aspartic proteases (proteases A or saccharopepsin).

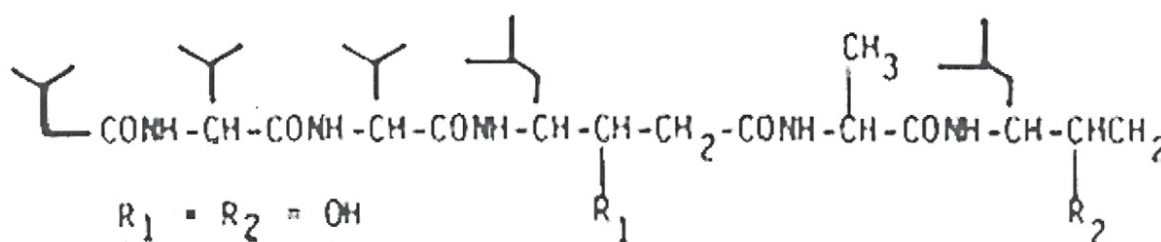
### *Low-Molecular-Weight Inhibitors*

In contrast to the proteinaceous nature of the proteases inhibitors from plants and animals, the inhibitors produced by microorganisms are of smaller molecular nature. The presence of proteases inhibitors in microorganisms came into existence from the studies on antibiotics because they act as inhibitors of enzymes that are involved in growth and multiplication. Extracellular proteolytic enzymes hydrolyze organic nitrogen compounds in the medium and are thought to be harmful to cells. The production of inhibitors of the proteolytic enzymes by microorganisms has probably evolved as a mechanism to provide cell protection. Specific inhibitors of microbial origin have been used as useful tools in biochemical analysis of biological functions and diseases. Polysaccharide sulfates have been reported to be pepsin inhibitors; however, their antipepsin activity is weak, and the effect of such polyanionic compounds is not specific. Pepstatin, a low-molecular-weight aspartic proteases inhibitor, isolated from various species of *Streptomyces*, is a specific inhibitor of pepsin (Umezawa et al., 1970). Pepstatin also inhibits the activities of cathepsin D, cathepsin E, renin, pseudorenin and aspartyl proteases produced by microorganisms.

*Streptomyces testacus* was reported to produce various pepstatins that differed from one another in the fatty acid moiety (C2-C10). A pepstatin containing an isovaleryl group has been most widely used for biological and biochemical studies (Figure 6).



Moreover, as minor components, pepstanone containing (S)-3-amino-5-methylhexane-2-one instead of the C-terminal (3S, 4S)-4-amino-3-hydroxy-6-methylheptanoic acid (AHMHA), and hydroxyepstatin containing L-serine instead of L-alanine, have also been isolated. Pepstatin containing an acetyl group and propanoyl or isobutyryl groups were isolated from *Streptomyces naniwaensis* and *Streptomyces* no. 2907 (Dash et al., 2003).



**Figure 6** Chemical structure of pepstatin, a pepsin inhibitor

Pepstatins, pepstanones, and hydroxyepstatins have almost identical activity against pepsin and cathepsin D. Pepstatin also binds to procathepsin D and inhibits its autoactivation. However, pepstatin is more effective against renin than are pepstanone or hydroxyepstatin, and its potency against renin increases with the increasing numbers of carbon atoms in the fatty acid moiety. The inhibition of aspartyl proteases by pepstatin depends to a large extent on the presence of acid residue in their structure.

The inhibitory effect of pepstatin on cathepsin D does not depend on the carbon chain length of acid radicals (Gacko et al., 2007). Esters of pepstatin, pepstatinal and pepstatinol possess anti-pepsin activity similar to pepstatins. Several pepstatin analogs have also been synthesized to date. AHMHA and its N-acyl derivative exhibit no potency toward pepsin; however, N-acetyl-valyl-AHMHA is active, and the addition of another valine between the acetyl and valyl groups does not increase their activity. The addition of L-alanine to the C-terminal group increases the activity about 100 times. This suggests that the acetyl-valyl-AHMHA-L-alanine is the smallest molecular structure that exhibits inhibition against pepsin and cathepsin D similar to pepstatin. Acetyl- L-valyl-L-valyl-[(3S, 4R)-4-amino-3-hydroxy-6-methyl]

heptanoic acid prepared by chemical synthesis shows absence of activity. This suggests that the 4S-configuration of AHMHA is essential for activity.

The bacterial enzyme that hydrolyzes the isovaleryl bond in pepstatin has been identified, and from the residual peptide benzoyl-L-valyl-AHMHAL- alanyl-AHMHA and L-lactyl-L-valyl-AHMHA-Lalanyl- AHMHA have been synthesized. These analogs are more water-soluble than pepstatin and have almost identical activity against pepsin and cathepsin D. However, these water-soluble analogs have much weaker activity against renin when compared with pepstatin. The addition of aspartic acid or arginine to the C-terminus of pepstatin increases its water solubility. Such water-soluble analogs have same activity against renin as does pepstatin and also have a hypotensive action (Rich 1985). Pepstatin also inhibits carageenin-induced edema and suppresses the generation of Shay rat ulcer. Therapeutic effects on stomach ulcers in man have also been observed. Pepstatin has been reported to be effective against experimental muscle dystrophy and enhances the effect of leupeptin. Pepstatin also inhibits leukokinin formation and ascites accumulation in ascites carcinoma of mice. Pepstatin inhibits the growth of *Plasmodium beghei* and inhibits focus formation in murine sarcoma virus (Yuasa et al., 1975).

Alkalo thermophilic *Bacillus* Inhibitor (ATBI) is a low molecular weight hydrophilic peptidic aspartic protease inhibitor extracellularly produced by an alkalothermophilic *Bacillus* sp isolated from the soil sample of a hot spring at Vajreswari, Maharashtra, India (Dey *et al.* 1991). Another low molecular weight aspartic protease inhibitor was obtained from *Bacillus licheniformis* isolated from tomato (Kumar and Rao 2006).

### *Inhibitors of pepsin*

Pepsin is a well studied enzyme whose activity has been extensively studied since Northrop crystallized it in 1929 (Northrop 1930). It belongs to the family of the aspartic proteases, together with cathepsin D, quinosine, renin and the HIV-protease. The recognition of the HIV-protease as a member of this family (Pearl and Taylor 1987) has renewed the interest in this type of enzymes and in their inhibition (Velazquez-Campoy *et al.*, 2000). There is a wide range of specific inhibitors that can

bind to the active site and selectively remove the activity of pepsin. One of the best known ones is pepstatin (Umezawa 1970) that, at acidic pH, tightly binds to the catalytic site of both pepsin and its precursor: pepsinogen. The pepstatin-pepsinogen complex, however, cannot be formed above pH 3 because the active site is blocked by a propeptide sequence. Below pH 5, pepsinogen is self-cleaved to produce active pepsin (Dash et al., 2003). A simplified analogs of pepstatin A representing 'tripeptides' with two valine residues which are C-terminated by an amino alcohol moiety was found to exhibit inhibition against pepsin (Kratzel et al., 2000). 1,2-Epoxy-3-(p-nitrophenoxy)propane (EPNP) is known to inhibit pepsin and other aspartic proteinases by reacting with the active site aspartic acid residue. However, the reaction is considerably slow in general, and therefore, it is desirable to develop similar reagents that are capable of inhibiting these enzymes more rapidly. Hishashi et al (2008) have reported the synthesis of a novel inhibitor which have a reactive epoxide group linked with peptide by a hydrazide bond, with a general structure: Iva-L-Val-L-Val-(L-AA)<sub>n</sub>-N<sub>2</sub>H<sub>2</sub>-ES-OEt (Iva, isovaleryl; AA, bulky hydrophobic or aromatic amino acid residue; ES, epoxysuccinyl). These inhibitors were shown to inhibit porcine pepsin remarkably faster than EPNP.

ATBI was found to inhibit pepsin with a two-step inhibition mechanism. Kinetic analysis showed that pepsin is competitively inhibited by ATBI. Comparative analysis of the kinetic parameters with pepstatin, the known inhibitor of pepsin, revealed a higher value of  $k_5/k_6$  for ATBI (Dash et al., 2001). A low molecular weight aspartic protease inhibitor was isolated from a thermotolerant *Bacillus licheniformis* and exhibited a slow tight binding mechanism towards pepsin. The  $IC_{50}$  and  $K_i$  values were in nanomoles and was higher than that of pepstatin (Kumar and Rao 2006). Recently, a new class of peptidomimetics, the unsymmetrical peptidyl ureas, have emerged as powerful inhibitors of aspartic proteases (Dales et al., 2001). These were developed using mechanism-based and substrate-based design techniques and using the computational method GrowMol (Ripka et al., 2001). These newly synthesized inhibitors possess a distinct advantage over the natural inhibitors. The natural inhibitors such as antipain, elastinal, etc. contain urea bonds in place of the amide bonds between the P3 and P4 residues and not between the P1 and P2

residues. Ureas have the ability to form stronger hydrogen bonds than the amide groups. The synthesis of ureas as inhibitors was therefore a natural choice. These synthetic inhibitors of porcine pepsin were generated through computational programs that analyze the target enzyme structure, predict inhibitor structures, and analyze the enzyme-inhibitor complex formed. These structures would help to chemically build up molecules of medicinal value and would give rise to newer classes of drugs (Dash et al., 2003).

### *Inhibitors of cathepsin D*

Cathepsin D is a soluble lysosomal aspartic endopeptidase (EC 3.4.23.5) studied mainly from the perspective of its role in degenerative diseases & cancer development. Cathepsin D activity is regulated on a few levels: through stimulation and inhibition of its biosynthesis, at the stage of post-translatory modifications in the Golgi apparatus, proenzyme activation and interlysosomal pH regulation (Turk et al., 1981). This ensures that cathepsin D can operate at the proper time, site and intensity, and prevents uncontrolled protein degradation. The 20-kDa cytoplasmic protein, glycine ethyl ester, tripolyphosphates, phospholipids and ATP increase the activity of cathepsin D (Watabe et al., 1996).

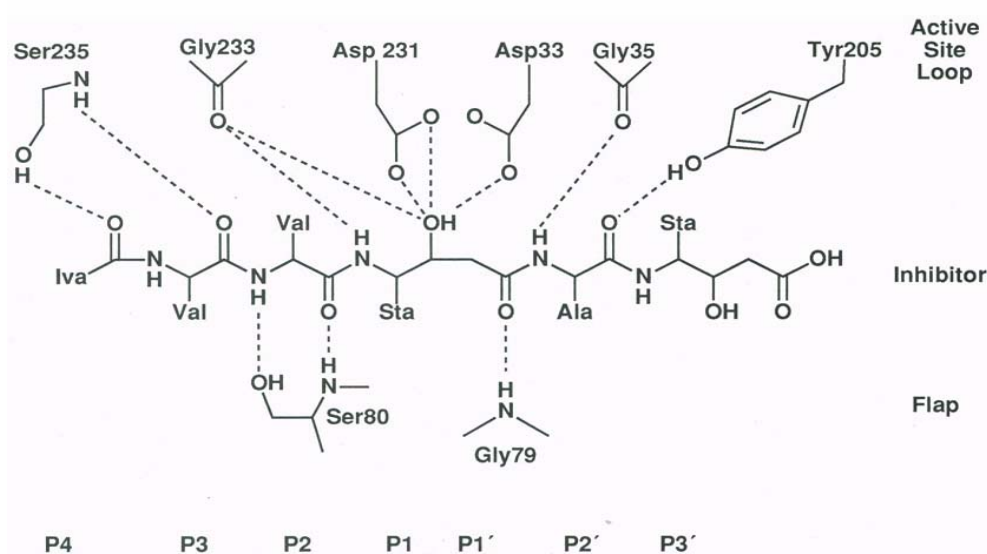
Most cathepsin D inhibitors are synthetic, peptide and polypeptide produced by microorganisms, plants and animals (Richardson M 1977; Xie et al., 1997). Synthetic inhibitors of cathepsin D are micromolecular organic compounds estrifying the carboxyl group of the Asp33 or Asp231 residue in the catalytic site. The Asp33 residue reacts with 1,2-epoxy-3-(p-nitrophenyloxy)-propan. The compounds reacting with the Asp231 residue include diazacyl derivatives of amino acid methyl esters. The carboxyl groups of cathepsin D are estrified by these compounds in the presence of copper ions having a catalytic function (Smith et al., 1969). Other cathepsin D inhibitors are: diazoacetyl-glycine ethyl ester (Bayliss et al., 1969), diazoacetyl-phenylalanin methyl ester, diazoacetyl-2,4-dinitrophenyl-ethylenediamine and other diazol compounds (Stepanov et al., 1969; Tang 1979). The reaction of cathepsin D with diazol compounds occurs most rapidly at pH 4.5. Other cathepsin D inhibitors also include many derivatives of 4-(morpholinylsulphonyl)-L-Phe-P2-

(cyclohexyl)Ala[isostere]-P1'-P2'. Also ditiophosgen and 2,2-dichloro-1,3-ditiocyclobutanone (Rakitzis et al., 1976), and methyl blue and tetranitrometane (Keilova et al., 1969) have been found to inhibit cathepsin D activity. These compounds inactivate pepsin as well. However, 2,4'-dibromoacetophenone and 2-bromo-2-phenylacetophenone inhibit pepsin but not cathepsin D activity (Smith et al., 1969; Tang 1971).

Cathepsin D activity is inhibited by structural analogues of synthetic substrates. These are oligopeptides containing at least five amino acid residues in the molecule and having L-amino acid replaced by D-amino acid. In the pentapeptide Pro1-Phe2-Phe3-Val4-Leu5, cathepsin D causes the cleavage of the Phe2-Phe3 bond (Keilova 1971). Replacement of L-Leu5 residue by D-Leu5 makes this pentapeptide resistant to the action of cathepsin D and able to inhibit hydrolysis of matrix pentapeptide. In the Gly1-Phe2-Leu3-Gly4-Phe5-Leu6 hexapeptide, cathepsin D causes the cleavage of the Phe2-Leu3 bond. The hydrolysis of peptides of analogous structure but containing D-amino acids in positions P1, P3 or P4 is considerably hindered; moreover they inhibit decomposition of a hexapeptide built up of L-amino acids. Cathepsin D vulnerability to hydrolysis and degree of inhibition by these analogues depend on the number and location of D amino acids in the molecule. The analogues with one D-amino acid at a maximum distance from the site sensitive to cathepsin D exert the strongest inhibitory effect. However, the analogues with two D-amino acids at the site of a cleaved Phe3-Leu3 bond and constituting a cyclic hexapeptide are not hydrolyzed and do not exhibit an inhibitory effect. Cathepsin D activity is also inhibited by Gly-Glu-Gly-Phe-Leu-Gly-D-Phe-Leu and aldehydes of such peptides as Ac-Leu-Leu-Nle-H, Ac-Leu-Val-Phe-H and [(s)-1-carboxy-2-phenyl-ethyl]-carbamoil-Arg-Val-Arg-H (Ikezawa et al., 1972).

Pepstatin acts as an inhibitor of cathepsin D. The mechanism of cathepsin D inhibition by pepstatin can be illustrated by a simplified model and a spatial model of these substances (Figure 7). Pepstatin also binds to procathepsin D and inhibits its autoactivation (Hasilik et al., 1982). A comparison between the inhibitory effect of pepstatins with variously structured acid residue on the activities of pepsin, cathepsin D and rennin shows that the inhibitory effects are similar in the case of the

first two proteases, whereas that of rennin increases with elongation of carbon chain of the residue. This is due to the structural similarity of the catalytic site of pepsin and cathepsin D and its different structure in the rennin molecule. The inhibitory effect of pepstatins on cathepsin D does not depend on the carbon chain length of the acid radical. Hydroxypepstatin exerts a similar inhibitory effect to that of pepstatins. However, the inhibitory effect of pepstanon is less pronounced. This indicates the significance of the presence of hydroxyl groups in the C-terminal fragment for the action of these inhibitors (Gacko et al., 2007)



**Figure 7** Interactions between pepstatin and cathepsin D. Schematic hydrogen-bonding diagram for pepstatin bound to cathepsin D. Inhibitor side chain numbering is according to the nomenclature of Schechter and Berger (1967), where  $P_n$  designates inhibitor side chain residues that interact with the corresponding  $S_n$  subsites within the enzyme active site. Iva and Sta indicate isovaline and statine, respectively (Baldwin et al., 1993).

Polypeptide inhibitors of aspartyl proteases can be found in spare plant organs such as seeds, bulbs and fruits, and more seldom in vegetative organs like leaves, roots and flowers (Gacko et al., 2007). Potato bulbs contain six or eight polypeptide inhibitors of cathepsin D, depending on the species (Baudys et al., 1991; Strukelj et al., 1990). They show a considerable similarity in the amino acid composition, sequence and in the number and location of disulphide bridges. Potato inhibitors possess two inhibitory sites: one binding cathepsin D and the other binding trypsin (Ishikawa et al., 1994), and they do not inhibit the activity of pepsin. Cathepsin D inhibitor, which also inhibits the activity of pepsin and acid protease from fungus *Glomerella cingulata* has been isolated from pumpkin fruit (Christeller et al., 1998). It is

composed of 96 amino acid residues and occurs in three molecular forms differing slightly in the amino acid sequence. Cathepsin D inhibitors can be found in the seeds of lentil and vicia but are not found in the seeds of 25 cereal species and pulses consumed by man. Cathepsin D inhibitors have been isolated from the seeds of wheat (Galleschi et al., 1993), barley (Sarkkinen et al., 1992), tomato leaves (Werner et al., 1993; Lison et al., 2006), tobacco leaves (Balandin et al., 1995), aubergine fruit (*Solanum melongea*) and from trailing nightshade leaves (*Solanum dulcamara*) and black nightshade (*Solanum nigrum*). The inhibitor obtained from tomato leaves have been found to inhibit several aspartic proteases. The comparison of cathepsin D inhibitors isolated from tomato leaves and potato bulbs revealed that the potato inhibitor was more potent. The synthesis of plant cathepsin D inhibitors is stimulated by mechanical tissue injury, as well as jasmonic acid, methyl ester of jasmonic acid and abscisic acid (Farmer et al., 1992; Kreft et al., 1997). Salicylic acid inhibits synthesis of these inhibitors.

Cathepsin D activity is inhibited by equistatin, a protein inhibitor isolated from *Actinia equine* (Lenarcic et al., 1999; Galesa et al., 2003). Equistatin inhibits the activity of cysteine proteases: papain, cathepsin B, cathepsin L and cathepsin D, but not the activity of pepsin, chymotrypsin or HIV protease. Equistatin has a domain structure. Trypsin digestion of equistatin leads to the formation of domain-1 and domain-2 and 3, which are connected by the disulphide bridge. These domains originate from cleavage of the peptide bonds Lys67-Ala68 and Arg151-Val152. Trypsin also splits the inactive C-terminal fragment off domain-3. Domain-1 inhibits the activity of cysteine proteases (papains), whereas domain-2 and domain-3 inhibit the activity of cathepsin D. *Ascaris lumbricoides* and *Ascaris suum* synthesize the inhibitors which block the activity of cathepsin E, pepsin and rennin but not cathepsin D (Wiederanders and Kirschke 1989; Ng et al., 2000). They are used to differentiate the activities of these proteases in the nonfractionated material. Endogenous cathepsin D inhibitors include  $\alpha$ 2-macroglobulin and polyanion compounds - glycozaminoglycans and deoxyribonucleic acids (Gacko et al., 2007).

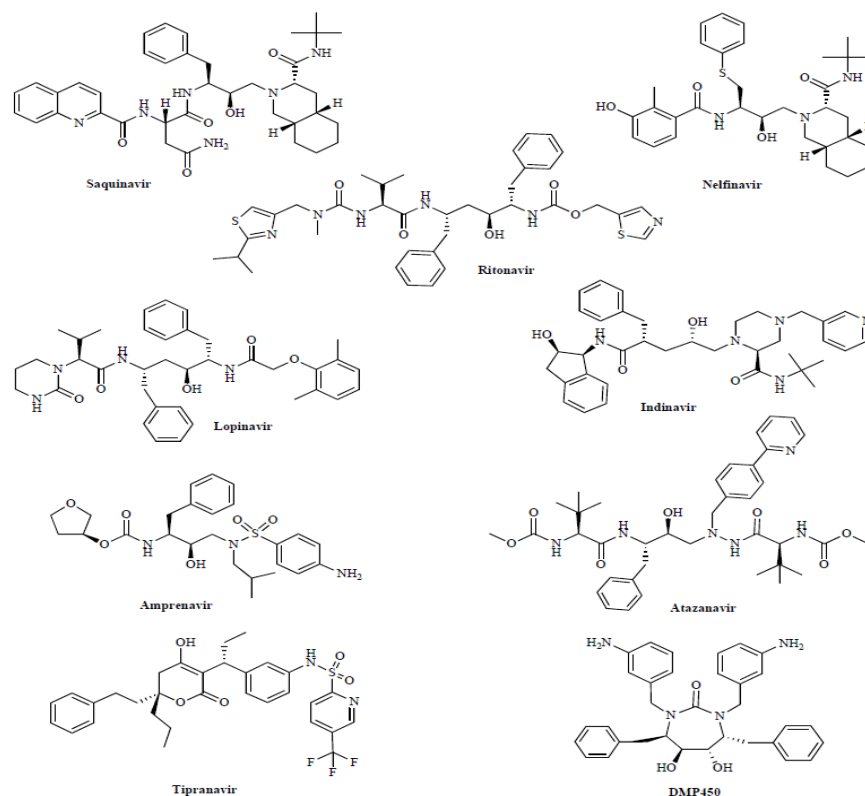
### *Inhibitors of HIV protease*

HIV-1 protease (PR) has been classified as an aspartic protease that functions as a homodimer, based on its primary amino acid sequence, its inhibition by pepstatin, and its crystal structure (Ratner et al., 1985; Richards et al., 1989). HIV-1 PR has been an attractive target for the development of drugs against AIDS (Blundell et al., 1991). The rational design of HIV-1 PR inhibitors may be considered under two broad categories based on (a) the substrate specificity and (b) the structural homology of HIV-1 PR dimer (Darke et al., 1988). Plethoras of synthetic inhibitory compounds targeting the active site of the HIV-1 PR have been reported (Wlodawer and Erickson 1993; Eder et al., 2007).

So far nine HIV protease inhibitor drugs have been approved and are clinically available: Saquinavir, Nelfinavir, Ritonavir, Lopinavir, Indinavir, Amprenavir, Fosamprenavir, Atazanavir, and Tipranavir (Figure 8). Saquinavir (Invirase<sup>®</sup>) was approved in 1996 as the first HIV-protease inhibitor despite its low oral bioavailability due to poor absorption and extensive first-pass degradation by cytochrome P<sub>450</sub>. It is a very potent inhibitor with an *IC*<sub>50</sub> value of 0.4 nM and is one of the first and most prominent examples of a structure-based designed drug (Roberts et al., 1990). Saquinavir is a hydroxyethylamine transition state analogue having a bulky decahydroquinoline moiety in P1' and a quinoline in P3. It is active in cell culture against both HIV-1 and HIV-2 viruses. All of the above compounds are very potent inhibitors of wild-type HIV protease. However, one of the key challenges in developing antiretroviral drugs is the high degree of genetic variability of the human immunodeficiency virus, which frequently leads to mutations in the viral proteins and, as a consequence, to reduced binding affinities of the inhibitors. At present, more than 50 mutations in the HIV protease have been reported, 22 of which may cause resistance against known inhibitors (Svicher et al., 2005). In particular, accumulation of several mutations may lead to complete drug resistance. The second generation of HIV protease inhibitors, therefore, also aims at improving clinical efficacy against multiple virus variants. An example is Atazanavir (Reyataz<sup>®</sup>), a 2-hydroxy-1,3-diaminopropane transition state isostere with an azadipeptide core and an extended P1' moiety (Robinson et al., 2000). Atazanavir inhibits the wild-type



HIV protease with a  $K_i$  value of 10 pM and exhibits good oral bioavailability. It also inhibits several mutant viral proteases which are resistant to a number of the other HIV protease inhibitors, but may ultimately induce itself drug-resistant mutations (Gong et al., 2000).



**Figure 8** Inhibitors of HIV protease. Peptidomimetics: Saquinavir, Nelfinavir, Ritonavir, Lopinavir, Indinavir, Amprenavir, Atazanavir. Non-peptidic inhibitors: Tipranavir, DMP450

The availability of numerous crystal structures in complex with inhibitors has also facilitated the discovery of potent and selective non-peptidomimetic inhibitors. Of these, Tipranavir (Aptivus®), a sulfonamide-based inhibitor is already on the market (Kandula et al., 2005). Its inhibition constant against wild-type HIV protease is in the low picomolar range (8 pM) (Turner et al., 1998) and it exhibits robust activity against various resistant forms of the HIV protease with  $K_i$  values against the clinically most important variants V82A and V82F/I84V of 3.0 nM and 0.25 nM, respectively (Larder et al., 2000). In addition, mechanistic information has been used to design a series of potent inhibitors based on cyclic ureas (Lam et al., 1994). For this compound class, the carbonyl oxygen of the cyclic urea mimics the hydrogen-bonding features of the structural water molecule. This structure permits an optimal

interaction of substituents with the corresponding S1, S2, S1' and S2' pockets. An example for this class of inhibitors is DMP450, a sub nanomolar inhibitor ( $IC_{50}$  value of 0.28 nM) with favorable pharmacokinetic properties (Hodge et al. 1996).

Identification of clinical viral isolates that are resistant to these drugs indicates that this is a significant problem and that new classes of inhibitors are continually needed. Research is also being focused on natural inhibitors from microbial sources. HIV-1 PR was inhibited by a peptidic inhibitor, ATBI isolated from an extremophilic *Bacillus* sp. and the kinetic parameters revealed ATBI as a noncompetitive and tight binding inhibitor with the  $IC_{50}$  and  $K_i$  values 18.0 and 17.8 nM respectively. The inhibitor was found to be a hydrophilic peptide with Mr of 1147, and an amino acid sequence of Ala-Gly-Lys-Lys-Asp-Asp-Asp-Asp-Pro-Pro-Glu (Dash and Rao 2001). Screening of microbial extracts followed by bioassay-guided isolation led to the discovery of a natural hinnuliquinone, a C2-symmetric bis-indolyl quinone natural product that inhibited the wild-type and a clinically resistant (A44) strain of HIV-1 protease with  $K_i$  values of 0.97 and 1.25  $\mu$ M, respectively. Crystallographic analysis of the inhibitor-bound HIV-1 protease helped explain the importance of the C2-symmetry of hinnuliquinone for activity (Singha et al., 2004).

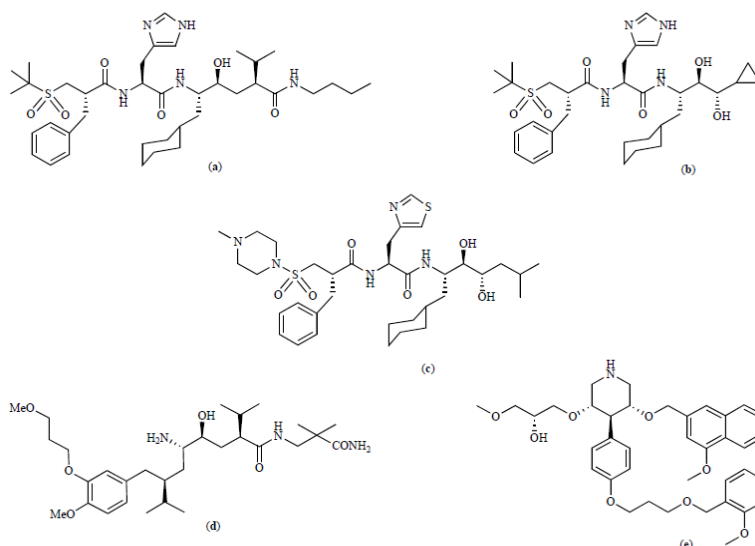
Current therapeutic strategies for several diseases including human immunodeficiency virus type 1 (HIV-1) infection have evolved from an initial single-target treatment to a multitarget one (Hammer et al. 2006). Single antiretroviral drug regimens are no longer recommended for clinical use against HIV-1 owing to the rapid emergence of drug-resistant strains after initiation of therapy (Volberding et al., 1995; Rusconi et al., 1996). A combination of antiretroviral drugs targeting different viral proteins is more effective at suppressing viral growth (Metzner et al., 2007). In many cases, however, these regimens are expensive and result in greater toxicity and in poor patient adherence (Jones and Gazzard 2006; Bisson et al., 2006; Moya et al., 2006). New paradigms in multitarget drug discovery have emerged (Faivre et al., 2006; Millan 2006), particularly for the treatment of HIV-1 infection (Litovchick et al., 2001; Bugatti et al., 2007). For example, the multitarget antiretroviral drug Cosalane has been developed to inhibit several HIV-1 proteins (gp120, integrase, protease and reverse transcriptase) simultaneously (Casimiro-

Garcia et al., 2000 De Clercq 2001). Over the past 20 years, many structural and mechanistic insights have been gained by studying the HIV protease and many inhibitory principles have been successfully established and refined. HIV protease inhibitors are the first aspartic protease inhibitors which have reached the market and as such also serve as prototype inhibitors for the whole enzyme family. They have now become an important component of antiretroviral therapy and, although there is currently no cure for AIDS, they are contributing significantly to the treatment options for this devastating disease.

### *Inhibitors of renin*

Since the early discovery of renin as an enzyme involved in the control of blood pressure regulation, extensive research went into unraveling the detailed mechanism of the renin-angiotensin system (RAS) (Oparil and Haber., 1974; Skeggs et al., 1980). Renin is produced mainly by kidney juxtaglomerular cells and released into the circulation following regulated and constitutive pathways. Different to most other aspartic proteases, renin is enzymatically active at neutral pH. Blocking the RAS is recognized since decades as attractive option for a treatment of hypertension and many anti-hypertensive drugs are now on the market. Most of these drugs either inhibit angiotensin converting enzyme (ACE), which converts angiotensin I to angiotensin II, or block the angiotensin II receptor, AT1. However by inhibiting ACE or blocking the angiotensin AT1 receptor, the negative feed back control exerted by angiotensin II disappear and consequently elevated plasma and tissue renin activities are observed. Renin inhibition leads also to an increased renin secretion and production but in contrast to other RAS blockers the newly release active renin is immediately neutralized by inhibitors present in the systemic circulation. Given its privileged position in the enzymatic cascade and its unique substrate specificity, it is surprising that there are no renin inhibitors on the market yet, even though there have been numerous attempts to find and design renin inhibitors since almost three decades.

Efforts into the elucidation of the molecular architecture of renin did not succeed until the enzyme could be expressed and purified from recombinant sources (Sielecki et al., 1989). The structure of renin complexed with statine-based inhibitors revealed how the active site of renin can accommodate substrates with eight amino acid residues spanning the specificity pockets S4 to S4' (Rahuel et al., 1991; Dhanaraj et al., 1992). The S1 and S3 pockets form a contiguous and large hydrophobic cavity with a sub-pocket, S3<sup>SP</sup> (Rahuel et al., 2000). Like in other aspartic proteases, a flexible flap constituted by amino acid residues Thr72 to Ser81 covers the active site cleft and plays an important role in the enzyme substrate interactions. In addition, protein flexibility and secondary structure re-arrangements within the active site, e.g. in S1' and S2', are important in understanding enzyme specificity (Cooper 2002). Initially, renin inhibitors were based on pepstatin analogues (Guegan et al., 1986) and substrate- or prosequence-derived (Cumin et al., 1985) peptides with the scissile amide bond being replaced by a non-cleavable transition state isostere or hydroxyisostere and CGP29287. Although these compounds were found highly active in lowering blood pressure in primate models when administered intravenously, they were characterized by a poor oral bioavailability and instability due to the presence of several peptide bonds in the molecule. Further optimization programs were pursued aiming at improving oral bioavailability by reducing the size and the peptidic character of the molecules. A variety of tetrapeptide transition state mimetics were synthesized including CGP038560A, Remikiren and Zankiren (Figure 9). These closely related compounds were tested in human volunteers, however, insufficient oral bioavailability was still observed as a major issue preventing their further development.



**Figure 9** Inhibitors of renin. Tetrapeptide transition state mimetics (a) CGP038560A ( $IC_{50} = 1$  nM), (b) Remikiren ( $IC_{50} = 0.7$  nM) and (c) Zankiren ( $IC_{50} = 1.1$  nM) (d) the non-peptidomimetic inhibitor Aliskiren ( $IC_{50} = 0.6$  nM) and (f) the 3,4,5 substituted piperidine Ro 66-1132 ( $IC_{50} = 0.07$  nM)

The current renin inhibitors represent another successful example of structure-based drug design. The combined use of structural information from renin/inhibitor complexes and computer-assisted molecular modelling allowed to further reduce the molecular weight and peptidic character of the inhibitors. In particular, the optimal use of the large S1/S3 pocket and the concomitantly discovered S3<sup>SP</sup> sub-pocket resulted in highly potent compounds. One of these is Aliskiren (SPP100), the first orally bioavailable, selective, and highly potent ( $IC_{50}$  value of 0.6 nM) renin inhibitor which has entered phase 3 clinical trials. It was shown to be well tolerated and to be as efficacious in blood pressure lowering as irbesartan, a known angiotensin II receptor blocker. In addition to transition state mimetics, novel compounds such as 3,4-disubstituted piperidines have also been identified by screening compound libraries. The binding of these compounds to the active site aspartic residues Asp 32 and Asp 215 (residues numbering are according to pepsin amino acid sequence) occurs via the protonated piperidine nitrogen. Their further optimization led to 3,4,5-trisubstituted piperidines, which were found to induce an open flap conformation with a change in the orientation of the side chains Tyr75 and Trp39 and thereby opening a large hydrophobic pocket. Moreover, novel compound classes derived from further optimization such as disubstituted amino-aryl piperidines and ketopiperazine, have been reported recently. Enzyme selectivity

against other human A1 aspartic proteases was readily achieved, probably reflecting the unique substrate specificity of renin.

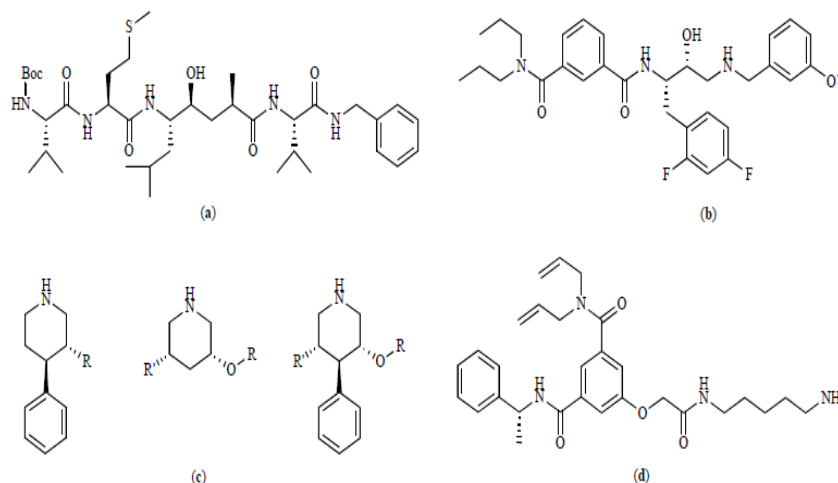
### *Inhibitors of BACE*

Alzheimer's disease (AD) is thought to be caused by the progressive brain accumulation of  $\beta$ -amyloid (Ab) peptides into fibrillar aggregates and insoluble plaques resulting severe memory loss and neuronal cell death (Selkoe 2001). The Ab peptides are generated by endoproteolysis of the  $\beta$ -amyloid precursor protein ( $\beta$ -APP) by two proteolytic enzymes,  $\beta$ - and  $\gamma$ -secretase. The  $\beta$ -secretase generates the N-terminus of Ab peptides by cleaving APP at Met670/Asp671, while  $\gamma$ -secretase cleaves the C-terminus of the peptides by proteolysis either at Val711 or Ala713, the resultant Ab peptides is either 40 or 42 amino acid residues in length (Dorrel 2000). The Ab42 peptide is the most abundant and which play critical roles on the induction of AD (Li et al., 2007).

Initially, the design of BACE inhibitors was facilitated by the knowledge gained in the development of HIV protease and renin inhibitors. These efforts were further supported by the early elucidation of the enzyme's molecular architecture using X-ray crystallography. Structures of complexes with statine-based peptide inhibitors show the inhibitor binding in an extended conformation. The catalytic centre is covered by a hairpin loop, the so-called flap region, which largely occludes the active site from access to solvent. The hydroxyl group of the statine moiety interacts directly with the catalytic residues Asp228 and Asp32 in a bi-dentate way. The specificity pockets S3, S1, S2', and S4' are of hydrophobic nature which is also reflected by the preference for bulky and hydrophobic groups at the corresponding positions in peptidic inhibitors. This is contrasted by more hydrophilic and open S4, S2, and S3' pockets. Of particular interest for the design of BACE-1 specific inhibitors is the comparison of these pockets with those of the other family members. For example, a unique feature of the BACE-1 structure is the loop defining the S1'/S3' pocket. This loop is truncated in comparison with the corresponding loop in cathepsin D and renin, allowing inhibitors to cover a larger space with more hydrophilic character. In contrast, the S1/S3 pocket of BACE-1 is

large and hydrophobic and may allow the design of inhibitors which show selectivity over cathepsin D and pepsin A, where this pocket is smaller and of more hydrophilic character.

The information derived from a number of crystal structures for BACE-1 in complex with substrate-based inhibitors has helped researchers to rapidly arrive at potent inhibitors ( $K_i$  values  $< 10$  nM) with moderate selectivity (100-fold) over cathepsin D (Ghosh et al., 2000; Hanessian et al., 2005). Most of these compounds are based on the hydroxyethylene transition state mimetic. Another scaffold successfully used for the inhibition of BACE-1 is the hydroxyethylamine isoster. While only modest affinities have been reported so far ( $IC_{50}$  value  $< 0.1$   $\mu$ M), the crystal structure of one example could be solved (Patel et al., 2004). This structure shows the distinct interaction pattern of a hydroxyethylamine with both catalytic aspartic acids in the active site. In addition to these more classical protease inhibitors, some publications and patents report also on the discovery of nonpeptide based inhibitors. Among these are inhibitors based on the cyclic amine principle first discovered in form of the piperidine scaffold for renin. So far, however, only modest *in vitro* affinities ( $K_i$  values in the low micromolar range) have been reported and no crystal structure unraveling the features governing the molecular recognition has been published (Bhisetti et al., 2002). Interestingly, a recent report describes a structure of a unique inhibitor which does not interact directly with the catalytic aspartates (Figure 10). This inhibitor binds exclusively to the non primed site of BACE-1 and shows an unprecedented interaction in the S3 pocket reminiscent of the situation first observed in the renin/Alliskiren complex. A chemical optimization program with the goal to increase the potency of the initial hit ( $IC_{50}$  value of 25  $\mu$ M) resulted in the generation of an inhibitor with  $IC_{50}$  values in the low nanomolar range in biochemical and cellular assays, respectively (Stachel et al., 2004). Recently there have been reports of inhibitors that do not directly engage the catalytic aspartates but interact through a water mediated hydrogen bond (Coburn et al., 2004). Ghosh et al (2012) have reported the first such inhibitor that displays modest inhibition of BACE-1 ( $IC_{50} = 24$   $\mu$ M) with no interaction with the catalytic dyad or primary active site region.



**Figure 10** Examples for (a) a hydroxyethylene-based inhibitor, (b) a hydroxyethylamine-based inhibitor, (c) the cyclic amine-based scaffold and (d) a novel, non-classical inhibitor

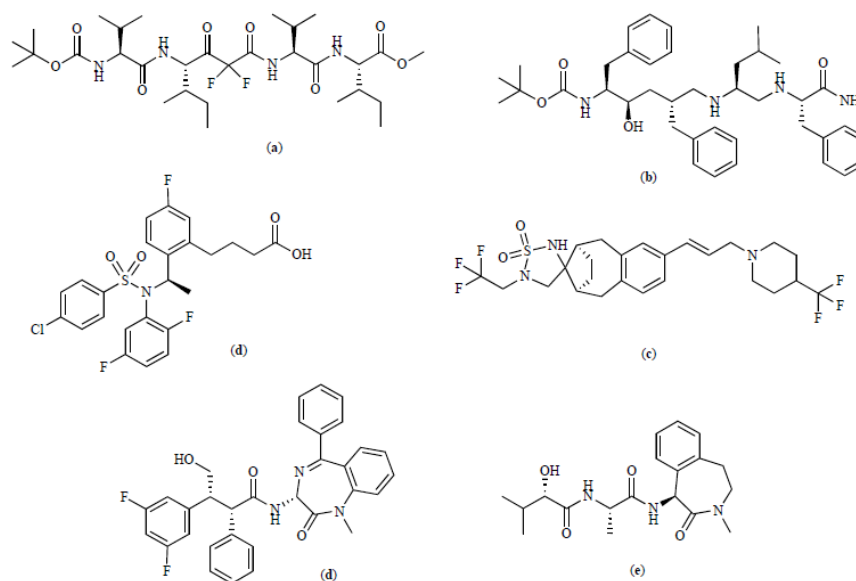
Six years after the discovery of BACE-1 as the enzyme responsible for the generation of the amyloid peptides A $\beta$ 40 and A $\beta$ 42, and despite the progress made so far towards potent and selective BACE-1 inhibitors, the discovery of drugs for the treatment of Alzheimer's disease remains a big challenge to researchers in the field. So far, to the best of our knowledge, no BACE-1 inhibitor has entered clinical trials highlighting the difficulty to develop compounds with high potency for BACE-1, sufficient selectivity over other aspartic proteases, appropriate pharmacokinetic properties and good blood-brain barrier penetration. However, the recent developments both in identifying non-peptide based inhibitors with potentially improved pharmacological properties and the positive results from studies using peptide carrier linked peptidomimetics suggest that the field is ready to make the next step in the near future.

### *Inhibitors of $\gamma$ -secretase*

Irrespective of the lack of any structural information and in the absence of a homogeneous preparation of the protease, a large variety of potent  $\gamma$ -secretase inhibitors have readily been identified (Josien 2002; Wolfe 2002). Early inhibitors were mainly peptidic transition state mimetics on the basis of difluoroketones or hydroxyethylenes, which exhibit competitive inhibition (Figure 11) (Esler et al., 2000; Shearman et al., 2000). Other series comprised sulfonamides (Barten et al., 2005) and sulfamides (Sparey et al., 2005), as well as benzodiazepins (Churcher et al.,



2003) and benzolactams, all of which show non-competitive inhibition of  $\gamma$ -secretase and up to sub-nanomolar inhibition constants. Most  $\gamma$ -secretase inhibitors successfully abrogated generation of A $\beta$  peptides in *in vitro* systems and substantially reduced A $\beta$  levels in animal models. However, none of these compounds, with the exception of LY450139 (currently in phase II clinical trials) (Valentine et al., 2004; Siemers et al., 2005), progressed beyond phase I clinical trials.



**Figure 11** Inhibitors of  $\gamma$ -secretase. (a) Difluoroketone ( $IC_{50} = 10 \mu\text{M}$ ) (b) hydroxyethylene ( $IC_{50} = 17 \text{ nM}$ ) (c) sulfonamide ( $IC_{50} = 7.1 \text{ nM}$ ) (d) sulfamide ( $IC_{50} = 0.5 \text{ nM}$ ) (e) benzodiazepin ( $IC_{50} = 0.07 \text{ nM}$ ) and (f) benzolactam (LY450139;  $IC_{50} = 15 \text{ nM}$ )

The major issue in development of  $\gamma$ -secretase inhibitors was found to lie in the multiple substrates of this protease. Besides APP, the currently known  $\gamma$ -secretase substrates include E-cadherin, nectin-1, low density lipoprotein receptor-related protein, CD44, Erb-B4, Notch and the Notch ligands Delta and Jagged (Brunkan and Goate 2005). Particularly the requirement for Notch signalling in many biological systems seems the prime hurdle for  $\gamma$ -secretase inhibitors, since potent inhibitors showed marked effects on lymphocyte development and intestine morphology, which both could be attributed to impaired Notch processing (Siemers et al., 2005; Wong et al., 2004). Defining a therapeutic window between beneficial reduction of A $\beta$  generation and adverse effects on Notch-related processes is therefore a major focus for the development of future  $\gamma$ -secretase inhibitors. Hope for a therapeutic window relies mainly in the fact that  $\gamma$ -secretase appears to cleave

its substrates at several sites (Okochi et al., 2002). For APP, three major cleavages have been established, the classical  $\gamma$ -cleavage in the middle of its transmembrane region resulting in secreted A $\beta$  peptides, mainly A $\beta$ 40/42, an  $\epsilon$ -cleavage between A $\beta$  residue 49 and 50 (Sastre et al., 2001), which produces the N-terminus of the liberated APP-ICD, and a  $\zeta$ -cleavage between A $\beta$  residue 46 and 47 (Zhao et al., 2004). In a recent study, the correlation of  $\epsilon$ - and  $\zeta$ -cleavage with the generation of A $\beta$ 40/42 has been unraveled by using a differential inhibitor strategy (Zhao et al., 2005). Transition state analogues were found to interfere with the production of A $\beta$ 40/42 at the level of  $\epsilon$ - and  $\zeta$ -cleavage, which precedes the downstream  $\gamma$ -cleavage, while non-transition state analogues preferentially inhibit the  $\gamma$ -cleavage with less effect on the  $\epsilon$ - and  $\zeta$ -cleavages. Since the  $\epsilon$ -cleavage is essential for the liberation of ICDs that are critical for cell signaling (e.g. the Notch-ICD), differentiating  $\gamma$ -secretase inhibitors might hold the key for the treatment of Alzheimer's disease.

### *Inhibitors of Plasmepsins*

Malaria is still one of the most widespread and lethal diseases in the world, affecting the tropical parts of the globe, with Africa being the most plagued continent. Every year there are more than 500 million clinical cases of malaria and several millions of them are children (Bremner et al., 2004). Malaria is caused by four major species, *Plasmodium falciparum*, *P. vivax*, *P. malariae*, and *P. ovale*. Among these four major species, *P. falciparum* alone accounts for more than 95% of the malaria cases (Oaks et al., 1991). Although many antimalarial drugs are available, emerging drug resistance and the lack of a functioning vaccine are two main reasons behind the failure to control and eradicate the disease (Rosenthal et al., 1988; Jiang et al., 2001). Three aspartic proteases (plasmepsin I, II and IV) and one histoaspartic protease (HAP) are involved in hemoglobin (Hb) degradation (Banerjee et al., 2002). Plasmepsins I and II are involved in the first phase of Hb degradation, while plasmepsin IV and HAP either partially digest Hb or act on the degradation products of the first phase to cleave them into smaller peptides. Genome data of *P. falciparum* revealed the presence of six more Plasmepsins (Plm) (plasmepsins V to X) in the parasite (Coombs et al., 2001). These enzymes share much less similarity among themselves and with the other four aspartic proteases and their functions are not yet known.

The Plasmeepsins have a varied degree of sequence identity with the human aspartyl proteases, the most similar being the lysosomal enzyme Cathepsin D (Silva et al., 1998). For this reason, Cathepsin D is commonly used as a marker for cross-inhibition. Comparison studies between Plm II and Cathepsin D show a 35% sequence identity, and even higher structural identity has been observed at the active site when comparing crystal structures of Plm II and Cathepsin D in complex with pepstatin A. In this regard it is therefore essential to develop Plm inhibitors exhibiting specificity for the *Plasmodium* aspartic proteases over the human homologue (Kay et al., 2011). Simultaneous inhibition of multiple plasmepsins would lead to a faster starvation of the parasite. By such action, the appearance of drug resistant mutants would also be impeded because the parasite would have to mutate several proteins in order to overcome the inhibition. Such an adaptive drug with the ability to inhibit several members of a protein family would be more advantageous than a combination regimen of multiple medications, due to cost-effectiveness, dosage, adverse effects, and compliance (Nguyen et al., 2008).

Since the identification of plasmepsins in 1994 (Coombs et al., 2001), numerous attempts have been made to design inhibitors of plasmepsins with a view to develop them into potent antimalarial drugs. A wide variety of them have been designed, synthesized, checked for activity by enzyme assays as well as in parasite cultures. They include both peptide-like (Noteberg et al., 2003; Johansson et al., 2005; Nguyen et al., 2008) and non-peptidyl (Mueller et al., 2003; Nguyen et al., 2008) inhibitors. Some of them were designed based on the substrate structure (Phe33-Leu34 of Hb) (Asojo et al., 2002) and/or statine residue (Dahlgren et al., 2003) of the universal aspartic protease inhibitor, pepstatin. C2 symmetric (Ersmark et al., 2004 & 2006) and achiral inhibitors (Jiang et al., 2001), were also reported. Inhibitor molecules were also designed based on the 'double-drug' approach in which a statine-based inhibitor of Plm II has been linked to the well known antimalarial Primaquine and was found to inhibit Plm II and *P. falciparum* in vitro (Romeo et al., 2004). Several transition state mimic inhibitors such as 1,2-dihydroxyethylene, hydroxyethylamine (Muthas et al., 2005), aminopiperidine, diamine clamp, hydroxymethylcarbonyl and 4-arylpiperidine are reported as Plm II inhibitors (Bjelic et al., 2007). The

determination of the crystal structure of plm II in complex with pepstatin revealed intricate details of the mode of binding and provided a platform for the structure-based design (Silva et al., 1996). Subsequent crystal structures of plm II with other inhibitors (Asojo et al., 2002 & 2003) revealed the conformational flexibility of the binding pocket and an entirely new type of binding (Prade et al., 2005). Further, recent reports show that poly-inhibition of plasmepsins, and other proteases such as falcipains, may be desirable in potential antimalarials to ensure clinical efficacy (Omara-Opyene et al., 2004; Liu et al., 2006). Modeling/docking, molecular dynamics and interaction energy calculations were also performed in many studies (Jiang et al., 2001; Ersmark et al., 2004). Some of the compounds could successfully inhibit the enzyme but failed to stop the parasite growth in cell culture (Silva et al., 1996; Jiang et al., 2001) probably because of their size that prevents the access to the food vacuole of the parasite where the Hb degradation occurs. Kasam et al (2007) have demonstrated the relevance of computational grids in drug discovery and have also identified several promising small molecules such as thiourea, diphenylurea, and guanidino scaffolds to serve as candidate inhibitors for *P. falciparum* plasmepsins. Recent study on molecular dynamics simulations were performed to analyze the flexibility of the Plm II in greater detail, leading to a binding mode hypothesis for the 3,4-bis(aminomethylene)pyrrolidines and providing further insight and general implications for the design of Plm II inhibitors (Luksch et al., 2010; Gil et al., 2011). Compounds containing novel structure from natural origin represent a major source for the discovery and development of new drugs for malaria. A number of natural products having antimalarial activities have been reviewed (Vangapandu et al., 2007; Kaur et al., 2009). The strategy for a viable drug is to find a relatively small, cost-effective and highly specific inhibitor. Although many inhibitors targeting the plasmepsin group of enzymes are available, none of them are in use as drugs for the treatment of malaria today.

### *Inhibitors of secretory aspartic proteases (SAPs)*

Cells of *Candida albicans* can invade humans and may lead to mucosal and skin infections or to deep-seated mycoses of almost all inner organs, especially in immunocompromised patients. In this context, both the host immune status and the

ability of *C. albicans* to modulate the expression of its virulence factors are relevant aspects that drive the candidal susceptibility or resistance; culminating in the establishment of successful infection known as candidiasis. *C. albicans* possesses a potent armamentarium consisting of several virulence molecules that help the fungal cells to escape of the host immune responses. A well-known virulence attribute is the secretion of aspartic proteases (Saps), which may contribute to colonization and infection of different host niches by degrading tissue barriers, destroying host defense molecules, or digesting proteins for nutrient supply. Saps are encoded by a gene family with 10 distinct members (SAP1-SAP10) that are located on five different chromosomes. Alignments show that the products of SAP1, SAP2 and SAP3 are approximately 75% identical. Another distinct subgroup contains SAP4, SAP5 and SAP6 showing 90% identity to each other, which falls to 65% when compared with SAP1-SAP3. SAP8 is most similar to SAP1 (65%) and SAP9 and SAP10 have a C-terminal extension. SAP7 is the most diverged member of this family (Monod et al., 1994; Monod et al., 1998).

Very little inhibitor design has been reported for SAP2. A-70450 was originally designed to inhibit renin and later found to be nonselective inhibitor of the SAP of *C. albicans*. This inhibitor incorporates the (S)-hydroxyethylene isostere with the hydroxyl group positioned in the crystal structure between two catalytic aspartate residues. Interestingly, the terminal methylpiperazine ring of A-70450 is found in a boat conformation that occupies the S3 subsite of the enzyme together with the benzyl group of the ketopiperazine ring. The large S3 subsite is not found in other aspartic proteases, and this difference could be exploited to develop selective inhibitors for SAP2 (Abad-Zapetero et al., 1996). The inhibition of SAP activity by HIV protease inhibitors was described for the first time in 1999 (Santos et al., 2010). Saquinavir and indinavir restrained SAP activity when bovine serum albumin (BSA), hemoglobin and human stratum corneum were used as proteinaceous substrates (Korting et al., 1999). In parallel, indinavir and ritonavir promoted a noticeable dose-dependent inhibition of SAP production and activity when evaluated both antigenically and as direct enzyme activity on BSA as substrate (Cassone et al., 1999). Similarly, Gruber et al (1998) showed that indinavir promoted a dose-dependent

decrease in cell wall-bound SAP antigen by flow cytometry analysis. Borg-von Zepelin et al (1999) demonstrated that purified SAP1, SAP2 and SAP3 were inhibited by ritonavir, saquinavir, indinavir and nelfinavir in a concentration-dependent manner, in which ritonavir was by far the most effective inhibitor of these SAP isoenzymes. In contrast, only a slight inhibition of activity was detected for purified SAP4, SAP5 and SAP6. Recently, Braga-Silva et al (2010) showed that amprenavir was found to be the most potent inhibitor of SAP2, which is the main pronounced virulence factor expressed during *C. albicans* infections, reducing the proteolytic activity by approximately 92%, while the other HIV PIs tested (ritonavir, saquinavir, indinavir, nelfinavir and lopinavir) inhibited around 45%-65% of the proteolytic activity. For that reason, amprenavir was selected to determine its dose response on SAP2, revealing that the inhibition increased from 85% to 100% as amprenavir concentration increased from 6.25 to 200  $\mu\text{mol/L}$  (Braga-Silva et al., 2010). Reduced amide monohydroxyethylene and diamonidiol-based transition state peptidomimetics were also reported to inhibit SAPs effectively (Skrbec and Romeo 2002). A few natural products were isolated from *Lycopodium cernuum* out of which lycernuic acid C and apigenin-4'-O- (2'', 6''-di-O-pcoumaryl)- beta-D-glucoside showed inhibition of SAP with  $IC_{50}$  values of 20 and 8.5  $\mu\text{g/ml}$  (Zhang et al., 2002). Further research efforts are needed to screen natural sources for the identification of new inhibitors.

## FUTURE PERSPECTIVE FOR INHIBITOR DESIGN

The family of aspartic proteases, although rather small, contains a number of validated and potential drug targets making drug discovery efforts in this area very fruitful and exciting. There have been substantive advances in our understanding of the use of protease inhibitors as therapeutic agents. Several synthetic protease inhibitors have been approved by the FDA for therapy of HIV and hypertension. These drugs represent prime examples of structure based drug design. Moreover, the inhibitory principles and compounds, which have been established and discovered, now enable mechanism-based drug discovery across the whole family. The initial generation of aspartic protease inhibitors was mainly derived from peptidic structures and, due to their unfavorable physicochemical and pharmacokinetic

properties, many compounds failed during clinical development. Today, we are witnessing a new generation of non-peptide derived aspartic protease inhibitors of which more and more are entering preclinical or clinical development. The sequencing of the human genome and the resulting knowledge on all human aspartic proteases allows an exhaustive profiling of inhibitors for specificity towards all family members thereby reducing the risk of unwanted side effects.

The majority of drug discovery efforts in the field of protease inhibition are still devoted to small molecules. Ideally, a small-molecule inhibitor would be completely selective for its target, have excellent absorption, distribution, metabolism, excretion and toxicology (ADMET) parameters for acute and chronic use, be orally available and be amenable to daily (or less frequent) administration. Several general strategies for small-molecule screening are also applicable to the design of protease inhibitors. More often, screening for protease inhibitors involves high-throughput screening, virtual screening, fragment-based screening and screening of small focused libraries of compounds (typically several thousand compounds). One limitation with screening for protease inhibitors is that some of these methods, such as virtual screening and fragment-based screening, require the three-dimensional structure of the target protease. However, knowledge of the three-dimensional structure of the protease is, although not essential, beneficial in all screening methods and for inhibitor design in general. For example, the development of drugs against the aspartic protease of the HIV-1 virus was only really enabled once the three dimensional protease structure was available; as a result the first drugs advanced to the market within 10 years of initial target identification.

A number of natural and peptidomimetic inhibitors performed well in different phases of clinical testing to treat other human disorders, including cancer, inflammation, cardiovascular, neurodegenerative, and various infectious diseases. Despite this impressive progress, there is much to learn about the cross talk between signal transduction pathways and protease activation cascades. Additionally, development of successful protease inhibitors for clinical use is reliant on maximizing bioavailability, specificity, and potency of inhibition of the target enzyme. Ideally, localizing protease inhibitors to a single target area of the body may

also help minimize the potential for complications and detrimental side effects. There is the further issue of the development of drug resistance to protease inhibitors in the face of a build up of substrate pressure, and selection of catalytically active mutant or other salvage proteases that do not have complementarity for carefully designed inhibitors of wild type proteases. The future appears to still hold considerable promise for protease inhibitors. We can anticipate new, overexpressed proteases from genomic/biochemical comparisons made between normal/diseased cells, host/ pathogen, healthy/unhealthy subjects leading to more effective and efficient validation of proteases as drug targets. New advances in protein chemistry will lead to faster production and greater quantities of pure recombinant proteases and advances in structural biology (crystallography, NMR spectroscopy) will produce faster and more accurate inhibitor-protease structures. Inhibitors (naturally occurring and synthetic) have permitted detailed biochemical and crystallographic investigations to be made, but an understanding of the selectivity of such inhibitors may be of just as much importance for the design and synthesis of specific inhibitors for use therapeutically in controlling individual aspartic proteases.

One of the major factors to be considered in protease drug discovery is whether to develop reversible or irreversible inhibitors. Although designing an irreversible inhibitor is fairly simple for some protease classes, and can be achieved by attaching the substrate recognition sequence to a warhead, the question is whether such an inhibitor would be sufficiently selective. Although both reversible and irreversible inhibitors would largely ablate the activity of the target, they would have differential activity against other off-target proteases. A reversible inhibitor, especially one with good selectivity, would only partially block the activities of other proteases; however, an irreversible inhibitor would, sooner or later (depending on the binding kinetics), block all proteases that it binds. Irreversible inhibitors are most useful as tools for elucidating the catalytic mechanisms of a protease, whereas they are not the most suitable strategy for a therapeutic that is intended to be used chronically to treat a disease. However, many of the protease inhibitors in development are of the covalent kind, and have been developed with the same rationale as used for the design of irreversible inhibitors. Non-covalent inhibitors are much more difficult to



design. Another factor in protease drug design is whether the inhibitor is competitive or non-competitive. With the exception of the first antiprotease therapeutic - heparin, an allosteric indirect inhibitor of blood coagulation proteases - all other protease inhibitors currently in use or in development are competitive inhibitors. Discovering competitive inhibitors is generally easier because of the simplicity of activity tests used, but there are also disadvantages with this approach. The ideal inhibitor would be a non-covalent reversible inhibitor, because such an inhibitor would generally provide better selectivity and should cause less side effects than covalent inhibitors.

Discovery of novel selective inhibitors can proceed only through combination of screening of chemical libraries, rational design, computational technology, and exploration of natural compounds. The exploitation of vast microbial diversity will also generate large amount of biologic aspartic protease inhibitors. Furthermore, future research into the synergistic capabilities of inhibitors will help elucidate the most effective combination therapies. These advances, together with more careful attention to inhibitor conformation, mechanism of action, and drug-like composition are expected to result in more potent, more selective, more bioavailable inhibitors with a higher probability of success rates in clinical trials.

## PRESENT INVESTIGATION

The present work enunciates various aspects of hydrolases and their inhibitors with special emphasis on aspartic protease inhibitor. The findings of the investigations have been presented in the following chapters:

**Chapter 1:** General introduction

**Chapter 2:** Isolation and identification of microbes for the production of aspartic protease inhibitor

**Chapter 3:** Purification and characterization of aspartic protease inhibitors from *Streptomyces* sp MBR04 and *Penicillium* sp VM24

**Chapter 4:** Mechanistic and structural insights into the inhibition of therapeutically significant aspartic protease by inhibitor from *Streptomyces* sp MBR04

**Chapter 5:** Aspartic protease inhibitor from *Penicillium* sp VM24 as antifungal peptide: Implications in combating mycotic infections

**Chapter 6:** Bifunctional role of aspartic protease inhibitor from *Penicillium* sp VM24: Inactivation of aspartic protease and xyloglucanases

**Chapter 7:** Functional aspects of hydrolyases

**BIBLIOGRAPHY**

- Abad-Zapatero C, Goldman R, et al. (1996) *Protein Sci* **5**, 640–652.
- Adams J (2004) *Cancer Cell* **5**, 417-421.
- Asojo OA, Afonina E, Gulnik SV, Yu B, Erickson JW, Randad R, Medjahed D, Silva AM (2002) *Acta Cryst* **58**, 2001–2008.
- Asojo OA, Gulnik SV, Afonina E, Yu B, Ellman JA, Haque TS, Silva AM (2003) *J Mol Biol* **327**, 173–181.
- Babe LM, Craik CS (1997) *Cell* **91**, 427-430.
- Baird TT, Wright WD, Craik CS (2006) *Protein Sci* **15**, 1229-1238.
- Balandin T, Van der Does C, Belles AJM, Bol JF, Linthorst HJM (1995) *Plant Mol Biol* **27**, 1197-1204.
- Baldwin ET, Bhat TN, Gulnik S, Hosur MV, et al. (1993) *Proc Natl Acad Sci* **90**, 6796-6800.
- Banerjee R, Liu J, Beatty W, Klemba M, Goldberg DE (2002) *Proc Natl Acad Sci* **99**, 990–995.
- Bang ML, Villadsen I, Sandal T (1999) *Appl Microbiol Biotechnol* **51**, 215–222.
- Barten DM, Guss VL, Corsa JA, Loo A, Hansel SB, Zheng M, et al. (2005) *J Pharmacol Exp Ther* **312**, 635-643.
- Basi G, Frigon N, Barbour R, Doan T, Gordon G, McConlogue L, et al. (2003) *J Biol Chem* **278**, 31512-31520.
- Baudys M, Ghosh M, Harlos K, Meres M, Fusek M, Kostka V, Blake CC (1991) *J Mol Biol* **218**, 21-22.
- Baumeister W, Lupas A (1997) *Curr Opin Struct Biol* **7**, 273-278.
- Bayliss RS, Knowles JR, Wybrandt EB (1969) *Biochem J* **113**, 377-386.
- Bennett B, Babu-Khan S, et al. (2000) *J Biol Chem* **275**, 20647–20651.
- Bevec T, Stoka V, Pungercic G, Dolenc I, Turk V (1996) *J Exp Med* **183**, 1331–1338.
- Cooper JB (2002) *Curr Drug Targets* **3**, 155-173.
- Bhaumik P, Xiao H, Parr CL, Kiso Y, Gustchina A, Yada RY, Wlodawer A (2009) *J Mol Biol* **388**, 520-540.
- Bhisetti GR, Saunders JO, Murcko MA, Lepre CA, Britt SD, Ome JH, et al. (2002) Inhibitors of BACE WO02088101

- Bisson, GP, Frank I, Gross R, Lo R, Strom JB, Wang X, Mogorosi M, et al. (2006) *AIDS* **20**, 1333-1336.
- Bjelic S, Nervalla M, Gutierrez-de-Teran H, Ersmarkb K, Hallbergb A, Aqvista J (2007) *Cell Mol Life Sci* **64**, 2285 – 2305
- Blundell TL, Cooper JB, Sali A, Zhu Z (1991) In Structure and Function of the Aspartic Proteinases: Genetics, Structures and Mechanisms ( (Dunn, B.N. Eds.), pp 443-453, Plenum, New York.
- Bode W, Huber R (1992) *Eur J Biochem* **204**, 433-451.
- Borg-von Zepelin M, Meyer I, Thomssen R, Würzner R, Sanglard D, Telenti A, Monod M (1999) *J Invest Dermatol* **113**, 747-751.
- Borth W (1992) *FASEB J* **6**, 3345-3353.
- Braga-Silva LA, Mogami SS, Valle RS, Silva-Neto ID, Santos AL (2010) *FEMS Yeast Res* **10**, 221-224.
- Breman JG, Alilio MS, Mills A (2004) *Am J Trop Med Hyg* **71**, 1-15.
- Broemme D (1999) *Drug News Perspect* **12**, 73-82.
- Brunkan AL, Goate AM (2005) *J Neurochem* **93**, 769-792.
- Bugatti A , Urbinati C , Ravelli C, De Clercq E, Liekens S, Rusnati M (2007) *Antimicrob Agents Chemother* **51**, 2337-2345.
- Carroll TM, Setlow P (2005) *J Bacteriol* **187**, 7119-7125.
- Casimiro-Garcia A, De Clercq E, Pannecouque C, Witvrouw M, et al. (2000) *Bioorg Med Chem* **8**, 191-200.
- Cassone A, De Bernardis F, Torosantucci A, Tacconelli E, Tumbarello M, Cauda R (1999) *J Infect Dis* **180**, 448-453.
- Celotti F, Laufer S (2001) *Pharmacol Res* **43**, 429-436.
- Chang C, Werb Z (2001) *Trends cell boil* **11**, 37-43.
- Chapman HA, Riese RJ, Shi G-P (1997) *Annu Rev Physiol* **59**, 63-88.
- Chatfield D, Brooks B (1995) *J Am Chem Soc* **117**, 5561-5572.
- Chen J, Ouyang Y, Wang L, Xie W, Zhang Q (2009) *Gene* **442**, 108-118.
- Chien J, Campioni M, Shridhar V, Baldi A (2009) *Curr Cancer Drug Targets* **9**, 451-468.
- Christeller JT, Farley PS, Ramsay RJ, Sullivan PA, Laing WA (1998) *Eur J Biochem* **254**, 160-167.

- Churcher I, Williams S, Kerrad S, Harrison T, Castro JL, Shearman MS, et al. (2003) *J Med Chem* **46**, 2275-2278.
- Coburn CA, Stachel SJ, Li YM, Rush DM, et al. (2004) *J Med Chem* **47**, 6117-6119.
- Coombs GH, Goldberg DE, Klemba M, Berry C, Kay J, Mottram JC (2001) *Trends Parasitol* **17**, 532–537.
- Cumin F, Evin G, Fehrentz JA, Seyer R, Castro B, Menard J, et al. (1985) *J Biol Chem* **260**, 9154-9157.
- Dahlgren A, Kvarnstrom I, Vrang L, Hamelink E, Hallberg A, Rosenquist, Samuelsson AB (2003) *Bioorg Med Chem* **11**, 3423–3437.
- Dales N, Bohacek R, Satyshur K, Rich D (2001) *Org Lett* **3**, 2313–2316.
- Damiano S, Domenico R (2002) *Biochem Biophys Res Commun* **297**, 1350–1353
- Darke PL, Nutt RF, Brady SF, Garsky VM, Ciccarone TM, et al. (1988) *Biochem Biophys Res Commun* **156**, 297-303.
- Dash C, Kulkarni A, Dunn B, Rao M (2003) *Crit Rev Biochem Mol* **38**, 89-119.
- Dash C, Phadtare S, Deshpande V, Rao M (2001) *Biochemistry* **40**, 11525–11532.
- Dash C, Rao M (2001) *J Biol Chem* **276**, 2487-2493.
- Dass SB, Dosoretz CG, Reddy CA, Grethlein HE (1995) *Arch Microbiol* **163**, 254–258.
- De Clercq E (2001) *Curr Med Chem* **8**, 1543–1572.
- De Strooper B (2003) *Neuron* **38**, 9-12.
- Dejonckheere E, Vandenbroucke RE, Libert C (2011) *Drug Discov Today* **16**, 762-778.
- Deveraux Q, Takahashi R, Salvesen GS, Reed JC (1997) *Nature* **388**, 300–304.
- Dey D, Hinge J, Shendye A, Rao M (1991) *Can J Microbiol* **38**, 436-442.
- Dhanaraj V, Dealwis CG, Frazao C, Badasso M, Sibanda BL, Tickle IJ, et al. (1992) *Nature* **357**, 466-472.
- Dorrel S (2000) *Drug Discov Today* **5**, 316–317.
- Dunn BM (2002) *Chem Rev* **102**, 4431–4458.
- Dupuy B, Deghmane AE & Taha MK (2004) Type IV prepilin peptidase. In: Handbook of Proteolytic Enzymes, Barret AJ, Rawlings ND, Woessner JF (Eds). Elsevier Academic Press, London, pp.204–208.
- Eder J, Hommel U, Cumin F, Martoglio B, Gerhartz B (2007) *Curr Pharm Design* **13**, 217-258.

- Elliott PJ, Zollner TM, Boehncke WH (2003) *J Mol Med* **81**, 235-245.
- Ersmark K, Feierberg I, Bjelic S, Hamelink E, Hackett F, Blackman MJ, et al. (2004) *J Med Chem* **47**, 110-122.
- Ersmark K, Samuelsson B, Hallberg A (2006) *Med Res Rev* **26**, 626-666.
- Esler WP, Kimberly WT, Ostaszewski BL, Diehl TS, Moore CL, Tsai JY, et al. (2000) *Nat Cell Biol* **2**, 428-434.
- Faivre S, Kroemer G, Raymond E (2006) *Nat Rev Drug Discov* **5**, 671-688.
- Farley PC, Christeller JT, Sullivan ME, Sullivan PA, Laing WA (2002) *J Mo Recognit* **15**, 135-144.
- Farmer EE, Johnson RR, Ryan CA (1992) *Plant Physiol* **98**, 995-1002.
- Faro C, Ramalho-Santos M, et al. (1999) *J Biol Chem* **274**, 28724-28729.
- Fear G, Komarnytsky S, Raskin I (2007) *Pharmacol Therapeut* **113**, 354-368.
- Fengwu L, Patra KP, Yowell CA, Dame JB, Chin K, Vinetz JM (2010) *J Biol Chem* **285**, 8076-8083.
- Fleischmann A, Darsow M, Degtyarenko K, Fleischmann W, Boyce S, Axelsen K, et al. (2004) *Nucleic Acids Re* **32**, 434-437.
- Frazao C, Bento I, Costa J, Soares C, Verissimo P, Faro C (1999) *J Biol Chem* **274**, 27694-27701.
- Frazão C, Bento I, et al. (1999) *J Biol Chem* **274**, 27694-27701.
- Fricker SP (2010) *Metallomics* **2**, 366-377.
- Friedmann E, Lemberg MK, Weihofen A, Dev KK, Dengler U, Rovelli G, et al. (2004) *J Biol Chem* **279**, 50790-50798.
- Fuetterer J, Hohn T (1987) *Trends Biochem Sci* **12**, 92-95.
- Fuetterer J, Hohn T (1987) *Trends Biochem Sci* **12**, 92-95.
- Fujinaga M, Cherney MM, Oyama H, Oda K, James MN (2004) *Proc Natl Acad Sci* **101**, 3364-3369.
- Gacko M, Minarowska A, Karwowska A, Minarowski L (2007) *Folia Histochem Cyto* **45**, 291-313.
- Galesa K, Pain R, Jongasma MA, Turk V, Lenarcic B (2003) *FEBS Lett* **539**, 120-124.
- Galleschi L, Friggeri M, Repiccioli R, Come D (1993) In: Proceedings of Fourth Int. Workshop Seeds: basic and applied aspects of seed biology. Corbineau F. Angers France. pp-207-211.
- Garcia-Lorenzo M, Sjodin A, Jansson S, Funk C (2006) *BMC Plant Biol* **6**, 30.

- Ghosh AK, Brindisi M, Tang J (2012) *J Neurochem* **120**, 71-83.
- Ghosh AK, Shin D, Downs D, Koelsch G, Lin X, Ermolieff J et al. (2000) *J Am Chem Soc* **122**, 3522-3523.
- Gil AL, Baliencie PA, Pascutti PG, Pons T (2011) *J Trop Med* doi : 10.1155/2011/657483.
- Gomis-Ruth FX, Maskos K, Betz M, et al. (1997) *Nature* **389**, 77-81.
- Gong YF, Robinson BS, Rose RE, Deminie C, Spicer TP, Stock D, et al. (2000) *Antimicrob Agents Chemother* **44**, 2319-2326.
- Gosh AK (2010) Aspartic acid proteases as therapeutic targets, Wiley-VCH Verlag GmbH & Co. KGaA.
- Gruber A, Lukasser-Vogl E, Borg-von Zepelin M, Dierich MP, Würzner R (1998) *J Infect Dis* **177**, 1057-1063.
- Guegan R, Diaz J, Cazaubon C, Beaumont M, Carlet C, Clement J, et al. (1986) *J Med Chem* **29**, 1152-1159.
- Hammer SM, Saag MS, Schechter M, Montaner JSG, Schooley RT, et al. (2006) *J Am Med Assoc* **296**, 827-843.
- Hanessian S, Yun H, Hou Y, Yang G, Bayrakdarian M, Therrien E, et al. (2005) *J Med Chem* **48**, 5175-5190.
- Hardy J (1997) *Trends Neurosci* **20**, 154-159.
- Hardy J, Selkoe DJ (2002) *Science* **297**, 353-356.
- Hardy JA, Higgins GA (1992) *Science* **256**, 184-185.
- Hasilik A, Figura K, Conzelman E, Nehrkorn H, Sandhoff K (1982) *Eur J Biochem* **125**, 317-321.
- Hellen CUT, Wimmer E (1992) *Experientia* **48**, 201-215.
- Hibbetts K, Hines B, Williams D (1999) *J Vet Intern Med* **13**, 302-308.
- Hill J, Phylip L (1997) *FEBS Lett* **409**, 357-360.
- Hishashi I, Tomoko H, Yusuke M, Yoshitaka N, Yong-Tae K, Kenji T (2008) *J Enzyme Inhib Med Chem* **23**, 352-356.
- Hodge CN, Aldrich PE, Bacheler LT, Chang CH, Eyermann CJ, Garber S, et al. (1996) *Chem Biol* **3**, 301-314.
- Holliday GL, Bartlett GJ, Almonacid DE, O'Boyle NM, Murray-Rust P, Thornton JM, Mitchell JBO (2005) *Bioinformatics* **21**, 4315-4316.
- Holliday GL, Murray-Rust P, Rzepa HS (2006) *J Chem Inf Model* **46**, 145-157.

- Holmes MA, Matthews BW (1981) *Biochemistry* **20**, 6912-6920.
- Hong L, Koelsch G, Lin X, Wu S, Terzyan S, Ghosh AK, et al. (2000) *Science* **290**, 150-153.
- Hong L, Turner RT, III, Koelsch G, Shin D, Ghosh AK, Tang J (2002) *Biochemistry* **41**, 10963-10967.
- Hussain I, Powell DJ, Howlett DR, Chapman GA, Gilmour L, Murdock PR, et al. (2000) *Mol Cell Neurosci* **16**, 609-619.
- Hwang KP, Chang SH, Wang LC (2010) *Acta Trop* **113**, 289-94.
- Ikezawa H, Yamada K, Aoyagi T, Takeuchi T, Umezawa H (1972) *J Antibiot* **25**, 738-740.
- Ishikawa A, Ohta S, Matsuoka K, Hattori T, Nakamura K (1994) *Plant Cell Physiol* **35**, 303-312.
- Ishikawa A, Yoshihara T, Nakamura K (1994) *J Plant Mol Biol* **26**, 403-414.
- Ito H, Hirono T, Morita Y, Nemoto Y, Kim YT, Takahashi K (2008) *J enzym inhib med ch* 2008,
- IUBMB (2005) Recommendations of the Nomenclature Committee of the International Union of Biochemistry and Molecular Biology on the nomenclature and classification of enzyme-catalysed reactions
- James M (1998) In: Structure and Function of Aspartic Protease, Retroviral and Cellular Enzymes, Plenum Press, New York, pp. 1-481.
- James MNG, Sielecki AR (1987) In: Jurnak FA, McPherson A (Eds). John Wiley & Sons, New York, Vol. 3, 413.
- Jiang S, Prigge ST, Wei L, Gao YE (2001) *Antimicrob Agents Chemother* **45**, 2577-2584.
- Johansson P-O, Lindberg J, Blackman MJ, Kvarnstrom I, Vrang L, et al. (2005) *J Med Chem* **48**, 4400-4409.
- Jones R, Gazzard B (2006) *Int J STD AIDS* **17**, 499-506.
- Josien H (2002) *Curr Opin Drug Discov Devel* **5**, 513-525.
- Kaehn KK, Morr M, Kula MR (1979) *Z Physiol Chem* **360**, 791-794.
- Kageyama T (1998) *Eur J Biochem* **253**, 804-809.
- Kandula VR, Khanlou H, Farthing C (2005) *Expert Rev Anti Infect Ther* **3**, 9-21.
- Kanehisa M, Goto S, Kawashima S, Okuno Y, Hattori M (2004) *Nucleic Acids Res* **32**, 277-280.



- Kasam V, Zimmermann M, Maab A, Schwichtenberg H, Wolf A, Jacq N, Breton V, Hofmann M (2007) *J Chem Inf Model* **47**, 1818-1828.
- Kaur K, Jain M, Kaur T, Jain R (2009) *Bioorg Med Chem* **17**, 3229–3256.
- Kay J, Meijer HJG, Have AT, van Kan JAL (2011) *BMC Genomics* **12**, 254 – 269.
- Kay J, Valle MJ, Dunn BN (1983) In: Katunuma N, Umezawa H, Holzer H (Eds). Japan Scientific Societies Press, Tokyo, pp. 201–210
- Keilova H (1971) On the specificity and inhibition of cathepsin D and B. In: *Tissue proteinases*. Barrett AJ, Diugle JT (ed) North-Holland Co Amsterdam, pp. 45-67.
- Keilova H, Markovic O, Keil B (1969) *Collect Czech Chem Commun* **34**, 2154.
- Kervinen J, Tobin G, et al. (1999) *EMBO J* **18**, 3947–3955.
- Kobayashi H, Kim H (2003) *Food Sci Technol Res* **9**, 30–34.
- Kobayashi H, Sekibata S, Shibuya H, Yoshida S, et al. (1989) *Agr Biol Chem* **53**, 1927–1933.
- Korting HC, Schaller M, Eder G, Hamm G, Böhmer U, Hube B (1999) *Antimicrob Agents Chemother* **43**, 2038-2042.
- Kratzel M, Bernkop-Schnürch A (2000) *Peptides* **21**, 289-293.
- Kraut J (1977) *Ann Rev Biochem* **46**, 331-358.
- Kreft S, Ravnikar M, Mesko P, Pungercar J, Umek A, Kregar I, Strukelj B (1997) *Phytochemistry* **44**, 1001-1006.
- Kumar A, Rao M (2006) *Biochim Biophys Acta* **1760**, 1845-1856.
- Lam PY, Jadhav PK, Eyermann CJ, Hodge CN, Ru Y, Bacheler LT, et al. (1994) *Science* **263**, 380-384.
- Larder BA, Hertogs K, Bloor S, van den Eynde CH, DeCian W, Wang Y, et al. (2000) *AIDS* **14**, 1943-1948.
- Laskowski MJ, Kato I (1980) *Annu Rev Biochem* **49**, 593-626.
- Laudon H, Hansson EM, Melen K, Bergman A, Farmery MR, Winblad B, et al. (2005) *J Biol Chem* **280**, 35352-35360.
- Lenarcic B, Turk V (1999) *J Biol Chem* **274**, 563-566.
- Leung-Toung R, Zhao Y, Li W, Tam TF, Karimian K, Spino M (2006) *Curr Med Chem* **13**, 547-581.
- Li M, Chen L, Lee DHS, Yu L-C a, Zhang Y (2007) *Prog Neurobiol* **83** 131–139.
- Li M, Dimaio F, Zhou D, et al. (2011) *Nat Struct Mol Biol* **18**, 227-229.
- Lison P, Rodrigo I, Conejero V (2006) *Plant Physiol* **142**, 1329-1339.

- Litovchick A, Eisenstein M, Kalinkovich A, Borkow G (2001) *Biochemistry* **40**, 15612–15623.
- Liu J, Istvan ES, Gluzman IY, Gross J, Goldberg DE (2006) *Proc Natl Acad Sci* **103**, 8840 – 8845.
- Loftus BJ, Fung E, Roncaglia P, Rowley D, Amedeo P (2005) *Science* **307**, 1321–1324.
- Lopez-Otín C, Bond JS (2008) *J Biol Chem* **283**, 30433–30437.
- Lowe J, Stock D, Jap B, Zwickl P, Baumeister W, Huber R (1995) *Science* **268**, 533-539.
- Luksch T, Blum A, Klee N, Diederich WE, Sotriffer CA, Klebe G (2010) *Chem Med Chem* **5**, 443–454.
- Mares M, Meloun B, Pavlik M, Kostka V, Baudys M (1989) *FEBS Lett* **251**, 94–98.
- Martoglio B, Golde TE (2003) *Hum Mol Genet* **2**, 201-206.
- Martzen MR, McMullen BA, Smith NE, Fujikawa K, Peanasky RJ (1990) *Biochemistry* **29**, 7366–7372.
- Mathialagan N, Hansen TR (1996) *Proc Natl Acad Sci* **93**, 13653–13658.
- McGrath M (1999) *Annu Rev Bioph Biom* **28**, 181-204.
- Medema JP, Scaffidi C, Kischkel FC, Shevchenko A, et al. (1997) *EMBO J* **16**, 2794–2804.
- Mercado-Flores Y, Trejo-Aguilar A, Ramirez-Zavala B, et al.. (2005) *Can J Microbiol* **51**, 171 – 175.
- Metzner KJ, Allers K, Rauch P, Harrer T (2007) *AIDS* **21**, 703–711.
- Millan MJ (2006) *Eur J Pharmacol* **500**, 371–384.
- Minarowska A, Gacko M, Karwowska A, Minarowski L (2008) *Folia Histochem Cyto* **46**, 23-38.
- Monod M, Hube B, Hess D, Sanglard D (1998) *Microbiology* **144**, 2731-2737.
- Monod M, Togni G, Hube B, Sanglard D (1994) *Mol Microbiol* **13**, 357-368.
- Morrison CJ, Butler GS, Rodriguez D, Overall CM (2009) *Curr Opin Cell Biol* **21**, 1-9.
- Moya J, Casado JL, Aranzabal L, Moreno A, Antela A, Dronda F, et al. (2006) *HIV Cli Trials* **7**, 210–214.
- Mueller R, Huerzeler M, Boss C (2003) *Molecules* **8**, 556–564.
- Muthas D, Noˆteberg D, SabnisYA, Hamelink E, Vrang L, Samuelsson B, Karle´nA, Hallberg A (2005) *Bioorg Med Chem* **13**, 5371–5390.

- Nagano N (2005) *Nucleic Acids Res* **33**, 407–412.
- Nehls U, Bock A, Einig W, Hampp R (2001) *Plant Cell Environ* **24**, 741–747.
- Neurath H, Walsh KA (1976) *Proc Natl Acad Sci* **73**, 3825–3832.
- Ng KKS, Petersen MM, Charney MM, Garen C, Zalatoris JJ, Rao-Naik C, Dunn BM, et al. (2000) *Nat Struct Biol* **7**, 653-657.
- Nguyen J-T, Hamada Y, Kimura T, Kiso Y (2008) *Arch Pharm Chem Life Sci* **341**, 523 – 535.
- Northrop D (2001) *Accounts Chem Res* **34**, 790–797.
- Northrop JH (1930) *J Gen Physiol* **13**, 739-766.
- Noteberg D, Hamelink E, Hulten J, Wahlgren M, Vrang, L, Samuelsson B, Hallberg A (2003) *J Med Chem* **46**, 734-746.
- Oaks SC, Mitchell VS, Jr Pearson GW, et al. (1991) Malaria: Obstacles and Opportunities. A report of the committee for the study on malaria prevention and control: Status review and alternate strategies. Division of International Health, Institute of Medicine, National Academy, Washington, DC.
- Okochi M, Steiner H, Fukumori A, Tanii H, Tomita T, Tanaka T, et al. (2002) *EMBO J* **21**, 5408-5416.
- Olson ST, Björk I, Bock SC (2002) *Trends Cardiovasc Med* **12**, 198–205.
- Omara-Opyene AL, Moura PA, Sulsona CR, Bonilla JA, Yowell CA, Fujioka H, Fidock DA, Dame JB (2004) *J Biol Chem* **279**, 54088–54096.
- Omara-Opyene AL, Moura PA, Sulsona CR, et al. (2004) *J Biol Chem* **279**, 54088-54096.
- Oparil S, Haber E (1974) *N Engl J Med* **291**, 389-401.
- Oparil S, Haber E (1974) *N Engl J Med* **291**, 446-457.
- Otlewski J, Jelen F, Zakrzewska M, Oleksy A (2005) *EMBO J* **24**, 1303–1310.
- Overall CM, Kleinfeld O (2006) *Nat Rev Cancer* **6**, 227-239.
- Page-McCaw A, Ewald AJ, Werb Z (2007) *Nat Rev Mol Cell Biol* **8**, 221–233.
- Park SK, Penas MM, Ramirez L, Pisabarro AG (2006) *Fungal Genet Biol* **43**, 376–387.
- Patel V, Vuillard L, Cleasby A, Murray CW, et al. (2004) *J Mol Biol* **343**, 407-416.
- Pearl LH, Taylor WR (1987) *Nature* **329**, 351-354.
- Pegg SCH, Brown SD, Ojha S, Seffernick J, Meng EC, et al. (2006) *Biochemistry* **45**, 2545–2555.

- Phylip LH, Lees WE, et al. (2001) *J Biol Chem* **276**, 2023-2030.
- Pinti M, Orsi CF, Gibellini L, Esposito R, et al. (2007) *FEBS Lett* **581**, 3882–3886
- Prade L, Jones AF, Boss C, Richard-Bildstein S, Meyer S, Binkert C, Bur D(2005) **280**, 23837–23843.
- Rahuel J, Priestle JP, Grutter MG (1991) *J Struct Biol* **107**, 227-236.
- Rahuel J, Rasetti V, Maibaum J, Rueger H, Goschke R, Cohen NC, et al. (2000) *Chem Biol* **7**, 493-504.
- Rakitzis ET, Malliopoulou TB (1976) *Biochem J* **153**, 737-739.
- Rao MB, Tanksale AM, Ghatge MS, Deshpande VV (1998) *Microbiol mol Biol R* **62**, 597-635.
- Ratner L, Haseltine W, Patarca R, Livak K.J, Starcich B, et al. (1985) *Nature* **313**, 277-284.
- Rawlings ND, Barrett AJ, Bateman A (2010) *Nucleic Acids Res* **38**, 227–233.
- Rawlings ND, Bateman A (2009) *BMC Genomics* **10**, 437–447.
- Reed JC (2002) *Nature Rev Drug Discov* **1**, 111–121.
- Rich D (1985) *J Med Chem* **28**, 263–73.
- Richards AD, Roberts R, Dunn BM, Graves MC, Kay J (1989) *FEBS Lett* **247**, 113-117.
- Richardson M (1977) *Phytochemistry* **16**, 159-169.
- Ripka A, Satyshur K, Bohacek R, Rich D (2001) *Org Lett* **3**, 2309–2312.
- Roberts NA, Martin JA, Kinchington D, Broadhurst AV, Craig JC, Duncan IB, et al. (1990) *Science* **248**, 358-361.
- Robinson BS, Riccardi KA, Gong YF, Guo Q, Stock DA, Blair WS, et al.(2000) *Antimicrob Agents Chemother* **44**, 2093-2099.
- Romeo S, Dell’Agli M, Parapini S, Rizzi L, Galli G, Mondani M, Sparatore A, Taramelli D, Bosisio E (2004) **14**, 2931–2934.
- Rosenblum JS, Kozarich JW (2003) *Curr Opin Chem Biol* **7**, 496-504.
- Rosenthal PJ, McKerrow JH, Aikawa M, Nagasawa H, Leech JH (1988) *J Clin Invest* **82**, 1560–1566.
- Rudenskaia GN, Gaida AV, Stepanov VM (1980) *Biokhimiia* **45**, 561–568.
- Runeberg-Roos P, Kervinen J et al. (1994) *Plant Physiol* **105**, 321–329.
- Rusconi S, De Pasquale MP, Mainini F, Bulgheroni E, et al. (1996) *Antivir Ther* **1**, 211–219.

- Sabotič J, Popovič T, Croat JB (2009) *Chem. Acta* **82**, 739–745.
- Saeki K, Ozaki K, Kobayashi T, Ito S (2007) *J Biosci Bioeng* **103**, 501–508.
- Sankaran K (2004) Signal peptidase II. In: Handbook of Proteolytic Enzymes, Barrett AJ, Rawlings ND, Woessner JF (eds). Elsevier Academic Press, London, pp. 201–204.
- Santos ALS (2010) *World J Biol Chem* **26**, 21-30.
- Sarkkinen P, Kalkkinen N, Tilgmann C, Siuro J, Kervinen J, Mikola L (1992) *Planta* **186**, 317-323.
- Sastre M, Steiner H, Fuchs K, Capell A, Multhaup G, Condrón MM, et al. (2001) *EMBO Rep* **2**, 835-841.
- Sauer RT, Bolon DN, Burton BM, Burton RE, Flynn JM, Grant RA, Hersch GL, Joshi SA, et al. (2004) *Cell* **119**, 9–18.
- Schechter I, Berger A (1967) *Biochem Biophys Res Commun* **27**, 157-162.
- Schomburg I, Chang A, Ebeling C, Gremse M, Heldt C, Huhn G, Schomburg D (2004) *Nucleic Acids Res* **32**, 431–433.
- Schu P, Suarez Rendueles P, Wolf DH (1991) *Eur J Biochem* **197**, 1–7.
- Selkoe D, Kopan R (2003) *Annu Rev Neurosci* **26**, 565-597.
- Selkoe DJ (2001) *Physiol Rev* **81**, 741-66.
- Shearman MS, Behr D, Clarke EE, Lewis HD, Harrison T, Hunt P, et al. (2000) *Biochemistry* **39**, 8698-8704.
- Shiozaki EN, Chai J, Rigotti DJ, Riedl SJ, et al. (2003) *Mol Cell* **11**, 519–527.
- Siegel RM (2006) *Nat Rev Immunol* **6**, 308–317.
- Sielecki AR, Hayakawa K, Fujinaga M, Murphy ME, Fraser M, Muir AK, et al. (1989) *Science* **243**, 1346-1351.
- Siemers E, Skinner M, Dean RA, Gonzales C, Satterwhite J, Farlow M, et al. (2005) *Clin Neuropharmacol* **28**, 126-132.
- Silva AM, Lee AY, Erickson JW, Goldberg DE (1998) *Adv Exp Med Biol* **436**, 363–373.
- Silva AM, Lee AY, Gulnik SV, Majer P, Collins J, Bhat TN, Collins PJ, et al. (1996) *Proc Natl Acad Sci* **93**, 10034–10039.
- Silverman GA, Bird PI, Carrell RW, Church FC, et al. (2001) *J Biol Chem* **276**, 33293–33296.
- Simões I, Faro C (2004) *Eur J Biochem* **271**, 2067-75.

- Simoes I, Faro R, Bur D, Kay J, Faro C (2011) *FEBS J* **278**, 3177–3186.
- Sims AH, Dunn-Coleman NS, Robson GD, Oliver SG (2004) *FEMS Microbiol Lett* **239**, 95-101.
- Singha SB, Ondeykaa JG, Tsipourasa N, Rubya C, et al. (2004) *Biochem Biophys Res Commun* **324**, 108-113.
- Skeggs LT, Dorer FE, Levine M, Lentz KE, Kahn JR (1980) *Adv Exp Med Biol* **130**, 1-27.
- Skrbec D, Romeo D (2002) *Biochem Biophys Res Commun* **297**, 1350-1353.
- Smith GD, Murray MA, Nichols LW, Trikojus VM (1969) *Biochim Biophys Acta* **171**, 288-298.
- Sparey T, Beher D, Best J, Biba M, Castro JL, Clarke E, et al. (2005) *Bioorg Med Chem Lett* **15**, 4212-4216.
- Stachel SJ, Coburn CA, Steele TG, Jones KG, Loutzenhiser EF, Gregro AR, et al. (2004) *J Med Chem* **47**, 6447-6450.
- Steiner H, Kostka M, Romig H, Basset G, Pesold B, Hardy J, et al. (2000) *Nat Cell Biol* **2**, 848-851.
- Stepanov VM, Orekhovich VN, Lobareva LS, Mzhelskaya TI (1969) *Biochemistry* **34**, 170-171.
- Strukelj B, Pungercar J, Ritonja A, Krizaj I, Gubensek F, Kregar I, Turk V (1990) *Nucleic Acids Res* **18**, 4605.
- Stubbs MT, Laber B, Bode W, Huber R, et al. (1990) *EMBO J* **9**, 1939–1947.
- Sun X, Wang Y, Qing H, Christensen MA, Liu Y, Zhou W, et al. (2005) *FASEB J* **19**, 739-749.
- Svicher V, Ceccherini-Silberstein F, Erba F, Santoro M, et al. (2005) *Antimicrob Agents Chemother* **49**, 2015-2025.
- Tang J (1971) *J Biol Chem* **246**, 4510-4517.
- Tang J (1979) *Mol Cell Biochem* **26**, 93-109.
- Tang J, James MN, Hsu IN, Jenkins JA, Blundell TL (1978) *Nature* **271**, 618–621.
- Terauchia K, Asakuraa T, Uedac H, Tamuraa T, et al. (2006) *J Plant Physiol* **163**, 856—862.
- Theodoratou E, Huber R, Bock A (2005) *Biochem Soc Trans* **33**, 108–111.
- Tormakangas K, Hadlington JL, Pimpl P, Hillmer S, Brandizzi F, Teeri TH, Denecke J (2001) *Plant cell* **13**, 2021-2032.

- Torruella M, Gordon K, Hohn T (1989) *EMBO J* **8**, 2819–2825.
- Torruella M, Gordon K, Hohn T (1989) *EMBO J* **8**, 2819–2825.
- Tschan S, Mordmuller B, Kun JF (2011) *Expert Opin Ther Tar* **15**, 365-378.
- Turk B (2006) *Nat Rev Drug Discov* **5**, 785-799.
- Turk B, Turk D, Turk V (2000) *Biochim Biophys Acta* **1477**, 98–111.
- Turk B, Turk D, Salvesen GS (2002) *Curr Pharm Des* **8**, 1623–1637.
- Turk D, Guncar G (2003) *Acta Crystallogr D Biol Crystallogr* **59**, 203-213.
- Turk V, Lah T, Puizdar V, Kregar I, Pain RH (1981) *Acta Biol Med Germ* **40**, 1439-1450.
- Turner SR, Strohbach JW, Tommasi RA, Aristoff PA, Johnson PD, Skulnick HI, et al. (1998) *J Med Chem* **41**, 3467-3476.
- Umezawa H, Aoyagi T, et al. (1970) *J Antibiot* **23**, 259-262.
- Valentine L, Kwon MO, Herrling PL (2004) *Neurodegenerative Dis* **1**, 269-322.
- van der Hoorn RAL (2008) *Annu Rev Plant Biol* **59**, 191–223.
- Vandeputte-Rutten L, Kramer RA, Kroon J, Dekker N, et al. (2001) *EMBO J* **20**, 5033–5039.
- Vangapandu S, Jain M, Kaur K, Patil P, Patel SR, Jain R (2007) *Med Res Rev* **27**, 65–107
- Vanlaere I, Libert C (2009) *Clin Microbiol Rev* **22**, 224-239.
- Vassar R (2005) *Biochem* **38**, 79-103.
- Vassar R, Bennet BD, et al. (1999) *Science* **286**, 735–741.
- Vattemi G, Engel WK, McFerrin J, Pastorino L, Buxbaum JD, Askanas V (2003) *Exp Neurol* **179**, 150-158.
- Velazquez-Campoy A, Luque I, et al. (2000) *Protein Sci* **9**, 1801-1909.
- Vieira M, Pissarr J, Veri' ssimo P, Castanheira P, Costa Y, Pires E, et al. (2001) *Plant Mol Biol* **45**, 529–39.
- Volberding PA, Volberding PA, Lagakos SW, Grimes JM, et al. (1995) *N Engl J Med* **333**, 401–407.
- Ward OP, Rao MB, Kulkarni A (2009) Proteases, production. In: Schaechter M (ed). *Encyclopedia of Microbiology*, Elsevier, USA, pp 495-511.
- Watabe S, Ikeda T, Yago N (1996) *Bioch Molec Biol Int* **39**, 703-710.
- Weihofen A, Binns K, Lemberg MK, Ashman K, Martoglio B (2002) *Science* **296**, 2215-2218.

- Weihofen A, Lemberg MK, Friedmann E, Rueeger H, Schmitz A, Paganetti P, et al. (2003) *J Biol Chem* **278**, 16528-16533.
- Werner R, Guitton MC, Muhlbach HP (1993) *Plant Physiol* **103**, 1473.
- Wiederanders B, Kirschke H (1989) *Arch Biochem Biophys* **272**, 516-521.
- Wolfe MS (2002) *Curr Top Med Chem* **2**, 371-383.
- Wong GT, Manfra D, Poulet FM, Zhang Q, Josien H, Bara T, et al. (2004) *J Biol Chem* **279**, 12876-12882.
- Xie D, Gulnik S, Collins L, Gustchina E, Suvorov L, Erickson JW (1997) *Biochemistry* **36**, 16166-16172
- Xin H, Stephans JC, Duan X, Harrowe G, Kim E, Grieshammer U, et al. (2000) *Biochim Biophys Acta* **1501**, 125-137.
- Yan R, Bienkowski MJ, Shuck ME, Miao H, Tory MC, Pauley AM, et al. (1999) *Nature* **402**, 533-537.
- Yuasa Y, Shimojo H, et al. (1975) *J Natl Cancer Inst* **54**, 1255-1256.
- Zhang Z, ElSohly HN, Jacob MR, Pasco DS, Walker LA, Clark AM (2002) *J Nat Prod* **65**, 979-85.
- Zhao G, Cui MZ, Mao G, Dong Y, Tan J, Sun L, et al. (2005) *J Biol Chem* **8**, 141-146.
- Zhao G, Mao G, Tan J, Dong Y, Cui MZ, Kim SH, et al. (2004) *J Biol Chem* **279**, 50647-50650.



# CHAPTER 2

*‘Scientists know we must protect microbial biodiversity  
because they are working parts of our life-support  
system’*

**Paul Ehrlich**

**Isolation and identification of microbes for the  
production of aspartic protease inhibitor**

## SUMMARY

The involvement of aspartic proteases in various human diseases has spurred stupendous research interest in isolating new inhibitors from different sources. Exploiting the soil biodiversity, we have isolated two potent cultures producing aspartic protease inhibitor. Preliminary morphological characteristics revealed one to be an actinomycetes and the other belonging to the kingdom fungi. Further the biochemical studies and 16S rDNA sequence homology affirmed that the actinomycetes isolate belong to the genus *Streptomyces*. The 16S rDNA of *Streptomyces* sp MBR04 was sequenced and the BLAST search analysis showed 99% homology to *Streptomyces cinerchromogenes*. The sequence was submitted to GenBank and accession number JN627518 was obtained. The optimum temperature and pH for growth of *Streptomyces* sp MBR04 were 28°C and 6.0 respectively. *Streptomyces* sp MBR04 produced 92 IU/ml of inhibitor in a medium containing soya meal (SBM) as inducer at 28°C in 48 h. The optimized process and nutritional parameters increased the inhibitor yield to 11.39 folds as compared to the basal medium.

The fungal isolate was identified as a *Penicillium* sp on the basis of ITS sequence homology. The ITS sequence of *Penicillium* sp VM24 was deposited to GenBank and an accession number of JN673378 was obtained. The optimum temperature and pH for growth of *Penicillium* sp VM24 were 28°C and 5.0 respectively. *Penicillium* sp produced 154 IU/ml of inhibitor in a medium supplemented with soy meal as inducer in 96 h under submerged fermentation (SmF). The culture also produced inhibitor units of 1148 IU/g in a media containing wheat bran and soy meal in 6 days under solid state fermentation (SSF) conditions. This is the first report of a fungal isolate producing aspartic protease inhibitor.

## INTRODUCTION

In the past decade rational drug discovery has taken the movement away from the development of enzyme inhibitors by screening of natural products, the biodiversity prevalent in soil, water, insects, and tropical plants still possess tremendous potential for the isolation of novel and effective enzyme inhibitors. The versatility of microbial biosynthesis is enormous (Demain 2000). Microorganisms are important for many reasons, but one of the principal ones is that they produce things of value to mankind. These may be very large materials such as proteins, nucleic acids, carbohydrate polymers, or even cells, or they can be smaller molecules such as metabolites essential for vegetative growth and those non-essentials (i.e. primary and secondary metabolites, respectively). The power of the microbial culture in the competitive world of commercial synthesis can be appreciated by the fact that even simple molecules (i.e. L-glutamic acid and L-lysine), are made by fermentation rather than by chemical synthesis. Low-molecular-weight inhibitors released from microbial cells are different from macromolecular endogenous inhibitors in that the latter have functional roles in the cells, whereas the former do not (Umezawa 1982). The main reason for the use of microorganisms to produce compounds that can otherwise be isolated from plants and animals or synthesized by chemists is the ease of increasing production by environmental and genetic manipulation. Thousand-fold increases have been recorded for small metabolites. The higher the specific level of production, the simpler is the job of product isolation. Despite the testing of thousands of synthetic compounds, only a few promising structures were uncovered. As new lead compounds became more and more difficult to be explored, vast microbes diversity filled the void and microbial products increased in importance in therapeutics. Many microbial products with important pharmacological activities were discovered by screening for inhibitors using simple enzymatic assays (Umezawa, 1982).

*Streptomyces* is a naturally occurring bacterium in soil and is likely to be present in aquatic habitats as well (Moran et al., 1995). Since the early discovery of this microorganism's ability to produce clinically useful antibiotics (Schatz et al., 1944;

Waksman and Woodruff 1940), the bacterium has received tremendous scientific attention (Paradkar et al., 2003). Furthermore, other noteworthy characteristics, such as its remarkably complex developmental features, make this microorganism an interesting subject of study. Different species of *Streptomyces* are reported to produce different classes of protease inhibitors (Umezawa 1982). *Penicillium* is a large anamorphic (asexual state) ascomycetous fungal genus with widespread occurrence in most terrestrial environments. This genus comprises more than 200 described species and many are common soil inhabitants, as well as food borne contaminants or food ingredients used in the preparation of cheese and sausages (Pitt, 2000; Frisvad and Samson, 2004). They have important implications in applied research, including medical aspects, toxicology, spoilage and biotechnology. *Penicillium* species produce a much diversified array of active secondary metabolites, including antibacterial (Rancic et al. 2006; Lucas et al. 2007), antifungal substances (Nicoletti et al. 2007), immunosuppressants, cholesterol-lowering agents (Kwon et al. 2002), and also potent mycotoxins (Frisvad and Samson, 2004). Thousands of *Penicillium* isolates have probably been screened in bioprospecting programs since the discovery of penicillin, and new bioactive metabolites continue to be discovered from these fungi nowadays (Larsen et al. 2007; Ge et al. 2008; Takahashi and Lucas, 2008), indicating their current importance as sources of high amounts of novel bioactive molecules to be used by pharmaceutical industry. We have exploited the vast biodiversity of soil from Pashan, Pune district, India and have isolated two cultures, *Streptomyces* sp MBR04 and *Penicillium* sp VM24 producing aspartic protease inhibitors. The present chapter deals with the isolation and identification of the isolates and production of inhibitors from *Streptomyces* sp MBR04 and *Penicillium* sp VM24.

## EXPERIMENTAL PROCEDURES

### *Materials*

Lysozyme, SDS, EDTA, phenol, chloroform, isoamyl alcohol, isopropanol, RNAase, deoxyribonucleoside triphosphate (dNTP), Taq DNA polymerase, agarose, tris base, boric acid, ethidium bromide, polyethylene glycol were from Sigma Chem. Co.USA. 16S rDNA primers commercially obtained from Life technologies, India, NaCl, activated charcoal, luria broth, agar, beef extract, yeast extract, peptone, glucose, magnesium sulfate, dipotassium hydrogen phosphate, soya meal were purchased from Himedia and Qualigens India. All other chemicals were of analytical grade.

### **Isolation and identification of actinomycetes**

#### *Isolation and preliminary morphological studies*

The organism was isolated in the laboratory from soil sample from Pashan, Pune district, India. The culture was purified by the single colony plating technique on LB agar plates. The organism was identified by carrying out biochemical tests as described in the Bergey's Manual of Determinative Bacteriology (Buchanan and Gibbons, 1974) and by 16S rDNA sequencing using ABI 3700 DNA sequencer.

#### *Isolation of genomic DNA*

The bacterial culture was grown in 100 ml of Luria Broth (pH 6.0) at 28°C for 48h with continuous shaking at 200 rpm. DNA was isolated according to the method described by Hopwood et al. (1985) with slight modifications. Bacterial cells (1 g) washed in 5ml TE buffer (pH 8.0) was centrifuged at 10,000 rpm for 10 min. at 4°C. The pellet was freezed in liquid nitrogen and powdered for better access by lysozyme. The powdered pellet was re-suspended in 5 ml TE containing 2 mg/ml lysozyme. It was incubated at 30°C, triturating every 15 min until a drop of suspension on a microscopic slide was completely cleared with a drop of 10% SDS (1 h). Further, 1.2 ml of 0.5 M EDTA was added to the mixture followed by 0.7 ml of 10% SDS. The solution was swirled and incubated at 37°C for 2 h. Proteins were

extracted from the aqueous phase by adding 6ml of a mixture of phenol: chloroform: IAA (isoamyl alcohol) (25:24:1). The mixture was shaken for 5 min and then centrifuged at 10,000 rpm, 4°C for 10 min. This step was repeated again for the aqueous phase in a new tube. Finally, 40 µg/g of RNAase from a stock of 10 mg/ml was added to pre-weighed aqueous phase and incubated at 37°C for 1 h. The genomic DNA was precipitated by adding equal volume of isopropanol and was stored at room temperature for 1 h. DNA was spooled with a glass rod and transferred to a fresh tube and dissolved in 5 ml of TE buffer, pH 8.0.

### *PCR amplification of 16S rDNA*

The primers used for the identification of *Streptomyces* sp were universal eubacterial 16S rDNA primers (16F27N- 5'CCA GAG TTT GAT CMT GGC TCA G, 16F536 (5'GTG CCA GCA GCC GCG GTR ATA), 16R1525XP (5'TTC TGC AGT CTA GAA GGA GGT GWT CCA GCC) commercially obtained from Life technologies, India. The 25 µl polymerase chain reaction (PCR) was set by using the genomic DNA and the reaction mixture typically contained genomic DNA; (0.50 µl), 10X buffer; (2.50 µl), 0.2 mM deoxyribonucleoside triphosphate (dNTP); (2.5 µl), forward and reverse primers; (10-20 pmoles), (1.25 µl each), distilled water; (16.87 µl), and 1 unit of *Taq DNA polymerase*; (0.25 µl) (Bangalore Genei). All the additions were done on ice and the PCR reaction was performed on Gene Amplifier PCR System 9700 (Perkin Elmer, USA). The PCR conditions for 16S rDNA gene amplification were: initial denaturation 95°C for 3 min; followed by 35 cycles of 94°C for 1 min, 55°C for 1 min, 72°C for 1 min and final extension at 72°C for 10 min. 5 µl of the above PCR amplified product was used for electrophoresis using 1.0 % agarose gel in 1X TBE buffer (Working solution: 0.5X; Stock: 5X, 54 g Tris base, 27.5 g boric acid, 20 ml 0.5 M EDTA [pH 8]). The gel was run at 80 V for 90 min using 1X TBE as running buffer. The gel was stained in 1% ethidium bromide for 45 min and was observed under UV illumination.

### *Purification of PCR amplified products*

To 20 µl PCR amplified product, 0.6 volumes of 20% PEG-NaCl (polyethylene glycol - NaCl) solution was added and incubated at 37°C for 30 min. It was then centrifuged at 12000 rpm for 20 min. The supernatant was discarded and the pellet

was washed twice with 70% ethanol and separated by centrifuging at 12000 rpm for 20 min. The pellet was dried and dissolved in 10 µl of double distilled water and stored at -20°C.

### *Sequencing of the purified products*

The sequencing reactions were carried out using *Taq* DNA polymerase dye terminator cycle sequencing using the 'ABI PRISM BigDye Terminator Cycle Sequencing Ready Reaction Kit' (Perkin Elmer Applied Biosystems Division, Foster City, CA) according to the manufacturer's protocol. This kit contains the four ddNTPs with different fluorescence labels termed as BigDye Terminators. 2 µl PCR product and 3 pmol of the sequencing primer were used in a 20 µl sequencing reaction. The sequencing primers were 355F (5'-GGCGGACGGGTGAGTAAT-3'), 704F (5'-GTAGCGGTGAAATGCGTAGA-3'), 907R (5'-CCGTCAATTCMTTGTGAGTTT-3'). The sequencing reaction mixes were subjected to 25 cycles in a Perkin Elmer thermal cycler 9700. Each cycle consisted of 95°C for 10 min, 50°C for 5 min and 60°C for 4 min. DNA sequencing was carried out on ABI 1500 Automated Sequencer at the DNA sequencing facility in National Centre for Cell Science (NCCS), Pune. The analysis of nucleotide sequence was done at NCBI server using BLAST-n ([www.ncbi.nlm.gov/blast](http://www.ncbi.nlm.gov/blast)).

## **Production of aspartic protease inhibitor**

### *Growth conditions*

*Streptomyces* sp was routinely maintained on malt extract (0.3%), glucose (1%), yeast extract (0.3%) and peptone (0.5%) (MGYP) slants. The pH of the slant was adjusted to 6.0. The actinomycete was grown at 28°C for 48 h. For long term storage, soil stocks were prepared by inoculating spore suspension (10<sup>6</sup> spores/ml) to sterile soil containing CaCO<sub>3</sub> and were preserved at 4°C.

### *Production of aspartic protease inhibitor*

*Streptomyces* sp MBR04 was grown and maintained on MGYP medium. The media composition for the production of inhibitor was malt extract – 1%, peptone – 0.75%, sodium chloride – 0.3%, magnesium sulphate – 0.1%, dipotassium hydrogen



phosphate – 0.1% and soy meal (SBM) – 2% at pH 6.0. Production of the inhibitor was carried out by inoculating a loop full of a 5 day old culture on MGYP slant into the inoculum flask containing liquid media with the above composition (1% SBM was used instead of 2%) at 28°C. The inoculum was developed for 48 h in the inoculum flask and 10 ml inoculum was transferred into 500 ml Erlenmeyer flask containing 100 ml of the above medium and was incubated under shaking condition (180 rpm) at 28°C for 48 h. The culture supernatant was assayed at different time intervals for anti-proteolytic activity.

#### *Aspartic protease inhibition assay*

The assay was carried out in a 2 ml reaction mixture containing enzyme, substrate and inhibitor. The reaction mixture contains pepsin (100 µg/ml), buffer (50mM glycine HCl buffer, pH 3.0), and 100 µL inhibitor. The reaction was initiated by incubating the mixture at 37°C for 5 min. Substrate (1% hemoglobin) was added to the reaction mixture and was incubated further for 30 min at 37°C. The reaction was ceased by adding 10% TCA acidified with 2.25% HCl. The tubes were kept at room temperature for 30 min. The samples were filtered and centrifuged (5000 rpm for 10 min at 4°C) to get a clear solution and the absorbance was recorded at 280 nm. One unit of pepsin was defined as amount of enzyme that produced an increase in absorbance of 0.001 at 280 nm per minute. One unit of inhibitor is defined as amount of inhibitor required to inhibit one aspartic protease unit under standard assay condition (Dash et al., 2001).

#### *Optimization of inhibitor production in fermentation flasks*

##### *Growth curve*

Cells from 5 day old slant of *Streptomyces* were transferred into 250 ml Erlenmeyer flask with 50 ml MGYP medium. The flasks were kept on rotary shaker at 28°C. Growth was measured as dry cell weight (g/L) after every 12 h. Cell mass was determined after drying at 50°C till constant dry weight was obtained.

### *Time profile for the production of inhibitor*

The production of the inhibitor at various time intervals was checked by removing samples at different time intervals and assaying for its anti-proteolytic activity. The time course of production of the inhibitor and the effect of various additives was estimated in terms of the inhibitor units, taking equal volume of the charcoal treated culture broth for the assay.

### *Inoculum age and level*

The production of inhibitor using different inoculums, 24 h, 48 h, 72 h and 96 h were carried out and samples were removed at different time intervals to determine the anti-proteolytic activity. Similarly different percentage of inoculum, 5%, 10%, 15% and 20% were used to optimize the production of inhibitor from *Streptomyces* sp MBR04.

### *Optimization of temperature and pH*

The effect of different temperatures (28°C, 37°C, 40°C) for fermentation and various pH of the fermentation medium (4, 5, 6, 7, 8, and 9) were studied for the production of inhibitor.

### *Carbon sources*

The effect of various carbon sources on the production of inhibitor was determined by supplementing with glucose, maltose, sucrose, carboxymethyl cellulose (CMC), starch, corn starch, rice flour and wheat flour, all at a concentration of 1% in the production flasks.

### *Nitrogen sources*

The medium was formulated for the maximum production of the inhibitor using 1% w/v of beef extract, yeast extract, casamino acids, tryptone, urea, ammonium chloride, ammonium nitrate, ammonium sulphate, casein acid hydrolysate, cornsteep liquor (CSL) as the nitrogen sources in the fermentation flasks.

### *Addition of inducers*

The fermentation medium was supplemented with various inducers and the effect on the production of the inhibitor was monitored. The inducers used in the production flasks were soya meal, skimmed milk powder, wheat bran, casein, hemoglobin and bovine serum albumin, all at a final concentration of 2%. Hemoglobin and bovine serum albumin were filter sterilized (0.22  $\mu$  Millipore filter) and added to the autoclaved fermentation medium.

## **Isolation and identification of the fungal isolate**

### *Isolation of the microorganism*

The organism was isolated in the laboratory from soil sample from Pashan, Pune district, India. The culture was purified by single colony plating technique on PDA agar plates. The preliminary morphological identification was carried out using lactophenol blue staining and slide culture technique.

### *Isolation of genomic DNA*

The genomic DNA from freeze-dried mycelia was isolated according to the method described by Lodhi et al (1994) with slight modifications. For the isolation of DNA, the fungus was grown in 500 ml flask containing 100 ml MGYP medium. The growth was initiated by inoculating spores from 7 days old MGYP slant. The flasks were incubated on a rotary shaker (180 rpm) for 48 h at 28°C. The contents were centrifuged at 8000 rpm for 15 min, washed repeatedly to remove the media constituents. 3-5 g of wet mycelium was freeze-dried in liquid nitrogen and ground in liquid nitrogen, followed by addition of 8-10 ml of cetyl trimethyl ammonium bromide (CTAB) extraction buffer, pH 8.0 containing 0.2%  $\beta$ -mercaptoethanol. The composition of 2X CTAB extraction buffer was -Tris-Base (100 mM; pH 8.0); CTAB (2% w/v); NaCl (1.4 M); EDTA (20 mM); PVP-40 (1-2%);  $\beta$ -mercaptoethanol (0.2-2%). After that 20  $\mu$ l of proteinase K (20 mg/ml) was added and incubated at 65°C for 1 h. This was followed by addition of 20  $\mu$ l RNase A (10 mg/ml) and further incubation at 65°C for 15 min. To the supernatant collected after centrifugation (8000 rpm, 10 min), 10 ml chloroform: isoamylalcohol (24:1) was added. The mixture was shaken for 5 min and centrifuged at 10,000 rpm, 4°C for 15 min. Two

volumes of CTAB precipitation buffer (1 % CTAB; 50 mM Tris (pH 8.0); 10 mM EDTA), was added to the supernatant and kept at room temperature for 1 h. The pellet collected after centrifugation was dissolved in 5 ml of 1.2 M NaCl and 5 ml of chloroform: isoamylalcohol (24:1) was added. Two volumes of absolute alcohol were added to the aqueous phase to precipitate the DNA. DNA was spooled out and washed with 70% ethanol and suspended in 5 ml of 0.1 M Tris EDTA buffer pH 8.0 and stored at -20°C. The quantification of DNA was done by measuring the absorbance of the sample at 260 nm on spectrophotometer.

### *PCR amplification of 18S rDNA and ITS gene*

PCR amplification of the internal transcribed spacer (ITS) region was done using primers ITS1-F (TCC GTA GGT GAA CCT GCG G) and ITS4-R (TCC TCC GCT TAT TGA TAT GC) (White et al., 1990). The polymerase chain reaction (25 µl) was set to amplify the 18S rDNA and ITS gene by using the genomic DNA. The reaction mixture typically contained genomic DNA- 0.70 µl, 10X PCR Buffer-2.50 µl, 0.2 mM dNTPs-2.5 µl, forward and reverse primers 10-20 pmoles-1.25 µl each, distilled water-16.60 µl, and 1 unit of *Taq* DNA polymerase-0.20 µl. All the additions were done on ice and the PCR reaction was performed on Gene Amplifier PCR System 9700 (Perkin Elmer, USA). The PCR conditions for 18S rDNA and ITS gene amplification were: initial denaturation-95°C for 3 min; followed by 35 cycles of 94°C for 1 min, 57°C for 30 sec, 72°C for 2 min and final extension at 72°C for 10 min. 5 µl of the above PCR amplified product was used to check the amplification on 1.0% agarose gel in 1X TBE buffer (Working solution: 0.5 X; Stock: 5 X, 54 g Tris base, 27.5 g boric acid, 20 ml 0.5 M EDTA, pH 8). The gel was run at 80 V for 90 min using 1 X TBE as running buffer. The gel was stained in 1% ethidium bromide for 45 min and was observed under UV illumination.

### *Purification of PCR amplified product*

To 20 µl PCR amplified product, 12 µl of 20% PEG-NaCl (Polyethylene glycol - NaCl) solution was added and incubated at 37°C for 30 min. It was then centrifuged at 12,000 rpm for 20 min. The supernatant was discarded and the pellet was washed

twice with 70% ethanol and separated by centrifuging at 12,000 rpm for 20 min. The pellet was dried and dissolved in 10 µl of double distilled water and stored at -20°C.

### *Sequencing of the purified PCR product*

The sequencing reactions of PCR product were carried out using *Taq* DNA polymerase dye terminator cycle applying automated DNA sequencing method based on dideoxynucleotide chain termination method (Sanger et al., 1977). The sequencing reactions were carried out using the 'ABI PRISM BigDye Terminator Cycle Sequencing Ready Reaction Kit' (Perkin Elmer Applied Biosystems Division, Foster City, CA) according to the manufacturer's protocol. This Kit contains the four ddNTPs with different fluorescence labels termed as BigDye Terminators. 2 µl PCR product and 3 pmol of the sequencing primer were used in a 20 µl sequencing reaction. The sequencing primers were ITS1 (TCC GTA GGT GAA CCT GCG G) and ITS4 (TCC TCC GCT TAT TGA TAT GC) for sequencing (White et al., 1990). The sequencing reaction mixes were subjected to 25 cycles in a Perkin Elmer thermal cycler 9700. Each cycle consisted of 95°C for 10 min, 50°C for 5 min and 60°C for 4 min. DNA sequencing was carried out on ABI 1500 Automated Sequencer at the DNA sequencing facility in National Centre for Cell Science (NCCS), Pune. The analysis of nucleotide sequence was done at NCBI server using BLAST-n ([www.ncbi.nlm.nih.gov/blast](http://www.ncbi.nlm.nih.gov/blast)).

## **Production of aspartic protease inhibitor**

### *Growth curve*

Cells from 7 day old slant of *Penicillium* were transferred into 250 ml Erlenmeyer flask with 50 ml MGYM medium. The flasks were kept on rotary shaker at 28°C. Growth was measured as dry cell weight (g/L) after every 12 h. Cell mass was determined after drying at 50°C till constant dry weight was obtained.

### *Production of aspartic protease inhibitor using submerged fermentation*

*Penicillium* sp VM24 was grown and maintained on PDA medium. The media composition for the production of inhibitor was glucose – 1%; beef extract – 0.75%;

sodium chloride – 0.3%; magnesium sulphate – 0.1%; dipotassium hydrogen phosphate – 0.1%, soy meal (SBM) – 2% at pH 5.0. Production of the inhibitor was carried out by inoculating a loop full of a 7 day old culture on PDA slant into the inoculum flask containing liquid media with the above composition (1% SBM was used instead of 2%) at 28°C. The inoculum was developed for 48h in the inoculum flask and 10ml inoculum was transferred into 500 ml Erlenmeyer flask containing 100 ml of the above medium and was incubated under shaking condition (180 rpm) at 28°C for 96 h. The culture supernatant was assayed for antiproteolytic activity at different time intervals.

#### *Fungal aspartic protease inhibition assay*

Proteolytic activity of aspartic protease from *Aspergillus saitoi* was measured by assaying the enzyme activity using hemoglobin as described by Dash et al (Dash et al., 2001). Enzyme (1.5  $\mu$ M) and inhibitor were incubated in glycine-HCl buffer, 0.05 M, pH 3.0 for 10 min. The reaction was started by the addition of 1 mL of hemoglobin (5 mg/mL) and incubated at 37°C for 30 min. The reaction was quenched by the addition of 2 mL of 10% trichloroacetic acid (TCA) acidified with 2.25% HCl followed by centrifugation (10000 g, 5 min) and filtration. The optical absorbance of the TCA-soluble products in the filtrate was read at 280 nm. One unit of fungal aspartic protease was defined as the amount of enzyme that produced an increase in absorbance of 0.001 at 280 nm per minute under the conditions of the assay. One protease inhibitor unit was defined as the amount of inhibitor that inhibited one unit of fungal aspartic protease activity (Dash et al., 2001).

#### *Time profile for the production of inhibitor*

The production of the inhibitor at various time intervals was checked by removing samples at different time intervals and assaying for its anti-proteolytic activity. The time course of production of the inhibitor was estimated in terms of the inhibitor units, taking equal volume of the charcoal treated culture broth for the assay.

### *Temperature and pH profile for inhibitor production*

The effect of different temperatures (28°C, 37°C, 40°C) for fermentation and various pH of the fermentation medium (4, 5, 6, 7, 8, and 9) were studied for the production of inhibitor.

### *Effect of mycelial and spore inoculum for inhibitor production*

The inhibitor production was carried out using mycelial and spore inoculum. For mycelial inoculum, *Penicillium* sp was grown in the inoculum medium for 48 h and 10% inoculum was added to the production medium. For spore inoculum, spores from freshly grown 7 day old slants of *Penicillium* sp VM24 were harvested using sterile distilled water containing 0.01% Tween 80 to obtain  $4 \times 10^6$  spores/ml and was used as inoculum.

### *Production of aspartic protease inhibitor using solid state fermentation (SSF)*

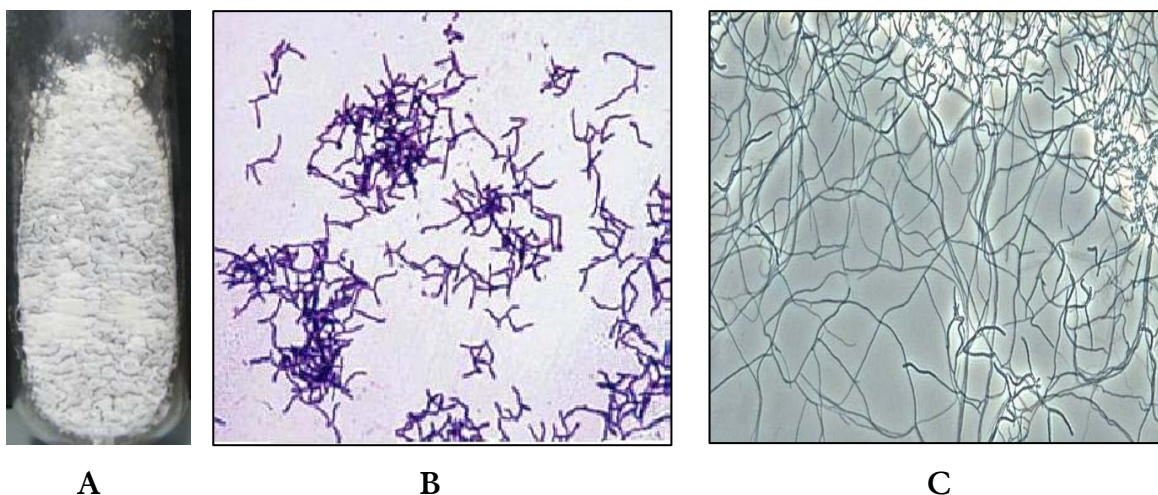
The spores from 7-day-old PDA slants were harvested to obtain  $5 \times 10^7$  spores/ml and were used as inoculum for SSF. The fermentation medium for SSF contained 0.5 g of wheat bran (WB) in a 250 ml Erlenmeyer flask supplemented with 1 g SBM. The flask was moistened with 2 ml 5X basal salt solution (sodium chloride – 0.3%; magnesium sulphate – 0.1%; dipotassium hydrogen phosphate – 0.1%) and 20 ml double distilled water and was autoclaved at 121°C for 30 min. On cooling, the fermentation medium was inoculated with 2.5% spore suspension and incubated for 6 days at 28°C in a humidity chamber with 75% humidity. After 6 days, the flask was harvested with 25 ml of 50 mM glycine-HCl buffer, pH 3.0 containing 0.01% Tween 80. The flask was kept on shaker (120 rpm) for 1 h at 28°C. The contents were centrifuged at 10,000 rpm for 30 min at 4°C. The supernatant before and after activated charcoal treatment was used for anti-proteolytic activity as described earlier. Similarly, the fermentation flasks were inoculated and incubated for different days (1-7) to determine the optimum time for the maximum production of inhibitor. Different combinations of WB (0.5, 1 and 1.5 g) and SBM (0.5, 1 and 1.5 g) were also studied for maximum inhibitor production.

## RESULTS

### Isolation and identification of actinomycetes

#### *Morphological and biochemical identification*

The morphological characteristics of the isolated organism on MGYP slants showed large, irregular, discrete, powdery, ash coloured colonies. The strain was aerobic, non-motile, Gram positive, spore-forming rod shaped bacterium (Figure 1A & B). The isolate produces vegetative hyphae which forms an extensively branched non-fragmented mycelium bearing spores (Figure 1C). The strain was found to utilize hexoses, amino acids, casein and peptone. The strain showed positive reaction for catalase, hydrolysis of starch and gelatin and reduction of nitrates (Table 1). Based on the morphological and biochemical characteristics and referring to Bergey's Manual of Determinative Bacteriology, the isolate belongs to the genus *Streptomyces*. The optimum pH and temperature for the growth of the isolate was 6.0 and 28°C respectively.



**Figure 1** Morphological characteristics of actinomycetes. (A) Large, irregular, discrete, powdery, ash coloured colonies. (B) aerobic, non-motile, Gram positive, spore-forming rod shaped bacterium. (C) Slide culture showing vegetative hyphae with extensively branched non-fragmented mycelium bearing spores.



**Table 1 Morphological and biochemical characteristics of the isolate**

Colony characters		Sugars	Growth	Nitrogen	Growth
Size	2 mm	Glucose	+ (+)	Yeast extract	+ (+)
Shape	Discrete	Xylose	+ (+)	Peptone	+ (+)
Margin	Entire	Sucrose	+ (+)	Casein	+ (+)
Colour	White	Raffinose	+ (+)	Valine	-(-/+)
Opacity	Opaque	Galactose	+ (+)	Histidine	+ (+)
Elevation	Convex	Maltose	+ (+)	Arginine	+ (-/+)
Consistency	Hard	Arabinose	+ (+)	Ammonium sulphate	-(-/+)
Motility	Non motile	Fructose	+ (+)	Ammonium nitrate	-(+)
Gram character	Gram positive	Glycerol	-(-)	Potassium nitrite	-(-/+)
		Mannitol	+ (+)	Sodium nitrite	+ (+)

Enzyme activities	
Gelatin	+ (+)
Starch	+ (+)
Casein	- (+)
Cellulose	-(-/+)
Lecithin	-(-/+)

*Note: Positive or negative results in parentheses were cited from Bergey's manual of systemic Bacteriology volume 4 (1989) and Bergey's Manual of Determinative Bacteriology 8<sup>th</sup> edition (1974)*

### *Identification of isolate by 16S rDNA sequencing*

The genomic DNA was isolated, loaded on agarose gel and was found to be high molecular weight, intact DNA (Figure 2). The spectrophotometric analysis of the DNA showed that the ratio of A<sub>260</sub> to A<sub>280</sub> was 2 indicating the purity of DNA preparation.



**Figure 2** Agarose gel (1%) electrophoresis of genomic DNA isolated from *Streptomyces* sp

The 16S rDNA sequence (449 bp) of *Streptomyces* sp. was obtained by sequencing with the primers 16F27N, 16R1525XP and 16F536. The sequences so obtained by each set of primer were then overlapped to get a 449 bp 16S rDNA sequence (Figure 3). The nucleotide sequences of 16S rDNA gene from the new isolate, *Streptomyces* sp MBR04 was deposited in NCBI GenBank database with the accession number JN627518.

```
5'CCACGTTGTCCGTGCCGCAGCTAACGCATTAAGTGCCCCGCCTGGG
GAGTACGGCCGCAAGGCTAAAAC TCAAAGGAATTGACGGGGGCCCG
CACAAGCGGCGGAGCATGTGGCTTAATTCGACGCAACGCGAAGAAC
CTTACCAAGGCTTGACATACACCGGAAACGTCTGGAGACAGGCGCC
CCCTTGTGGTCGGTGTACAGGTGGTGCATGGCTGTCGTCAGCTCGTG
TCGTGAGATGTTGGGTTAAGTCCCGCAACGAGCGCAACCCTTGTCCC
```

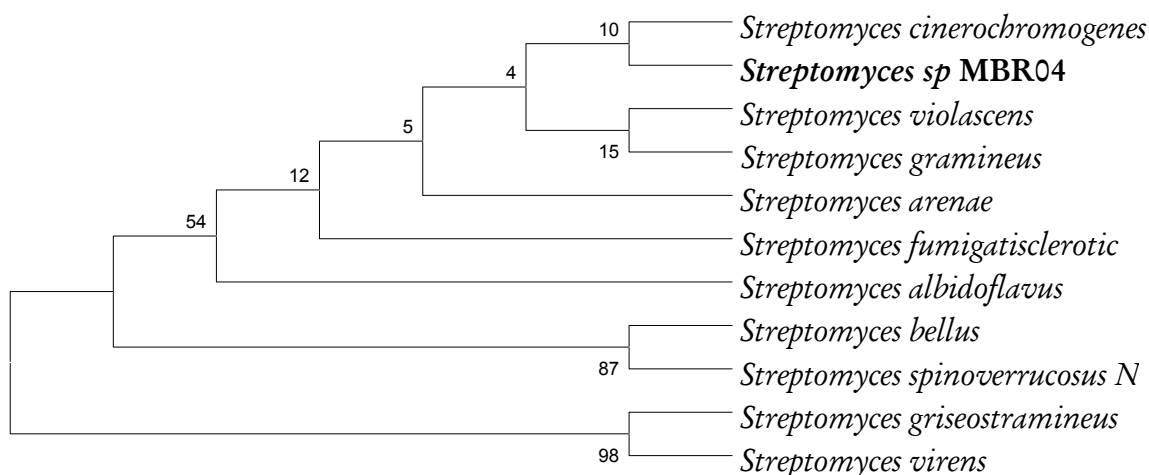
```

GTGTTGCCAGCAGGCCCTTGTGGTGCTGGGGACTCTCGGGAGACCG
CCGGGGTCAACTCGGAGGAAGGTGGGGACGACGTCAAGTCATCATG
CCCCTTATGTCTTGGGCTGCACACGTGCTACAATGGCCGGTACAATG
AGCTGCGATACCCGCGAGGTGGAGCGAATCTC3'

```

**Figure 3** 16S rDNA sequence of *Streptomyces* sp MBR04

The 16S rDNA nucleotide sequence was analyzed with the GenBank database using BLAST program. Multiple sequence alignment was performed with Clustal W program. The phylogenetic tree constructed using neighbour-joining method excluding the type strains, indicated that the *Streptomyces* sp MBR04 may be a type strain of *Streptomyces cinerochromogenes* (Figure 4). The optimum temperature and pH for growth were 28°C and 6.0 respectively.



**Figure 4** Dendrogram showing the similarity between different known *Streptomyces* species with the new isolate.

### Production of aspartic protease inhibitor from *Streptomyces* sp MBR04

The time course for inhibitor production was studied. It was found that the inhibitor production was growth associated and the inhibitor showed 90% inhibition for pepsin. *Streptomyces* sp MBR04 produced 92 IU/ml of inhibitor in unoptimized medium (Figure 5 A & B).

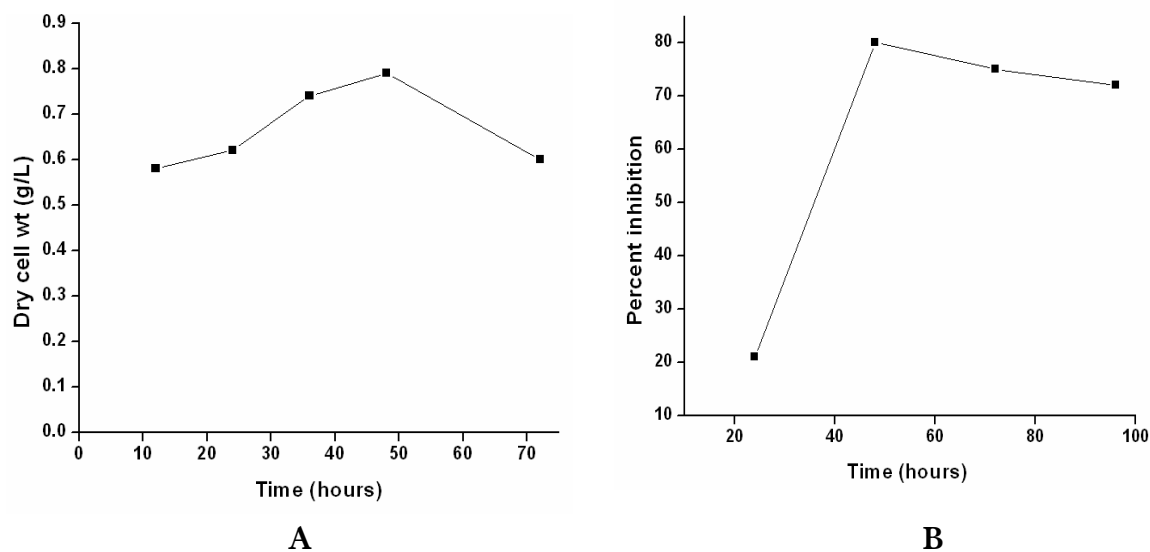
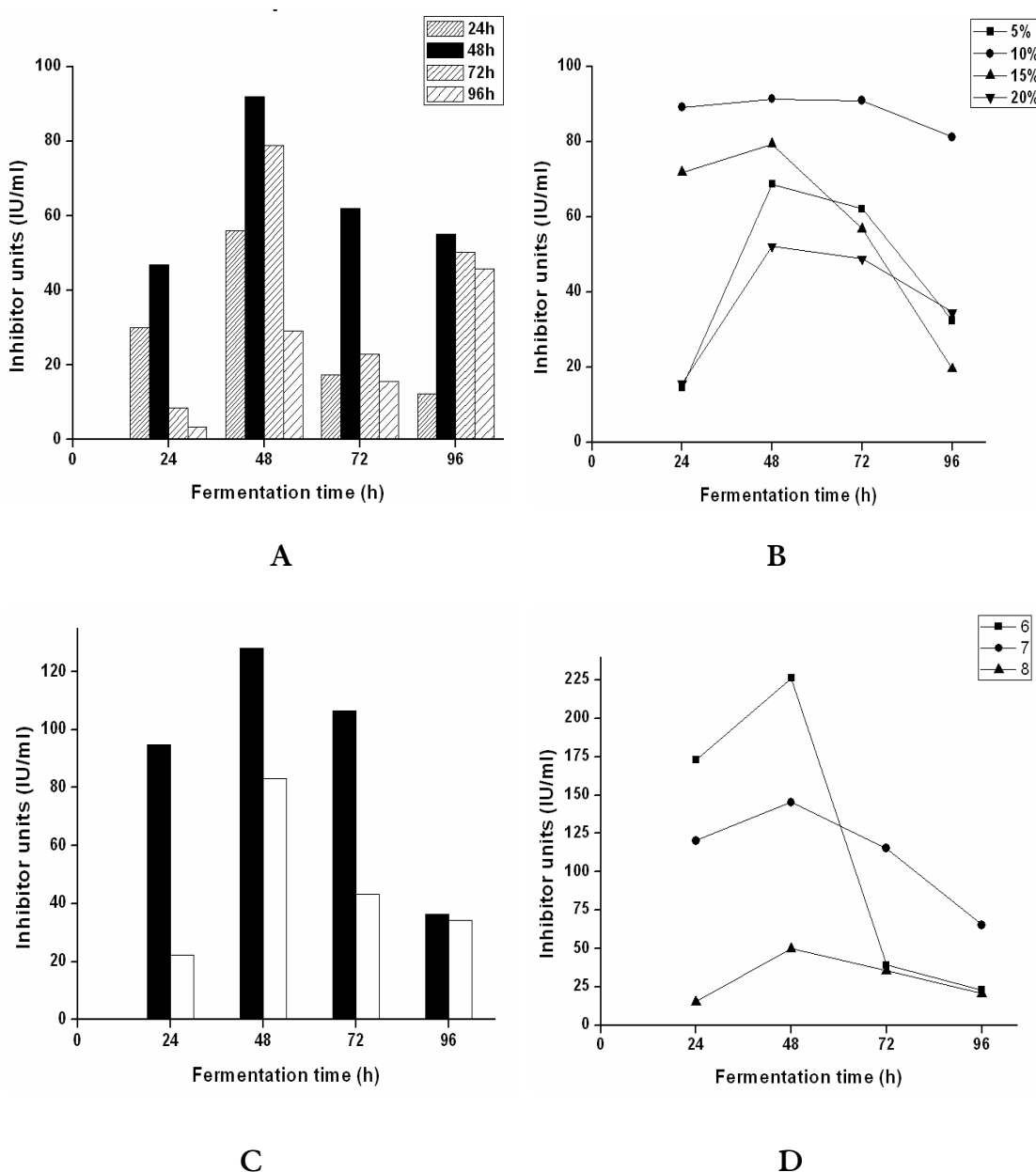


Figure 5 (A) Growth curve of *Streptomyces* sp MBR04. (B) Time profile for inhibitor production

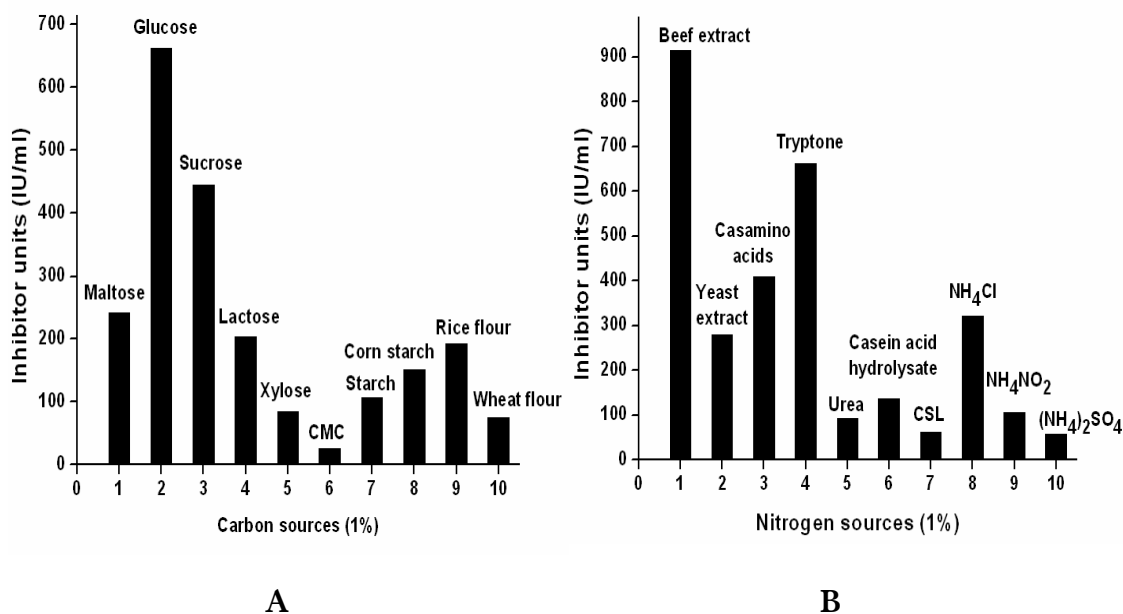
Various process and nutritional parameters were optimized in shake flask for the production of inhibitor from *Streptomyces* sp MBR04. Optimization of inoculum parameters revealed that maximum inhibitor production of 92 IU/ml was obtained with 48 h old 10% inoculum (Figure 6 A & B). Effect of different temperatures for the production of inhibitor showed that maximum inhibitor production of 128 IU/ml was obtained at 28°C. The optimum pH for maximum production of inhibitor was 6.0 which is similar to the growth pH (Figure 6 C & D). Further increase in temperature and pH showed a drastic decrease in inhibitor production.



**Figure 6** Process optimization of inhibitor production by *Streptomyces* sp MBR04. Production of inhibitor at different day old inoculum (A), percentages of inoculum (B), temperatures - filled bar: 28°C and unfilled bar: 37°C (C) and pH (D).

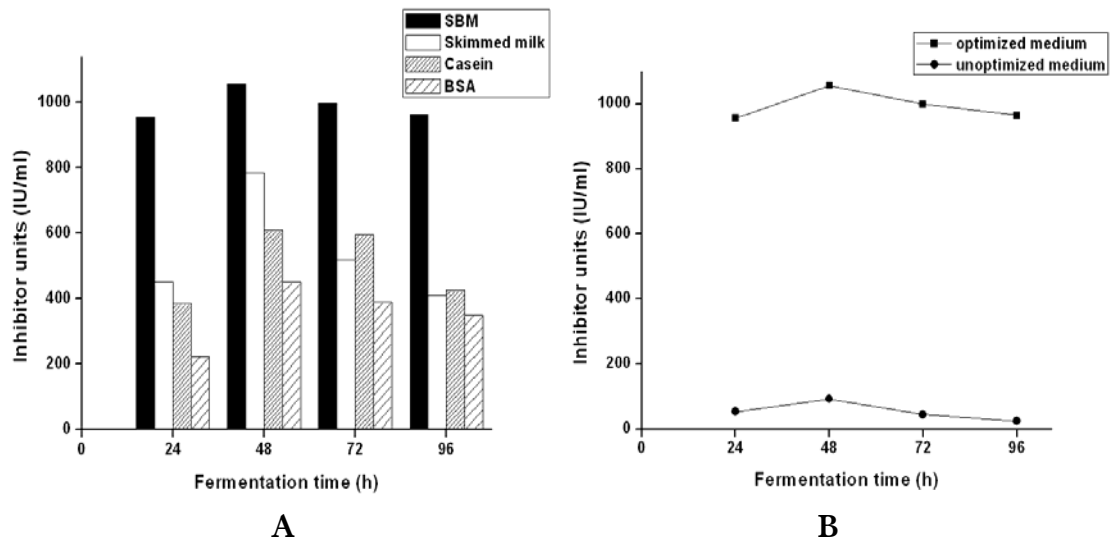
Effect of different carbon sources on inhibitor production was studied. Among the different carbon sources supplemented, glucose induced maximum production of inhibitor (Figure 7A). In case of nitrogen sources, maximum inhibitor production was obtained in presence of beef extract. The results indicated that inhibitor production was increased when organic nitrogen sources were present in the medium (Figure 7B). Among the organic sources tested, highest inhibitor production was observed with beef extract whereas among inorganic sources  $\text{NH}_4\text{Cl}$  proved to

be best. This suggests that beef extract contains some micronutrients essential for the production of the inhibitor.



**Figure 7** Effect of different carbon (A) and nitrogen (B) sources for inhibitor production by *Streptomyces* sp MBR04.

Among the different inducers studied for inhibitor production, SBM was found to induce maximum inhibitor production of 1058 IU/ml at 48 h followed by skimmed milk, casein and BSA (Figure 8A). The optimized process and nutritional parameters increased the inhibitor production yield to 11.39 folds as compared to the basal medium (Figure 8B).

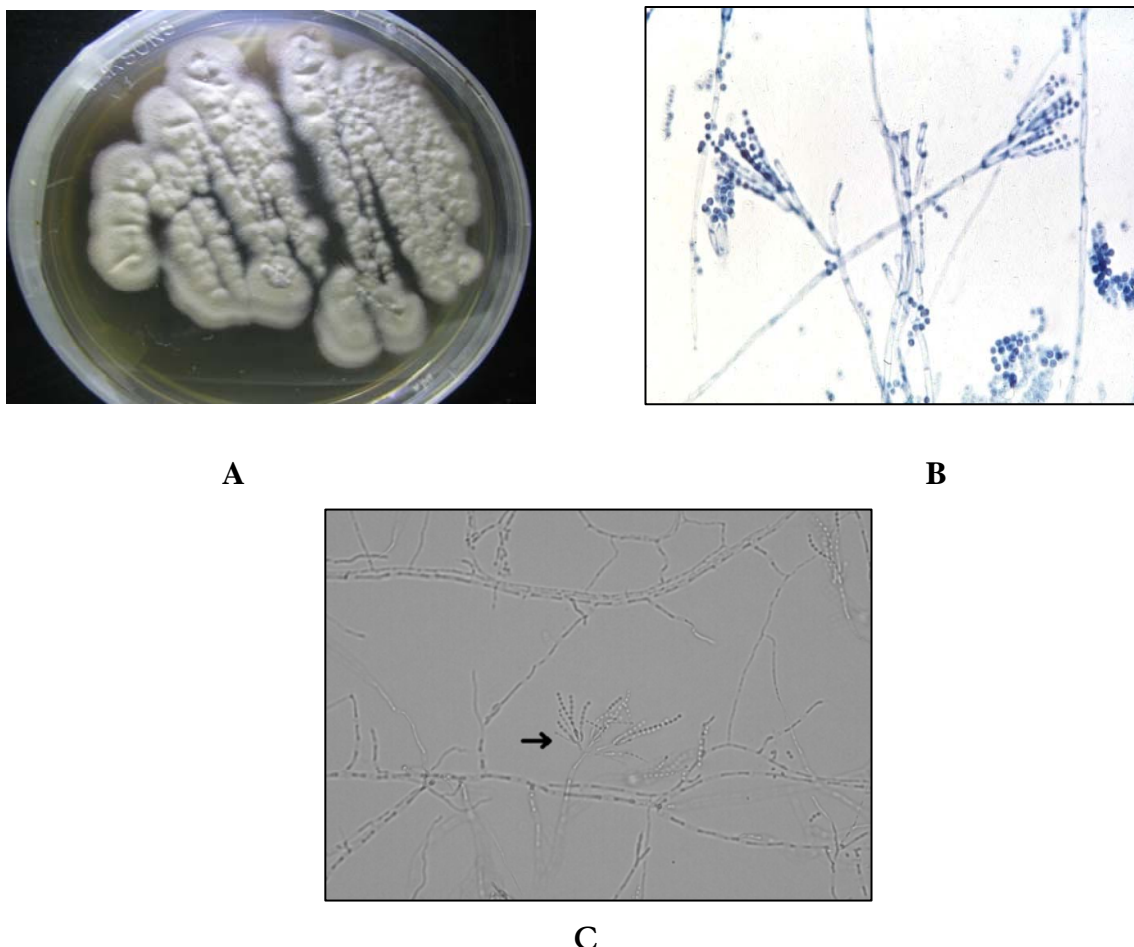


**Figure 8** Effect of different inducers (A) and optimized and unoptimized medium (B) on inhibitor production.

## Isolation and identification of the fungal isolate

### *Morphological characteristics*

The fungal strain was isolated from soil from Pashan, Pune district, India. The growth was aerobic with creamish white cottony mycelium on MGYP (Figure 9A). Microscopic observation (100X) showed that the organism formed thick network of thin mycelia and older cultures showed numerous spores. Preliminary morphological studies using Lactophenol blue staining (Figure 9B) and slide culture technique (Figure 9C) showed the presence of conidiophores with metulatae, phialides and conidia. The appearance of the spore head is like that of a brush or penicillus. Thus, based on microscopic investigations it was proved that examined fungal isolate was characterized by conidiophores and microscopic elements typical for *Penicillium* genus.



**Figure 9** Preliminary identification of the isolate. (A) Morphological characteristics of the fungus (B) Lactophenol staining (C) Light micrograph of slide culture for the fungal isolate



*Identification of isolate by ITS sequencing*

The genomic DNA was isolated, loaded on agarose gel and was found to be high molecular weight, intact DNA. The spectrophotometric analysis of the DNA showed that the ratio of A<sub>260</sub> to A<sub>280</sub> was 2 indicating the purity of DNA preparation. The ITS sequence (446 bp) of *Penicillium* sp was obtained by sequencing with the primers ITS1 and ITS4. The sequences so obtained by each set of primer were then overlapped to get a 446 bp ITS sequence (Figure 10).

```

5'CGGGAATTCTACCCTGAATCCGAGGTCACCGTGGTAAAACATGG
TGGTGACCAACCCCGCAGGTCCTTCTGAACAAGAGACAGAGCCCC
ATACGCTCGAGGACCAGACGGACCTCGCCGCTGCCTTTCGGGCAGG
TCCCCGGGGGGACCACACCCAACACACAAGCCGTGCTTGAGGGCA
GAAATGACGCTCGGACAGGCATGCCCCCGGAATGCCAGGGGGCG
CAATGTGCGTTCAAAGATTCGATGATTCACGGAATTCTGCAATTCAC
ATTACTTATCGCATTTCGCTGCGTTCTTCATCGATGCCGGAACCAAT
AGATCCCTTGTGAAAGTTTTTGACAATTTTCACAGTACTCAGAACG
GCCCTTCTTTCATCAGGGCTTCACAGAAGGGCTTCAGGCGGGCGAT
GGGCCCCGGAACGTGCGTCCCCCGGGTAAAC 3'

```

**Figure 10** Sequence of ITS gene

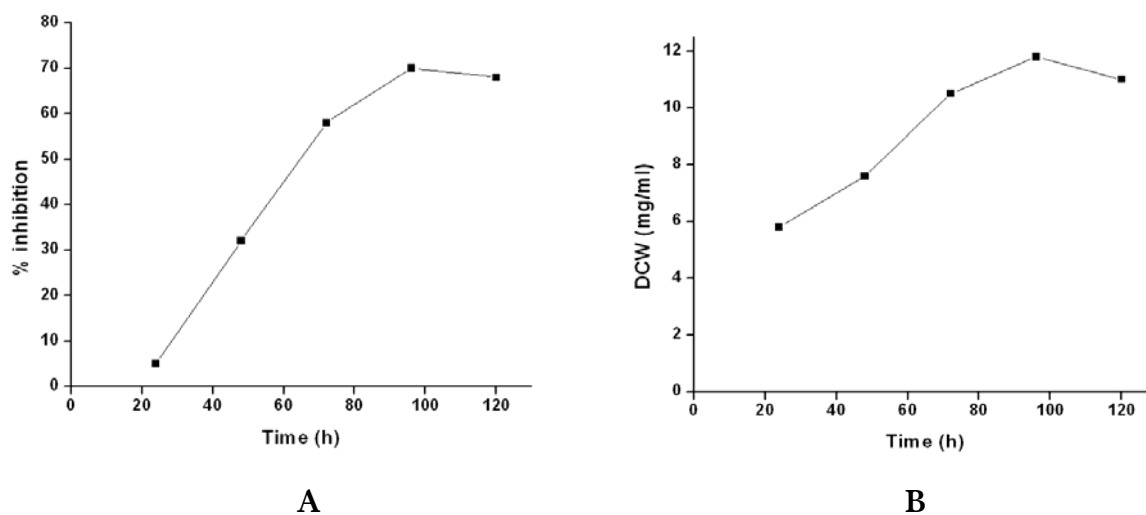
The nucleotide sequence of the ITS region from the new isolate, *Penicillium* sp VM24 was deposited in NCBI GenBank database with the accession number JN673378. The ITS sequence was analyzed with the GenBank database using BLAST program. The ITS sequence of the new isolate showed 94% homology with *Penicillium pinophilum* as well as with several other *Penicillium* species and strains (Table 2). As the percent homology of the new isolate was <99%, the isolate may be a new species of *Penicillium*.

**Table 2** BLAST hits for ITS sequence

Accession	Description	Max Score	E value	Max identity
AB606412.1	<i>Penicillium pinophilum</i> FKI-5653	660	0.0	94%
AB455516.1	<i>Penicillium pinophilum</i> FKI-3864	660	0.0	94%
HM371219.1	<i>Penicillium</i> sp. W1	660	0.0	94%
JN198417.1	<i>Penicillium pinophilum</i>	660	0.0	94%
HQ607835.1	<i>Penicillium verruculosum</i> isolate ATT099	660	0.0	94%
HM469418.1	<i>Penicillium pinophilum</i> strain KUC1758	660	0.0	94%
HQ839772.1	<i>Penicillium pinophilum</i> strain F01	660	0.0	94%
HQ671193.1	<i>Penicillium</i> sp. MJM1981	660	0.0	94%

### Production of aspartic protease inhibitor from *Penicillium* sp VM24

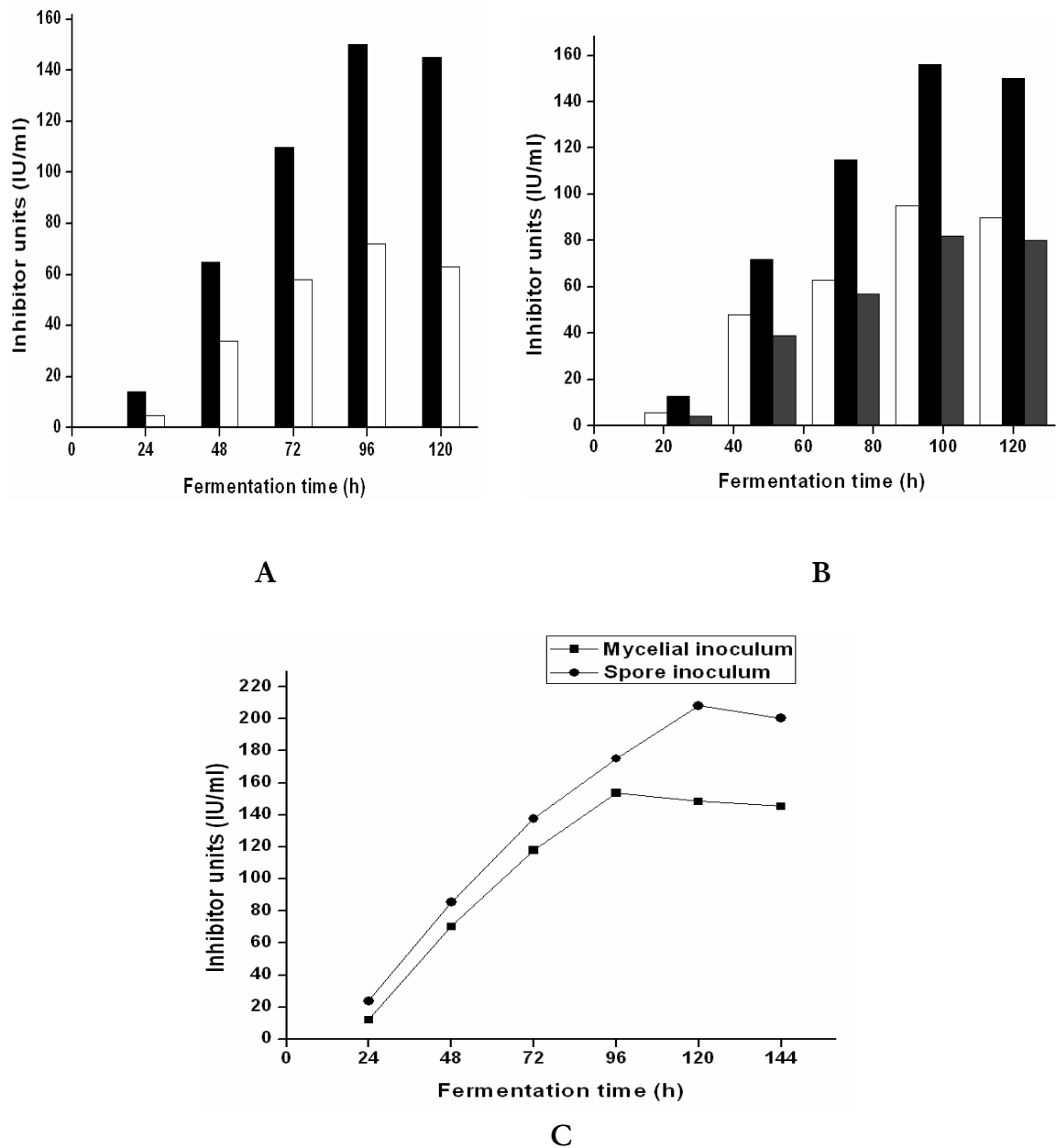
Time profile for inhibitor production from *Penicillium* sp VM24 was studied in shake flask (Figure 11A). It was found that inhibitor production was growth associated (Figure 11B).



**Figure 11** (A) Time course of inhibitor production (B) Growth curve of *Penicillium* sp.

Effect of different temperatures for inhibitor production showed that 28°C was optimum with 154 IU/ml of inhibitor (Figure 12A). The optimum pH for maximum production of inhibitor was 5.0 (Figure 12B). There was a drastic reduction in inhibitor production with increase in temperature and pH. Effect of

mycelial and spore inoculum on inhibitor production was studied. Maximum inhibitor production of 207 IU/ml was obtained with spore inoculum at 120 h. Mycelial inoculum produced 153 IU/ml of inhibitor in 96 h. Inhibitor units was increased with spore inoculum as compared to mycelial inoculum with an increase in time of 24 h (Figure 12 C).



**Figure 12** Production of inhibitor at different temperatures, filled bar: 28°C and unfilled bar: 37°C (A), pH, Unfilled bar: 4, Black bar: 5, Gray bar: 6 (B), mycelial and spore inoculum (C).

Inhibitor production using *Penicillium sp* VM24 was also studied in solid state fermentation (SSF). Inhibitor was produced on solid support (WB) supplemented with the inducer, SBM. The time profile for inhibitor production was studied under SSF. It was observed that maximum inhibitor production was obtained at 6<sup>th</sup> day of fermentation (Figure 13). Different combinations of WB and SBM were used for the optimization of appropriate cocktail of the support and the inducer. As revealed from Table 3, the optimum combination of WB and SBM was found to be 0.5% and 1g% respectively.

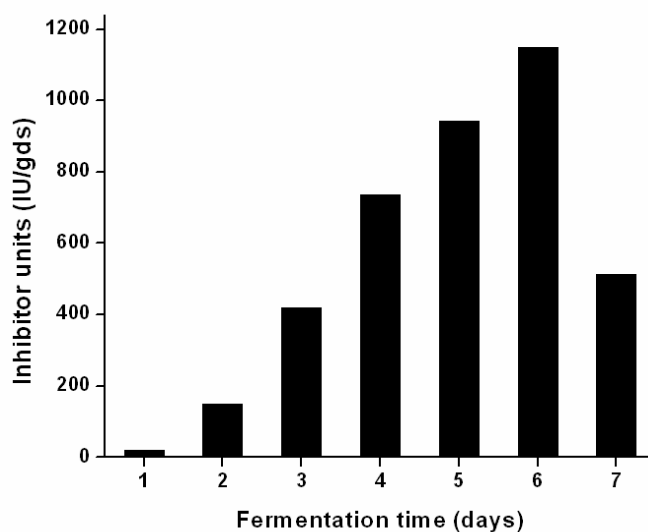


Figure 13 Time course for inhibitor production in SSF using *Penicillium sp* VM24

Table 3 Different combination of WB and SBM for inhibitor production in SSF

Wheat bran (WB)	Soybean meal (SBM)	IU/gds
0.5	0.5	428
	1	1150
	1.5	634
1	0.5	318
	1	212
	1.5	519
1.5	0.5	638
	1	420
	1.5	123

## DISCUSSION

Recently rational drug design using the three-dimensional structure of an enzyme's active site to predict inhibitors are being well-studied. Computer-based methods of predicting the affinity of an inhibitor for an enzyme are also being developed, such as molecular docking and molecular mechanics (Dash et al., 2004). There have been numerous reports of synthetic inhibitors of aspartic proteases over past few decades. However, there is a paucity of inhibitors from natural resources. To our knowledge, there are only two genus reported for aspartic protease inhibitors ie *Streptomyces* (Umezawa 1982) and *Bacillus* (Dash et al., 2001; Kumar and Rao 2006). After extensive screening of various microbes, we have isolated two potent cultures, *Streptomyces* sp MBR04 and *Penicillium* sp VM24 for the production of aspartic protease inhibitor. The isolates were purified and identified based on the morphological, biochemical and DNA sequencing studies. The 16S rDNA sequence of *Streptomyces* sp MBR04 and the ITS gene sequence of *Penicillium* sp VM24 were submitted to NCBI GenBank with the accession numbers JN627518 and JN673378 respectively. The medium was optimized for the production of inhibitor from *Streptomyces* sp MBR04 and the inhibitor production in optimized medium was increased 11 fold as compared to basal medium. The inhibitor exhibited inhibitory activity towards pepsin. Aspartic protease inhibitor production was studied from *Penicillium* sp VM24 in SmF and SSF. The inhibitor was found to inhibit fungal aspartic protease from *Aspergillus saitoi*. SmF produced 154 IU/ml of inhibitor in a complex media containing glucose beef extract with soya meal as inducer at 28°C and pH 5.0 in 96 h wherein SSF produced 1148 IU/g of inhibitor in a media containing wheat bran and soy meal in 6 days. This is the first report of a fungal isolate producing aspartic protease inhibitor. More over the inhibitors being extracellular and from microbial origins offers tremendous potential for commercial production.

**BIBLIOGRAPHY**

Buchanan RH, Gibbons NE (1974) Bergeys manual of determinative bacteriology. 8<sup>th</sup> ed, William and Wilkins Co, Baltimore, pp 747-842.

Dash C, Kulkarni A, Dunn B, Rao M (2003) *Crit Rev Biochem Mol* **38**, 89-119.

Dash C, Phadtare S, Desphande VV, Rao M (2001) *Biochemistry* **40**, 11525-11532.

Demain AL (2000) *Biotechnol Adv* **18**, 499-514.

Frisvad, JC, Samson RA (2004) *Stud Mycol* **49**, 1-174.

Ge HM, Shen Y, Zhu CH, Tan SH, Ding H, Song, YC, Tan, RX (2008) *Phytochemistry* **69**, 571-576.

Hopwood DA, Bibb MJ et al (1985) In: Genetic Manipulation of *Streptomyces*-A laboratory manual. The John Innes Foundation, Norwich, England.

Krieg NR, Ludwig W, Whitman, WB, Hedlund BP, et al (1989) Bergey's Manual of Systematic Bacteriology. 2<sup>nd</sup> ed, Williams and Wilkins, Baltimore, pp 948.

Kumar A, Rao M (2006) *Biochim Biophys Acta* **1760**, 1845-1856.

Kwon OE, Mun-Chual R, Young SH, Woong LS, Yeon CM, Hyun J, Ho KY, Sun LH, Young-Kook K (2002) *J Antibiot* **55**, 1004-1008.

Larsen TO, Lange L, Schnorr K, Stender S, Frisvad JC (2007) *Tetrahedron Lett* **48**, 1261-1264.

Lodhi MA, Ye GN, Weeden NF, Reisch BI (1994) *Plant Mol Biol Reporter* **12**, 6-13.

Lucas EMF, Castro MCM, Takahashi JA (2007) *Braz J Microbiol* **38**, 785-789.

Moran MA, Rutherford LT, Hodson RE (1995) *Appl Environ Microbiol* **61**, 3695-3700.

Nicoletti R, Lopez-Gresa MP, Emiliano M, Angela C, Letizia CM (2007) *Mycopathologia* **163**, 295-301.

- Paradkar A, Trefzer A, Chakraborty R, Stassi D (2003) *Crit Rev Biotechnol* **23**, 1-27.
- Pitt JI (2000) A laboratory guide to common *Penicillium* species. 3rd Ed, Food Science Australia Publishers, pp 197.
- Rancic A, Sokovic M, Karioti A, Vukojevic, J, Skaltsa H (2006) *Environ Toxicol Phar* **22**, 80-84.
- Sanger F, Nicklen S, Coulson AR (1977) *Proc Natl Acad Sci USA* **74**, 5463-5467.
- Schatz A, Bugie E, Waksman SA (1944) *Proc Soc Exptl Biol Med* **55**, 66-69.
- Takahashi JA, Lucas EMF (2008) *Quim Nova* **31**, 1807-1813.
- Umezawa H (1982) *Ann Rev Microbiol* **36**, 75-99.
- Waksman SA, Woodruff HB (1940) *J Bacteriol* **40**, 581-600.
- White TJ, Bruns T, Lee S, Taylor JW (1990) Amplification and direct sequencing of fungal ribosomal RNA genes for phylogenetics. In PCR protocols: a guide to methods and applications, New York, Academic press, pp. 315-322.

# CHAPTER 3

*‘Nothing has such power to broaden the mind as the ability to investigate systematically and truly all that concerns under your observation in life’*

Marcus Aurelius



**Purification and characterization of aspartic  
protease inhibitors from *Streptomyces* sp  
MBR04 and *Penicillium* sp VM24**

## SUMMARY

The extracellular culture filtrates of *Streptomyces* sp MBR04 and *Penicillium* sp VM24 were subjected to activated charcoal treatment, ultrafiltration and gel filtration to remove high molecular weight impurities and salts. The inhibitors were concentrated by lyophilization and were further purified to homogeneity by rp-HPLC. The purified inhibitor showed a specific activity of 429 U/mg and a 59 fold increase in purification with a yield of 15% from *Streptomyces* sp MBR04. The inhibitor was stable in a broad range of pH (2-6) and temperatures (25-40°C). The molecular mass of the inhibitor was 1078 Da as determined by mass spectrometry (MALDI-TOF) and revealed a single homogenous band with a Mr of 1072 on Tricine-SDS-PAGE. Amino acid composition of inhibitor showed the presence of D, D G, A, K, L, Y, W residues and CD spectrum conceded the absence of any periodic structure in the secondary structure of the inhibitor.

The purified inhibitor from *Penicillium* sp VM24 showed a specific activity of 350 U/mg and a 52 fold increase in purification with a yield of 18%. The inhibitor showed stability in a broad range of pH (2-6) and temperatures (25-40°C). The molecular mass of the inhibitor was 1585 Da as determined by mass spectrometry (MALDI-TOF) and revealed a single homogenous band with Mr of 1580 on Tricine-SDS-PAGE. Amino acid composition of inhibitor showed D, D, D, E, A, H, K, L, I, Y, W residues. The secondary structure determination by CD analysis revealed the presence of 6.5%  $\alpha$ -helix, 49%  $\beta$ -sheet, and 45% aperiodic structures. The inhibitor from *Streptomyces* sp was found to inhibit pepsin and cathepsin D and the inhibitor from *Penicillium* sp inhibited fungal aspartic protease. The inhibitors exhibited no inhibitory activity against other classes of proteases like trypsin, chymotrypsin, papain and subtilisin.

## INTRODUCTION

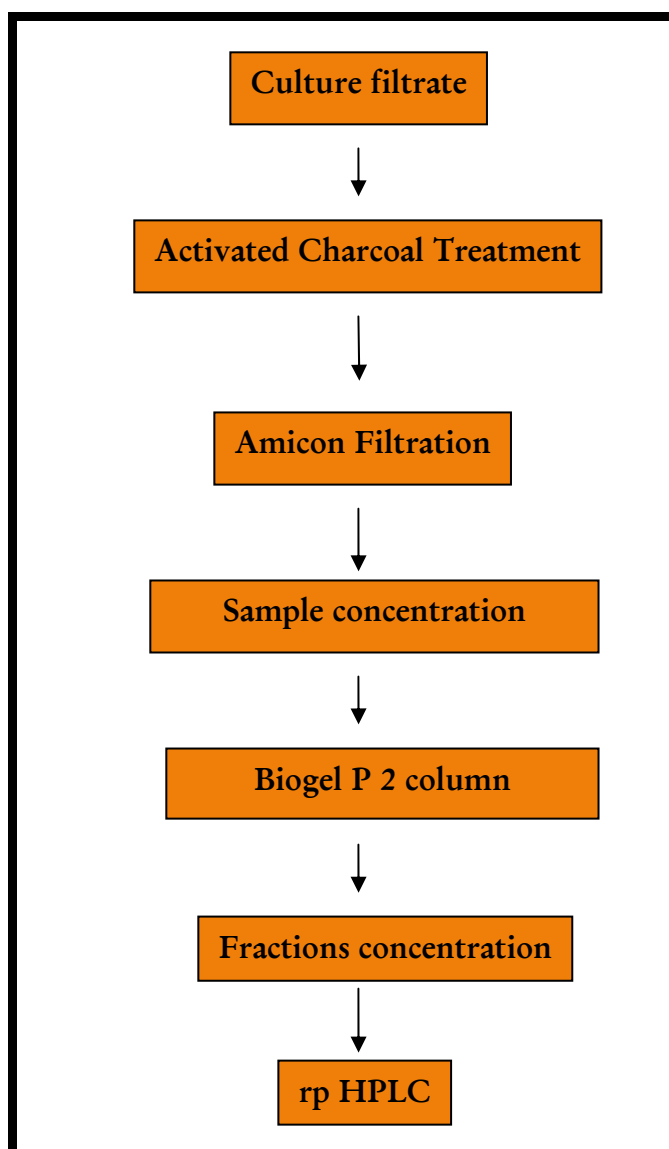
The development of potent enzyme inhibitors has led to a detailed understanding of enzyme mechanisms and has provided effective therapeutic agents for the treatment of diseases. Inhibitors serve as probes for kinetic and chemical processes during catalysis. For example, they help in elucidating the mode of ligand binding, where the ligand may be an inhibitor, substrate, or substrate analogue. Alternative applications for inhibitors are the detection of short-lived enzyme-bound reaction intermediates, or the identification of amino acid residues at the active site that are necessary for the catalytic activity of the enzyme. Inhibitors are also used for *in vivo* studies to localize and quantify enzymes in organs or to mimic certain genetic diseases that involve the absence of an enzyme in given biosynthetic pathway. An increased understanding of the enzymes specificity for the substrate and inhibitor binding enables a more rational design of potent inhibitors, selective for a particular enzyme.

For assessing the physiological function of newly isolated protease inhibitors, the purification of the inhibitor to homogeneity is highly recommended. Most of the proteinaceous inhibitors of proteases range in molecular size from 3000 - 80,000 Da (Dubin 2005; Joanitti 2006) and microbial inhibitors range from 1000 - 2000 Da (Umezawa 1982; Dash and Rao 2001; Kumar and Rao 2006; Kulkarni and Rao 2009). The conventional purification procedures such as ion exchange chromatography, gel filtration chromatography, reversed-phase high-performance liquid chromatography (rp-HPLC), fast protein liquid chromatography, isoelectric focusing and preparative gel electrophoresis are applied to purify inhibitors from various sources. The most relevant method of protease inhibitor purification is the use of affinity ligands. Aspartic proteases play an important role in digestion, lysosomal protein degradation, regulation of blood pressure and in several diseases (Dash et al., 2003). The understanding of the structure and function relationships of aspartic protease have a direct impact on the design of inhibitor drugs. The present chapter describes the purification and biochemical characterization of aspartic protease inhibitors from *Streptomyces* sp MBR04 and *Penicillium* sp VM24.

## EXPERIMENTAL PROCEDURES

### *Production and purification of inhibitors from Streptomyces sp MBR04 and Penicillium sp VM24*

*Streptomyces* sp MBR04 and *Penicillium* sp VM24 were cultured in a liquid medium containing soy meal (SBM) (2%) as an inducer and other nutrients such as glucose (1%), beef extract (0.75%), sodium chloride (0.3%), magnesium sulfate (0.1%) and dipotassium hydrogen phosphate (0.1%) for inhibitor production at 28°C.



Purification protocol for inhibitors

The extracellular culture filtrate was obtained by centrifugation of growth medium constituents at 10,000 rpm at 4°C for 30 min. The supernatant was subjected to treatment with activated charcoal to remove the coloring impurities. The resulting filtrate was subjected to ultrafiltration using membrane cutoffs of 10,000, 3000 and 500 daltons successively. The resulting filtrate from 500 dalton cutoff was desalted using gel filtration (Biogel P-2). The sample was eluted with 0.05 M glycine-HCl buffer, pH 3.0. The fractions were assayed for inhibitor activity towards pepsin and fungal aspartic protease for *Streptomyces* sp MBR04 and *Penicillium* sp VM24 respectively. The active fractions were lyophilized and loaded onto a prepacked UltroPac column (fluka RP-C 8) pre-equilibrated with 90% acetonitrile (CH<sub>3</sub>CN) and 0.05% trifluoroacetate (TFA). The fractions were eluted on a linear gradient of 0–90% acetonitrile with H<sub>2</sub>O containing 0.05% TFA at a flow rate of 0.5 ml/min and monitored at a wavelength of 210 nm. The eluted sample was lyophilized and dissolved in deionized water and checked for inhibitory activity as mentioned above. The active fractions were rechromatographed on rp-HPLC under similar experimental conditions as mentioned above. The active peak was finally purified by rp-HPLC.

#### *Assay for inhibitory activity towards pepsin and fungal aspartic protease for purification of the inhibitors*

Pepsin and fungal aspartic protease inhibition assay were performed as described in chapter 2 for the purification of inhibitors from *Streptomyces* sp MBR04 and *Penicillium* sp VM24 respectively.

#### *Determination of molecular weight of the inhibitors*

##### *a. MALDI-TOF*

The molecular weight of the inhibitors was determined by the mass spectroscopy (MALDI-TOF). Mass spectral analysis was performed on a Voyager-De-STR (Applied Biosystems) MALDI-TOF. Spectra were acquired in the range of 500–2000 Da, in linear mode with delayed ion extraction and with an accelerating voltage of 25 kV. All the analyses were performed in four replications.

### *b. Tricine-SDS-PAGE*

Tricine-sodium dodecyl sulfate-polyacrylamide gel electrophoresis (Tricine-SDS-PAGE) was done as described by Schagger (2006). Inhibitor samples (1  $\mu$ g) were electrophoresed in 16% Tris-Tricine gels at a constant voltage of 200 V using Tris-HCl as anode buffer and Tris-Tricine-SDS as cathode buffer for 5 h. The gels were fixed with 50% methanol, 10% acetic acid and 100 mM ammonium acetate for 30 min. The peptides were visualized in the gel by silver staining.

### *Amino acid analysis*

The amino acid analysis was done by hydrolyzing 100 pM of inhibitor with 6N HCl at 110°C for 24 h in vacuum sealed tubes. The hydrolyzed amino acids were derivatized with AccQ Fluor Reagent (6-amino quinolyl-N-hydroxysuccinimide carbamate) and run on a prepacked rp-HPLC 3.9 $\times$ 150mm column AccQ.Tag. The amino acids were eluted with acetonitrile gradient (5-95%) and monitored with a fluorescence detector. To calculate the molar proportion of constituents, the peak areas of individual amino acids were compared with standards running under identical conditions. Total cysteine and tryptophan were estimated with intact peptide according to the method of Cavallini et al (1966) and Spande and Witkop (1967) respectively.

### *Protein concentration*

Protein concentration was determined according to Bradford method (1976), using bovine serum albumin as the standard.

### *Secondary structure determination of the inhibitors*

CD spectra were recorded in a Jasco-J715 spectropolarimeter at ambient temperature using a cell of 1-mm path length. Replicate scans were obtained at 0.1 nm resolutions, 0.1 nm band widths and at a scan speed of 50 nm/min. Spectra were averages of six scans with the base line subtracted spanning from 280 to 200 nm in 0.1 nm increments. The CD spectrum of the inhibitors (10  $\mu$ M and 25  $\mu$ M for *Streptomyces* sp MBR04 and *Penicillium* sp VM24 respectively) was recorded in 50

mM HCl. Secondary structure content of the inhibitors were calculated using the algorithm of the K2d program (Andrade 1993).

### *Temperature and pH stability*

For the temperature stability experiments, the inhibitors (10  $\mu$ M) were incubated at temperatures 25–50°C for 6 h and the inhibitory activity was determined towards pepsin and aspartic protease from *Aspergillus saitoi* for *Streptomyces* sp MBR04 and *Penicillium* sp VM24 respectively at different intervals of time. The pH stability of the inhibitor was determined by pre-incubating the inhibitor (10  $\mu$ M) in a range of pH values in appropriate buffers for 1 h and estimating the anti-proteolytic activities as mentioned above.

### *Assay for inhibitory activity of inhibitors towards cathepsin D and other classes of proteases*

The inhibitory activity of the inhibitors against cathepsin D (5 nM) was assayed using hemoglobin as the substrate under aspartic protease inhibition assay conditions mentioned in chapter 2.

#### *a. Chymotrypsin Assay*

The inhibitory activity of the inhibitors against chymotrypsin, was determined by assaying the proteolytic activity of 25  $\mu$ l of chymotrypsin (1 mg/ml) in 0.05 M borax-boric acid buffer, pH 8.0, in the presence of 0.1 M CaCl<sub>2</sub>, using casein (1%) as the substrate in the presence or absence of the inhibitor. The assay was also performed with the synthetic substrate Bz-Tyr-pNA under similar conditions (Walsh 1970).

#### *b. Trypsin Assay*

The anti-trypsin activity of the inhibitors was determined by incubating 5  $\mu$ l of trypsin (1 mg/ml) in the presence and absence of the inhibitor in a reaction mixture containing 0.05 M phosphate buffer pH 7.5 using casein (1%) as the substrate. The assay was also performed with the synthetic substrate Bz-L-Arg-pNA.HCl under similar conditions (Arnon 1970).

### *c. Subtilisin Assay*

The inhibitory activity of the inhibitor against subtilisin was determined by assaying the proteolytic activity of 15  $\mu$ l of subtilisin (0.5 mg/ml) in 0.05 M carbonate-bicarbonate buffer, pH 10.0, using casein (1%) as the substrate, in the presence or absence of the inhibitor. The assay was also performed with the synthetic substrate Z-Ala-Ala-Leu-pNA under similar conditions (Grant et al., 1981).

### *d. Papain Assay*

The anti-papain activity of the inhibitors was determined by incubating 25  $\mu$ l of papain (0.5 mg/ml), in the presence or absence of inhibitor in a reaction mixture containing 0.05 M Tris-HCl buffer, pH 7.5, 20  $\mu$ l dithiothritol (1 M), using casein (1%) as the substrate. The assay was also performed with the synthetic substrate Bz-L-Arg-pNA.HCl under similar conditions (Arnon 1970).

### *Stability of the inhibitors in human serum and plasma*

Inhibitor stabilities were assayed in diluted serum as previously described (Cudic et al., 2002). 25% human serum was centrifuged at 10,000 rpm for 10 min to remove lipids and the supernatant was collected and incubated at 37°C for at least 15 min. The assay was initiated upon the addition of the inhibitor to the serum for a final concentration of 10 nM and 5  $\mu$ M for *Streptomyces* sp MBR04 and *Penicillium* sp VM24 respectively. The aliquots (200  $\mu$ l) were withdrawn at different time intervals and mixed with 40  $\mu$ L of 10% acidified TCA and incubated at 4°C for 30 min to precipitate serum proteins. The supernatant was collected after centrifugation at 10,000 rpm for 20 min. These assays were performed in triplicate. The inhibitory activity of the supernatant was assayed towards pepsin and fungal aspartic protease as described in chapter 2. The supernatant was also subjected to rp-HPLC under similar conditions mentioned above. A zero time sample (peptide, and serum, at pH 3) was used as a control. Similarly the inhibitors were subjected to *in vitro* human plasma stability studies to investigate their resistance toward proteolytic cleavage. *In vitro* plasma incubation closely reproduces the proteolytic activity in the blood (Falciani et al., 2007) and provides a good estimation of *in vivo* metabolism. The

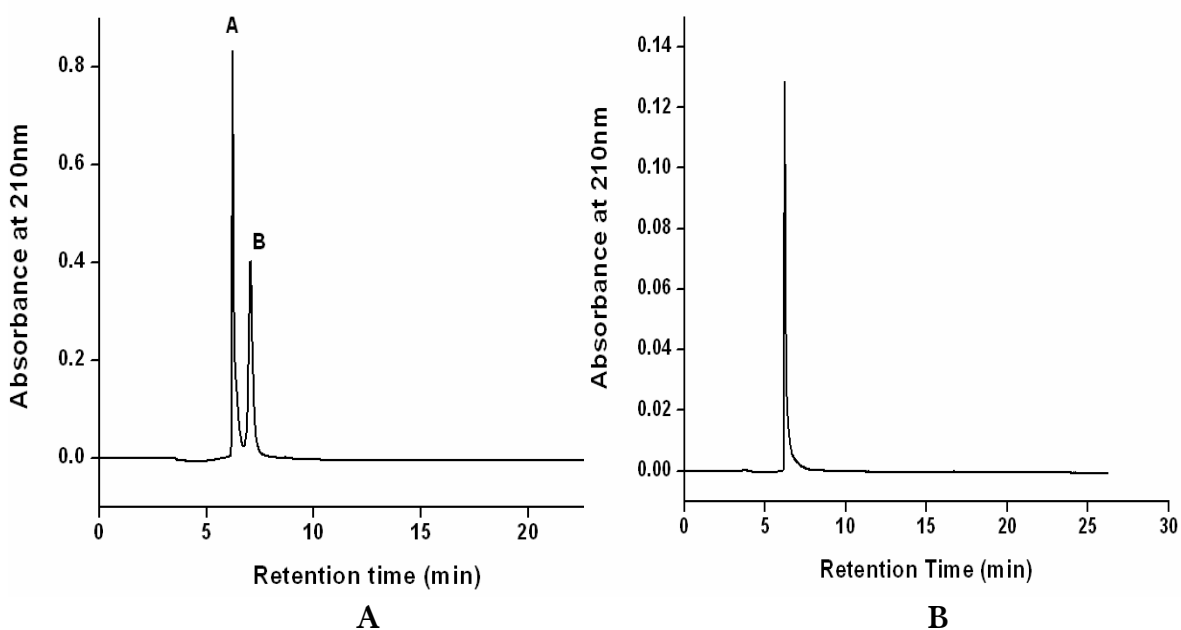


inhibitors (10 nM and 5  $\mu$ M for *Streptomyces* sp MBR04 and *Penicillium* sp VM24 respectively) were incubated in human plasma for different time intervals and assayed and detected under similar conditions as described for serum stability studies.

## RESULTS

### *Purification of inhibitor from Streptomyces sp MBR04*

The extracellular culture filtrate was subjected to activated charcoal treatment, ultrafiltration and gel filtration to remove high molecular weight impurities and salts. The gel filtration fractions showing the anti pepsin activity were concentrated and loaded on a C 8 pre packed column for rp-HPLC. The anti pepsin activity was associated with the peak A, having a retention time of 6.223 min (Figure 1A) and other eluted peak, B with retention times 7.049, showed no inhibitory activity. The fractions showing the inhibitory activity were pooled and lyophilized. Homogeneity of the active fractions containing peak A was indicated by a single peak as analyzed on rp-HPLC with the retention time of 6.223 (Figure 1B). The inhibitor was purified with 59 fold purification. Table 1 summarizes the results for the purification of inhibitor.



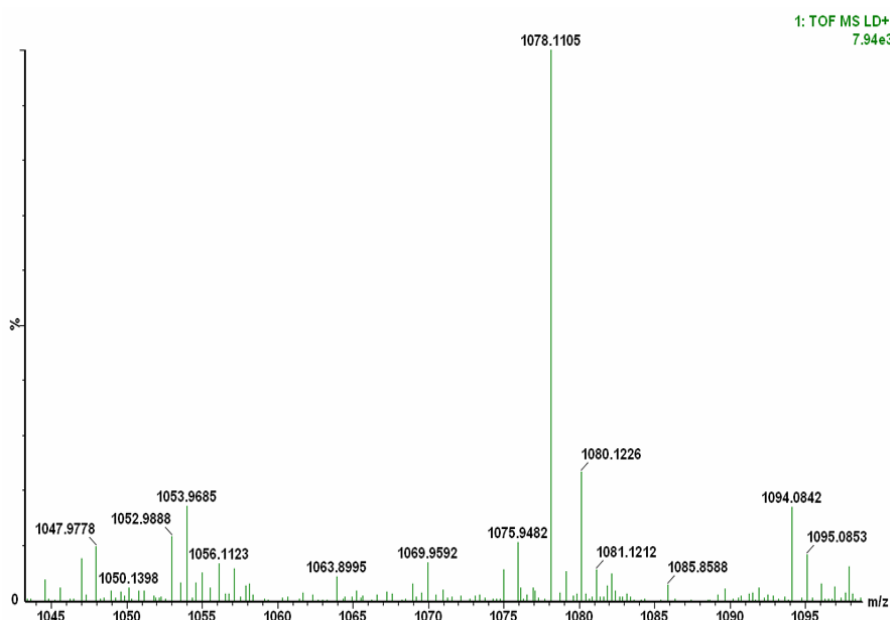
**Figure 1** Reverse phase-HPLC purification of the inhibitor (A) 5  $\mu$ l of the lyophilized inhibitor sample was loaded on prepacked UltroPac column (fluka RP-C 8) pre-equilibrated with acetonitrile ( $\text{CH}_3\text{CN}$ ) and trifluoroacetate (TFA). The fractions containing the peaks A, and B were collected manually and assayed for the antipepsin activity. (B) 10  $\mu$ l of the pooled fractions containing the peak A (associated with the antipepsin activity) was reloaded onto the reverse-phase HPLC system under similar experimental conditions. The peak detected showed a retention time of 6.223 min.

**Table 1** Purification of the inhibitor from *Streptomyces* sp MBR04

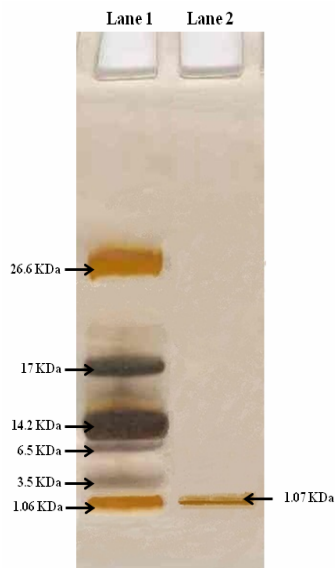
Purification step	Volume (ml)	Total activity (Units)	Total protein (mg)	Specific activity (Units/mg)	Purification (fold)	Yield (%)
Centrifugation	850	7650	1063	7.19	1	100
Activated charcoal	700	6300	630	10	1.39	82.35
Ultrafiltration 10kDa cut off	650	5850	390	15	2.06	76.47
Ultrafiltration 3kDa cut off	625	5488	125	43.90	6.03	71.74
Ultrafiltration 0.5kDa cut off	600	5352	80	66.9	9.19	69.96
Biogel P-2 column	15	2200	12.5	176	24.18	28.76
rp-HPLC	5	1200	2.8	429	58.94	15.69

### *Biochemical characterization of the inhibitor*

Homogeneity of the active fractions containing peak A was indicated by the single peak as analyzed on rp-HPLC, mass spectrometry (MALDI-TOF) showing Mr 1078 (Figure 2) and by Tricine SDS-gel electrophoresis showing Mr 1072 (Figure 3).

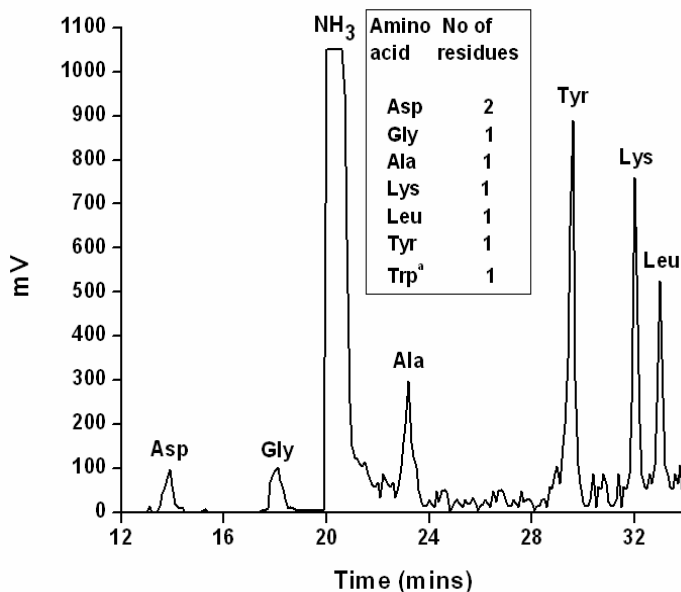


**Figure 2** Molecular weight of the inhibitor. The purified inhibitor was analyzed for the determination of molecular weight (1078 Da) by MALDI TOF.



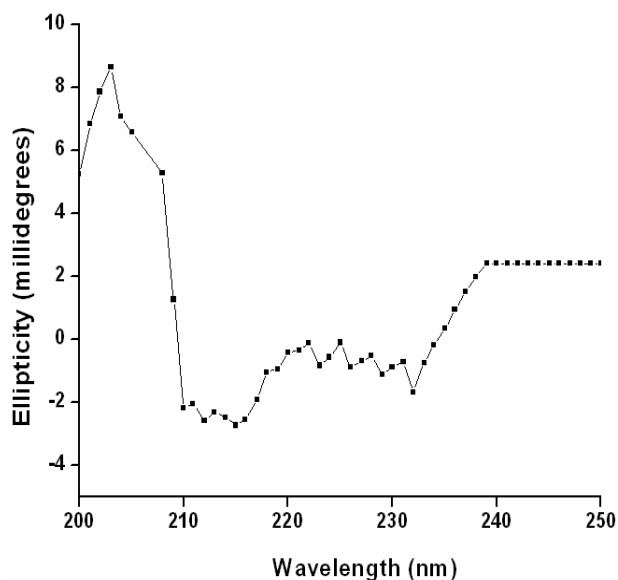
**Figure 3** Tricine-SDS-PAGE of the inhibitor loaded on 16% T, 6% C tris-tricine gel. Lane 1 shows the ultra-low standard molecular weight markers (Sigma) and Lane 2 shows the HPLC purified inhibitor.

The amino acid analysis of the inhibitor revealed the presence of 8 amino acid residues, D, D, G, A, K, L, Y, W (Figure 4) and a positive ninhydrin test indicated the peptidic nature of the inhibitor.



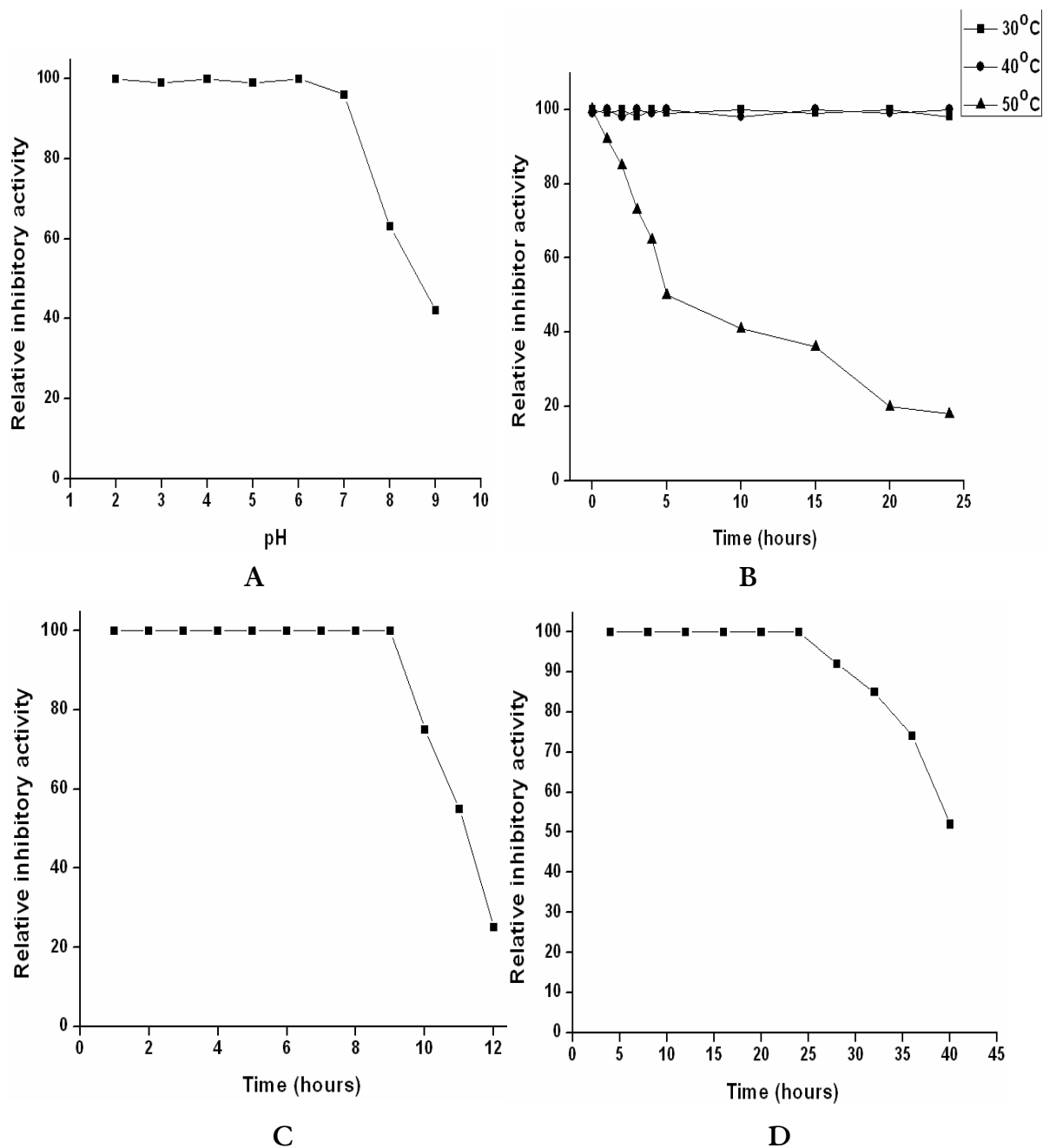
**Figure 4** The amino acid analysis was done by hydrolyzing 100  $\mu$ M of inhibitor with 6N HCl at 110°C for 24 h in vacuum sealed tubes. The hydrolyzed amino acids were derivatized with AccQ Fluor Reagent (6-amino quinolyl-N-hydroxysuccinimide carbamate) and run on a prepacked rp-HPLC 3.9 $\times$ 150 mm column AccQ.Tag. The amino acids were eluted with acetonitrile gradient (5-95%) and monitored with a Waters fluorescence detector. <sup>a</sup>Tryptophan determined by 2-nitrobenzenesulfonyl chloride (NBS).

CD spectra of the inhibitor was analyzed to determine the secondary structure of the inhibitor. The secondary structure revealed a negative band at approximately 205 nm, which is characteristic feature of random coil (Figure 5). The secondary structure content calculated from the data obtained from the CD spectrum by the algorithm of K2d program showed no periodic structure in the peptidic inhibitor.



**Figure 5** Far-UV CD spectrum of the inhibitor. Inhibitor (10  $\mu\text{M}$ ) was dissolved in 50 mM HCl and the CD spectrum was recorded from 280 to 200 nm at 25°C. The spectrum shown is the average of six scans with the baseline subtracted. The data are expressed in terms of ellipticity as measured in millidegrees.

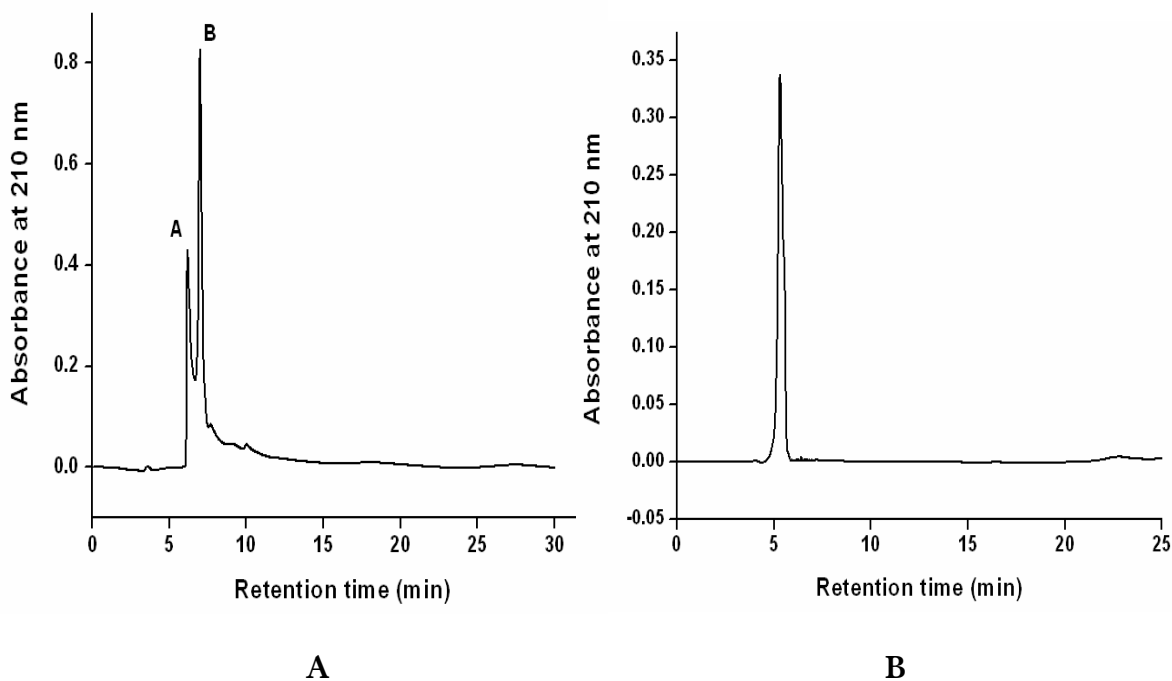
The inhibitor was stable in a broad range of pH (2-6) and temperatures (25-40°C) (Figure 6 A & B). Inhibitor was stable in human serum and plasma for 9 and 24 h respectively at 37°C (Figure 6 C & D).



**Figure 6** pH (A), temperature (B), serum (C) and plasma (D) stability of the inhibitor. The inhibitor was treated with various buffers of different pHs and its anti-pepsin activity was determined at different time intervals. Inhibitor was incubated at 30, 40 and 50°C for different time intervals and the anti-pepsin activity was determined at 37°C. For serum and plasma stability, inhibitor was incubated in human serum and plasma for specified time and the inhibitory activity was determined against pepsin and the intact peptide was detected using rp-HPLC as mentioned in experimental procedures.

### *Purification of inhibitor from Penicillium sp VM24*

The extracellular culture filtrate of the *Penicillium* sp VM24 was subjected to activated charcoal treatment and ultra filtration to remove the high molecular weight impurities. The inhibitor sample was concentrated by lyophilization. This concentrated inhibitor sample was further purified by rp-HPLC. The anti-aspartic protease activity was associated with the peak A, having a retention time of 5.532 min (Figure 7A) and other eluted peak B showed no inhibitory activity. The fractions showing the inhibitory activity were pooled and lyophilized. Homogeneity of the active fractions containing peak A was indicated by the single peak as analyzed on rp-HPLC with the retention time of 5.560 (Figure 7B). The purified inhibitor showed a specific activity of 350 U/mg and a 52 fold increase in purification with a yield of 18% (Table 2).



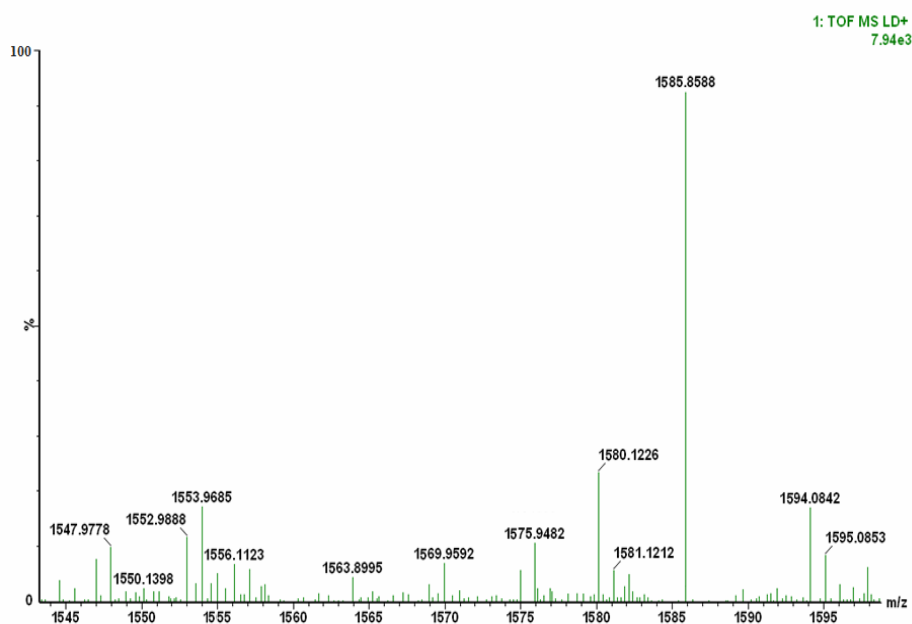
**Figure 7** Reverse phase-HPLC purification of the inhibitor. (A) 10  $\mu$ l of the lyophilized inhibitor sample was loaded on a linear gradient of 0-50% acetonitrile with water containing 0.01% trifluoroacetate for 15 min at a flow rate of 0.5 ml/min and monitored at 210 nm. The fractions containing the peaks A and B were collected manually and assayed for the antiproteolytic activity. (B) 2.5  $\mu$ l of the pooled fractions containing the peak A (associated with the antiproteolytic activity) was reloaded onto the reverse-phase HPLC system under similar experimental conditions. The peak detected showed a retention time of 5.560 min.

**Table 2** Purification of inhibitor from *Penicillium* sp VM24

Purification step	Volume (ml)	Total activity (Units)	Total protein (mg)	Specific activity (Units/mg)	Purification (fold)	Yield (%)
Centrifugation	650	4083	607.61	6.72	1	100
Activated charcoal	600	3498	280	12.49	1.86	85.67
Ultrafiltration 10kDa cut off	575	2942	86.25	34.11	5.08	72.05
Ultrafiltration 3kDa cut off	550	2648	48.03	55.13	8.12	64.85
Ultrafiltration 0.5kDa cut off	525	2458	35.62	69.03	10.28	60.19
Biogel P-2 column	12	1821	10.38	176.75	26.32	44.59
rp-HPLC	3.5	735	2.14	350	52.12	18.14

### *Biochemical characterization of the inhibitor*

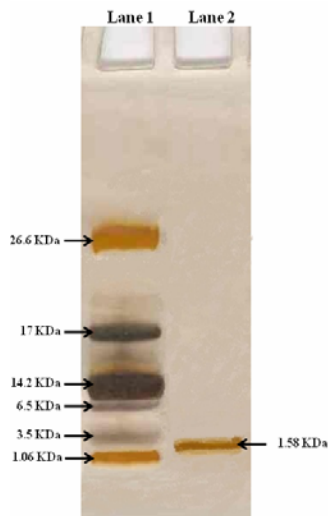
The molecular weight of inhibitor as determined by mass spectrometry (MALDI-TOF) was 1585 Da (Figure 8).



**Figure 8** Molecular weight of the inhibitor. The purified inhibitor was analyzed for the determination of molecular weight (1585 Da) by MALDI TOF.

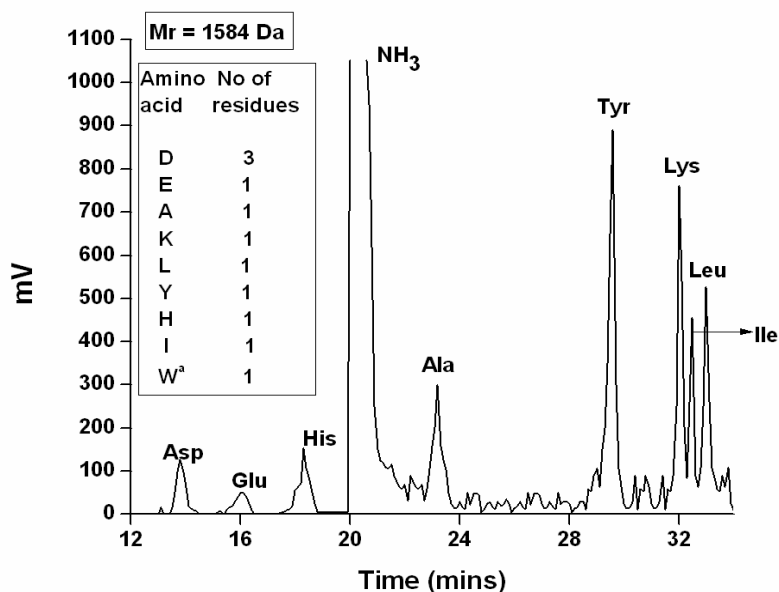


The inhibitor revealed a single homogenous band with a Mr of 1580 on Tricine-SDS-PAGE (Figure 9).



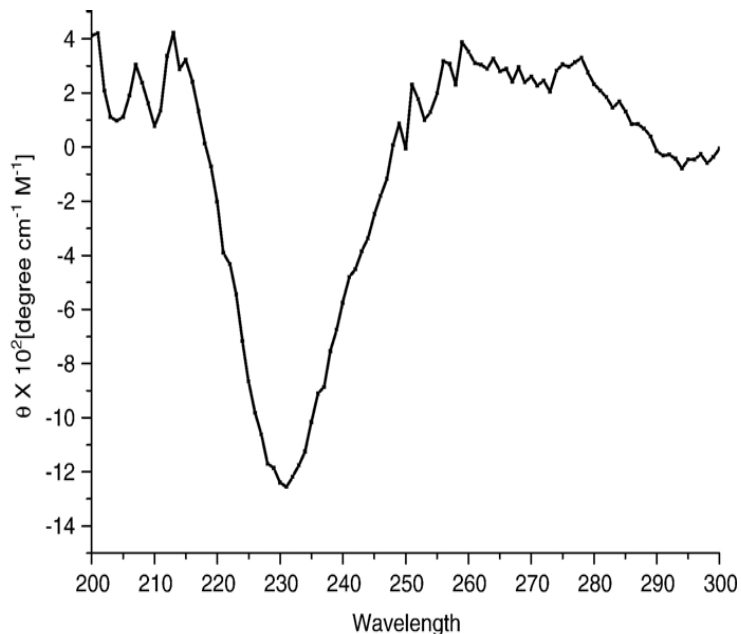
**Figure 9** Tricine-SDS-PAGE of the inhibitor loaded on 16% T, 6% C tris-tricine gel. Lane 1 shows the ultra-low standard molecular weight markers and Lane 2 shows the purified inhibitor.

The positive ninhydrin test with the purified inhibitor revealed its peptidic nature. Amino acid composition data showed the predominance of aspartic acid in the inhibitor. The amino acid composition of the purified inhibitor revealed the presence of D, D, E, A, K, L, Y, H, I, W residues (Figure 10).



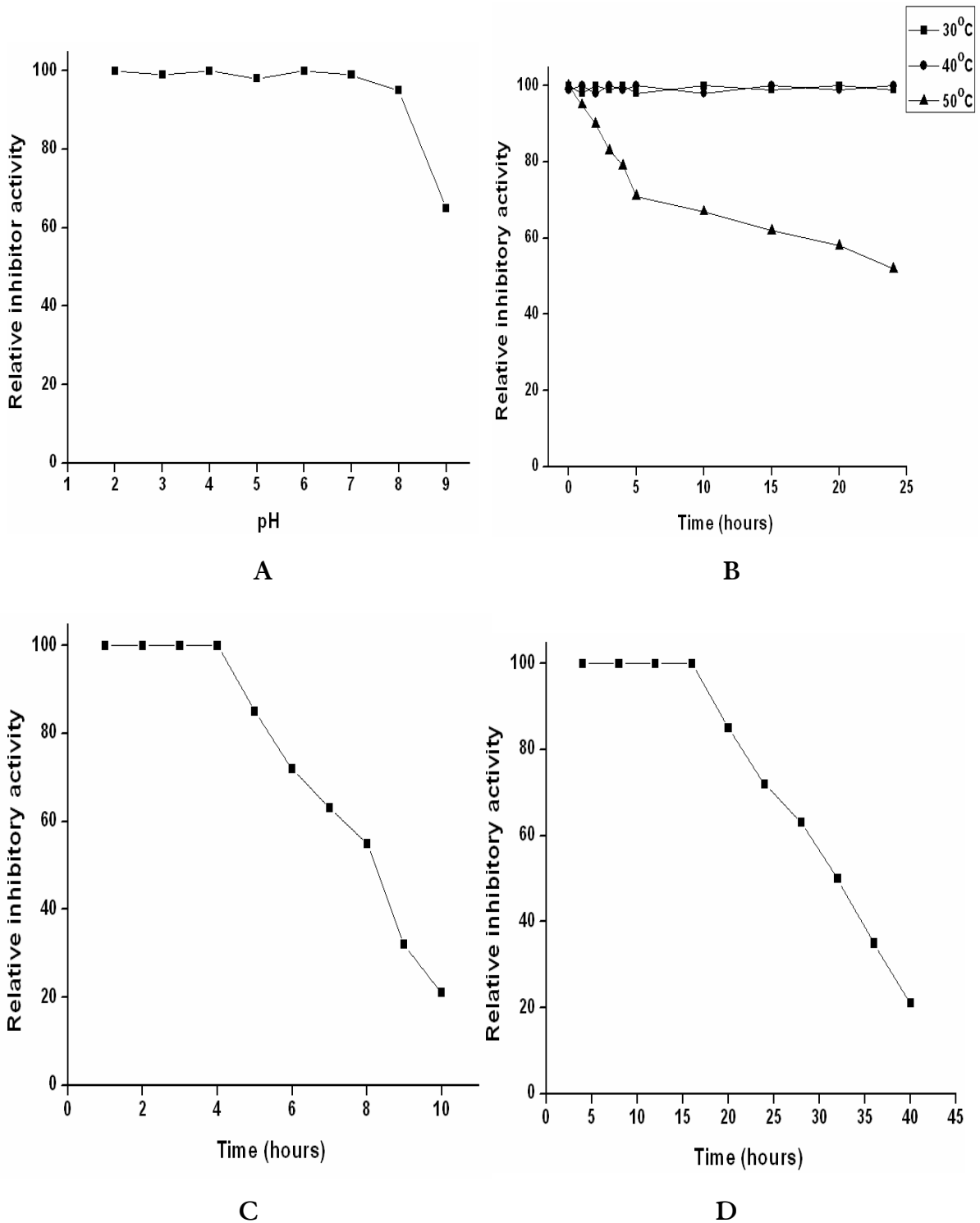
**Figure 10** The amino acid analysis was done by hydrolyzing 100 pM of inhibitor with 6N HCl at 110°C for 24 h in vacuum sealed tubes. The hydrolyzed amino acids were derivatized with AccQ Fluor Reagent and run on a prepacked rp-HPLC. The amino acids were eluted with acetonitrile gradient (5-95%) and monitored with a Waters fluorescence detector. <sup>a</sup>Tryptophan determined by NBS.

To evaluate the secondary structure of the inhibitor, the CD spectrum was analyzed. The estimated secondary structure contents from the CD analysis were 6.5%  $\alpha$ -helix, 49%  $\beta$ -sheet, and 45% aperiodic structure (Figure 11).



**Figure 11** Far-UV CD spectra analysis of the inhibitor to analyze the secondary structure of the inhibitor. The inhibitor (25  $\mu\text{M}$ ) was dissolved in 0.05N HCl and the CD spectra were recorded from 300 to 190 nm at 25  $^{\circ}\text{C}$ . Spectrum represents the average of six scans.

The inhibitor was stable in a broad range of pH (2-6) and temperatures (25-40 $^{\circ}\text{C}$ ) (Figure 12 A & B). Inhibitor was stable in human serum and plasma for 4 and 16 h respectively at 37 $^{\circ}\text{C}$  (Figure 12 C & D).



**Figure 12** pH (A), temperature (B), serum (C) and plasma (D) stability of the inhibitor. The inhibitor was treated with various buffers of different pHs and its anti-pepsin activity was determined at different time intervals. Inhibitor was incubated at 30, 40 and 50°C for different time intervals and the anti-pepsin activity was determined at 37°C. For serum and plasma stability, inhibitor was incubated in human serum and plasma for specified time and the inhibitory activity was determined against pepsin and the intact peptide was detected using rp-HPLC as mentioned in experimental procedures.

The inhibitor from *Streptomyces* sp MBR04 was found to inhibit cathepsin D and pepsin and showed less inhibitory activity towards fungal aspartic protease. The inhibitor from *Penicillium* sp VM24 showed inhibitory activity towards fungal aspartic protease and had very low inhibitory activity towards pepsin and no inhibitory activity towards cathepsin D. Inhibitors when tested for its anti-proteolytic potency towards proteases belonging to other classes, such as trypsin, chymotrypsin, subtilisin, and papain, exhibited no inhibitory activity. These results indicated the specificity of the inhibitors towards the aspartic protease class (Table 3).

**Table 3** Inhibitory activity of the inhibitors towards aspartic proteases

Source of inhibitors	Enzymes		
	Pepsin	Fungal aspartic protease	Cathepsin D
	Percent inhibition		
<i>Streptomyces</i> sp MBR04	85	26	90
<i>Penicillium</i> sp VM24	35	70	No inhibition

*Substrate used for the assay was hemoglobin. For assay conditions and buffer compositions, refer to experimental procedures.*

## DISCUSSION

Low molecular weight peptidic aspartic protease inhibitors from microbes are reported from *Streptomyces* sp and *Bacillus* sp. *Streptomyces* sp is reported to produce pepstatin, an aspartic protease inhibitor containing an isovaleryl group with an Mr of 685 (Umezawa 1982). A low molecular weight peptidic inhibitor purified from the extracellular culture broth of an extremophilic *Bacillus* sp was found to exhibit inhibitory activity against HIV protease, pepsin and F-prot (Dash and Rao 2001; Dash et al., 2001). The molecular weight of the inhibitor was 1147 Da. Another low molecular weight peptidic inhibitor was isolated from a thermotolerant *Bacillus licheniformis* and exhibited inhibitory activity against pepsin. The molecular weight of the inhibitor was 1363 Da as shown by MALDI-TOF spectra and 1358 Da as analyzed by SDS-PAGE. The amino acid analysis of the peptide shows the presence of 12 amino acid residues. The secondary structure of the inhibitor as analyzed by the CD spectra showed  $\alpha$ -helix,  $\beta$ -sheet and aperiodic structure (Kumar and Rao 2006). In the present work, the extracellular culture filtrates of *Streptomyces* sp MBR04 and *Penicillium* sp VM24 were subjected to activated charcoal treatment, ultrafiltration and gel filtration to remove high molecular weight impurities and salts. The concentrated inhibitor samples were further purified to homogeneity by rp-HPLC. The molecular mass of inhibitor from *Streptomyces* sp MBR04 and *Penicillium* sp VM24 as determined by mass spectrometry (MALDI-TOF) were 1078 and 1585 Da respectively. Inhibitor from *Streptomyces* sp and *Penicillium* sp revealed a single homogenous band with a Mr of 1072 and 1580 Da on Tricine-SDS-PAGE respectively. Amino acid composition of the inhibitor from *Streptomyces* sp showed the presence of D, D, G, A, K, L, Y, W residues and from *Penicillium* sp showed D, D, D, E, A, H, K, L, I, Y, W residues. The inhibitor from *Streptomyces* sp MBR04 was found to inhibit cathepsin D and pepsin and the inhibitor from *Penicillium* sp VM24 showed inhibitory activity towards fungal aspartic protease. The inhibitors had no inhibitory activity against other classes of proteases like trypsin, chymotrypsin, papain and subtilisin.

**BIBLIOGRAPHY**

- Andrade MA, Chacon P, Merelo JJ, Moran F (1993) *Protein. Eng* **6**, 383-390
- Arnon R (1970) Proteolytic enzymes. In: Perlmann GE, Lorand L (eds) *Methods in enzymology*, Academic press, NY, pp 226-244
- Bradford MM (1976) *Anal. Biochem* **72**, 248-254
- Cavallini D, Graziani MT, Dupre S (1966) *Nature* **212**, 294-295
- Cudic M, Condie BA, Weiner DJ, Lysenko ES, Xiang ZQ, et al (2002) *Peptides* **23**, 2071-2083.
- Dash C, Kulkarni A, Dunn B, Rao M (2003) *Crit Rev Biochem Mol* **38**, 89-119.
- Dash C, Phadtare S, Desphande VV, Rao M (2001) *Biochemistry* **40**, 11525-11532.
- Dash C, Rao M (2001) *J Biol Chem*, **276**, 2487-2493.
- Dubin G (2005) *Cell Mol Life Sci.* **62**, 653-669.
- Falciani C, Lozzi L, Pini A, Corti F, Fabbrini M, Bernini A, Lelli B, Niccolai N, Bracci L (2007) *Chem Biol Drug Des* **69**, 216-221.
- Grant GA, Eisen AZ, Bradshaw RA (1970) Proteolytic enzymes. In: Perlmann GE, Lorand L (eds) *Methods in enzymology*, Academic press, NY, pp 722-734
- Joanitti GA, Freitas SM, Silva LP (2006) *Current Enzyme Inhibition* **2**, 199-217
- Kulkarni A, Rao M (2009) *Peptides* **30**, 2118-2126.
- Kumar A, Rao M (2006) *Biochim Biophys acta* **1760**, 1845-1856.
- Schagger H (2006) *Nature Protocols* **1**, 16-22
- Spande TF, Witkop B (1967) Determination of tryptophan content of proteins with N-bromosuccimide. In: Hirs CHW (ed). *Methods in Enzymology*, Academic press, NY, pp 498-506
- Umezawa H (1982) *Ann Rev Microbiol* **36**, 75-99.
- Walsh KA (1970) Proteolytic enzymes. In: Perlmann GE, Lorand L (eds) *Methods in enzymology*, Academic press, NY, pp 41-63.

# CHAPTER 4

*‘Every great advance in science has issued from a new  
audacity of the imagination’*

**John Dewey**

**Mechanistic and structural insights into the inhibition of therapeutically significant aspartic protease by inhibitor from *Streptomyces* sp MBR04**



## **PART A**

### **Kinetic interactions of pepsin with the inhibitor: Correlation to inhibitor induced conformational changes**

## SUMMARY

A low molecular weight aspartic protease inhibitor from *Streptomyces* sp MBR04 exhibiting a two-step inhibition mechanism against pepsin is reported. The kinetic interactions revealed a reversible, competitive, time-dependent slow-tight binding inhibition with an  $IC_{50}$  and  $K_i$  values of 4.5 nM and 4 nM respectively. The inhibition followed a rapid equilibrium step to form a reversible enzyme-inhibitor complex (EI), which isomerizes to the second enzyme inhibitor complex (EI\*), which dissociated at a very slow rate. The rate constants determined for the isomerization of EI to EI\* and for the dissociation of EI\* were  $2.65 \pm 0.32 \text{ s}^{-1}$  and  $0.070 \pm 0.01 \text{ s}^{-1}$ , respectively. The overall inhibition constant  $K_i^*$  was 0.12 nM. The binding of the inhibitor with the enzyme and the subsequent conformational changes induced were monitored by exploiting the intrinsic tryptophanyl fluorescence. The rate constants derived from fluorescence studies were in agreement with the kinetic data correlating the conformational alterations to isomerization of EI to EI\*. The conformational changes induced upon inhibitor binding to pepsin were monitored by far and near UV analysis. A comparative analysis in the fluorescence spectra of pepsin upon binding of APD or the classical known active site directed inhibitor, pepstatin was found to be similar to that of inhibitor, suggesting that the inhibitor binds in the active site of the enzyme. To evaluate the effects of the inhibitor on the secondary structure of the enzyme, we have analyzed the CD spectra of pepsin-inhibitor complex. Interestingly, the pepsin-inhibitor complex, pepsin-APD complex and pepsin-pepstatin complex exhibited a similar pattern of negative ellipticity in the far-UV region, suggesting that the inhibitor causes similar structural changes in the enzyme as that of the substrate. These studies revealed that the inhibitor binds to the active site and causes inactivation of pepsin. Chemical modification of the inhibitor with group specific reagents WRK and TNBS abolished the antiproteolytic activity of the inhibitor due to the involvement of Asp and Lys residues.

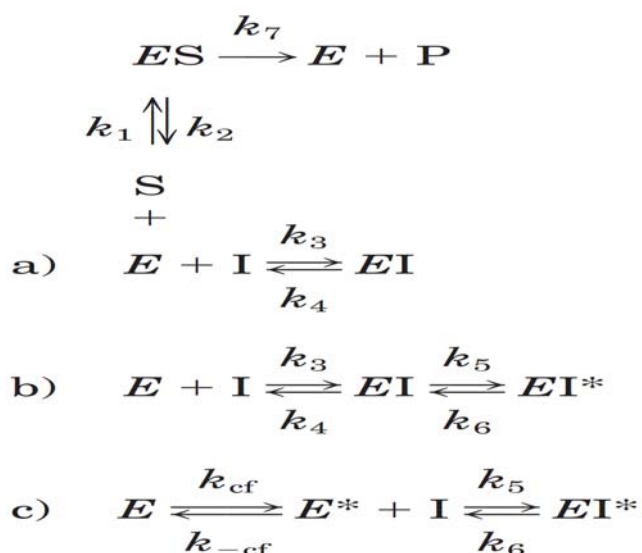
## INTRODUCTION

Pepsin, the well-known aspartic proteinase, is produced by the human gastric mucosa in seven different zymogen isoforms (Samloff 1969; Foltmann 1981). These have been subdivided into two types: pepsinogen I (pepsinogen A), consisting of PGA 1-5, and pepsinogen II (pepsinogen C or progastricsin), consisting of PGC 6 and 7. Three major species of pepsinogen A - PGA 3, 4, 5 - have been sequenced; these sequences show that PGA 3 and 5 differ only in the proenzyme part so that after conversion to the mature enzymes, the resulting pepsins are identical (Fujinaga et al., 1995). Pepsin is a monomeric, two domain, mainly L-protein, with a high percentage of acidic residues (43 out of 327) leading to a very low pI. The catalytic site is formed by two aspartate residues, Asp32 and Asp215, one of which has to be protonated, and the other deprotonated, for the protein to be active (Antonov et al., 1978; Lin et al., 1992). Pepsin is studied mainly from the perspective of its role in gastro-esophageal reflux diseases (GERD) and peptic ulcers (Tobey et al., 2001). Although in many cases the etiologic agent of the ulcer is unknown, it is accepted that ulcerative processes occur as results of a balance between aggressive endogenous factors such as acid, pepsin and the maintenance of the integrity of the gastric mucosa, and environmental factors like the use of non-steroidal anti-inflammatory drugs (NSAID), the presence of *Helicobacter pylori* in the gastro-intestinal mucosa, smoking habit, environmental stress, and population feeding habits (Lanza et al., 1984). Recently, with a remarkable advance in the pharmacological studies with regard to ulceration of digestive organs, many attempts are directed to the aspect of enzymatic action of pepsin in order to solve the causes of ulceration as well as developments of ulcers. So far there are no drugs that produce 100% remission of gastroduodenal ulcers (Friedman and Peterson 1998), which is considered a major health problem. It is vital to explore anti-ulcerogenic agents that are more effective and less toxic from microbial origin.

The classification of inhibitors depends on the reversibility, strength, and rates of their interaction with the enzyme. The four categories of reversible inhibitors are

classical, tight-binding, slow binding, and slow, tight-binding inhibitors (Morrison 1982). The categories are generally differentiable based on the ratio of total inhibitor ( $I_t$ ) to total enzyme ( $E_t$ ) under experimental conditions and the qualitative time required for attainment of the equilibrium between the enzyme, inhibitor, and enzyme-inhibitor complex. The classification is essentially for inhibitors whose actions cannot be described by Michaelis-Menten kinetics. For classical reversible inhibitors, the affinity for the inhibitor is sufficiently low that  $I_t \gg E_t$  and the rates at which the inhibitor associate and dissociate from the enzyme are relatively high. When the affinity of an enzyme for the inhibitor is very high, tight-binding situations arise, then the experiment would be performed in concentration regimes where  $I_t \approx E_t$ . Under such conditions steady-state treatments are inadequate and incorrect, even though the net binding and release of inhibitors may be described by fast steps (Morrison 1969; Henderson 1972; Cha 1975; Cha 1976).

While classical and tight-binding inhibitors have been recognized for a very long time, awareness of compounds that cause inhibition of enzymes in a time-dependent manner is much more recent (Cha 1975; Cha 1976; Williams and Morrison 1979; Morrison 1982). A number of enzymatic reactions do not respond to the presence of competitive inhibitors instantly, but rather display a slow-onset of the inhibition. In some cases the inhibitor interacts slowly with the enzyme, in others the formation of the enzyme-inhibitor complex takes place in a very short time. Such inhibition is called slow-binding inhibition and the inhibitor is referred to as slow-binding inhibitor (Williams and Morrison 1979; Szedlacsek and Duggleby 1995; Sculley et al., 1996). From the kinetic point of view, the possible mechanisms for the slow-binding inhibition phenomena are described in Scheme I.



**Scheme I** The possible mechanisms for the slow-binding inhibition phenomenon. E stands for free enzyme, I is free inhibitor, EI is a rapidly forming pre-equilibrium complex, and EI\* is the final enzyme-inhibitor complex. E may undergo inter conversion into another form E\*, which binds to the inhibitor by a fast step, where  $k_{cf}$  and  $k_{-cf}$  stand for the rate constants for forward and backward reaction respectively, for the conversion of the enzyme.

Scheme Ia assumes that the formation of an EI complex is a single slow step and the magnitude of  $k_3I$  is quite small relative to the rate constants for the conversion of substrate to product. However, scheme I b demonstrates the two-step slow-binding inhibition, where the first step involves the rapid formation of a reversible EI complex, which undergoes slow isomerization to a stable, tightly bound enzyme-inhibitor complex, EI\* in the second step. The two-step mechanism of inhibition can be considered as the prototype of slow-binding inhibition on a steady state time scale. The ratio between the kinetic constants of  $k_5/k_6$  can be taken as an index of the accumulation of EI\* and the energetic of its formation. The higher the values of  $k_5/k_6$  ratio, the longer-lived is the EI\* and the more likely the inhibitor is to have a useful *in vivo* lifetime. The weakness in the use of classical enzyme inhibitors as drugs of clinical condition is that enzyme inhibition results in the upstream accumulation of the substrate for the enzyme, which has an impact on the isomerization of EI\* to EI and hence reversal of the inhibition which will be of immense value in clinical applications. Inhibitors which inhibit the enzyme-catalyzed reactions at concentrations comparable to that of the enzyme and under conditions where the equilibria are set up rapidly are referred as tight binding inhibitors. The establishment of the equilibria between enzyme, inhibitor, and

enzyme inhibitor complexes, in slow binding inhibition occurs slowly on the steady-state time scale (Morrison 1982), which has been thoroughly reviewed (Kati et al., 1998; Ploux et al., 1999; Dash et al., 2001; Kumar and Rao 2010). As yet, no general paradigm has emerged for relating inhibitor and/or enzyme structure which allows the predictions to be made about the design of compounds that would give rise to slow-binding inhibition. However, understanding the basis of the isomerization of EI complex to EI\* complex could lead to design inhibitors that allow titration of the lifetime of the EI\* complex. Early investigations of pepsin and the fungal aspartic proteases gave rise to a variety of mechanistic proposals, which were resolved in favor of the mechanisms shown in Scheme I (Suguna et al., 1987; James et al., 1992). The future development of slow-tight binding inhibitors will undoubtedly depend on application of kinetic techniques that yield quantitative information about the properties of the inhibitors.

Investigations of the inhibition mechanism have generated enormous attention to unravel the interaction between potent inhibitors and the target enzymes. The best-known slow-binding inhibitor of pepsin is pepstatin (Umezawa et al., 1978), with the  $t_{1/2}$  for the dissociation 2.5 h. Several analogs of pepstatin have been prepared to analyze the structural features required to express slow, time-dependent onset of enzyme inhibition (Rich and Sun 1980). There have been also reports where two approaches have been combined in protease inhibitor design, by the use of a statyl-type residue along with a group that could accumulate as a stabilized tetrahedral (Gelb et al., 1985). However, the hydrophobic nature of pepstatin holds a disadvantage for its poor oral bioavailability. There is plethora of synthetic inhibitory compounds targeting the active site of pepsin; however there is paucity on biologic inhibitors from microorganisms. Till date, the known peptidic slow-binding inhibitors of pepsin from microbial origin other than pepstatin are reported from *Bacillus* sp from our laboratory (Dash and Rao 2001; Kumar and Rao 2006). The application of biologic inhibitors will stimulate renewed interest in the therapeutic targeting of aspartic proteases (Scott and Taggart 2010). Considering the physiological importance of the aspartic proteases and their role in various diseases,

the newly isolated biologic inhibitor would provide greater insight into the inhibition mechanism and their *in vivo* efficacies.

This part of the chapter deals with the evaluation of kinetic and thermodynamic parameters of a low-molecular weight pepsin inhibitor from *Streptomyces* sp MBR04. We have investigated the localized conformational changes induced in pepsin upon binding of the inhibitor by monitoring the intrinsic tryptophanyl fluorescence and the effects on the secondary structure of pepsin by circular dichroism studies. We have also compared the results obtained with that of the synthetic substrate and a classical aspartic protease inhibitor, pepstatin. These results demonstrated that the inhibitor binds to the active site of pepsin and causes inactivation. Further, by chemical modification, we have assigned the residues of the inhibitor responsible for enzyme inactivation.

## EXPERIMENTAL PROCEDURES

### *Materials*

Porcine gastric mucosa pepsin, N-acetyl-L-phenylalanyl-L-3, 5-diiodotyrosine (APD), Hemoglobin, Pepstatin, Woodward's reagent (WRK) and 2, 4, 6-trinitrobenzenesulphonic acid (TNBS) were obtained from Sigma chemical Co., St Louis, MO. All other chemicals used were of analytical grade.

### *Pepsin assay for inhibition kinetics*

Pepsin was assayed in the presence of the synthetic substrate N-acetyl-L-phenylalanyl-L-3, 5-diiodotyrosine (APD). Pepsin, 50 nM (porcine gastric mucosa), was pre-incubated at 37°C in glycine-HCl buffer, pH 3.0. After 10 min 0.125 ml of APD solution was added to the test and 0.5 ml of ninhydrin reagent was added to the blanks (final enzyme conc. 12.5 nM). After 30 min, 0.5 ml ninhydrin reagent was added to the test and at any time 0.125 ml of APD solution was added to the blanks. The tubes were kept in boiling water bath for 15 min and the contents of tubes were diluted with 2.5 ml of 60% (v/v) ethanol. The absorbance was measured at 570 nm. The activity was expressed in APD units (Kumar and Rao 2006). One APD unit is the quantity of enzyme which liberates 1 micromole of diiodotyrosine per minute under the above conditions (Ryle 1970). For the kinetic analysis and rate constant determinations, the assays were carried out in triplicate, and the average value was considered throughout this work.

### *Initial kinetic analysis for the determination of $K_M$ and $K_i$*

The kinetic parameters for the substrate hydrolysis were determined by measuring the initial rate of enzymatic activity. The inhibition constant  $K_i$  was determined by Dixon (Dixon 1953) method and also by the Lineweaver-Burk equation. The  $K_m$  value was also calculated from the double-reciprocal equation by fitting the data to Origin 8.1. For the Lineweaver-Burk analysis of pepsin (12.5 nM) was incubated with the inhibitor at 1 nM and 5 nM and assayed at increased concentration of APD (10–100  $\mu$ M) at 37°C for 30 min. The reciprocals of substrate hydrolysis ( $1/v$ ) for



each inhibitor concentration were plotted against the reciprocals of the substrate concentrations, and the  $K_i$  was determined by fitting the resulting data. In Dixon's method, hydrolytic activity of pepsin (12.5 nM) was measured in the presence of 50  $\mu$ M and 100  $\mu$ M APD, at concentrations of the inhibitor ranging from 1 to 10 nM at 37°C for 30 min. The reciprocals of substrate hydrolysis ( $1/v$ ) were plotted against the inhibitor concentration and the  $K_i$  was determined by fitting the data using ORIGIN 8.1.

### *Determination of initial apparent inhibition constants*

Inhibition studies were performed by adding 0.25 ml of pepsin (12.5 nM), to 0.25 ml of 1 mM APD solution in standard buffer containing varying concentrations of inhibitor (1–10 nM) at 37°C. After 30 min the release of diiodotyrosine was quantified as described above. Relative enzymatic activity, R, was computed from the ratio of product amounts obtained in the presence and absence of the inhibitor as  $R = 1 - [P] / [P]_0$ . The relative inhibition was fit by nonlinear least-squares regression to Eq (1), where  $[I]_0$  is the total concentration of the inhibitor and  $K_{app}$ , the fitting parameter, is the apparent inhibition constant.

$$R = [I]_0 / (k_{app} + [I]_0) \quad (1)$$

To determine the time dependence of the apparent inhibition constants, experiments were conducted as described above, except that the pepsin was added to the inhibitor at varying concentrations, and then assayed after pre-incubation for 0, 15, or 30 min.

### *Inhibitor progress curve analysis*

The progress curves for the interaction between the inhibitor and pepsin were analyzed using Eq (2).

$$p = p_0 + Vst + (V_0 - V_s)[1 - \exp(-k_{app}t)] / k_{app} \quad (2)$$

Each individual progress curve was fitted separately. The local fitting parameters were the initial velocity  $V_0$ , the steady-state velocity  $V_s$ , the apparent first order rate constant  $K_{app}$ , and the instrumental offset  $p_0$ . These fitting parameters were analyzed

to extract approximate inhibition constants. Several reaction progress curves, obtained in the presence and absence of inhibitor at various concentrations, were combined and fitted as a whole in the Equation (3),

$$p = p_0 + r_p[P]t \quad (3)$$

in which the concentration of product  $[P]_t$  at time  $t$  is obtained by numerical integration of the system of differential Equations (4a–g).

$$d[E]/dt = -k_1[E][S] + (k_2 + k_7)[ES] - k_3[E][I] + k_4[EI] \quad (4a)$$

$$d[S]/dt = -k_1[E][S] + k_2[ES] \quad (4b)$$

$$d[ES]/dt = k_1[E][S] - (k_2 + k_7)[ES] \quad (4c)$$

$$d[P]/dt = k_7[ES] \quad (4d)$$

$$d[I]/dt = -k_3[E][I] + k_4[EI] \quad (4e)$$

$$d[EI]/dt = k_3[E][I] - (k_4 + k_5)[EI] + k_6[EJ] \quad (4f)$$

$$d[EJ]/dt = k_5[EI] - k_6[EJ] \quad (4g)$$

Numerical integration of the differential system [Eq's (4a), (4b), (4c), (4d), (4e), (4f), and (4g)] was performed by using the Livermore Solver of Ordinary Differential Equations (Hindmarsh 1983). A modification of the Marquardt–Levenberg leastsquares fitting algorithm (Reich 1992) was used to perform the regression of experimental data as described by Moss et al (1996). The optimized fitting parameters were all rate constants except the bimolecular association rate constant  $k_1$ , the total enzyme concentration  $[E]_0$  for each progress curve (within 10% titration error), the molar response coefficient  $r_p$ , and the offset  $p_0$  for each progress curve. The regression analysis was performed by using the computer programs DYNAFIT (BioKin, Ltd., Madison, WI), ORIGIN 8.1 and GRAPH PAD PRISM.

### *Fluorescence analysis*

Fluorescence measurements were performed on a Cary Varian Eclipse fluorescence spectrophotometer connected to a Cary Varian temperature controller. Protein fluorescence was excited at 295 nm, and the emission was recorded from 300 to 500

nm at 25°C. The slit widths on both the excitation and emission were set at 5 nm, and the spectra were obtained at 1 nm/min. Fluorescence data were corrected by running control samples of buffer and smoothed. For inhibitor binding studies, pepsin (10 nM) was dissolved in 0.05 N HCl. Titration of pepsin with the inhibitor was performed by the addition of different concentrations of inhibitor to the pepsin solution. The magnitude of the rapid fluorescence decrease ( $F_0 - F$ ) occurring at each inhibitor concentration was computer fitted to the equation  $(F_0 - F) = \Delta F_{\max} / \{1 + (K_i / [I])\}$  to determine the calculated value of  $K_i$  and  $\Delta F_{\max}$ . The first-order rate constants for the slow loss of fluorescence  $K_{obs}$ , at each inhibitor concentration  $[I]$  were calculated by computer fitting of the remaining data, starting 1s after inhibitor addition, to the equation  $K_{obs} = k_5 [I] / (K_i + [I])$  for the determination of  $k_5$  under the assumption that, for a tight-binding inhibitor,  $k_6$  can be considered negligible at the onset of the slow loss of fluorescence (Houtzager et al., 1996). Time courses of the protein fluorescence following the addition of inhibitor were measured for up to 5 min with excitation and emission wavelengths fixed at 295 and 342 nm, respectively. Data points were collected at 1 s intervals during time courses. Corrections for the inner filter effect were performed as described by the formula  $F_c = F \text{ antilog } [(A_{ex} + A_{em})/2]$ , where  $F_c$  and  $F$  are the corrected and measured fluorescence intensities, respectively, and  $A_{ex}$  and  $A_{em}$  are the solution absorbance at the excitation and emission wavelengths, respectively (Lakowicz 1983). Background buffer spectra were subtracted to remove the contribution from Raman scattering.

### *Secondary structural analysis of pepsin-APD-inhibitor complexes*

CD spectra were recorded in a Jasco-J715 spectropolarimeter at ambient temperature using a cell of 1-mm path length. Replicate scans were obtained at 0.1-nm resolution, 0.1-nm bandwidth, and a scan speed of 50 nm/min. Spectra were averages of six scans with the base line subtracted spanning from 280 to 200 nm in 0.1-nm increments. The CD spectrum of pepsin (50 nM) was recorded in 0.05 N HCl in the absence/presence of APD (10  $\mu$ M) or inhibitor (10 nM) or pepstatin (10 nM). Secondary structure content of pepsin and the complexes were calculated using the algorithm of the K2d program (Andrade et al., 1993; Merelo et al., 1994).

*Chemical Modification of the inhibitor with 2,4,6-Trinitrobenzenesulfonic acid (TNBS) and N-Ethyl-5-phenylisoxazolium-3 $\epsilon$ -sulfonic acid (WRK)*

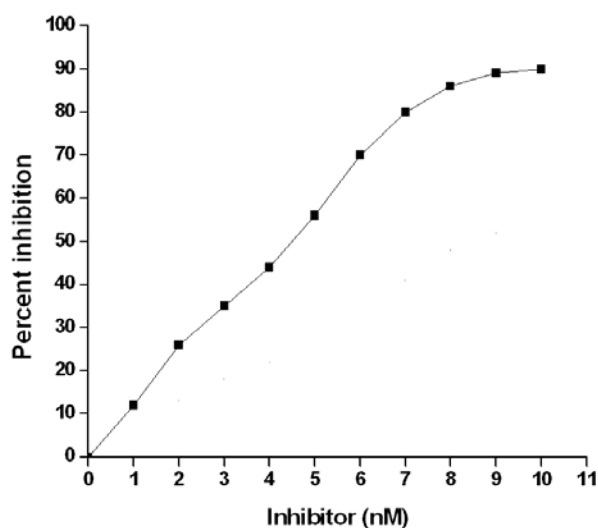
N-Ethyl-5-phenylisoxazolium-3 $\epsilon$ -sulfonic acid (Woodward's reagent K, WRK) has been known to react with the carboxyl group of aspartate and glutamate residues (Arana and Vallejos 1981; Sinha and Brewer 1985). To modify the carboxylic groups, the inhibitor (50  $\mu$ M) was incubated in the absence or presence of different concentrations of WRK at 28°C for 1 h. Aliquots were removed at different time intervals, and the reaction was quenched by the addition of sodium acetate buffer, pH 5.0, to a final concentration of 100 mM. Excess reagent was then removed by gel filtration on a Bio-Gel P2 column, equilibrated with sodium phosphate buffer, 0.05 M, pH 6.0. The fractions were eluted at a flow rate of 12 mL/h. The active fractions were detected by the differential absorption at 210/340 nm and concentrated by lyophilization, and the residual activity of the inhibitor was determined by assaying for the antiproteolytic activity.

The inhibitor (50  $\mu$ M) and 0.25 mL of 4% sodium bicarbonate were incubated with varying concentrations of 2,4,6-trinitrobenzenesulfonic acid (TNBS), a lysine group modifier (Okuyama and Satake 1960), at 37°C in a reaction mixture of 0.5 mL in the dark. Aliquots were withdrawn at suitable intervals, and the reaction was terminated by adjusting the pH to 4.6. A control without the modifier was routinely included, and the residual activity at any given time was calculated relative to the control. The extent of inactivation of pepsin was determined with the modified inhibitor as described before.

## RESULTS

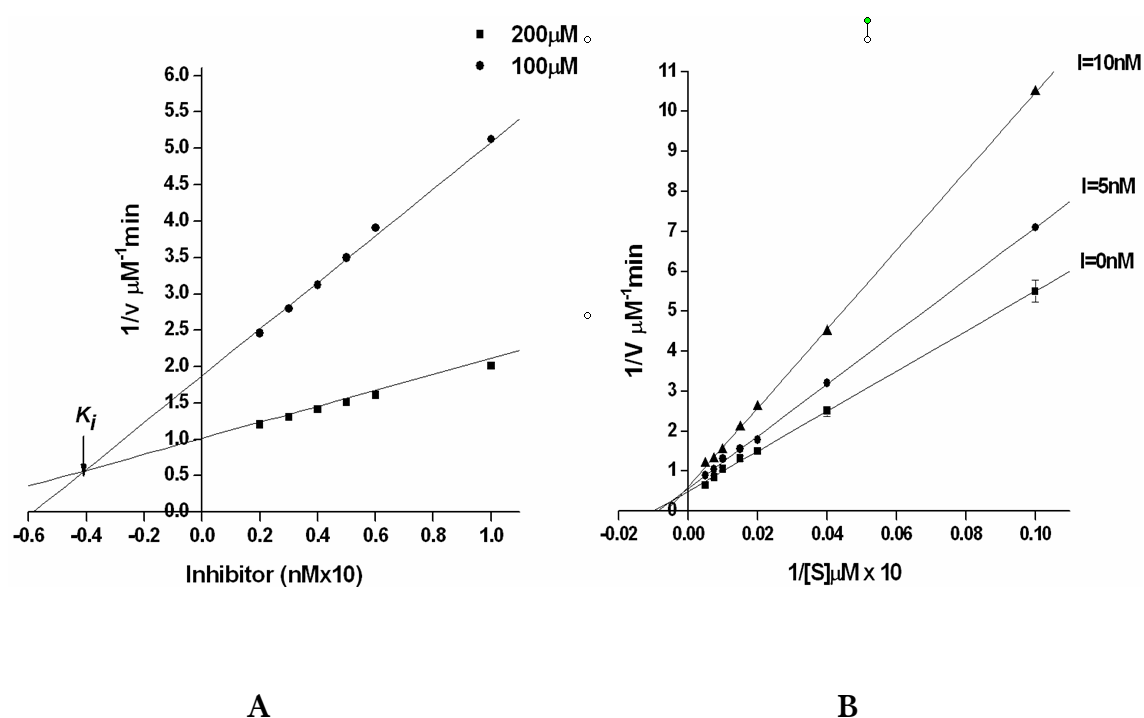
### *Kinetic analysis of the inhibition of pepsin*

The aspartic protease inhibitor was produced extracellularly by *Streptomyces* sp MBR04. The inhibitor was found to inhibit pepsin with an  $IC_{50}$  value (50% inhibitory concentration) of 4.5 nM (Figure 1). The inhibition of pepsin followed a hyperbolic pattern with increasing concentrations of the inhibitor. However, the secondary plot (the slope of inhibition graph versus inhibitor concentration) was not linear, suggesting that the application of Michaelis–Menten inhibition kinetics was not appropriate in this study.



**Figure 1** Inhibition kinetic analysis. The activity of the pepsin (12.5 nM) was determined with increasing concentrations of inhibitor. The percent inhibition was calculated from the residual enzyme activity. The sigmoidal curve indicates the best fit for the percent inhibition data obtained, and the  $IC_{50}$  value was calculated from the graph.

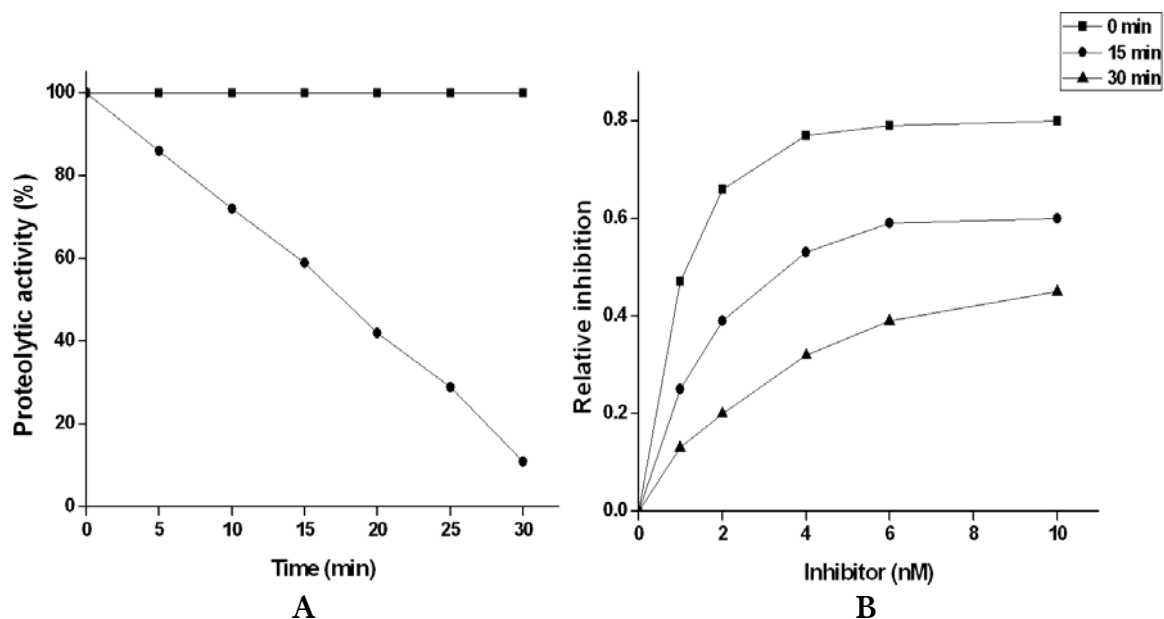
The inhibition constant  $K_i$ , determined by the classical double reciprocal plot and also by Dixon plot was 4.1 nM (Figure 2A), which is almost equal to the  $IC_{50}$  value of the inhibitor. The Lineweaver–Burk reciprocal plot (Figure 2B) showed a competitive mode of inhibition of pepsin with a  $K_M$  and  $K_i$  values of 75  $\mu$ M and 4.3 nM respectively.



**Figure 2 (A)** Enzyme activity of pepsin (12.5 nM) was estimated using the substrate N-acetyl-L-phenylalanyl-L-3, 5-diiodotyrosine (APD) at different concentrations of the inhibitor. Reciprocals of the reaction velocity were plotted against the inhibitor concentrations. The straight lines indicated the best fits for the data obtained and the inhibition constant  $K_i$  was calculated from the point of intersection of the plots. **(B)** Initial rate of enzymatic reaction of pepsin in the presence of the inhibitor. Enzymatic activity was estimated using APD in glycine-HCl buffer, 0.05 M, pH 3.0. Pepsin (12.5 nM) was incubated without or with the inhibitor and assayed at increased concentration of the substrate at 37°C for 30 min. The reciprocal of substrate hydrolysis ( $1/v$ ) for each inhibitor concentration were plotted against the reciprocal of the substrate concentration. The straight lines indicated the best fits for the data obtained by non-linear regression analysis and analyzed by Lineweaver-Burk's reciprocal equation.

Examination of progress curves suggested that, in absence of inhibitor the steady-state rate of proteolytic activities were reached rapidly, whereas in its presence, the rate decreased in a time-dependent manner (Figure 3A). The concentration of APD was set to a value below the Michaelis constant ( $K_m$ ) 50  $\mu\text{M}$ , so that the reactions were approximately first-order in APD. The results from the preincubation experiments with the inhibitor are shown in Table 1. The apparent inhibition constants decreased 5 fold over a 30 min period (Figure 3B). In an independent method to determine the conversion of pepsin-inhibitor\* to pepsin-inhibitor, high concentration of enzyme and inhibitor were preincubated for 60 min to allow the

system to reach equilibrium. Further the enzyme-inhibitor mixture was diluted 1000 fold into the assay mixture containing the substrate at  $10 K_m$ , which resulted in the dissociation and regeneration of enzymatic activity. At the specified time, aliquots were removed and assayed for the proteolytic activity. From the rate of product formation, the recovered enzyme concentration could be estimated as approximately 6nM and the reduction of APD was observed at a steady-state velocity of approximately 45% relative to the control.



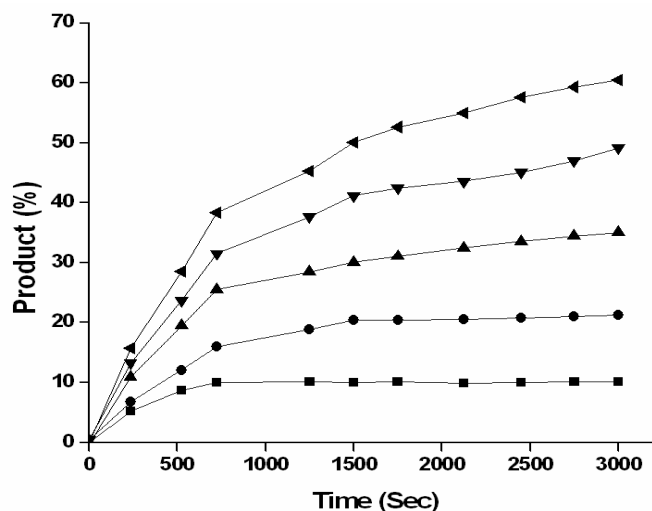
**Figure 3** Pre-incubation kinetic studies with the inhibitor (A) Loss of residual enzyme activity upon pre-incubation of pepsin (12.5 nM) without (●) or with the inhibitor at 10 nM (■). See experimental procedures for details. (B) Apparent inhibition constants with or without pre-incubation of the inhibitor (0-10nM) with pepsin for 0, 15 or 30 min before the assay. Residual enzyme activity was measured as mentioned in the text.

**Table 1** Apparent inhibition constant with or without preincubation of the inhibitor (0-10 nM) with pepsin (12.5 nM)

$K_{app}$ (nM)		
t = 0 min	t = 15 min	t = 30 min
$5.2 \pm 0.18$	$2.4 \pm 0.2$	$0.86 \pm 0.13$

*Pepsin was preincubated with varying concentrations of inhibitor for 0, 15 or 30 min before the assay. Residual enzyme activity was measured as mentioned in the text.*

The progress curves for the inhibitor were analyzed by two different methods (Moss et al., 1996). The results of a preliminary analysis, based on the assumption of rapid equilibrium, are shown in Figure 4. The progress curves obtained at 1, 2, 4, 6 and 10 nM of inhibitor were fitted individually to Eq's (2). The best-fit values of adjustable parameters for each concentration of the inhibitor are listed in Table 2.



**Figure 4** Least-square fit of progress curve data of the inhibition of pepsin by the inhibitor to the equation mentioned in the text. The initial concentration of substrate was 200  $\mu\text{M}$  and the inhibitor concentrations were 1 ( $\blacktriangleleft$ ), 2 ( $\blacktriangledown$ ), 4 ( $\blacktriangle$ ), 6 ( $\bullet$ ) and 10 nM ( $\blacksquare$ ). The experimental conditions and best fit values are mentioned in the text.

**Table 2** Best fit values of adjustable parameters obtained in fitting the progress curves shown in figure 4 (Pepsin – 12.5 nM, APD – 200  $\mu\text{M}$ , 37°C, pH 3.0)

$[\text{I}]_0$ (nM)	$V_s$ (%P $\text{s}^{-1}$ )	$V_0$ (%P $\text{s}^{-1}$ )	$K_{app}$ ( $\text{s}^{-1}$ )
0	0.0924	0.08995	-
1	0.0061	0.0686	0.0168
2	0.0048	0.0532	0.0316
4	0.0036	0.0436	0.0445
6	0.0022	0.0368	0.0541
8	0.0016	0.0346	0.0619
10	0.0010	0.0374	0.0666



For a one-step inhibition mechanism, without an intermediate enzyme-inhibitor complex, the initial velocity  $V_0$  should be constant, and the apparent rate constant  $K_{app}$  should increase linearly with the inhibition concentration  $[I]_0$ . These properties of the one-step mechanism are expressed in Eq's (5a-c) (Szedlacsek and Duggleby 1995).

$$V_0 = V_{max}[S]_0/([S]_0 + K_M) \quad (5a)$$

$$V_S = V_{max}[S]_0/\{[S]_0 + K_M(1 + [I]_0/K_i)\} \quad (5b)$$

$$K_{app} = k_6 + k_5[I]_0/(1 + [S]_0/K_M) \quad (5c)$$

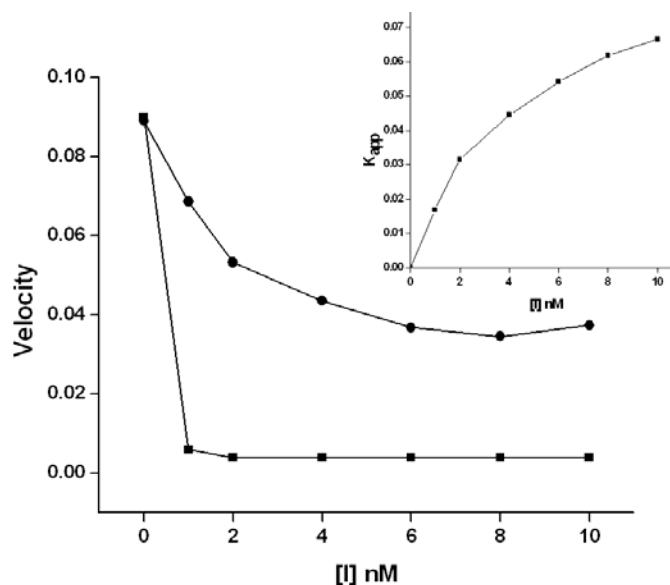
On the other hand, for a two-step mechanism (Scheme 1), the initial velocity should decrease with the inhibitor concentration, by following a typical binding curve, and the apparent rate constant should depend on  $[I]_0$  as a hyperbola, according to Eq's (6a-c).

$$V_0 = V_{max} [S]_0/\{[S]_0 + K_M(1 + [I]_0/K_i)\} \quad (6a)$$

$$V_S = V_{max} [S]_0/\{[S]_0 + K_M(1 + [I]_0/K_i^*)\} \quad (6b)$$

$$K_{app} = k_6 + k_5([I]_0/K_i)/(1 + [S]_0/K_M + [I]_0/K_i) \quad (6c)$$

The parameters listed in Table 2 favor the two-step mechanism, because the initial velocity does decrease with the concentration of the inhibitor, as predicted by Eq (6a). Also, the increase of the apparent rate constant with  $[I]_0$  is hyperbolic, instead of linear. The nonlinear least squares fit of  $V_0$ ,  $V_S$ , and  $K_{app}$  to Eq's (6a-c) is shown in Figure 5. From fitting of  $V_0$  to Eq (6a), the dissociation constant  $K_i$  of the initial complex is  $4.03 \pm 0.41$  nM; the fitted value of  $V_{max}$  is  $0.095 \pm 0.001$  au  $s^{-1}$ , in good agreement with the substrate kinetic analysis  $V_{max}$  (Kumar and Rao 2006). From fitting of  $V_S$  to Eq (6b), the overall dissociation constant  $K_i^*$  is  $0.039 \pm 0.005$  nM; the fitted value of  $V_{max}$  is  $0.096 \pm 0.001$  au  $s^{-1}$  in this case. From fitting of  $K_{app}$  to Eq (6c) (Figure 5 inset), the initial inhibition constant  $K_i$  was  $4.2 \pm 0.12$  nM. The isomerization rate constants were  $k_5 = 5.84 \pm 0.1 \times 10^{-2}$   $s^{-1}$  and  $k_6 = 0.31 \pm 0.06 \times 10^{-2}$   $s^{-1}$ , from which the total dissociation constant  $K_i^* = K_i k_6 / k_5$  is 0.22 nM.

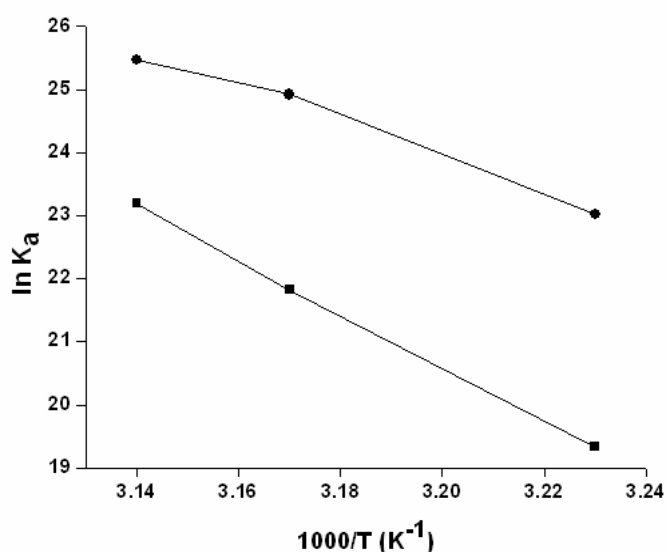


**Figure 5** Least-square fit of the initial velocity  $V_0$ , steady state velocity  $V_s$ , apparent first-order rate constant  $K_{app}$ , to the equations mentioned in the text. The best fit values of the adjustable parameters are listed in the text.

The inhibition progress curves for inhibitor were analyzed more thoroughly, by using a complete differential model where the rapid equilibrium assumption is not made (Moss et al., 1996). The collection of progress curves in Figure 4 was fitted as a whole to the system of Eq's (3) and (4a-g). The constant parameters were the initial concentration of the substrate ( $[S]_0 = 200 \mu\text{M}$ ) and the inhibitor ( $[I]_0 = 0, 1, 2, 4, 6,$  and  $10 \text{ nM}$ ), the initial concentration of the pepsin in the assay where inhibitor was absent ( $[E]_0 = 12.5 \text{ nM}$ ), and the bimolecular rate constant for the formation of the Michaelis complex ( $k_1 = 100 \mu\text{M}^{-1} \text{ s}^{-1}$ ). The best-fit values of globally optimized parameters were  $k_2 = 4.90 \pm 0.5 \text{ s}^{-1}$ ,  $k_7 = 0.95 \pm 0.02 \text{ s}^{-1}$ ,  $k_3 = 5.0 \pm 0.5 \text{ nM}^{-1} \text{ s}^{-1}$ ,  $k_4 = 21.43 \pm 2.5 \text{ s}^{-1}$ ,  $k_5 = 2.65 \pm 0.32 \text{ s}^{-1}$ ,  $k_6 = 0.070 \pm 0.006 \text{ s}^{-1}$  and  $r_P = 0.44 \pm 0.02$ . All enzyme concentrations in assays where the inhibitor was present were considered as locally optimized parameters, within the estimated 10% titration error. The best fit values of locally optimized concentrations were  $[E]_0 = 13 \pm 1 \text{ nM}$ ,  $[E]_0 = 15 \pm 2 \text{ nM}$ ,  $[E]_0 = 13 \pm 1 \text{ nM}$ ,  $[E]_0 = 11 \pm 0.5 \text{ nM}$ , and  $[E]_0 = 12 \pm 1 \text{ nM}$ , for the assays at 1, 2, 4, 6, and 10 nM of inhibitor, respectively. From the best-fit values of rate constants  $k_3$  and  $k_4$ , the dissociation constant of the initial complex,  $K_i$ , was calculated as  $k_4/k_3 = 4.29 \text{ nM}$ . Similarly, the overall dissociation constant of the final complex,  $K_i^*$ , was calculated as  $k_4 k_6 / k_3 k_5 = 0.12 \text{ nM}$ .

### *Thermodynamics of inhibitor binding to pepsin*

The thermodynamic feasibility of the inhibitor isolated from the culture supernatant of *Streptomyces* sp MBR04 by activity guided fractionation was evaluated with pepsin. The effect of temperature on  $K_i$  was investigated and the thermodynamic parameters for the association of inhibitor with pepsin were calculated using Vant Hoff plots (Figure 6).



**Figure 6** Vant Hoff plot for association of pepsin with inhibitor (■) ( $r=0.9995$  and  $N=3$ ) and pepstatin (●) ( $r = 0.9863$  and  $N = 3$ )

The thermodynamic parameters were also determined with a known potent inhibitor of pepsin, pepstatin A (Table 3). The Vant Hoff plots were further analyzed to obtain values for the changes in Gibbs free energy, enthalpy and entropy.  $K_i$  was found to increase with increase in temperature between 37 and 45°C, indicating that the inhibitor binding decreases with increasing temperatures and the Vant Hoff plots were straight line having a negative slope. The Gibbs free energy ( $\Delta G$ ) was negative; indicating that the interaction between the *Streptomyces* inhibitor and pepsin is spontaneous while negative  $\Delta H$  suggests that the overall reaction is exothermic. The positive entropy ( $\Delta S$ ) suggests that the inhibition of pepsin by the inhibitor may be due to hydrophobic interactions and association is

driven by increase in randomness. The thermodynamic interactions of pepstatin and pepsin were of similar pattern in comparison to *Streptomyces* inhibitor (Table 3).

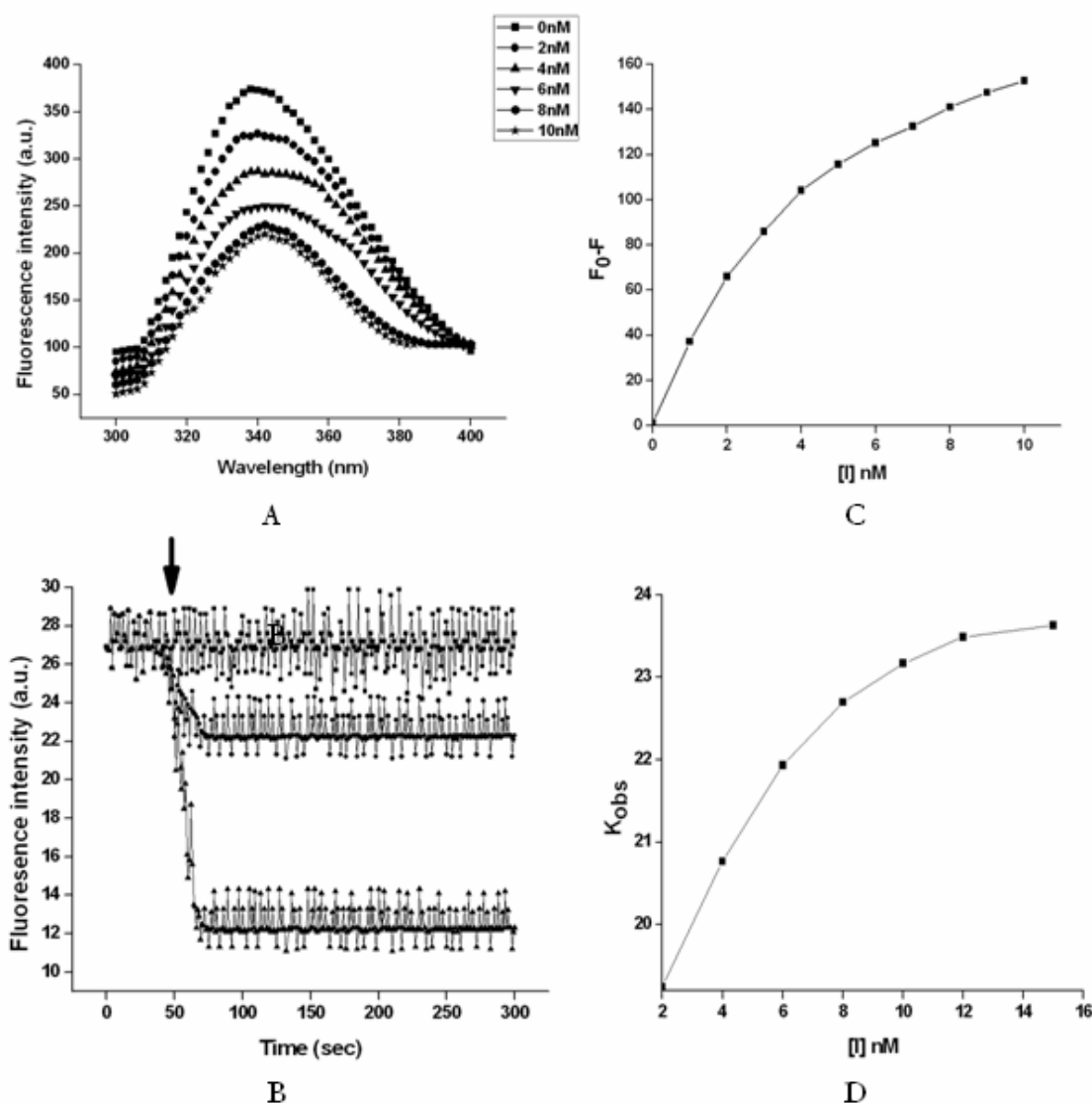
**Table 3** Thermodynamic parameters for the binding of the inhibitor to pepsin

Inhibitors	Temperature (°C)	$K_i$ (M)	$\ln K_a$	$\Delta G$ (KJ/mol <sup>-1</sup> )	$\Delta H$ (KJ/mol <sup>-1</sup> )	$\Delta S$ (J/mol <sup>-1</sup> /K <sup>-1</sup> )
<i>Streptomyces</i> Inhibitor	37	$4.0 \times 10^{-9}$	19.34	-49.85	-2.22	0.15
	40	$3.3 \times 10^{-10}$	21.83	-56.81	-2.24	0.17
	45	$8.5 \times 10^{-11}$	23.19	-59.95	-2.29	0.18
Pepstatin A	37	$1.0 \times 10^{-10}$	23.03	-59.35	-2.35	0.18
	40	$1.5 \times 10^{-11}$	24.92	-64.85	-2.37	0.19
	45	$8.7 \times 10^{-12}$	25.47	-65.85	-2.42	0.19

$K_i$  determined by Dixon method,  $\Delta G = -RT \ln K_a$ ,  $\Delta H = E_a - RT$ ,  $\Delta G = \Delta H - T\Delta S$

#### *Fluorescence analysis of pepsin-inhibitor interactions*

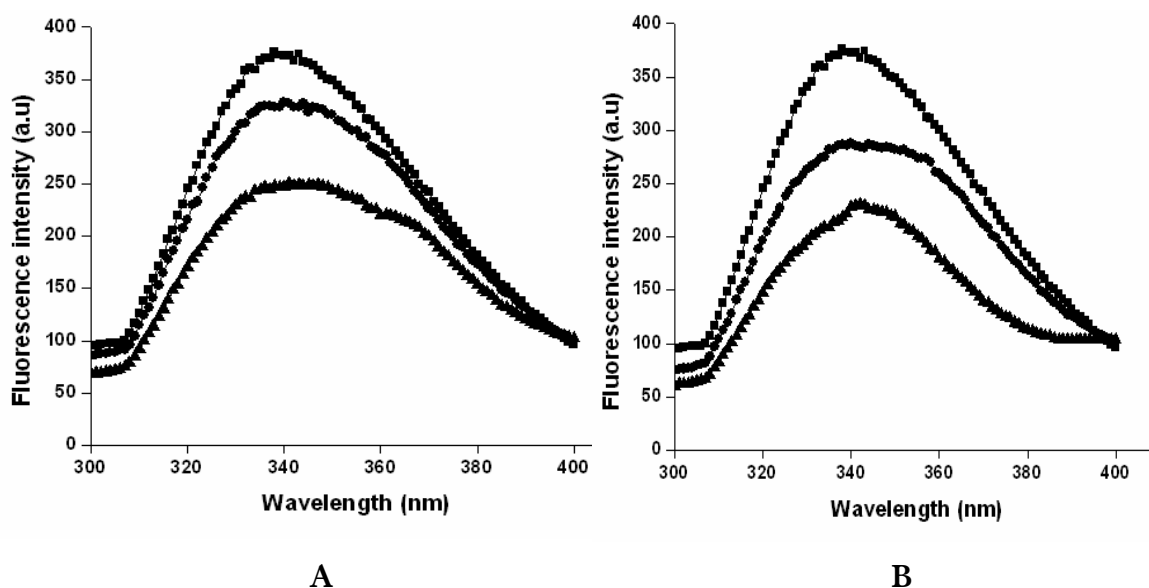
The kinetic analysis revealed a two-step inhibition mechanism, where the EI complex isomerizes to a tightly bound, slow dissociating EI\* complex. To delineate the conformational changes induced in pepsin due to the binding of the inhibitor, the fluorescence spectra of the enzyme-inhibitor complexes were monitored. The tryptophanyl fluorescence spectra of pepsin exhibited an emission maxima ( $\lambda_{\max}$ ) at 340 nm, as a result of the radiative decay of the  $\delta$ - $\delta^*$  transition from the Trp residues (Figure 7A). The binding of the inhibitor resulted in a concentration-dependent progressive quenching of the emission spectra of pepsin with saturation reaching at or above 10 nM inhibitor. However,  $\lambda_{\max}$  of pepsin indicated the absence of the blue or red shift in the intrinsic fluorescence, negating any drastic gross conformational changes in the three-dimensional structure of the enzymes. To monitor the isomerization of pepsin-inhibitor to pepsin-inhibitor\*, we have followed the intrinsic tryptophanyl fluorescence of the complexes as a function of time. Upon the addition of the inhibitor, a rapid decrease in the quantum yield of fluorescence was observed, followed by a slow decline to a final stable value over a period of 60 s for pepsin (Figure 7B), indicating an exponential decay of the fluorescence intensity.



**Figure 7** Steady-state fluorescence emission spectra of pepsin as a function of inhibitor and the time-dependent effect of the inhibitor on the fluorescence quenching of pepsin (A) Protein fluorescence was excited at 295 nm, and emission was monitored from 300 to 400 nm at 25°C. Titration was performed by the addition of different concentrations of the inhibitor to a fixed concentration of pepsin. (B) The inhibitor was added to pepsin (10 nM) at the specified time (indicated by the arrow), and the fluorescence emission was monitored for 300 s, at a data acquisition time of 0.1 s. The excitation and emission wavelength were fixed at 295 and 342 nm respectively. The data are the average of five scans with the correction for buffer and dilutions. The concentrations of inhibitor used were 0 (■), 5 (●) and 10 nM (▲). (C) The fluorescence changes ( $F_0 - F$ ) were plotted against the inhibitor concentrations. The resulting hyperbola curve was fitted to the equation  $(F_0 - F) = \Delta F_{\max} / \{1 + (K_i / [I])\}$  to give the calculated value of  $K_i$ . (D) The slow decay of pepsin fluorescence at each concentration was fitted to a first order rate equation to obtain  $K_{obs}$  (see Materials and methods). The  $K_{obs}$  values were then computer fitted to the equation mentioned in the text to give the calculated value of  $K_i$  and  $k_6$ .

The magnitude of the rapid fluorescence decrease as a function of time was found to be similar to the total fluorescence quenching observed at a specific inhibitor concentration. Thus we have concluded that both pepsin-inhibitor and pepsin-inhibitor\* complexes have the same intrinsic fluorescence. Further, titration was performed in which an increased concentration of inhibitor was added to the pepsin. The magnitude of the initial rapid fluorescence loss ( $F_0 - F$ ) increased hyperbolically (Figure 7C), corroborating the two-step, slow-tight binding inhibition of the pepsin by the inhibitor. The estimated value of  $K_i$  determined by fitting the data for the magnitude of the rapid fluorescence decrease ( $F_0 - F$ ) was  $4.64 \pm 0.15$  nM, and the  $k_s$  value determined from the data derived from the slow decrease in fluorescence was  $2.41 \pm 0.2$  s<sup>-1</sup> for pepsin (Figure 7D). These rate constants are in good agreement with that obtained from the kinetic analysis of pepsin; therefore, the initial rapid fluorescence decrease can be correlated to the formation of the reversible complex pepsin-inhibitor, while the slow, time-dependent decrease reflected the accumulation of the tight-bound slow dissociating complex pepsin-inhibitor\*.

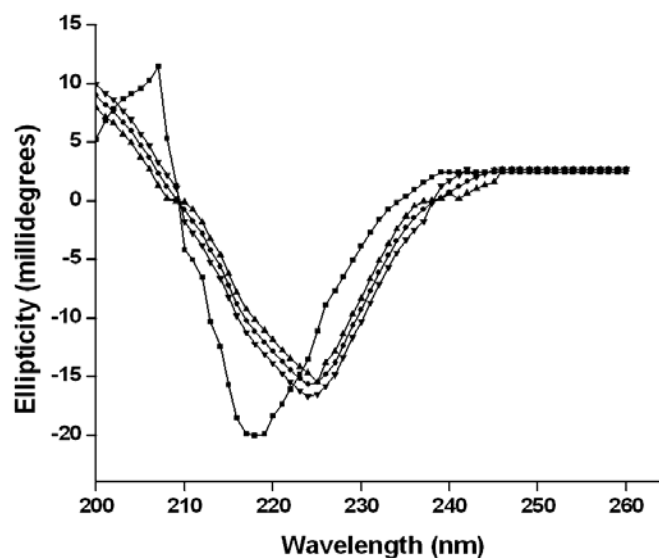
A progressive quenching in the fluorescence of pepsin at 340 nm was observed concomitant to the binding of APD (Figure 8A). Further, to conclude the mechanism of inactivation of the enzyme by the inhibitor, we have analyzed the interaction of a known potent competitive inhibitor, pepstatin by steady-state intrinsic fluorescence measurements. The binding of the competitive inhibitors led to decrease in the quantum yield of tryptophanyl fluorescence as indicated by the quenching of the emission spectra of the enzyme (Figure 8B). The comparative analysis of the intensity changes in the fluorescence spectra of pepsin upon binding of the substrate or the known active site-based inhibitor was found to be similar to that of the peptidic inhibitor, suggesting the binding of the inhibitor to the active site of the enzyme.



**Figure 8** (A) Fluorescence spectra of pepsin in the absence (■) or presence of APD at concentrations, 50  $\mu\text{M}$  (●) and 100  $\mu\text{M}$  (▲). Experiments were performed at 4°C to avoid substrate hydrolysis. (B) Effect of pepstatin on the fluorescence quenching of pepsin at concentrations, 0 (■), 5 (●), 10 (▲) nM.

#### *Circular dichroism analysis of pepsin-APD-inhibitor complexes*

To elucidate the effects of the inhibitor on the secondary structure of pepsin, CD spectra of enzyme-inhibitor complex was analyzed. The secondary structure content of pepsin as determined from the crystal structure data were 11.04%  $\alpha$ -helix and 40.49%  $\beta$ -structures (Berman et al., 2000). The estimated secondary structure contents from the CD analysis were 10.28%  $\alpha$ -helix and 42.05%  $\beta$ -structures, which are in total agreement with the crystallographic data. The CD spectrum of the enzyme-inhibitor complex showed a pronounced shift in the negative band at 218 nm of the native enzyme to 224 nm (Figure 9). This shift reveals a subtle change in the secondary structure of the enzyme upon ligand binding. To elucidate the changes in the secondary structure of the enzyme-inhibitor complex, a comparative analysis was performed with pepsin-APD and pepsin-pepstatin complexes. Interestingly, the pepsin-inhibitor, pepsin-APD and pepsin-pepstatin complexes exhibited a similar pattern of negative ellipticity in the far-UV region, suggesting that the inhibitor causes similar structural changes and was distinctly different from that of the unliganded enzyme.

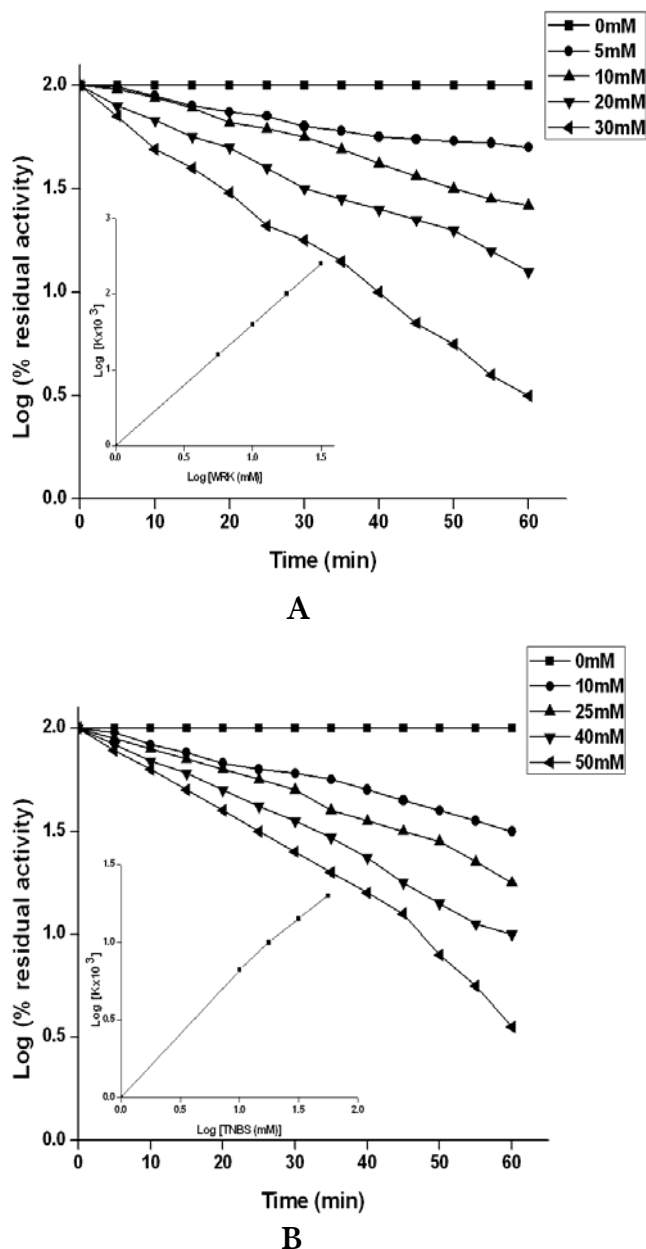


**Figure 9** Effect of the secondary structure of pepsin upon binding of the substrate or inhibitor Far-UV circular dichroism spectra of the unliganded pepsin (■) and its complexes with the substrate (▲), pepstatin (◄) and the inhibitor (●) are shown. Pepsin (50 nM) was dissolved in 0.05 N HCl and the CD spectra were recorded in the absence or in the presence of the substrate (10  $\mu$ M) or pepstatin (10 nM) or inhibitor (10 nM) from 260 to 200 nm at 25°C. Each spectrum represents the average of six scans.

#### *Chemical modification of inhibitor and its antiproteolytic activity*

The functional groups involved in the inhibitory activity of the inhibitor were elucidated by employing chemical modifiers with specific reactivity. The amino acid analysis of the inhibitor revealed the presence of Lys and Asp residues with ionizable side chains. The involvement of these groups in the mechanistic pathway was investigated using WRK, a carboxyl group modifier, and TNBS, an amine group modifier of lysine. Semilogarithmic plots of residual inhibitory activity against pepsin as a function of time were linear (Figure 10A). The modification of the carboxyl groups of inhibitor by WRK was monitored by the differential absorption at 210/340 nm. Analysis of the order of reaction (Levy et al., 1963) for pepsin yielded a slope of 1.65 (Figure 10A inset), thus suggesting the involvement of two carboxyl groups in enzyme inactivation. TNBS caused time- and concentration-dependent loss of the inhibitory activity of inhibitor. A reaction order of 0.82 (Figure 10B inset) for pepsin was determined from the slope of the double logarithmic plot, indicated the involvement of a single amine group of inhibitor in the enzyme inactivation.





**Figure 10** Differential labeling of the ionizable groups of the inhibitor with WRK and TNBS (**A**) Inactivation of the inhibitor by WRK. The inhibitor ( $50 \mu\text{M}$ ) was treated without or with different concentrations of WRK at  $28^\circ\text{C}$  for 1 h. Aliquots of the reaction mixture were removed at times indicated and the reaction was quenched with the addition of sodium acetate buffer to a final concentration of 100 mM. (**B**) Inactivation of the inhibitor by TNBS. The inhibitor ( $50 \mu\text{M}$ ) was treated without or with different concentrations of TNBS at  $37^\circ\text{C}$  for 1 h in dark. The lines represent the best fit of the data obtained as the natural logarithm of percent of residual inhibitory activity versus time. Inset represents the double logarithmic plots for the pseudo first order rate constants versus the concentration of the modifiers.

## DISSCUSSION

The data presented here showed that the peptidic inhibitor from *Streptomyces* sp MBR04, was a slow-tight binding inhibitor of pepsin. The determined kinetic data for the enzyme-inhibitor interactions were linked with the conformational changes induced in the enzymes due to the inhibitor binding. During our initial kinetic analysis, the inhibitor showed competitive inhibition against pepsin in vitro. The 1:1 molar ratio of the interaction of the inhibitor with the target enzymes classified it under the “tight-binding inhibitor” group (Wolfenden 1976; Williams and Morrison 1979). These results were reinforced by the equilibrium binding studies of the enzyme and inhibitor and by the estimation of the residual proteolytic activity. Inhibitor was found to inhibit pepsin with an  $IC_{50}$  value of 4.5 nM and inhibition constant  $K_i$ , determined by the different methods was found between 4 nM to 4.5 nM, which are almost equal to the  $IC_{50}$  value of the inhibitor.

The slow-binding inhibition of enzymes can be illustrated kinetically by three mechanisms as described in Scheme I. The kinetic properties of pepsin studied in this report provide a unique opportunity to quantitate these rates and affinities. As found in most of the ground-state inhibitors, formation of the first reversible complex, pepsin-inhibitor, was too rapid to be measured at steady-state kinetics and was likely to be near diffusion control. The rate of formation of the second enzyme inhibitor complex, pepsin-inhibitor\*, was slow and relatively independent of the stability of the pepsin-inhibitor complex or of the ability of the inhibitor to stabilize the pepsin-inhibitor\* complex. Thus the major variable for slow-binding inhibition is  $k_6$ , the first-order rate at which pepsin-inhibitor\* relaxes to pepsin-inhibitor. An equivalent statement is that the apparent inhibitor constant,  $K_i^*$ , depends on the ability of the inhibitor to stabilize the pepsin-inhibitor\* complex. It is interesting to comment on the kinetic data of inhibitor in the light of the extensive kinetic analysis of pepstatin, a known tight-binding inhibitor of pepsin. The values of  $K_i$  and  $K_i^*$  for the inhibitor were higher than those of pepstatin. Table 4 describes the comparison of kinetic parameters of biologic inhibitors reported in the literature with the newly isolated inhibitor against pepsin.

**Table 4** Comparison of kinetic data of the biologic inhibitors exhibiting inhibitory activity against pepsin

Inhibition constants (M)	Pepstatin <sup>a*</sup>	ATBI <sup>b*</sup>	API <sup>c</sup>	Present work
$IC_{50}$	$1 \times 10^{-10}$	$22 \times 10^{-9}$	$4.5 \times 10^{-9}$	$4.5 \times 10^{-9}$
$K_i$	$1.3 \times 10^{-8}$	$1.7 \times 10^{-9}$	$5.31 \times 10^{-9}$	$4 \times 10^{-9}$
$K_i^*$	$4.5 \times 10^{-11}$	$55 \times 10^{-12}$	$0.107 \times 10^{-9}$	$0.12 \times 10^{-9}$

\* - substrate used for the assay was hemoglobin. For composition of buffers and assay conditions, see experimental procedures. a – Rich and Sun (1980), b – Dash et al., 2001; c – Kumar and Rao 2006.

The onset of slow-binding inhibition is caused by a normal conformational mode of the enzyme-inhibitor complex that attains the stable configuration. The slow-binding inhibitors combine at the active site and induce conformational changes that cause the enzyme to clamp down in the inhibitor, resulting in the formation of a stable enzyme-inhibitor complex. The time-dependent inhibition kinetics of pepsin with the inhibitor followed a two-step mechanism, which was also reflected in the quenching pattern of the fluorescence. On the basis of our fluorescence studies, we propose that the rapid fluorescence loss was due to the formation of the reversible pepsin-inhibitor complex, whereas the subsequent slower decrease was a result of the accumulation of the tightly bound pepsin-inhibitor\* complex. The kinetically observable isomerization of pepsin-inhibitor to pepsin-inhibitor\* does not involve a major alteration in the three-dimensional structure of the enzymes as reflected in the absence of any shift in the tryptophanyl fluorescence. Further, agreement of the rate constant values determined from kinetic and fluorescence analysis prompted us to correlate the localized conformational changes to the isomerization of pepsin-inhibitor to pepsin-inhibitor\*. Any changes in the environment of individual tryptophan residues may result in an alternation of fluorescence characteristics such as emission wavelength, quantum yield, and susceptibility to quenching (Pawagi and Deber 1990). Fluorescence quenching can also result from the energy transfer to an acceptor molecule having an overlapping absorption spectrum (Cheung 1991). As the inhibitor has no absorption in the region of 290-450 nm, we ruled out the quenching of fluorescence due to the energy transfer between the inhibitor and the

tryptophan residues. The possibility that can be considered for the above inhibitor induced fluorescence decrease is due to the presence of multiple sites; binding at one induced rapid fluorescence change and at a second caused the slow fluorescence decrease. To verify this possibility, a fixed concentration of the enzymes was titrated with increasing concentrations of the inhibitor. The proteolytic activity of pepsin decreased linearly with increasing concentrations of the inhibitor, yielding a stoichiometry close to 1:1 expected for the slow-tight binding inhibition. The effect of inhibitor concentration on the fluorescence quenching of the enzymes was also consistent with a 1:1 molar ratio. These results are therefore inconsistent with the presence of multiple high-affinity sites. Irrespective of the physical explanation for the quenching process, it was apparent that the inhibitor-induced fluorescence quenching followed the formation of both the complexes pepsin-inhibitor to pepsin-inhibitor\*. The comparison of the emission spectra of pepsin upon binding of the peptidic inhibitor with that of the substrate or pepstatin led us to conclude that the inhibitor binds to the active site of the enzyme and exhibits localized conformational changes, thereby reducing the radioactive decay of the intrinsic Trp fluorescence. Our interpretation for the changes observed in the secondary structure of pepsin due to the binding of the substrate to the active site can be correlated to the similar pattern of changes observed due to the binding of the peptidic inhibitor. Thus, we have concluded from the fluorescence and CD studies, that the peptidic inhibitor binds to the active site of pepsin and causes inactivation.

The amino acids comprising the active center and the correlation between these residues with the inhibitory function are essential to understand the mechanism of action of the inhibitor. Chemical modification and the kinetic analysis indicated the participation of one amine and two carboxyl groups of the inhibitor in the inhibition of pepsin. The probable explanation for the involvement of two carboxyl groups of the inhibitor is that they may form a network of hydrogen bonds with the catalytic water molecule and with the ionizable groups in the active site of the enzyme. The participation of the Lys residue may be explained by considering its ability to form hydrogen bonding with the catalytic carboxyl groups of the

enzymes. These interactions may interfere in the native weak interactions between the carboxyl groups of the active site and the lytic water molecule, leading toward the inactivation of the enzymes. However, the crystal structure will aid in understanding the mechanism of inactivation of pepsin in depth and will further shed light on the molecular interactions between the enzyme and inhibitor.

The results of our investigation demonstrated that the inactivation of pepsin by the inhibitor followed a slow tight binding inhibition mechanism and can be conveniently monitored by fluorescence spectroscopy. The fluorescence studies revealed that the binding of the inhibitor causes localized conformational changes in pepsin, as reflected during the isomerization of the pepsin-inhibitor complex to pepsin-inhibitor\* complex. Based on the fluorescence and circular dichorism studies, we demonstrate that the inhibitor binds to the active site of pepsin and causes inactivation. Further, by chemical modification, we have assigned the residues of the inhibitor responsible for the enzyme inactivation. All these kinetic, thermodynamic and quenching studies suggest that the newly isolated peptidic inhibitor can be used to develop potent therapeutic lead molecules for the development of drugs targeted towards pepsin.

## **PART B**

### **Slow-tight binding inhibition of Cathepsin D: Implications in mechanism of inactivation**

## SUMMARY

Cathepsin D, a lysosomal aspartic protease is of potential interest as a target for drug design due to its implication in the pathology of breast and ovarian cancer. The active site cleft of cathepsin D is bound by a conformationally mobile loop known as flap, which is important in substrate binding and catalysis. Investigations of the steady-state kinetic interactions of cathepsin D and the *Streptomyces* sp inhibitor revealed reversible, competitive, time-dependent slow-tight binding nature of the inhibitor with an  $IC_{50}$  and  $K_i$  values of 3.2 nM and 2.5 nM respectively. The binding of the inhibitor with the enzyme and the subsequent conformational changes in the flap region were monitored by exploiting the intrinsic fluorescence of the surface exposed Trp-54 residue, which is present at the proximity of the flap. We have demonstrated by fluorescence and circular dichroism studies that the inhibitor binds in the active site of cathepsin D. The localized conformational changes induced in cathepsin D due to the interaction with the inhibitor were investigated by fluorescence spectroscopic studies. The titration of the enzyme with increasing concentrations of the inhibitor resulted in a concentration dependent quenching of the tryptophan fluorescence. A comparative analysis in the fluorescence spectra of cathepsin D upon binding of the synthetic substrate or the known active site directed inhibitor, pepstatin was found to be similar to that of the inhibitor, suggesting that the inhibitor binds in the active site of the enzyme. To evaluate the effects of the inhibitor on the secondary structure of the enzyme, we have analyzed the CD spectra of cathepsin D-inhibitor complex. Interestingly, the cathepsin D-inhibitor complex, cathepsin D-substrate complex and the cathepsin D-pepstatin complex exhibited a similar pattern of negative ellipticity in the far-UV region, suggesting that the inhibitor causes similar structural changes in the enzyme. Based on our results, we propose that the inactivation is due to the reorganization of the flaps impairing its flexibility leading towards inaccessibility of the substrate to the active site of the enzyme. The inhibitor will be significant as a potential lead molecule for the development of drugs targeted towards overactive and/or deregulated expression of cathepsin D in cancers and Alzheimers.

## INTRODUCTION

Cathepsin D [E.C. 3.4.23.5] is an lysosomal aspartic endoproteinase of the pepsin superfamily that requires an acidic pH to be proteolytically active and found in nearly all cells, tissues and organs, but not in mature lysosome-free erythrocytes (Yamamoto K 1999). Interest in cathepsin D as a target for drug design results from its association with several biological processes of therapeutic significance including lysosomal biogenesis and protein targeting (Von Figura and Hasilik 1986; Kornfeld and Mellman 1989), antigen processing and the presentation of peptide fragments to class II major histocompatibility complexes (Gaugliardi et al., 1990; Peters et al., 1991), connective tissue disease pathology (Woessner 1971), muscular dystrophy (Gopalan et al., 1987), breast and ovarian cancers, degenerative brain changes (Matus and Green 1987; Kenessey et al., 1989), cleavage of amyloid precursor protein within senile plaques of Alzheimer brain (Cataldo and Nixon 1990) and neuronal ceroid lipofuscinosis. In normal cells, cathepsin D is localized in intracellular vesicles (lysosomes and endosomes). In cancer cells, overexpressed cathepsin D accumulates in cells, where it may affect their degradative capacities, and the pro-enzyme is hyper-secreted in the tumor microenvironment. In addition, during apoptosis, lysosomal cathepsin D is released into the cytosol, where it may interact with and/or cleave pro-apoptotic, anti-apoptotic, or nuclear proteins. A number of hypotheses have been developed and tested to explain the potential causes for cathepsin D secretion in cancer cells (Benes et al., 2008).

The human cathepsin D gene contains 9 exons, and is located on chromosome 11p15 (Augereau et al., 1988). Cathepsin D is synthesized in the rough endoplasmic reticulum (RER) in a form of preprocathepsin D, built up of 412 amino acid residues. The RER is the site of glycosylation and formation of disulphide bridges in preprocathepsin D. Splitting off of the N-terminal 20 amino acid prepeptide by signalase causes release of procathepsin D and its passage to the Golgi apparatus and primary lysosomes. In an acid environment of the primary lysosomes, intramolecular autocatalytic splitting off of the 44 amino acid propeptide and the formation of active enzyme occur. The actions of cysteine proteases,



aminopeptidases, carboxypeptidases and the autocatalytic process lead to the formation of a mature two-chain cathepsin D molecule, 12 + 34 kDa. These protease inhibitors inhibit maturation of cathepsin D, which can also be found on the cell surface due to fusion of lysosomes with the plasma membrane. Cathepsin D may pass to cytosole, to the intracellular environment and to the blood. Cathepsin D activity is regulated on a few levels: through stimulation and inhibition of its biosynthesis, at the stage of post-translatory modifications in the Golgi apparatus, proenzyme activation and interlysosomal pH regulation. This ensures that cathepsin D can operate at the proper time, site and intensity, and prevents uncontrolled protein degradation.

Cathepsin D, like other aspartic proteases such as renin, chymosin, pepsinogen, has a bilobed structure. The crystal structures of the native and pepstatin-inhibited form of mature human cathepsin D (Metcalf and Fusek 1993; Baldwin et al., 1993; Lee et al., 1998; Goldfarb et al., 2005) have been shown to have a high degree of tertiary structural similarity with other members of the aspartic protease family (e.g. pepsinogen and human immunodeficiency virus protease). The high-resolution structure of pro-cathepsin D remains to be elucidated. The catalytic site of cathepsin D is constituted by two asparagine acid residues - Asp33 and Asp231, located in the triad sequences of Asp-33-Thr34-Gly35 and Asp31-Thr232-Gly233 (Hunt and Dayhoff 1970). In the acidic environment, the carboxyl group of Asp33 undergoes dissociation, whereas that of Asp231 does not. The carboxyl group of Asp33 activates the water molecule and allows proton release from this molecule. However, the protonated carboxyl group of Asp231 polarizes the carbonyl group of the peptide bond, facilitates formation of a tetraedric intermediate and allows cleavage of the bond. The reactions are performed by ionizing groups of cathepsin D and therefore their velocity is pH-dependent. Cathepsin D shows the highest activity in an acidic pH (pH=3.5-5.5). Cathepsin D contains three topologically distinct regions that are typical of aspartic proteases: an N-terminal domain (residues 1-188), a C-terminal domain (residues 189-346), and an interdomain, anti-parallel  $\beta$ -sheet composed of the N terminus (residues 1-7), the C terminus (residues 330-346), and

the interdomain-linking residues (160-200). The latter region links the pseudo-twofold-related N and C domains, each of which contributes an aspartic acid, Asp-33 and Asp-231, to the active site. Several structural features distinguish cathepsin D from other aspartic proteases. The cleavage and excision of an external loop between residues 98 and 106 in the N domain results in the noncovalent association of light and heavy chains (Barrett 1977). Electron density maps of cathepsin D show main-chain density for the light chain from Gly-1 through Gln-97. Continuous density for the heavy chain extends from Gly-106 to the C-terminal residue, Ala-346. Peptide sequencing of the protein preparation used for our crystallization experiments indicated that the light chain terminates with Ser-98 and that the heavy chain usually begins with Gly-106 (59%) and less frequently with Leu-105 (27%) or Gly-107 (13%). Electron density maps also indicated the presence of a disulfide bridge in cathepsin D between Cys-27 and Cys-96, which has not been observed for other aspartic proteases. This disulfide bridge, which had been predicted from modeling studies of porcine cathepsin D (Yonezawa et al., 1988), is within the light chain region and may stabilize the C terminus of the light chain against further proteolytic degradation. There are three proline residues in cathepsin D that refined in a cis-peptide conformation. A cis-peptide bond involving Pro-24 is conserved among all the aspartic proteases except for penicillopepsin, which has a deletion in this region. The other proline residues with cis-peptide bonds are localized within a proline-rich segment, termed the "proline loop," that consists of residues Pro-312, Pro-313, cis-peptide Pro-314, Ser-315, Gly-316, and cis-peptide Pro-317. An analogous structure has been described for human renin (Dhanraj et al., 1992).

Cathepsin D inhibitors have played a substantial role in the studies concerning the structure and mechanism of action of this protease and its tissue location (Rich 1986; Leung 2000; Huo et al., 2002). The design and synthesis of specific cathepsin D inhibitors are of great interest and may have important research and therapeutic consequences. The extensive pharmaceutical experience with HIV protease inhibitors suggests that cathepsin D selective inhibitors could also be developed. There is plethora of synthetic inhibitory compounds targeting the active site of

Cathepsin D; however there is paucity on biologic inhibitors from microorganisms. Considering the physiological importance of cathepsin D and their role in various diseases, there is a lacuna in the studies of the mechanism of inhibition by slow-binding inhibitors. This part of the chapter describes the kinetic and thermodynamic parameters of a low molecular weight cathepsin D inhibitor from *Streptomyces* sp MBR04. The mechanism of inactivation of cathepsin D upon inhibitor binding was elucidated using fluorescence and CD spectroscopic studies.

## EXPERIMENTAL PROCEDURES

### *Materials*

Human liver cathepsin D, BOC-Phe-Ala-Ala-Phe(*p*-NO<sub>2</sub>)-Phe-Phe-Val-Leu-OM4P, Hemoglobin, Pepstatin, Synthetic substrates, Proteases were obtained from Sigma chemical Co., St. Louis, MO. All other chemicals used were of analytical grade.

### *Cathepsin D inhibition assay for inhibition kinetics*

Cathepsin D was assayed in the presence of synthetic substrate N-t-BOC-Phe-Ala-Ala-Phe(*p*-nitro)-Phe-Val-Leu-4-hydroxymethylpyridine ester (BOC-Phe-Ala-Ala-Phe(*p*-NO<sub>2</sub>)-Phe-Phe-Val-Leu-OM4P) as described by Agarwal and Rich (1983) with some modifications. The cathepsin D activity was assayed at 37°C at different concentrations of the substrates in a 1ml reaction mixture containing 0.02 M sodium citrate buffer, pH 3.0. After 15 min the reaction was stopped by addition of 10% acidified TCA and followed by 30 min incubation at room temperature. The rate of the cleavage of peptide was followed spectrophotometrically at 310 nm.

### *Determination of initial inhibition parameters*

For initial kinetic analysis, the kinetic parameters for the substrate hydrolysis were determined by measuring the initial rate of enzymatic activity. The inhibition constant ( $K_i$ ) was determined by Dixon method (Dixon 1953) and also by the Lineweaver-Burk's equation. For the Lineweaver-Burk's analysis human liver cathepsin D (10 nM) was incubated with inhibitor at (1 nM) and (2.5 nM) and assayed at increased concentration of BOC-Phe-Ala-Ala-Phe(*p*-NO<sub>2</sub>)-Phe-Phe-Val-Leu-OM4P (1–10  $\mu$ M) at 37 °C for 30 min. The reciprocals of substrate hydrolysis (1/v) for each inhibitor concentration were plotted against the reciprocals of the substrate concentrations, and the  $K_i$  was determined by fitting the resulting data. In Dixon's method, proteolytic activity of cathepsin D (10 nM) was measured in the presence of 5 and 10  $\mu$ M of BOC-Phe-Ala-Ala-Phe(*p*-NO<sub>2</sub>)-Phe-Phe-Val-Leu-OM4P, at concentrations of inhibitor ranging from 0.5 to 5 nM at 37°C for 30 min. The

reciprocals of substrate hydrolysis ( $1/v$ ) were plotted against the inhibitor concentration and the  $K_i$  was determined by fitting the data using Origin 8E.

For the progress curve analysis, assays were carried out in a reaction mixture of 1 ml containing enzyme, substrate, and inhibitor at various concentrations. The reaction mixture contained cathepsin D (10 nM) in 0.02 M sodium citrate buffer, pH 3 and varying concentrations of inhibitor (0.5–3 nM) and BOC-Phe-Ala-Ala-Phe(*p*-NO<sub>2</sub>)-Phe-Phe-Val-Leu-OM4P (5 μM). Reaction was initiated by the addition of cathepsin D at 37°C, and the release of products were monitored at different time intervals by estimating the *p*-nitrophenylalanyl carboxylate at 310 nm. In each slow binding inhibition experiment, five to six assays were performed with appropriate blanks. For the kinetic analysis and rate constant determinations, the assays were carried out in triplicates, and the average value was considered throughout. Further details of the experiments are given in the respective figure legends.

#### *Evaluation of kinetic parameters*

Initial rate studies for reversible, competitive inhibition were analyzed according to Eq 1,

$$v = \frac{V_{\max}S}{K_m(1 + I/K_i) + S} \quad (1)$$

where  $K_m$  is the Michaelis constant,  $V_{\max}$  is the maximal catalytic rate at saturating substrate concentration (S),  $K_i = (k_4/k_3)$  is the dissociation constant for the first reversible enzyme-inhibitor complex, and I is the inhibitor concentration. The progress curves for the interactions between the inhibitor and cathepsin D were analyzed using Eq 2 (Morrison and Stone 1985; Beith 1995),

$$[P] = v_s t + \frac{v_0 - v_s}{k}(1 - e^{-kt}) \quad (2)$$

where (P) is the product concentration at any time  $t$ ,  $v_0$  and  $v_s$  are the initial and final steady-state rates, respectively, and  $k$  is the apparent first-order rate constant for the

establishment of the final steady-state equilibrium. As a prerequisite for tight binding inhibitors, corrections have been made for the reduction in the inhibitor concentration that occurs on formation of the enzyme-inhibitor (EI) complex. This is because, in the case of tight binding inhibition, the concentration of EI is not negligible in comparison to the inhibitor concentration and the free inhibitor concentration is not equal to the added concentration of the inhibitor. The corrections of the variation of the steady-state velocity with the inhibitor concentrations were made according to Eq's 3 and 4 as described by (Morrison and Walsh 1988),

$$v_s = \frac{k_7 S Q}{2(K_m + S)} \quad (3)$$

$$Q = [(K_i' + I_t - E_t) + 4K_i' E_t]^{1/2} - (K_i' + I_t - E_t) \quad (4)$$

where  $K_i' = K_i^* (1 + S/K_m)$ ,  $k_7$  is the rate constant for the product formation and  $I_t$  and  $E_t$  stands for total inhibitor and enzyme concentration, respectively. The relationship between the rate constant of enzymatic reaction  $k$ , and the kinetic constants for the association and dissociation of the enzyme and inhibitor was determined as per Eq 5,

$$k = k_6 + k_5 \left( \frac{I/K_i}{1 + (S/K_m) + (I/K_i)} \right) \quad (5)$$

The progress curves were analyzed by Eq's 2 and 5 using nonlinear least-square parameter minimization to determine the best-fit values with the corrections for the tight binding inhibition. The overall inhibition constant is determined as given by Eq 6,

$$K_i^* = \frac{[E][I]}{[EI] + [EI^*]} = K_i \left( \frac{k_6}{k_5 + k_6} \right) \quad (6)$$

For the time-dependent inhibition, there exists a time range in the progress curves wherein formation of EI\* is small. Within this time range, it is possible to directly measure the effect of the inhibitor on  $v_0$ , i.e. to measure  $K_i$  directly. Values for  $K_i$

were obtained from Dixon analysis at a constant substrate concentration as described in Eq 7,

$$1/v = 1/V_{max} + K_M/V_{max} (1 + I/K_i) \quad (7)$$

The rate constant  $k_6$ , for the dissociation of the second enzyme inhibitor complex was measured directly from the time-dependent inhibition. Concentrated cathepsin D and inhibitor were incubated in a reaction mixture to reach equilibrium, followed by large dilutions in assay mixtures containing near-saturating substrate. Cathepsin D (10 nM) was preincubated with equimolar concentrations of the inhibitor for 120 min in 0.02 M sodium citrate buffer, pH 3.0. 5  $\mu$ l of the preincubated sample was removed, diluted 10,000 fold in the same buffer, and assayed at 37°C using BOC-Phe-Ala-Ala-Phe(*p*-NO<sub>2</sub>)-Phe-Phe-Val-Leu-OM4P at 5  $\mu$ M for different time intervals.

#### *Fluorescence analysis of cathepsin D-inhibitor interactions*

Fluorescence measurements were performed as mentioned in part A. For inhibitor binding studies, cathepsin D (2.5 nM) was dissolved in 0.05N HCl. Titration of the enzyme with inhibitor was performed by the addition of different concentrations of the inhibitor to a fixed concentration of enzyme solution. The magnitude of the rapid fluorescence decrease ( $F_0 - F$ ) occurring at each inhibitor concentration was computer fitted as described in part A to determine the calculated value of  $K_i$  and  $F_{max}$ . The first order rate constants for the slow loss of fluorescence  $k_{obs}$ , at each inhibitor concentration ( $I$ ) were computer-fitted as mentioned in part A for the determination of  $k_5$ . The time course of the protein fluorescence following the addition of inhibitor was measured for 10 min with data acquisition at 0.1 s intervals as described in part A.

#### *Secondary structural analysis of cathepsin D-inhibitor complexes*

CD spectra were recorded as described in part A. The CD spectrum of cathepsin D (50  $\mu$ M) was recorded in 20 mM sodium citrate buffer (pH 3) in absence/presence of substrate (10 mM) or inhibitor (5 nM and 10 nM). Secondary structure content of

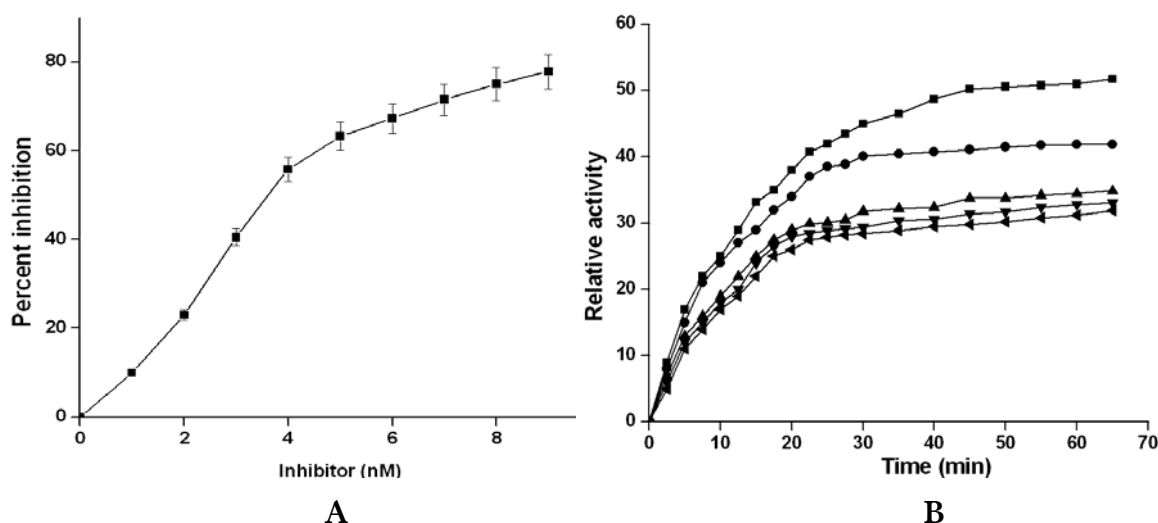
the cathepsin D, the cathepsin D-substrate complex, and the cathepsin D-inhibitor complex was calculated using the algorithm of the K2d program (35, 36).



## RESULTS

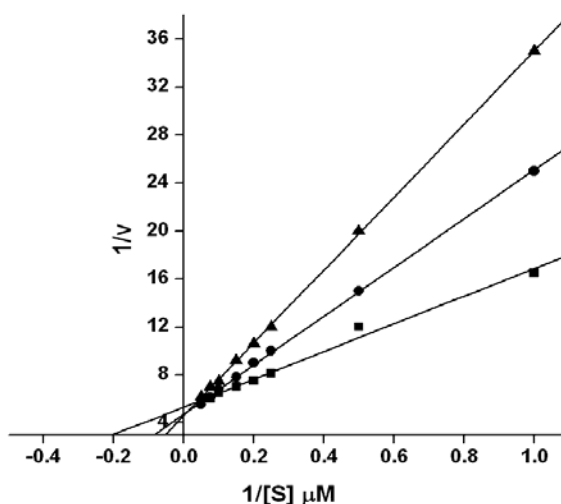
### *Inhibitor progress curve analysis*

Initial kinetic studies revealed that the inhibition of human liver cathepsin D is competitive with an  $IC_{50}$  value of  $3.2 \pm 0.5$  nM (Figure 11A). In the absence of inhibitor a steady state rate of proteolytic activity of cathepsin D was obtained rapidly whereas, in its presence a time dependent decrease in the rate as a function of the inhibitor concentration was observed. The analysis of the progress curves revealed a time range wherein the initial rate of reaction did not deviate from linearity (Figure 11B), and the conversion of EI to EI\* was minimal. For a low concentration of inhibitor, this time range was 7.5 min, within which the classic competitive inhibition experiments were used to determine the  $K_i$  values (Eq 5).



**Figure 11** (A) The activity of the cathepsin D (10 nM) was determined with increasing concentrations of inhibitor. The percent inhibition was calculated from the residual enzyme activity. The sigmoidal curve indicates the best fit for the percent inhibition data obtained, and the  $IC_{50}$  value was calculated from the graph. (B) Time course of inhibition of cathepsin D by the inhibitor. The reaction mixture contained cathepsin D (5 nM) in sodium-citrate buffer, 0.02 M, pH 3.0, and varying concentrations of inhibitor and synthetic substrate (10  $\mu$ M). The reaction was initiated by the addition of cathepsin D at 37°C. The points represent the hydrolysis of substrate as a function of time, and the lines indicate the best fits of data obtained from Eq's 2 and 5, with the corrections made as per Eq's 3 and 4. The concentrations of inhibitor were 0.5 nM (■), 0.72 nM (●), 1 nM (▲), 1.55 nM (▼) and 3 nM (◄).

The inhibition constant  $K_i$  associated with the formation of the reversible enzyme-inhibitor complex (EI) was  $2.5 \pm 0.5$  nM as determined by classical double reciprocal plot and Dixon plot (Figure 12) which is almost equal to the  $IC_{50}$  value of the inhibitor.

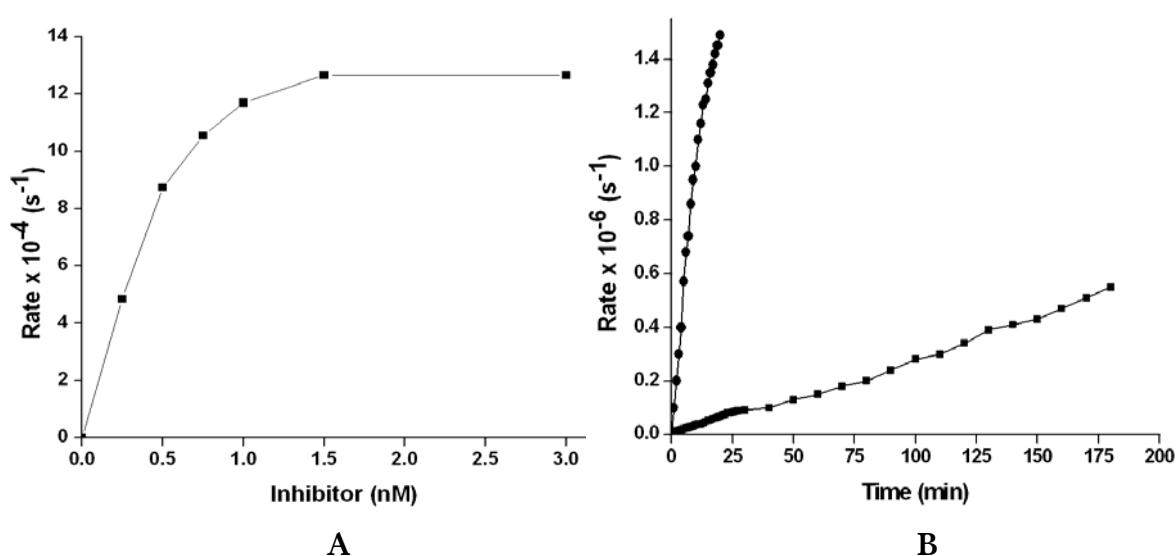


**Figure 12** Initial rate of enzymatic reaction of cathepsin D in the presence of the inhibitor. Enzymatic activity of cathepsin D was estimated using BOC-Phe-Ala-Ala-Phe(p-NO<sub>2</sub>)-Phe-Phe-Val-Leu-OM4P in sodium-citrate buffer, 0.02 M, pH 3.0, Cathepsin D (10 nM) was incubated without (■) or with the inhibitor at 1 nM (●) and 2.5 nM (▲) and assayed at increased concentration of the substrate (1–10 μM) at 37°C for 30 min. The reciprocal of substrate hydrolysis (1/v) for each inhibitor concentration were plotted against the reciprocal of the substrate concentration. The straight lines indicated the best fits for the data obtained by non-linear regression analysis and analyzed by Lineweaver-Burk's reciprocal equation.

The apparent rate constant  $K_{app}$ , derived from the progress curve, when plotted against the inhibitor concentration followed a typical hyperbolic binding curve (Figure 13A), thus favouring a fast equilibrium that precedes the formation of the final slow dissociating enzyme-inhibitor complex (EI\*) and thus indicating a two-step, slow tight inhibition mechanism (Scheme I). The data was fitted to Eq 5 by non-linear regression analysis and the best estimate of the overall inhibition constant  $K_i^*$  of  $6.7 \pm 0.8$  pM was obtained.

The rate constant  $k_6$  for the conversion of EI\* to EI was determined by pre incubating high concentrations of cathepsin D and inhibitor for sufficient time (60 min) to reach equilibrium. Further the enzyme inhibitor mixture was diluted into a relatively large volume of assay mixture containing saturating concentrations of the substrate causes dissociation of the enzyme-inhibitor complex and thus regeneration

of the proteolytic activity of cathepsin D. Under these conditions,  $V_0$  and the effective inhibitor concentration can be considered approximately zero and the rate of regeneration will be provided by the  $k_6$  value. After preincubating cathepsin D with inhibitor, the complex was diluted 10,000 fold into the assay mixture containing the substrate at  $25 K_m$ .  $k_6$  value of  $4.7 \pm 0.4 \times 10^{-6} \text{ s}^{-1}$  was determined by least square minimization of equation 2, which clearly indicates a very slow dissociation of  $EI^*$  (Figure 13B). The final steady state rate  $V_s$  was determined from the control that was preincubated without the inhibitor.



**Figure 13** (A) Dependence of cathepsin D inhibition on inhibitor concentration. The rate constants  $K_{app}$  were calculated from the progress curves recorded following the addition of cathepsin D to the reaction mixture containing synthetic substrate and inhibitor. The solid line indicates the best fit of the data obtained. (B) Dissociation rate constant ( $k_6$ ) for cathepsin D-inhibitor complex. Cathepsin D (10 nM) was preincubated without (●) or with (■) equimolar concentrations of the inhibitor for 120 min in sodium-citrate buffer, 0.02 M, pH 3.0, at 37°C. At the specified times indicated by the points, 5  $\mu\text{l}$  of the preincubated sample was removed, diluted 10,000 fold in the same buffer, and assayed for the proteolytic activity using synthetic substrate at  $25K_m$ . The rate constant associated with the regeneration of activity ( $k_6$ ) was determined as described in the text.

The value of the rate constant  $k_5$  associated with the isomerization of  $EI$  to  $EI^*$  was  $12.7 \pm 0.5 \times 10^{-4} \text{ s}^{-1}$  as obtained from fits of Eq 5 to the onset of inhibition data using the experimentally determined values of  $K_i$  and  $k_6$  (Table 5). The  $k_6$  value indicated a slower rate of dissociation of  $EI^*$  complex and the half-life  $t_{1/2}$  for the reactivation of  $EI^*$  as determined from  $k_6$  values was 40 h, suggesting a higher binding affinity of the inhibitor towards cathepsin D.

**Table 5** Inhibition constants of the inhibitor against human cathepsin D

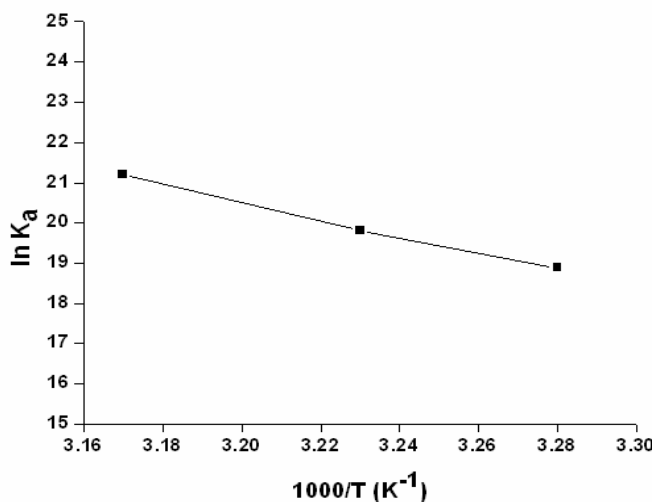
Inhibition constants	Values
$IC_{50}$	$3.2 \pm 0.5$ nM
$K_i$	$2.5 \pm 0.5$ nM
$K_i^*$	$6.7 \pm 0.8$ pM
$k_5$	$12.7 \pm 0.5 \times 10^{-4} \text{ s}^{-1}$
$k_6$	$4.7 \pm 0.4 \times 10^{-6} \text{ s}^{-1}$
$k_5/k_6$	$27 \pm 1.5 \times 10^2$
$t$	$40 \pm 2.2 \times 10^2$ h

From the kinetic point of view, the possible mechanisms for the slow-binding inhibition phenomena are described in Scheme 1. Scheme 1a assumes that the formation of an EI complex is a single slow step and the magnitude of  $k_3I$  is quite small relative to the rate constants for the conversion of substrate to product. This mechanism is ruled out based on the data of table 5, where the inhibitor has measurable effect on the initial rates before the onset of slow-tight binding inhibitions. Scheme 1c illustrates the inhibition model where the inhibitor binds only to the free enzyme that has slowly adopted the transition state configuration, can also be eliminated by the observed rates of onset of inhibition. Our results are in accordance with the two-step slow-binding inhibition, where the first step involves the rapid formation of a reversible EI complex, which undergoes slow isomerization to a stable, tightly bound enzyme-inhibitor complex,  $EI^*$ , in the second step (Scheme 1b).

#### *Thermodynamics of inhibitor binding to human cathepsin D*

The thermodynamic feasibility of the inhibitor isolated from the culture supernatant of *Streptomyces* sp MBR04 by activity guided fractionation was evaluated with human cathepsin D. The effect of temperatures on  $K_i$  was investigated and the

thermodynamic parameters for the association of inhibitor with human cathepsin D were calculated using Vant Hoff plot. The thermodynamic analysis shows that the  $K_i$  kept on increasing with respect to the increase in temperature between 32 and 42°C, and the Vant Hoff plot were linear (Figure 14).



**Figure 14** Vant Hoff plot for association of inhibitor with cathepsin D ( $r=0.9956$  and  $N=3$ )

The quantitative analysis of these plots yielded values for changes in the Gibbs free energies, enthalpies and entropies for binding of the inhibitor to cathepsin D (Table 6). As shown in the table, the Gibbs free energy ( $\Delta G$ ) is negative; indicating that the interaction between the inhibitor and cathepsin D is spontaneous while positive  $\Delta H$  suggests that the overall reaction is endothermic and probably reflects the electrostatic bonding and hydrophobic interactions accompanying the release of constrained water molecules upon inhibitor binding. The negative entropy ( $\Delta S$ ) suggests that the association of inhibitor with cathepsin D is driven by decrease in randomness.

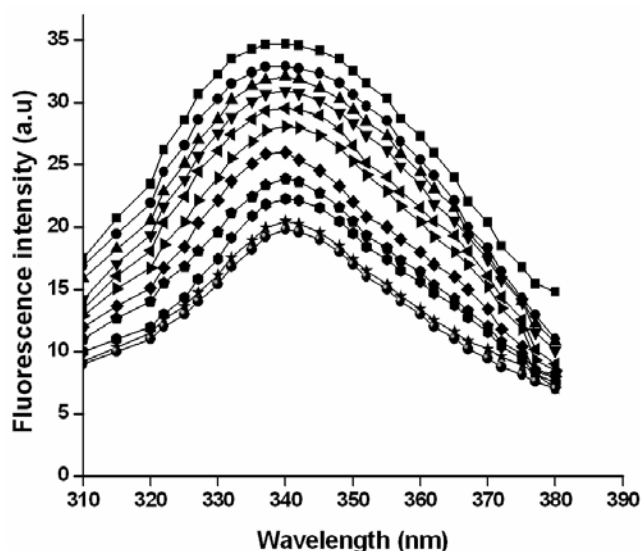
**Table 6** Thermodynamic parameters for the binding of the inhibitor to human cathepsin D

Temperature (K)	$K_i$ (M)	ln $K_a$	$\Delta G$ (kJ/mol)	$\Delta H$ (kJ/mol)	$\Delta S$ (J/mol/K)
305	$-6.24 \times 10^{-9}$	18.891	-47.903	172.554	48.469
310	$-2.52 \times 10^{-9}$	19.807	-51.049	172.523	51.606
315	$-6.21 \times 10^{-10}$	21.199	-54.289	172.471	54.837

$K_i$  determined by Dixon method,  $\Delta G = -RT \ln K_a$ ,  $\Delta H = E_a - RT$ ,  $\Delta G = \Delta H - T\Delta S$

*Fluorometric analysis of cathepsin D-inhibitor interactions*

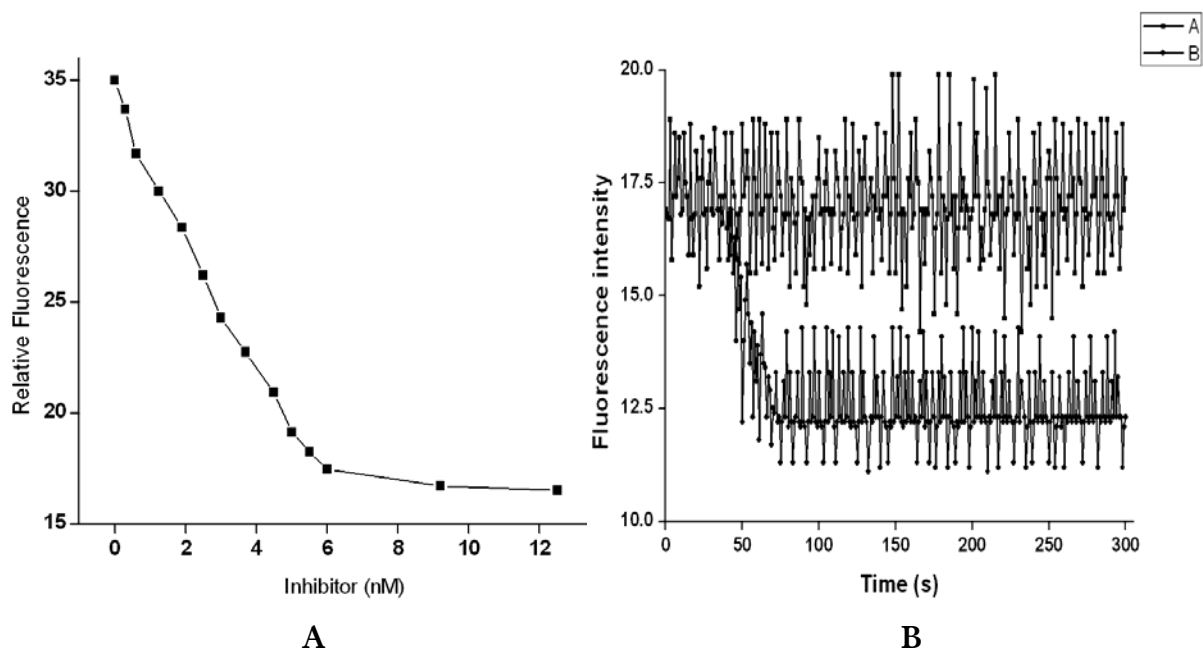
The localized changes induced in the human cathepsin D due to interactions with the inhibitor were investigated by fluorescence spectroscopic analysis. The sequence data reveals the presence of four Trp residues: Trp-40, Trp-54, Trp-206 and Trp-319, two on each chain of the human liver cathepsin D (Gieslmann et al., 1983). The visualization and accessibility calculations of these Trp residues revealed that they are present on the surface of the enzyme and thus are excellent probes to monitor the changes in the tertiary structure due to ligand binding (Swiss PdbViewer v4.0.3). Therefore, the conformational changes induced in the cathepsin D upon binding of the inhibitor were monitored by exploiting the intrinsic fluorescence by excitation of the  $\pi$ - $\pi^*$  transition in the Trp residues. The fluorescence emission spectra of the human liver cathepsin D exhibited an emission maxima ( $\lambda_{\text{max}}$ ) at 342 nm as a result of the radiative decay of the  $\pi$ - $\pi^*$  transition from the Trp residues, confirming the hydrophilic nature of the Trp environment (Figure 15).



**Figure 15** Steady-state fluorescence emission spectra of cathepsin D as a function of inhibitor. Protein fluorescence was excited at 295 nm, and emission was monitored from 300–400 nm at 25 °C. Titration was performed by the addition of different concentrations of the inhibitor to a fixed concentration of enzyme. Cathepsin D was dissolved in 0.05N HCl, and the concentrations of inhibitor used were 0 nM, 0.4 nM, 0.68 nM, 1.3 nM, 2 nM, 2.5 nM, 3.1 nM, 4.12 nM, 4.5 nM, 5 nM, 6 nM (■ - □ respectively).

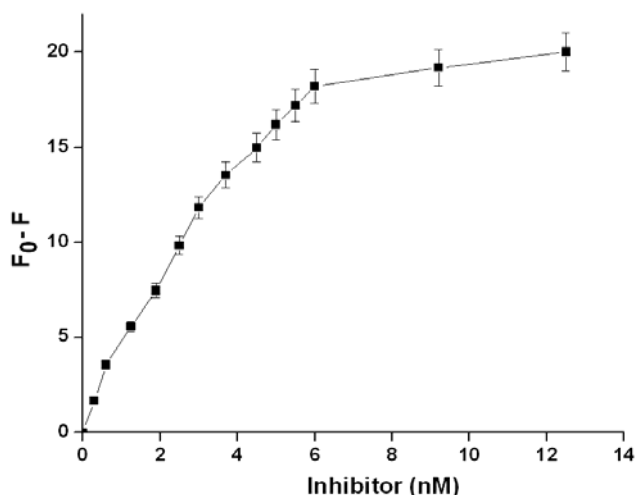
The titration of the native enzyme with increasing concentrations of inhibitor resulted in a concentration dependent quenching of the tryptophanyl fluorescence

(Figure 16A). However, the  $\lambda_{\max}$  of the fluorescence profile indicated no blue or red shift, revealing that the ligand binding caused reduction in the intrinsic protein fluorescence. The subtle conformational changes induced during the isomerization of EI to EI\* was monitored by analyzing the tryptophanyl fluorescence of the complexes as a function of time. Binding of the inhibitor resulted in an exponential decay of the fluorescence intensity as indicated by a sharp decrease in the quantum yield of fluorescence followed by a slower decline to a stable value (Figure 16B).



**Figure 16** (A) The curve represents the best fit of the fluorescence quenching data of cathepsin D at 342 nm ( $\lambda_{\max}$ ) as a function of inhibitor concentration. (B) Time-dependent effect of inhibitor on the fluorescence quenching of cathepsin D. The inhibitor was added to (10 nM) at the specified time (indicated by the arrow), and the fluorescence emission was monitored for 300 s, at a data acquisition time of 0.1 s. The excitation and emission wavelength were fixed at 295 and 342 nm, respectively. The data are the average of five scans with the correction for buffer and dilutions. The concentrations of inhibitor used were 0 nM (A) and 1.25 nM (B).

Furthermore, the titration of the inhibitor against cathepsin D revealed that the magnitude of the initial rapid fluorescence loss ( $F_0 - F$ ) increased in a saturation-type manner (Figure 17), which corroborated the two-step slow-tight binding inhibition of the enzyme by the inhibitor.



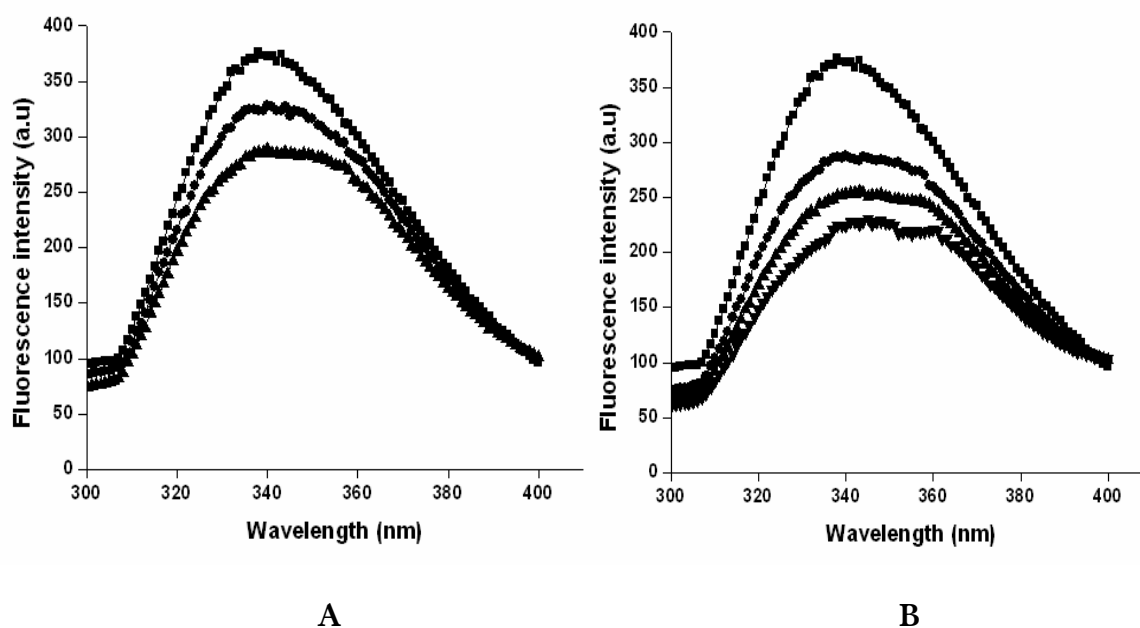
**Figure 17** Effect of inhibitor concentration on the tryptophan fluorescence of cathepsin D. A specified concentration of cathepsin D (10 nM) was treated with increasing concentrations of inhibitor (0–12 nM). The fluorescence was measured at 25 °C (excitation, 295 nm; emission, 342 nm). Each measurement was repeated five times, and the average values of the fluorescence intensity at 342 nm were recorded. Control experiments with the buffer and inhibitor were performed under identical conditions. The fluorescence changes ( $F - F_0$ ) were plotted against the inhibitor concentrations. The resulting hyperbola indicates the best fit of the data obtained and is fitted to equation 8 to give the calculated value of  $K_i$ .

From the data in figure 16B, the magnitude of the rapid fluorescence decrease at a specific inhibitor concentration was found to be close to the total fluorescence quenching observed figure 15, indicating that the EI and EI\* complexes have the same intrinsic fluorescence. The value of  $K_i$  determined by fitting the data for the magnitude of the rapid fluorescence decrease ( $F_0 - F$ ) was  $2.6 \pm 0.5$  nM, and the  $k_s$  value was determined from the data derived from the slow decrease in fluorescence was  $12.7 \pm 0.5 \times 10^{-4} \text{ s}^{-1}$ . These rate constants are in good agreement with that obtained from the kinetic analysis, therefore, the initial rapid fluorescence decrease can be correlated to the formation of the reversible complex EI, whereas the slow, time-dependent decrease reflected the accumulation of the tight bound slow dissociating complex EI\*.

A progressive quenching in the fluorescence of the cathepsin D at 342 nm was observed concomitant to the binding of synthetic substrate (N-t-BOC-Phe-Ala-Ala-*p*-nitro-Phe-Phe-Val-Leu-4-hydroxymethylpyridine ester). Further, to conclude the mechanism of inactivation of the enzyme by the inhibitor, we have analyzed the interaction of a known potent competitive inhibitor, pepstatin by steady-state



intrinsic fluorescence measurements. The binding of the competitive inhibitors led to decrease in the quantum yield of tryptophanyl fluorescence as indicated by the quenching of the emission spectra of the enzyme (Figure 18 A & B). The comparative analysis of the intensity changes in the fluorescence spectra of cathepsin D upon binding of the substrate or the known active site-based inhibitor was found to be similar to that of the peptidic inhibitor, suggesting the binding of the inhibitor to the active site of the enzyme.

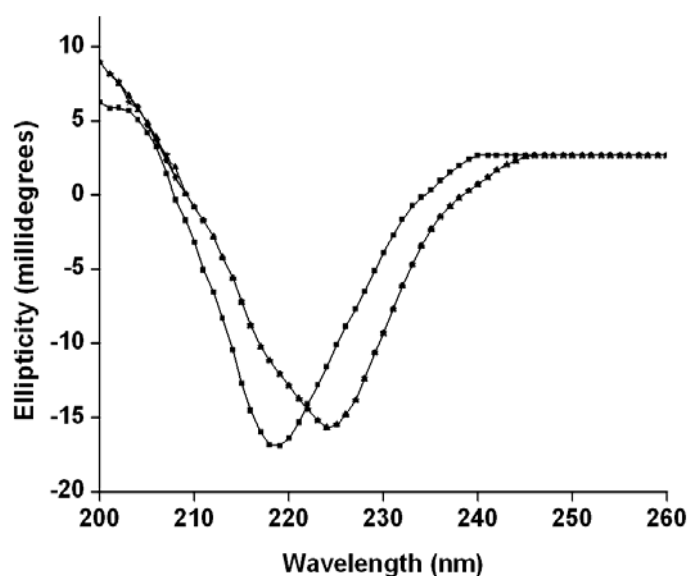


**Figure 18** (A) Fluorescence spectra of cathepsin D in the absence (■) or presence of synthetic substrate at concentrations, 25  $\mu\text{M}$  (●) and 50  $\mu\text{M}$  (▲). Experiments were performed at 4°C to avoid substrate hydrolysis. (B) Effect of pepstatin on the fluorescence quenching of cathepsin D at concentrations, 0 (■), 2.5 (●), 5 (▲) and 10 (▼) nM.

### *Circular dichroism analysis of enzyme substrate-inhibitor complexes*

To elucidate the effects of the inhibitor on the secondary structure of cathepsin D, CD spectra of enzyme-inhibitor complex was analyzed. The secondary structure content of the human liver cathepsin D were 5%  $\alpha$ -helix, 51%  $\beta$ -structure and 29% aperiodic conformation. The circular dichroism spectrum of the enzyme-inhibitor complex showed a pronounced shift in the negative band at 220 nm of the native enzyme to 225 nm (Figure 19). This shift reveals a subtle change in the secondary structure of the enzyme upon ligand binding. To elucidate the changes in the

secondary structure of the enzyme-inhibitor complex, a comparative analysis was performed with cathepsinD-substrate (experiments performed at 4°C to avoid substrate hydrolysis) and cathepsin D-pepstatin complexes. Interestingly, the cathepsin D-inhibitor, cathepsin D-substrate and cathepsin D-pepstatin complexes exhibited a similar pattern of negative ellipticity in the far-UV region, suggesting that the inhibitor causes similar structural changes and was distinctly different from that of the unliganded enzyme.



**Figure 19** Effect of the secondary structure of the cathepsin D upon binding of the substrate or inhibitor. Far-UV circular dichroism spectra of the unliganded cathepsin D (■) and its complexes with the substrate (\*), pepstatin (○) and the inhibitor (●) are shown. Cathepsin D (10 nM) was dissolved in the buffer and the CD spectra were recorded in the absence or in the presence of the substrate 10  $\mu$ M or pepstatin 10 nM or inhibitor 10 nM from 260 to 200 nm at 25 °C. Each spectrum represents the average of six scans.

## DISCUSSION

Currently the research strategies are focusing on the need for improved comprehension of protease-regulated cascades, along with precise selection of targets and improved inhibitor specificity. These inhibitors are mainly synthetic molecules; however there is paucity on biologic inhibitors from microbes. The application of biologic inhibitors will stimulate renewed interest in the therapeutic targeting of aspartic proteases (Scott and Taggart 2010). The data presented here showed that a low molecular weight octapeptide from a *Streptomyces* sp MBR04, as a slow tight binding inhibitor of the aspartic protease, human liver cathepsin D. The inhibitor was found to be specific for cathepsin D and did not show any activity towards other classes of proteases. The determined kinetic data for the enzyme-inhibitor interactions were linked with the conformational changes induced in the enzymes due to the inhibitor binding. The active site of many aspartic proteases has been suggested to accommodate a peptide segment of 5 to 8 residues (Sampath-Kumar and Fruton 1974; James et al., 1982). The inhibitor being an octapeptide can accommodate the active site of cathepsin D which is revealed by the fluorescence and CD studies. During our initial kinetic analysis, the inhibitor showed competitive inhibition against cathepsin D in vitro. The 1:1 molar ratio of the interaction of inhibitor with the target enzyme classified it under the “tight-binding inhibitor” group (Wolfenden 1976; Williams and Morrison 1979). These results were reinforced by the equilibrium binding studies of the enzyme and inhibitor and by the estimation of the residual proteolytic activity. The establishment of equilibria between enzyme, inhibitor, and enzyme-inhibitor complexes, in slow binding inhibition occurs slowly on the steady state time scale (Morrison 1982; Pegg and Itzstein 1994; Kati et al., 1998). The slow-binding inhibition of enzymes can be illustrated kinetically by three mechanisms as described in Scheme 1. Simple second-order interaction between the enzyme (E) and the inhibitor (I) could result in slow-binding inhibition where the rate of complex formation is slow. Kinetically, when an inhibitor has a low  $K_i$  value and the concentration of I varies in the region of  $K_i$ , both  $k_3I$ , and  $k_4$  values would be low. These low rates of association and dissociation

would lead to slow-binding inhibition (Scheme 1a). Alternatively, binding may also involve two steps where there is a rapid formation of an initial collisional complex EI, that subsequently undergoes slow isomerization to form the final tight complex EI\* (Scheme 1b). The extent of EI\* formation depends on the affinity of the EI complex and the relative rates of formation of EI\* and its relaxation to EI. Slow-binding inhibitor can also arise due to an initial slow inter conversion of the enzyme E into another form E\* which binds the inhibitor by a fast step (Scheme 1c). Kinetically, these mechanisms can be differentiated by investigating the behavior of the enzyme-inhibitor system at varying concentrations of the inhibitor. Scheme 1a would predict that in the presence of substrate the initial rate of substrate hydrolysis will be independent of inhibitor concentrations as the concentration of EI would be significantly low. However, in Scheme 1b, the inhibitor will inhibit the enzyme competitively at the onset of the reaction, and at increasing concentration of inhibitor, the initial rate of substrate hydrolysis will decrease hyperbolically. The kinetic properties of the aspartic protease studied in this report provide a unique opportunity to quantitative these rates and affinities. The formation of the first reversible complex, cathepsin D-inhibitor, was too rapid to be measured at steady-state kinetics and was likely to be near diffusion control as revealed for most of the ground-state inhibitors. The rate of formation of the second enzyme inhibitor complex, cathepsin D-inhibitor\*, was slow and relatively independent of the stability of the cathepsin D-inhibitor complex or of the ability of the inhibitor to stabilize the cathepsin D-inhibitor\* complex. Thus the major variable for slow-binding inhibition is  $k_6$ , the first-order rate at which cathepsin D-inhibitor\* relaxes to cathepsin D-inhibitor. An equivalent statement is that the apparent inhibitor constant,  $K_i^*$ , depends on the ability of the inhibitor to stabilize the cathepsin D-inhibitor\* complex. The longer half-life of the cathepsin D-inhibitor\* signified better stability and the slow dissociating nature of these complexes, being the essential parameters for an inhibitor to have biomedical applications.

The crystal structure of cathepsin D and its inhibitor complexes are gaining immense interest among the crystallographers. From the available crystallographic data, it is

deduced that binding of substrate or peptide-analogue inhibitors in the substrate-binding site of cathepsin D induces conformational changes in the flap region. The apparent function of the flap is to force the peptide substrate into a  $\beta$ -sheet in the active site and to correctly position its scissile bond between the two catalytic aspartyl residues (Metcalf and Fusek 1993). The flap accomplishes this by the establishment of a series of hydrogen-bonding interactions between amide nitrogens and carbonyl oxygens of the peptide substrate and the flap region (Baldwin et al., 1993). Our interpretation for the changes observed in the secondary structure of cathepsin D due to the binding of the substrate to the active site can be correlated to the inward movement of the flap. It is significant to note that the secondary structure of cathepsin D undergoes similar pattern of changes upon binding of the substrate or peptidic inhibitor. Thus, we have attributed the observed secondary structure changes in the cathepsin D-inhibitor complex to the inward movement of the flap of cathepsin D.

The characteristic feature of slow binding inhibition is the induction of conformational changes in the enzyme-inhibitor complex, resulting in the clamping down of the enzyme to the inhibitor, thus the formation of a stable enzyme-inhibitor complex. The two-step inhibition mechanism of cathepsin D by inhibitor was reflected in the quenching pattern of the fluorescence of the enzyme-inhibitor complexes. The tryptophanyl fluorescence appears to be uniquely sensitive to shielding by a variety of ligands because of the propensity of the excited indole nucleus to emit energy in the excited state. The Trp residues (Trp-40 and Trp-54) of the cathepsin D are present near to the Thr-72, the first residue of the flap region, which extends from Thr-72 to Leu-87. The inhibitors that bind to the active site induce small structural changes in the flap region of the cathepsin D and decrease the flexibility of flap (Baldwin et al., 1993). The binding of the inhibitor-substrate and the subsequent movement of the flaps may have influence on the intrinsic fluorescence of the Trp residues. Based on the above assumption, we have exploited these Trp residues of the cathepsin D to investigate the localized conformational changes induced upon substrate or inhibitor binding. Our foregoing results have

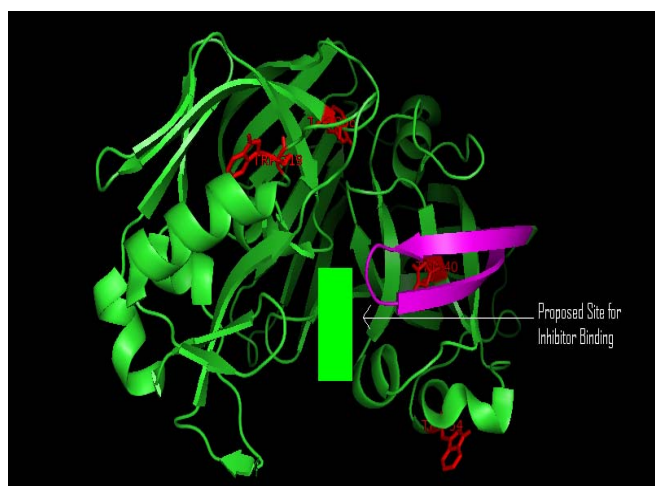
suggested that the inhibitor binds in the active site of the enzyme and is a unique example where the conformational changes in the flaps were investigated by monitoring the radiative decay of the  $\pi$ - $\pi^*$  transition from the Trp residues without mutating any of the residues in the flaps. The fluorescence quenching of cathepsin D by inhibitor revealed that the binding of the inhibitor reduces the quantum yield of the Trp emission. These results were further corroborated by the quenching studies of the cathepsin D in the presence of the substrate and the known classical competitive inhibitor. The inhibition of the cathepsin D by pepstatin is well documented (Knight and Barret 1976; Agarwal and Rich 1983). The quenching of the tryptophanyl fluorescence upon binding of the substrate or the active site inhibitors can be very well explained by the shielding effect of the Trp residues due to the inward movement of the flaps. Residues 79 and 80 at the tip of the flap moved in towards the inhibitor. The comparison of the emission spectra of cathepsin D upon binding of the peptidic inhibitor with that of the substrate or pepstatin led us to conclude that the inhibitor binds to the active site of the enzyme and induces the inward movement of the flap, thereby reducing the radiative decay of the intrinsic Trp fluorescence. The concentration-dependent quenching of Trp fluorescence showed that  $\lambda_{\text{max}}$  did not undergo any red or blue shift, wherein the quenching of fluorescence was considerably high. These findings indicated that the polarity of the Trp environment was negligibly altered after binding of the inhibitor, suggesting minimal conformational changes in the tertiary structure of the cathepsin D.

The rate constants derived from the fluorescence analysis of the complexes reinforced the values derived from the kinetic analysis. Therefore, we propose that the initial rapid fluorescence loss reflected the formation of the reversible complex EI, whereas the subsequent slower decrease was correlated to the accumulation of the tightly bound complex EI\*. Any disturbance in the environment of tryptophan residues may be reflected in an alternation in emission wavelength, quantum yield, and susceptibility to quenching (Pawagi and Deber 1990). Energy transfer to an acceptor molecule having an overlapping absorption spectrum can also contribute to fluorescence quenching (Cheung 1991). However, because the inhibitor has no

absorption in the region of 290–450 nm, the fluorescence quenching due to the energy transfer between the inhibitor and the tryptophan residues of cathepsin D have been neglected. The other possibility is the presence of multiple sites, where binding at one induced rapid fluorescence change and at a second site caused the slow fluorescence decrease. This was verified by titrating a fixed concentration of cathepsin D with increasing concentrations of the inhibitor. The proteolytic activity decreased linearly with increasing concentrations of inhibitor yielding a stoichiometry close to 1:1 (also revealed by fluorescence) expected for the slow-tight binding inhibition, therefore inconsistent with the presence of multiple high affinity sites. From the physical explanation for the quenching process, it was apparent that the inhibitor induced fluorescence quenching followed the formation of both the complexes. The agreement of the rate constants concomitant with the fluorescence changes observed during the time-dependent inhibition led us to correlate the localized conformational changes in the enzyme-inhibitor complex to the isomerization of the EI to EI\*.

Most of the synthetic oligopeptides and proteinaceous inhibitors of cathepsin D reported in literature (Gacko et al., 2007) are required in high molar concentrations for inhibitory activities, hence have not found application in therapeutic formulations to target cathepsin D in human diseases and are maximally restricted to use in research laboratories as protease inhibitor cocktails. Pepstatin and its derivatives are competitive inhibitors of cathepsin D (Lin and William 1979). Pepstatin-cathepsin D is stabilized by numerous hydrogen bonds between the backbone atoms of inhibitor and both main and side chain atoms of the enzyme. Pepstatine side chains make extensive van der Waals contacts with enzyme subsites (Baldwin et al., 1993). Being a peptidic inhibitor containing Asp, Ala, Gly and Leu residues, the inhibitor will have a similar mode of interaction with the residues in the active site of cathepsin D to that of pepstatin, however it is not feasible to understand the interactions at the atomic level at present. However the crystal structure will aid in understanding the mechanism of inactivation of cathepsin D by the inhibitor in depth and will further shed light on the molecular interactions

between the enzyme and inhibitor. With the existing experimental evidence, we visualize that the charged side chains of the amino acids, the amide nitrogens, and the carbonyl oxygen groups of the inhibitor could form many intermolecular hydrogen bonds and other weak interactions (van der Waals, ionic, etc.) with the  $\beta$ -sheet of the flaps and with the other residues present in or near the active site. Further, we propose that the tight binding and competitive nature of the inhibitor in conjunction with the multiple nonbonded interactions may be sufficient to cause the loss of the dynamic flexibility of the flap, which is crucial for the substrate binding and catalysis of the enzyme. A schematic diagram representing the proposed mechanism is depicted in figure 20. The binding of the inhibitor indicated that the inhibitor-complex form of the cathepsin D loses its binding ability to the substrate, since the flap can no more open up for the substrate to be aligned in the active site of cathepsin D, which subsequently results in the inactivation of the enzyme. These observations are at variance with the binding of the substrate to the enzyme in the absence of inhibitor, where the flexibility of the flap can be regained after catalysis.



**Figure 20** Schematic representation of the proposed mechanism of inhibition of the cathepsin D by inhibitor. Secondary structure of the cathepsin D is shown by the stereoview ribbon diagram derived from PDB database (PDB 1LYA). The cathepsin D and other aspartic proteases have the structural feature called the “flap region” (magenta color) which is important for the substrate binding and catalysis. The binding of the inhibitor (as indicated by the solid block) in the active site induces inward movement of the flaps. Further, we propose that the slow-tight binding nature of the inhibitor, along with its multiple non-bonded interactions with the flaps, is responsible for the loss of the dynamic flexibility of the flaps, resulting in the inactivation of the cathepsin D.



The kinetic analysis demonstrated that the inhibition of cathepsin D by the inhibitor, followed slow-tight binding inhibition mechanism and the induced conformational changes, is conveniently monitored by fluorescence spectroscopy. Based on our observations, we conclude that, concomitant with the kinetic analysis, fluorescence spectroscopy plays a very important role in the determination of kinetic constants of enzyme inhibition, as discussed for the characterization of the mechanism of inhibition of cathepsin D by the slow-tight binding inhibitor. All these kinetic, thermodynamic and quenching studies suggest that the newly isolated peptidic inhibitor could be a potential scaffold to study and can be used to develop new potent therapeutic lead molecule for the development of drugs targeted towards diseases associated with cathepsin D such as carcinomas and degenerative diseases.

**BIBLIOGRAPHY**

- Agarwal N, Rich DH (1983) *Anal. Biochem.* **130**, 158-165.
- Andrade MA, Chacon P, Merelo JJ and Moran F (1993) *Protein. Eng.* **6**, 383-390.
- Antonov VK, Ginodman LM et al (1978) *FEBS Lett.* **88**, 87-90.
- Arana JL and Vallejos RH (1981) *FEBS Lett.* **123**, 103-106.
- Augereau P, Garcia M, Mattei MG, Cavailles V, Depadova F et al (1998) *Mol. Endocrinol.* **2**, 186-192.
- Baldwin ET, Bhat N, Gulnik S, Hosur MV, Sowder RC, Cachau RE, Collins J, Silva AM, Erickson JW (1993) *Proc. Natl. Acad. Sci. USA.* **90**, 6796-6800.
- Barrett AJ (1977) *Proteinases in mammalian cells and tissue*, Elsevier, North-Holland, New York, pp. 209-248.
- Beith JG (1995) *Methods Enzymol.* **248**, 59-84.
- Benes P, Vetvicka V Fusek M (2008) *Cr. Rev. Oncol-Hem.* **68**, 12-28.
- Berman HM, Westbrook J, Feng Z, Gilliland G, Bhat TN, Weissig H, Shindyalov IN and Bourne PE (2000) *Nucleic Acids Res.* **28**, 235-242.
- Caffrey CR, Placha L, Barinka C, Hradilek M, Dostal J, Sajid M, McKerrow JH, Majer P, Konvalinka J Vondrasek J (2005) *Biol. Chem.* **386**, 339-349.
- Capony F, Rougeot C, Montcourrier P, Cavailles V, Salazar G, Rochefort H (1989) *Cancer Res.* **49**, 3904-3909.
- Cataldo AM & Nixon RA (1990) *Proc. Natl. Acad. Sci. USA* **87**, 3861-3865.
- Cha S (1975) *Biochem. Pharmacol.* **24**, 2177-2185.
- Cha S (1976) *Biochem. Pharmacol.* **25**, 1561-1569.
- Cheung HC (1991) In *Topics in Fluorescence Spectroscopy, Principles*. Lakowicz JR (ed), Plenum Press, NY

Dash C, Phadtare S, Desphande V, Rao M (2001) *Biochemistry* **40**, 11525-11532.

Dash C, Rao M (2001) *J. Biol. Chem.* **276**, 2487-2493.

Dhanraj V, Dealwis CG, Frazao C, Badasso M et al. (1992) *Nature (London)* **357**, 466-472.

Dixon M (1953) *Biochem. J.* **55**, 170-171.

Foltmann B (1981) *Essays Biochem* **17**, 52-84.

Friedman LS, Peterson WL (1998) Harrison's principles of internal medicine, McGraw & Hill.

Fujinaga M, Chernaia MM, Tarasova NI, Mosimann SC, James MNG (1995) *Protein Science* **4**, 960-972.

Gacko M, Minarowska A, Karwowska A, Minarowski L (2007) *Folia. Histochem. Cyto.* **45**, 291-313.

Gelb M, Svaren J and Abeles R (1985) *Biochemistry* **24**, 1813-1817.

Gieselmann VR, Pohlmann A, Hasilik A, Figura K (1983) *J. Cell. Biol.* **101**, 824-829.

Goldfarb NE, Lam MT, Bose AK, Patel AM, Duckworth AJ, Dunn BM (2005) *Biochemistry* **44**, 15725-15733.

Gopalan P, Dufrense MJ, Warner AH (1987) *Can. J. Physiol. Pharmacol.* **65**, 124-129.

Guagliardi LE, Koppelman B, Blum JS, Marks MS, Cresswell P, Brodsky FM (1990) *Nature (London)* **343**, 133-139.

Henderson P (1972) *Biochem. J.* **127**, 321-333.

Hindmarsh AC (1983) In: Scientific Computing. Stepleman, RS (ed). North Holland, Amsterdam, pp 55-64.

Houtzager V, Oullet M, Falguyret JP, Passmore LA, Bayly C, Percival MD (1996) *Biochemistry* **35**, 10974-10984.

Hunt LT, Dayhoff O (1970) *Biochem Biophys Res Commun.* **39**, 757-765.

- Huo S, Wang J, Cieplak P, Kollman PA, Kuntz ID (2002) *J Med Chem.* **45**, 1412-1419.
- James MNG, Sielecki A, Salituro F, Rich DH, Hofmann T (1982) *Proc.Natl.Acad.Sci. U.S.A.* **79**, 6137-6141.
- James MNG, Sielecki AR, Hayakawa K, Gelb MH (1992) *Biochemistry* **31**, 3872-3888.
- Kati WM, Saldivar AS, Mohamadi F, Sham HL, Laver WG, Kohlbrenner WE (1998) *Biochem. Biophys. Res. Commun.* **244**, 408-413.
- Kenessey A, Banay-Schwartz M, DeGuzman T, Lajtha AJ (1989) *Neurosci. Res.* **23**, 454-456.
- Knight CG, Barret AJ (1976) *Biochem. J.* **155**, 117-125.
- Kornfeld S, Meilman I (1989) *Annu. Rev. Cell Biol.* **5**,483-525.
- Kumar A, Rao M (2006) *Bio. Biophys. Acta.* **1760**, 1845-1856.
- Kumar A, Rao M (2010) *Bio. Biophys. Acta.* **1800**, 526-536.
- Lakowicz JR (1983) Principles of fluorescence spectroscopy, Plenum Press, NY, USA.
- Lanza FL, Nelson RS, Rack MF (1984) *J Clin Pharmacol* **24**: 89-95.
- Lee AY, Gulnik SV, Erickson JW (1998) *Nat. Struct. Biol.* **5**,866-871.
- Leung D, Abbenate G, Fairlie DP (2000) *J Med Chem.* **43**; 305-341.
- Levy HM, Leber PD, Ryan EM (1963) *J. Biol.Chem.* **238**, 3654-3659.
- Lin TY, William HR (1979) *J. Biol. Chem.* **254**, 11875-11883.
- Lin Y, Fusek M, Lin X et al (1992) *J. Biol. Chem.* **267**, 18413-18418.
- Masson O, Bach AS, Derocq D, Prebois C, Laurent-Matha V, Patingre S Liaudet-Coopman E (2010) *Biochimie.* **92**, 1635-1643.

Matus A, Green GDJ (1987) *Biochemistry* **26**, 8083-8086.

Merelo JJ, Andrade MA, Prieto A, Moran F (1994) *Neurocomputing* **6**, 443-454.

Metcalf P and Fusek M (1993) *EMBO. J.* **12**, 1293 – 1302.

Morrison JF (1982) *Trends. Biochem. Sci.* **7**, 102-105.

Morrison JF (1969) *Biochim. Biophys. Acta* **185**, 269.

Morrison JF, Stone SR (1985) *Comments. Mol. Cell. Biophys.* **2**, 347-368.

Morrison JF, Walsh CT (1988) *Adv. Enzymol. Relat. Areas. Mol. Biol.* **61**, 201-302.

Moss ML, Kuzmic P, Stuart JD, Tian G, Peranteau AG, Frye SV, Kadwell SH, Kost TA, Overton LK, Patel IR (1996) *Biochemistry* **35**, 3457-3464.

Okuyama T , Satake K (1960) *J. Biochem.* **47**, 454-466.

Pawagi AB, Deber CM (1990) *Biochemistry-US.* **29**, 950–955.

Pegg MS, Itzstein MV (1994) *Biochem. Mol. Biol. Int.* **32**, 851-858.

Peters PJ, Neeijes JJ, Oorschot V, Ploegh HL & Geuze HJ (1991) *Nature (London)* **349**, 669-676.

Ploux O, Breyne O, Carillon S and Marquet A (1999) *Eur. J. Biochem.* **259**, 63-70.

Reich JG (1992) *Curve Fitting and Modelling for Scientists and Engineers*, Graw-Hill, NY, USA.

Reid WA, Valler MJ Kay J (1986) *J. Clin. Pathol.* **39**, 1323-1330.

Rich D, Sun E (1980) *Biochem. Pharmacol.* **29**, 2205-2212.

Rich DH (1986) Inhibitors of aspartic proteinases. In: *Proteinase inhibitors*. Barrett AJ, Salvesen G (eds). Elsevier (Amsterdam) 179-217.

Ryle AP (1970) *Methods Enzymol.* **19**, 316-336.

Samloff IM (1969) *Gastroenterology* **57**,659-669.

Sampath-Kumar PS, Fruton JS (1974) *Proc.Natl.Acad.Sci. U.S.A.* **71**, 1070-1072.

Scott CJ, Taggart CC (2010) *Biochimie.* **92**, 1681-1688.

Sculley MJ, Morrison JF, Cleland WW (1996) *Bio. Biophys. Acta.* **1298**, 78-86.

Siintola E, Partanen S, Stromme P, Haapanen A, Haltia M et al. (2006) *Brain.* **129**, 1438-1445.

Sinha U, Brewer JM (1985) *Anal. Biochem.* **151**, 327-333.

Suguna K, Padlan EA, Smith, CW, Catlson WD, Davies DR (1987) *Proc. Natl. Acad. Sci. U.S.A.* **84**, 7009-7013.

Szedlacsek SE, Duggleby RG (1995) *Methods Enzymol.* **249**, 144-180.

Tobey NA, Hosseini SS, Caymaz-Bor C, Wyatt HR, Orlando GS, Orlando RC (2001) *Am. J. Gastroenterol.* **96**, 3062-3070.

Umezawa H, Takita T, Shiba T (1978) "Bioactive Peptides Produced by Microorganisms" Halsted, New York.

Vetvicka V, Vektvickova J, Fusek M (1994) *Cancer. Lett.* **129**, 131-135.

Von Figura K, Hasilik A (1986) *Annu. Rev. Biochem.* **55**, 167-193.

Williams JW, Morrison JF (1979) *Methods. Enzymol.* **63**, 437-467.

Woessner JF Jr (1971) In Tissue Proteinases, Barrett AJ, Dingle JT (eds). North-Holland, New York, pp 291-308.

Wolfenden R (1976) *Annu. Rev. Biophys. Bioeng.* **5**, 271-306.

Yamamoto K (1999) Cathepsin E and Cathepsin D. In: Proteases. New perspectives. Turk V (ed). Birkhäuser Verlag Basel, pp 59-71.

Yonezawa S., Takahashi T., Wang X., Wong RNS (1988) *J. Biol. Chem.* **263**, 16504-16511.

# Chapter 5

*‘The study of establishment and spread of plant diseases is an exercise in plant ecology. The interactions involved are multidimensional and the partial control of such leads to disease management’*

Robert Schein

**Aspartic protease inhibitor from *Penicillium* sp  
VM24 as antifungal peptide: Implications in  
combating mycotic infections**



## SUMMARY

A low molecular weight inhibitor from *Penicillium* sp VM24 was found to exhibit inhibitory activity against phytopathogenic fungi, including *Aspergillus fumigatus*, *Aspergillus niger*, *Aspergillus oryzae*, *Claviceps purpurea*, *Colletotrichum* sp., *Curvularia fallax*, *Fusarium oxysporum*, *Fusarium moniliforme*, *Fusarium udum*, *Fusarium solani* and *Rhizopus* sp. The 50% inhibitory concentrations of the peptidic inhibitor ranged from 0.58 to 4.5 µg/ml, whereas the MIC varied from 0.30 to 2.8 µg/ml for the fungal growth inhibition. Microscopic observation of the fungal cultures treated with the inhibitor revealed a reduction in mycelial growth or retardation of spore germination. Growth of representative phytopathogenic fungi on synthetic selective media containing specified carbon sources produced xyloglucanase or aspartic protease. The fungal growth inhibition in the presence of inhibitor revealed the role of these enzymes in growth. The chemical modification of Asp/Glu or Lys residues of the inhibitor by 2,4,6-trinitrobenzenesulfonic acid and Woodward's reagent K respectively, abolished the antifungal activity. The kinetic analysis of the TNBS and WRK modified inhibitor abolished its antixyloglucanolytic and antiproteolytic activity. In addition, the inhibitor inhibited xyloglucanase and aspartic protease with  $K_i$  values of 500 nM and 0.85 µM respectively. Our investigations led us to envisage a paradigm shift in the concept of fungal growth inhibition for the role of antixyloglucanolytic and antiproteolytic activity.

## INTRODUCTION

Plant diseases caused by viruses, bacteria and fungi affect crops, and are responsible for significant losses or decrease in the quality and safety of agricultural products. Their control relies mainly on chemical pesticides (Agrios 2005). Effective control of fungal plant pathogens is achieved by application of fungicides. Currently available antifungal compounds raise human health and environmental safety concerns that have resulted in the withdrawal of some of them. In addition, resistance problems have been encountered and could result in loss of effectiveness of fungicides (Knight et al., 1997; Holmes and Eckert 1999). New agents, which could substitute for or complement available fungicides, should therefore have properties that differentiate them from existing compounds. The past decade has witnessed a dramatic growth in knowledge of natural peptides. Antimicrobial peptides (AMPs) have been the object of attention in past years as candidates for plant protection products. Antimicrobial peptides have been isolated from very diverse organisms, bacteria (Cooter et al., 2005; Raaijmakers et al., 2006), fungi (Degenkolb et al., 2003; Ng 2004), insects (Hancock 2001; Bulet et al., 2004), marine invertebrates (Tincu and Taylor 2004), amphibians and mammals (Zaslhoff 2002; Toke 2005), and plants (Lay and Anderson 2005). A number of them have received attention because of their low toxicity against mammalian cells (Steiner et al., 1988). They are short sequence peptides, with generally fewer than 50 amino acid residues reported in living systems, which are a first line of defence in plants and animals.

### Classification of AMPs

AMPs are classified based on their structural characteristics and mode of action. Based on structural characteristics they are grouped to linear peptides often adopting helical structures, cysteine-rich open-ended peptides containing disulphide bridges, and cyclopeptides forming a peptide ring. Linear and cyclic peptides may be lipopeptides or pseudopeptides. On the basis of mode of action, the first group of AMPs acts by lysis, which occurs via several mechanisms (Shai 1995). Lytic peptides may be amphipathic, that is, molecules with two faces, with one being positively charged and the other being neutral and hydrophobic. Some amphipathic peptides

bind only to the membrane surface and can disrupt the membrane structure without traversing the membrane. Others traverse membranes and interact specifically with certain molecules. Finally, other amphipathic peptides aggregate in a selective manner, forming aqueous pores of variable sizes, allowing passage of ions or other solutes. The second peptide group interferes with cell wall synthesis or the biosynthesis of essential cellular components such as glucan or chitin (Debono and Gordee 1994).

### **Microbial AMPs**

Microorganisms produce a wide range of antimicrobial peptides that include small bacteriocins and fungal defensins synthesized through ribosomal synthesis, and peptaibols, cyclopeptides and pseudopeptides that are secondary metabolites produced by non-ribosomal synthesis.

#### *Bacteriocins and fungal defensins*

Bacteriocins are a type of protein and peptide secreted by major groups of bacteria that kill closely related species. Examples of large bacteriocins that inhibit plant pathogenic bacteria have been reported from bacteria associated with plants (Ishimaru et al., 1988; Jabrane et al., 2002; Lavermicocca et al., 2003; Pham et al., 2004), but small bacteriocins have not been tested. Several filamentous fungi secrete AMPs of 51–58 amino acid residues similar to defensins from animals and plants, with a compact structure of antiparallel strands stabilized by disulphide bridges. Proteins with such properties with antifungal activity have been isolated from four fungal species belonging to the Ascomycetes, *Penicillium chrysogenum*, *Penicillium nalgiovense*, *Aspergillus giganteus* and *Aspergillus niger*. Furthermore, *in silico* investigation of genomic databases has revealed putative proteins with high homology to those already isolated in *Gibberella zeae*, *Aspergillus clavatus* and *Neosartorya fischeri* (Marx 2004; Meyer 2008). The peptides AFP from *Aspergillus giganteus* (Lacadena et al., 1995), PAF from *Penicillium chrysogenum* and *Penicillium nalgiovense* (Kaiserer et al., 2003) and Anafp from *Aspergillus niger* (Lee et al., 1999) have antifungal activity. AFP is active against *Botrytis cinerea*, *Fusarium* sp and *Pyricularia oryzae*, but is inactive against bacteria (Vila et al., 2001; Moreno et al.,

2003 & 2005). PAF and AFP are the most intensively studied fungus-derived antifungal peptides. It has been shown that, in sensitive fungi, PAF is internalized by receptor-mediated endocytosis and exerts multiple detrimental effects: induction of morphological changes, membrane perturbation, intracellular oxidative stress and apoptosis (Kaiserer et al., 2003; Leiter et al., 2005; Marx et al., 2008). In susceptible organisms a small proportion of the applied AFP binds electrostatically to the cell membrane and induces pore formation. A large amount of AFP accumulated in the cell wall, digesting it; furthermore, AFP inhibits chitin synthesis (Theis et al., 2003 & 2005; Hagen et al., 2007) and also binds to DNA via an oligonucleotide/oligosaccharide binding motif and causes chromatin condensation (del Pozo et al., 2002). AFP is highly stable- it has been shown to preserve its antifungal activity up to 14 days after application (Moreno et al., 2003).

The effects of filamentous fungi-derived antifungal peptides have only been investigated in a very limited number of filamentous fungal isolates to date. They have a narrow antimicrobial spectrum but their species specificity is different (Marx 2004). AFP and PAF treatment results in strong antifungal effects in the case of some opportunistic human and/or plant pathogens belonging to the Ascomycetes and Zygomycetes (Galgoczy et al., 2005; Barna et al., 2008). This inhibition acts by disrupting sporangium and conidium formation, the germination of sporangiospores and conidia and/or hyphal extension. Treated mycelia are swollen and short, with multiple branches and spores displaying abnormal and delayed germination when cultivated in antifungal peptide-containing medium (Kaiserer et al., 2003; Moreno et al., 2003). Activity against yeasts has not been reported for any of the above-mentioned antifungal proteins so far and only *A. niger* antifungal inhibited growth of *Candida albicans*, *Saccharomyces cerevisiae* and *Trichosporon beigelii* (Marx 2004). It may be hypothesized that a combined application of different species specific antifungal peptides against fungal infection represents a promising novel broad-spectrum antifungal therapy or fungicide.

### *Peptaibols*

Peptaibols are linear peptides, usually composed of a C-terminal amino alcohol and an acyl N-terminus, which are rich in dialkylated aminoacids such as  $\alpha$ -diaminobutyric acid (Degenkolb et al., 2003). The lipopeptaibols have an acylated N-terminus composed of a short fatty acid chain (Toniolo et al., 2001). Peptaibols have been reported in several fungi. Their antimicrobial activity affects mainly fungi and plant pathogenic Gram positive bacteria by a mechanism of membrane disruption. Trichokonins are active against the plant pathogenic bacterium *Clavibacter michiganensis* and the fungi *Fusarium oxysporum*, *Botrytis cinerea*, *Rhizoctonia solani*, *Bipolaris sorokiniana* and *Colletotrichum* sp (Xiao-Yan et al., 2006). Trichorzins and harzianins show antifungal activity against *Sclerotium cepivorum* (Goulard et al., 1995). Some strains of fungi that are biological control agents of plant diseases and pertain to species of *Trichoderma* and *Gliocladium*, produce such compounds, which have been implicated in its mechanism of action (Schirmbock et al., 1994).

### *Cyclopeptides*

Antimicrobial cyclopeptides are secondary metabolites reported from bacteria, fungi and cyanobacteria that are composed of amino acid residues including D- and L-forms as well as allo- and diamino derivatives, arranged in a cyclic ring, usually without disulphide bridges. Depending on the nature of the cyclization, the cyclopeptides have only the peptide ring or may have an additional peptide tail and may be lipidic due to the presence of an acyl group (DeLucca & Walsh, 1999; Bonmatin et al., 2003; Raaijmakers et al., 2006). Lipidic cyclopeptides (LCPs) are produced by several plant-associated and soil-inhabiting bacteria and have antifungal and antibacterial, cytotoxic or surfactant properties. LCPs from *Pseudomonas* sp are mainly of the depsipeptide type and are classified into seven major groups (i.e. amphisins, corpeptins, putisolvins, syringomycins, syringopeptins, tolaasins and viscosins), based on the length and composition of the fatty acid, and the peptide ring and tail (Raaijmakers et al., 2006). These peptides mainly exhibit inhibitory activity towards Gram-positive bacteria, *Rhizoctonia solani* (Bassarrello et al., 2004), *Botrytis cinerea* (Lavermicocca et al., 1997), *Sclerotinia sclerotiorum* (Pedras et al., 2003), *Pythium ultimum* (Nielsen & Sorensen, 2003).

### *Other antifungal peptides derived from bacteria and fungi*

#### *Bacterial peptides*

***Bacillus licheniformis* peptides.** CB-1 is a chitin-binding peptide containing fatty acids bound to amino acids and inhibits *F. oxysporum* (Oita et al., 1996). A *B. licheniformis* isolate, M-4, produces fungicin M-4 (Lebbadi et al., 1994). It is a hydrophilic, narrow-spectrum antifungal peptide and inhibits the growth of *Microsporium canis*, *Mucor* species, and *Sporothrix schenckii*. *B. licheniformis* also produces A12-C, a fungal cell growth and hyphal proliferation inhibitor. A12-C inhibited *S. schenckii*, *T. mentagrophytes*, and *M. canis* growth, as observed in zone-of-inhibition studies (Galvez et al., 1993).

***Extremophilic Bacillus* sp.** A low molecular weight bifunctional peptidic inhibitor from an extremophilic *Bacillus* sp was found to inhibit several phytopathogenic fungi belonging to *Aspergillus* sp, *Fusarium* sp, *Penicillium* sp (Dash et al., 2001).  
***Cepacidines.*** Cepacidines A1 and A2 are glycopeptides that have similar structures and that are produced by *Burkholderia cepacia* (Lee et al., 1994; Lim et al., 1994). Together, they displayed potent antifungal properties against *Candida* species, *C. neoformans*, *A. niger*, *T. mentagrophytes*, *Trichophyton rubrum*, *M. canis*, and *F. oxysporum* (Lee et al., 1994).

#### *Fungal peptides*

**1907-II and 1907-VIII.** *P. lilacinus* produces two antifungal peptides, 1907-II and 1907-VIII, consisting of several amino acids, a methylamine, and a fatty acid (Sato et al., 1980). In vitro, peptides exhibit inhibitory activity against *Candida* species.  
***Leucinostatin-trichopolyn* group.** The leucinostatin-trichopolyn group is structurally related to 1907-II and 1907-VIII. Leucinostatins A and B are produced by submerged cultures of *Penicillium lilacinum* (Fukushima et al., 1983). Leucinostatins D, H, and K were isolated from *Paecilomyces marquandii* (Masse) Hughes and had a wide spectrum of antimicrobial properties against *Candida* species, *C. neoformans*, and other clinically important fungi (Radics et al., 1987; Rossi et al., 1987). Trichopolyns A and B are produced by *Trichoderma polysporum* (Fujita et al., 1981) and exhibit antifungal activity towards *C. albicans*, *C. neoformans*, *A. niger*, *A. fumigatus*, and *T. mentagrophytes*.

*Helioferins.* *Mycogone rosea* produces helioferins A and B, which are members of the leucinostatin-trichopolyn group that inhibiting *C. albicans*.

AMPs are attractive as antimicrobial compounds for plant disease control due to their mechanism of action against the target microorganism. Most AMPs are cationic and bind to the surface of microorganisms through receptor-mediated interaction and insert into the cytoplasmic membrane. Several AMPs are membrane disruptive, but others are non-membrane disruptive and cross the cell membrane to interact with intracellular targets and inhibit nucleic acid or protein synthesis, or enzymatic activity (Powers & Hancock, 2003; Brogden, 2005). Unfortunately, AMPs from microbial origin like LCPs and peptaibols have significant phytotoxicity that limits its direct use as plant protection products. However, several AMPs have been used as the basis for the development of shorter and less toxic analogues by synthetic procedures. Some AMPs play a role in biocontrol agents of plant diseases (Belen et al., 2002). The fact that animal and plant AMPs are produced by ribosomal synthesis, has provided tools for developing transgenic plants expressing genes coding for the synthesis of these compounds conferring partial or total resistance to plant pathogens.

Successful use of AMPs has been achieved through the commercial development as biopesticides of several microorganisms secreting these compounds. Although numerous transgenic plants expressing AMPs that confer different degrees of protection against diseases have been developed, commercial cultivars have not been marketed because of regulatory limitations and social concerns. Synthetic approaches to obtain AMPs guided by combinatorial chemical methods provide powerful tools to optimize molecules derived from natural compounds with improved activity against selected target pathogens, including decreased cytotoxicity and increased protease stability (Montesinos 2007). However, exploitation of the great number of AMPs as active ingredients of pesticides has not been accomplished yet. The majority of AMPs with potential uses have been studied at the *in vitro* level, fewer compounds have been tested on plant pathosystems, and only a few are on the market (De Lucca and Walsh 1999). Development of compounds suitable for

agricultural use as pesticide ingredients have several constraints mainly due to the intrinsic toxicity and low stability of some of the compounds, the requirement to develop suitable formulations, and the need for inexpensive products in plant protection. Therefore, future areas of interest consist of developing less toxic and more stable compounds as well as decreasing production costs by improving preparative synthesis and biotechnological procedures using microbial systems (Wimley 2010).

In the present chapter we have evaluated the antifungal potential of a low molecular weight peptidic inhibitor from *Penicillium* sp VM24 against phytopathogenic fungi *in vitro*. The kinetic studies revealed the bifunctional characteristics of the inhibitor, as it was found to inhibit xyloglucanase and aspartic protease (Chapter 6). Chemical modification of the carboxylic and amine groups of the inhibitor resulted in the loss of inhibitory activity against xyloglucanase and aspartic protease and also in the loss of antifungal property, indicating the correlation of these enzymatic activities to fungal growth. The inhibitor will be significant as a biocontrol agent for the protection of plants against phytopathogenic fungi.



## EXPERIMENTAL PROCEDURES

### *Materials*

Mueller-Hinton agar, Potato dextrose, bactoagar and other microbiological media components were from Himedia, India. DNSA was from Sigma Chemical co. USA. Filter discs were from Whatman. All other chemicals were of analytical grade.

### *Fungal Strains*

The fungal strains, *Aspergillus fumigatus* (NCIM 902), *Aspergillus niger* (NCIM 773), *Aspergillus oryzae* (NCIM 637, 643, 649, 1032), *Claviceps purpurea* (NCIM 1046), *Colletotrichum* sp., *Curvularia fallax* (NCIM 714), *Fusarium oxysporum* (NCIM 1008, 1043, 1072), *Fusarium moniliforme* (NCIM 1099, 1100), *Fusarium solani*, *Penicillium roqueforti* (NCIM 712), and *Rhizopus* sp (NCIM 1299) were from our in-house culture collection unit, National Collection of Industrial Micro-Organisms (NCIM), Pune, India. *Fusarium udum* was isolated in our laboratory from infected pigeon pea plants (Kulkarni A 2007).

### *Antifungal activity assay*

Antifungal activity of the inhibitor was assayed by a) hyphal extension inhibition assay, b) spore suspension assay, and c) micro-spectrometric assay. The hyphal extension assay was carried out as described (Roberts and Selitrennikoff 1986), with some modifications. Freshly grown fungal mycelium was spot inoculated at the center of a petriplate containing Mueller-Hinton (MH) agar media and incubated at 28°C for 24-48 h. Wells were bored on the agar surface, and different concentrations of the inhibitor were placed in front of the growing fungal mycelium. The plates were further incubated at 28°C and the crescent zones of retarded mycelial growth were observed. The antifungal activity by the spore suspension assay was determined as described (Mauch et al 1988). All manipulations were carried out under sterile conditions. Fungal spores were harvested from the freshly grown fungal culture and suspended in sterile water. The concentration of the spore suspension was adjusted to  $1.0 - 3.0 \times 10^6$  spores/ml, depending on the fungus to be tested. To 1 ml of the freshly prepared spore suspension, 1 ml of half strength MH agar was added and was

immediately overlaid on petridishes containing MH agar. To allow for spore germination and initial vegetative growth, plates were incubated at 28°C for 24-48 h. At this time, wells were bored on the agar surface, and different concentrations of the inhibitor were applied. The plates were incubated at 28°C and photographed after 24-72 h. All test solutions were filtered through a 0.22 µm membrane prior to the application. Micro-spectrometric antifungal assay was performed for the quantitative demonstration of antifungal activity as described (Broekaert et al., 1990). Briefly, routine tests were performed with 20 µl of (0.22 µm filter sterilized) test solution and 80 µl of fungal spore suspension (10<sup>6</sup> spores/ml) in half strength MH broth. Control micro-culture contained 20 µl of sterile distilled water and 80 µl of the fungal spore suspension. Unless otherwise stated the incubation conditions for the experiments were 28°C for 48 h. Antifungal activity is expressed in terms of percent inhibition as defined in Cammue et al. (1992).

#### *Minimum Inhibitory Concentration*

The minimum inhibitory concentrations (MIC) of the inhibitor for the growth inhibition of the fungal strains were determined by broth dilution method (Amsterdam, 1991). Serial dilutions of the inhibitor were made in half-strength MH broth in micro titer plates. Each well was inoculated with 10 µl of 10<sup>6</sup> spores/ml of the test organism. The MIC was determined after overnight incubation of the plates and was taken as the lowest concentration of the inhibitor at which growth was inhibited.

#### *Production of xyloglucanase and aspartic protease from the fungal strains*

Freshly grown *A. niger* and *F. udum* were inoculated into a synthetic liquid media having the composition (g/L); KH<sub>2</sub>PO<sub>4</sub> 2; (NH<sub>4</sub>)<sub>2</sub>SO<sub>4</sub> 7; Urea 1.5; MgSO<sub>4</sub>.7H<sub>2</sub>O 0.3; CaCl<sub>2</sub>.2H<sub>2</sub>O 0.3; FeSO<sub>4</sub>.7H<sub>2</sub>O 0.005; MnSO<sub>4</sub>.H<sub>2</sub>O 0.002; ZnSO<sub>4</sub>.7H<sub>2</sub>O 0.001; CoCl<sub>2</sub> 0.001; Tween 80 1; and containing xyloglucan (5 g/l) or soy meal (20 g/l) for the production of xyloglucanase or aspartic protease respectively at 28°C for 96 h. The fungal cells were separated by filtration and centrifugation and the extracellular culture filtrate was tested for the presence of xyloglucanase and aspartic protease.

### *Xyloglucanase inhibition assay*

Xyloglucanase activity was measured by incubating 1ml of assay mixture containing 0.5 ml of 5 mg/ml of tamarind xyloglucan and 0.5ml of suitably diluted enzyme in 50 mM phosphate buffer (pH 7.0) for 30 min at 50°C (Menon et al., 2010). Enzyme and reagent blanks were also simultaneously incubated with test samples. The reducing sugar formed was estimated by dinitrosalicylic acid (Mandels and Weber 1969). One unit of enzyme activity is defined as the amount of enzyme required to liberate 0.5mg of reducing sugar per minute under assay conditions.

### *Fungal aspartic protease inhibition assay*

Aspartic protease inhibition assay was performed as described in chapter 2.

### *Chemical Modification of the inhibitor with 2,4,6-Trinitrobenzenesulfonic Acid and N-ethyl-5-phenylisoxazolium-3'-sulfonic Acid*

The inhibitor (50  $\mu$ M) was modified with TNBS and WRK as per the procedure mentioned in chapter 4. The extent of inactivation of aspartic protease and xyloglucanase was determined with the modified inhibitor by assaying for the anti-xyloglucanolytic and anti-proteolytic activity.

The TNBS and WRK modified inhibitor was used in the experiments to determine the antifungal potency against different species of *Aspergillus* and *Fusarium*. Control experiments with the chemical modifiers were performed to observe the impact of these compounds on the fungal growth inhibition.

## RESULTS

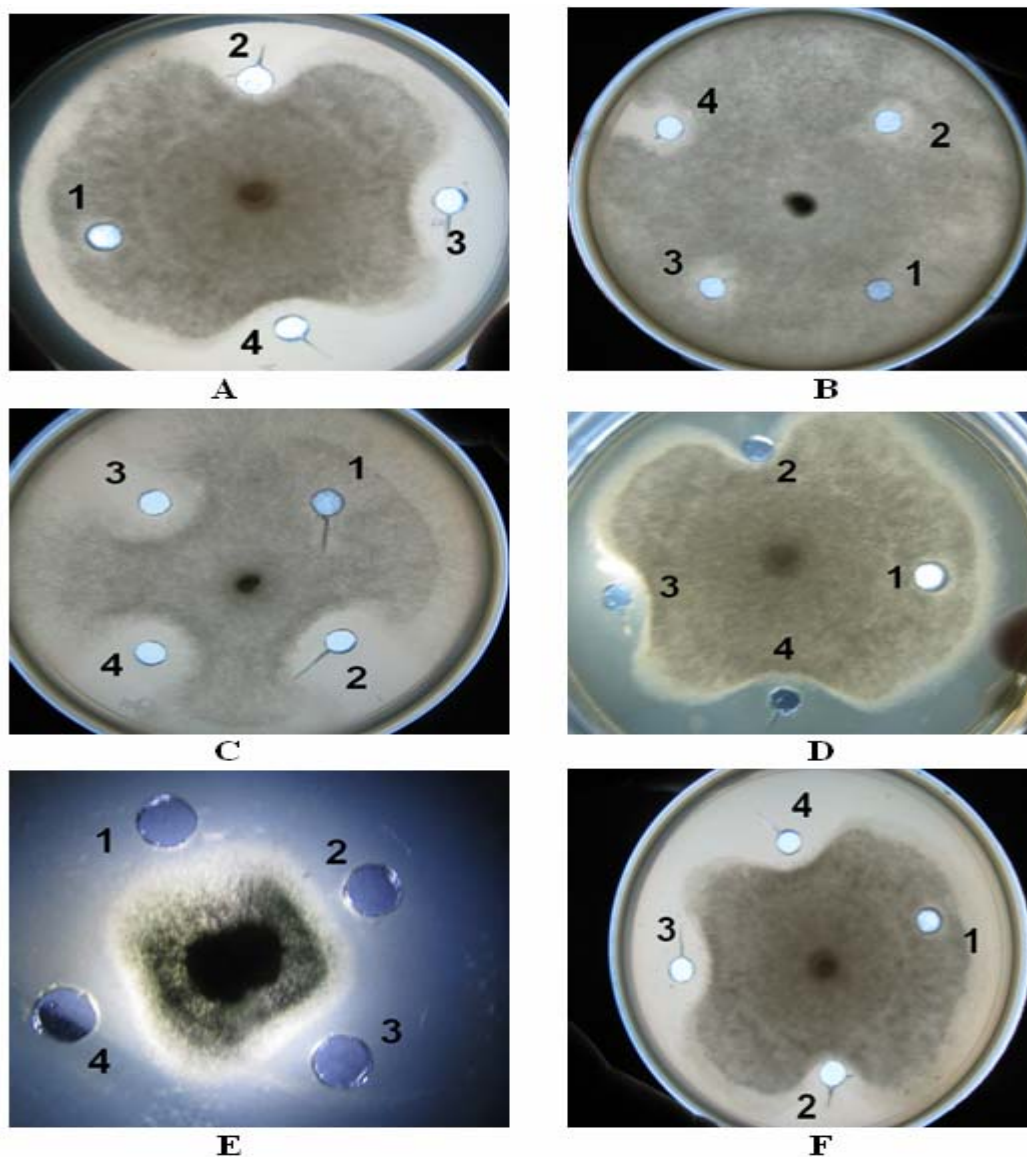
### *Antifungal activity of the inhibitor from Penicillium sp VM24*

The inhibitor was purified from the extracellular culture filtrate of *Penicillium* sp as described in chapter 3. The antifungal activity of the purified inhibitor against 12 fungal strains was assessed in a variety of standard biological assays (Table 1). The inhibitor exhibited strong inhibitory activity against *A. oryzae*, *A. niger*, *F. solani*, *F. udum*, *F. oxysporum* and moderate activity against *A. fumigatus*, *F. moniliforme*, *Colletotrichum* sp, *Rhizopus* sp, *Claviceps purpurea*, *Curvularia fallax* and *Penicillium roqueforti*.

**Table 1** Antifungal potency of the inhibitor against the tested fungal strains and the comparison of their  $IC_{50}$  and MIC values

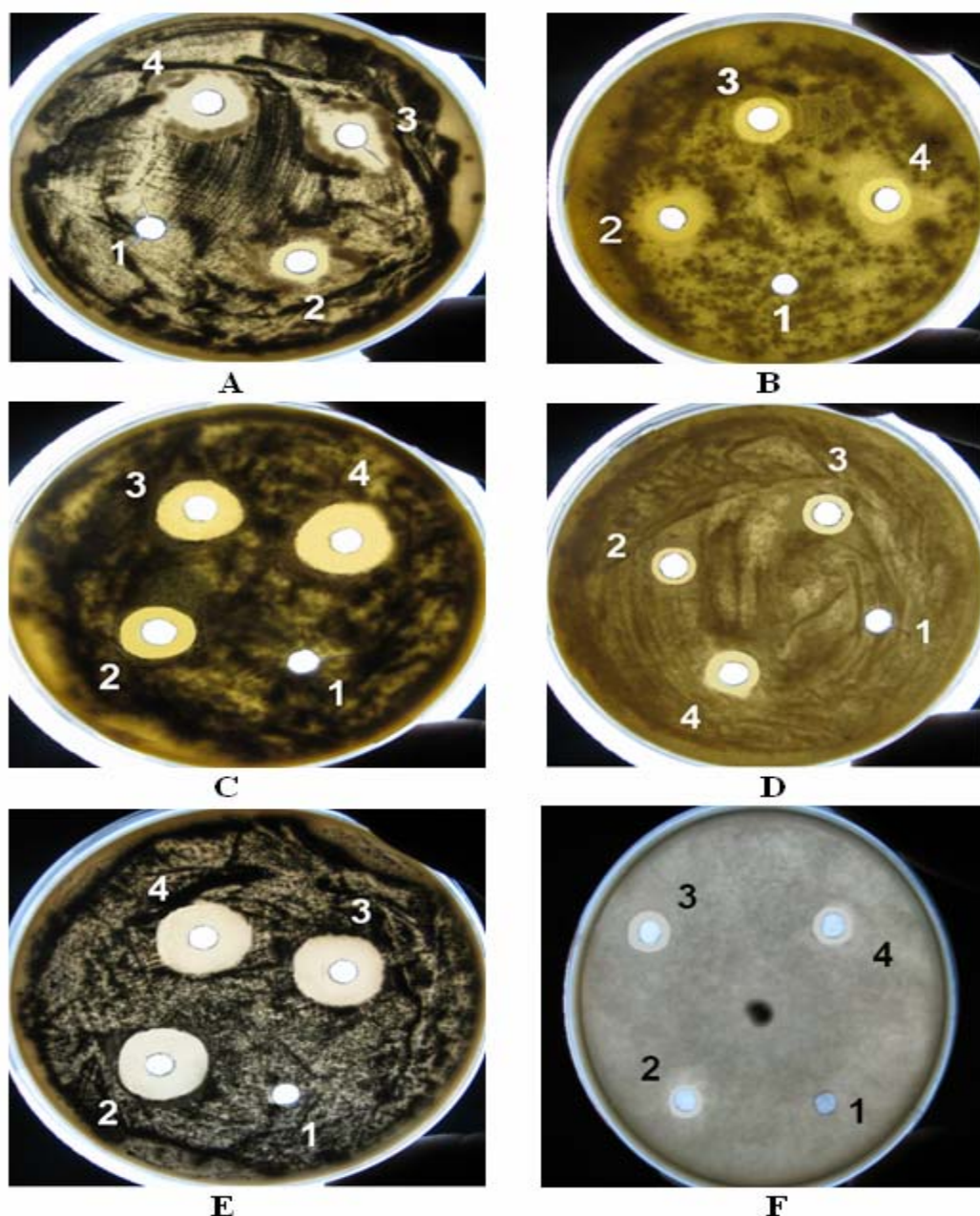
Organism	$IC_{50}$ ( $\mu\text{g/ml}$ )	MIC ( $\mu\text{g/ml}$ )
<i>Aspergillus oryzae</i>	1.84	1.23
<i>Aspergillus niger</i>	0.58	0.30
<i>Aspergillus fumigatus</i>	2.34	1.65
<i>Fusarium solani</i>	1.44	0.93
<i>Fusarium udum</i>	0.98	0.89
<i>Fusarium oxysporum</i>	1.59	1.24
<i>Fusarium moniliforme</i>	2.08	1.58
<i>Colletotrichum</i> sp	3.21	2.27
<i>Rhizopus</i> sp	4.5	2.88
<i>Claviceps purpurea</i>	2.82	1.79
<i>Curvularia fallax</i>	2.36	1.62
<i>Penicillium roqueforti</i>	2.05	1.80

The antifungal activity of the inhibitor was indicated by the zone of inhibition that developed around the wells against the vegetative growth (Figure 1). The radius of the crescent zone observed was found to be proportional to the concentration of the inhibitor applied.



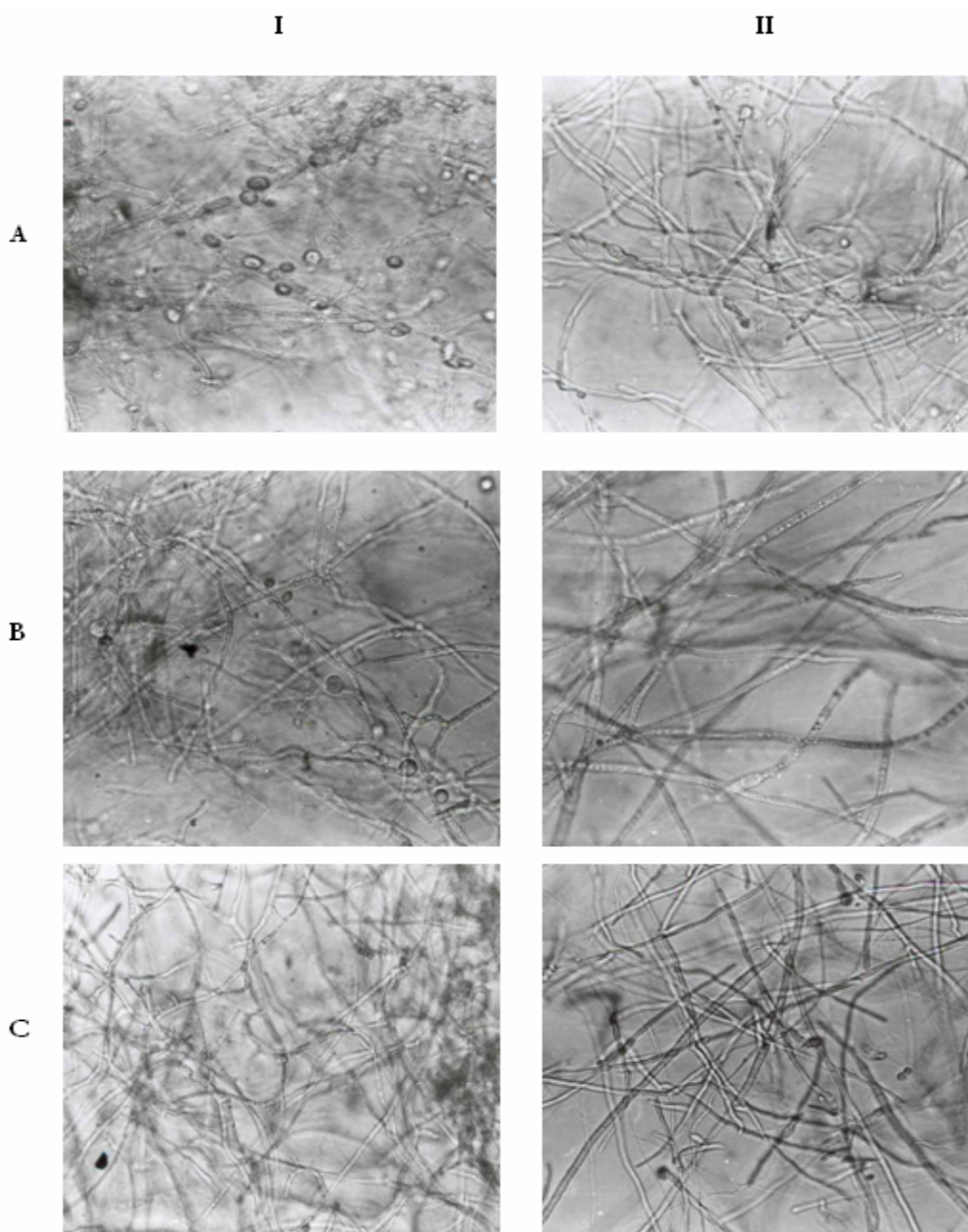
**Figure 1** Plate assay for mycelial growth inhibition. Fungal suspension were allowed to grow on MH agar for 24 h before the test solution was added. Subsequently, wells were bored on the agar, 25  $\mu$ l aliquots of test solutions were added to the wells, and the fungi were allowed to grow for 48-72 h. The test solution (25  $\mu$ l) contained 0  $\mu$ g (1), 1  $\mu$ g (2), 2  $\mu$ g (3), and 3  $\mu$ g (4) of the inhibitor. Fungal strains tested were *F. udum* (A), *Rhizopus* sp (B), *F. solani* (C), *F. moniliforme* (D), *A. niger* (E), and *Colletotrichum* sp (F).

The antifungal activity of the inhibitor was indicated by the zone of inhibition that developed around the wells against the vegetative growth after the spore germination (Figure 2). The diameter of the clearance zone observed was found to be proportional to the concentration of the inhibitor applied.

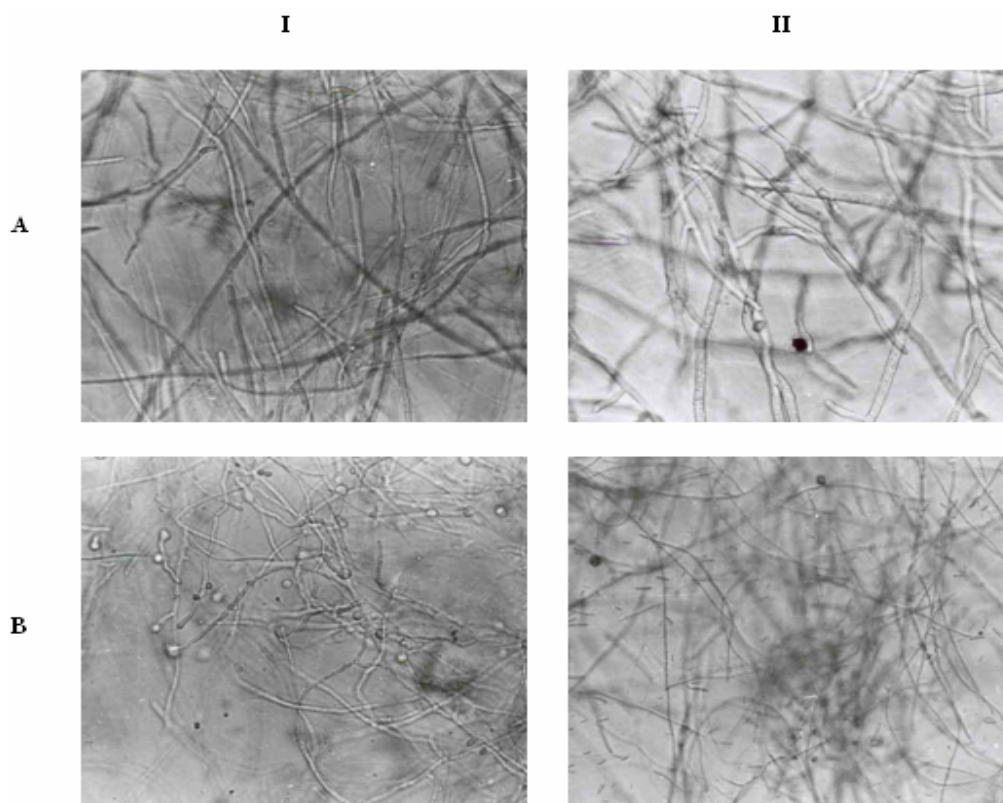


**Figure 2** Inhibition of fungal growth by purified inhibitor. Fungal spores were allowed to germinate on MH agar and grow for 24 h before the test solution was added. Subsequently, 25  $\mu$ l aliquots of test solutions were added to the wells, and the fungi were allowed to grow for 12 h. The test solution (25  $\mu$ l) contained 0  $\mu$ g (1), 1  $\mu$ g (2), 2  $\mu$ g (3), and 3  $\mu$ g (4) of the inhibitor. Fungal strains tested were *A. fumigatus* (A), *F. oxysporum* (B), *A. oryzae* (C), *F. solani* (D), *A. niger* (E), and *F. udum* (F).

Fungal growth inhibition was monitored in microscopic assay, wherein the spores were cultured in the presence of varied concentrations of the inhibitor. The morphological differences observed in the mycelial growth after 48 h are shown in Figure 3 A & B.



**Figure 3A** Morphological changes induced in the mycelia of the fungal strains in the presence of the inhibitor. Fungal spores were germinated in half-strength MH broth in the absence (panels in row I) or presence (panels in row II) of the inhibitor, and growth was observed after 24 h. The fungal strains tested were *A. niger* (A), *A. fumigatus* (B) and *F. udum* (C).

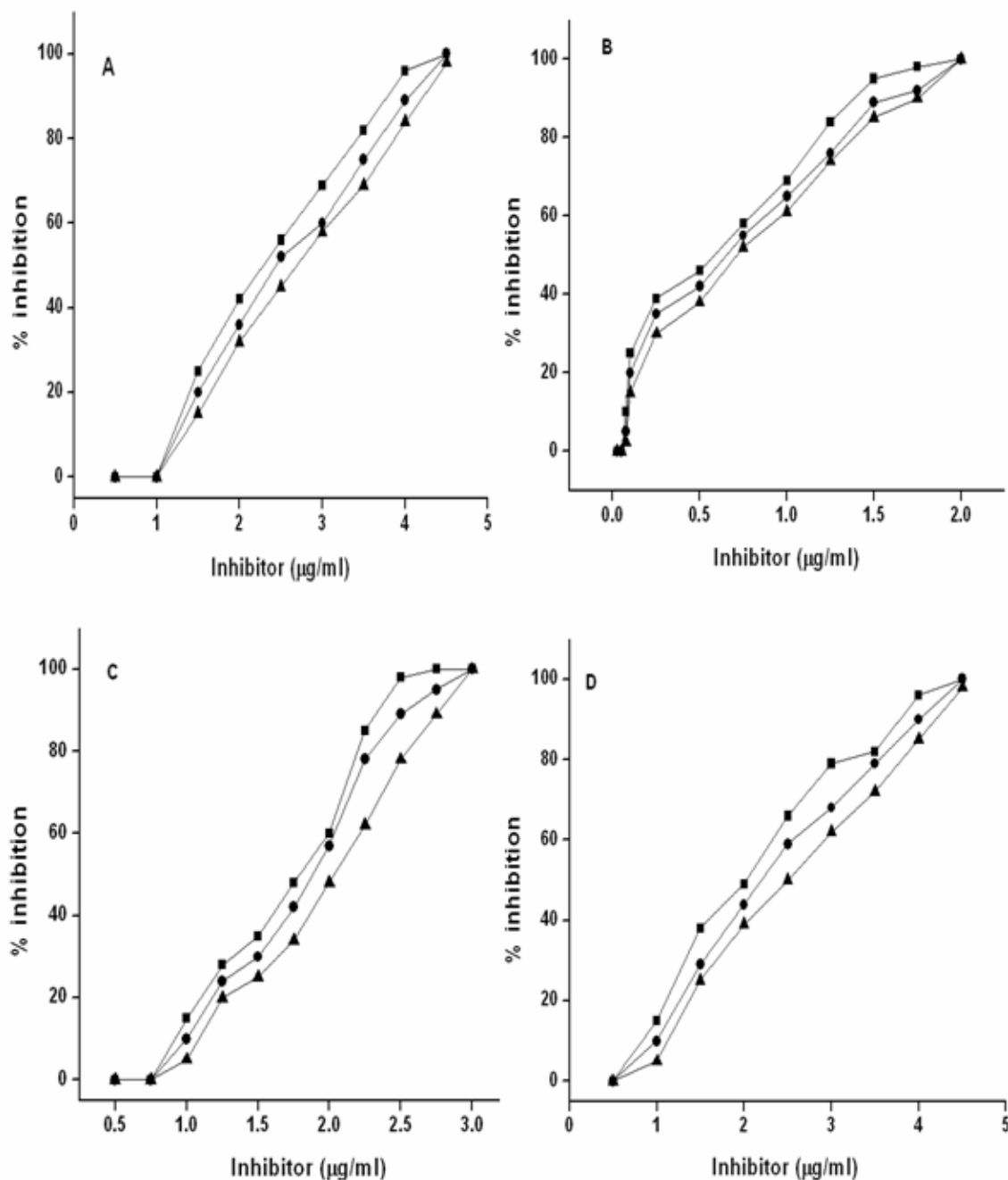


**Figure 3B** Morphological changes induced in the mycelia of the fungal strains in the presence of the inhibitor. Fungal spores were germinated in half-strength MH broth in the absence (panels in row I) or presence (panels in row II) of the inhibitor, and growth was observed after 24 h. The fungal strains tested were *Rhizopus* sp (A), *A.oryzae* (B).

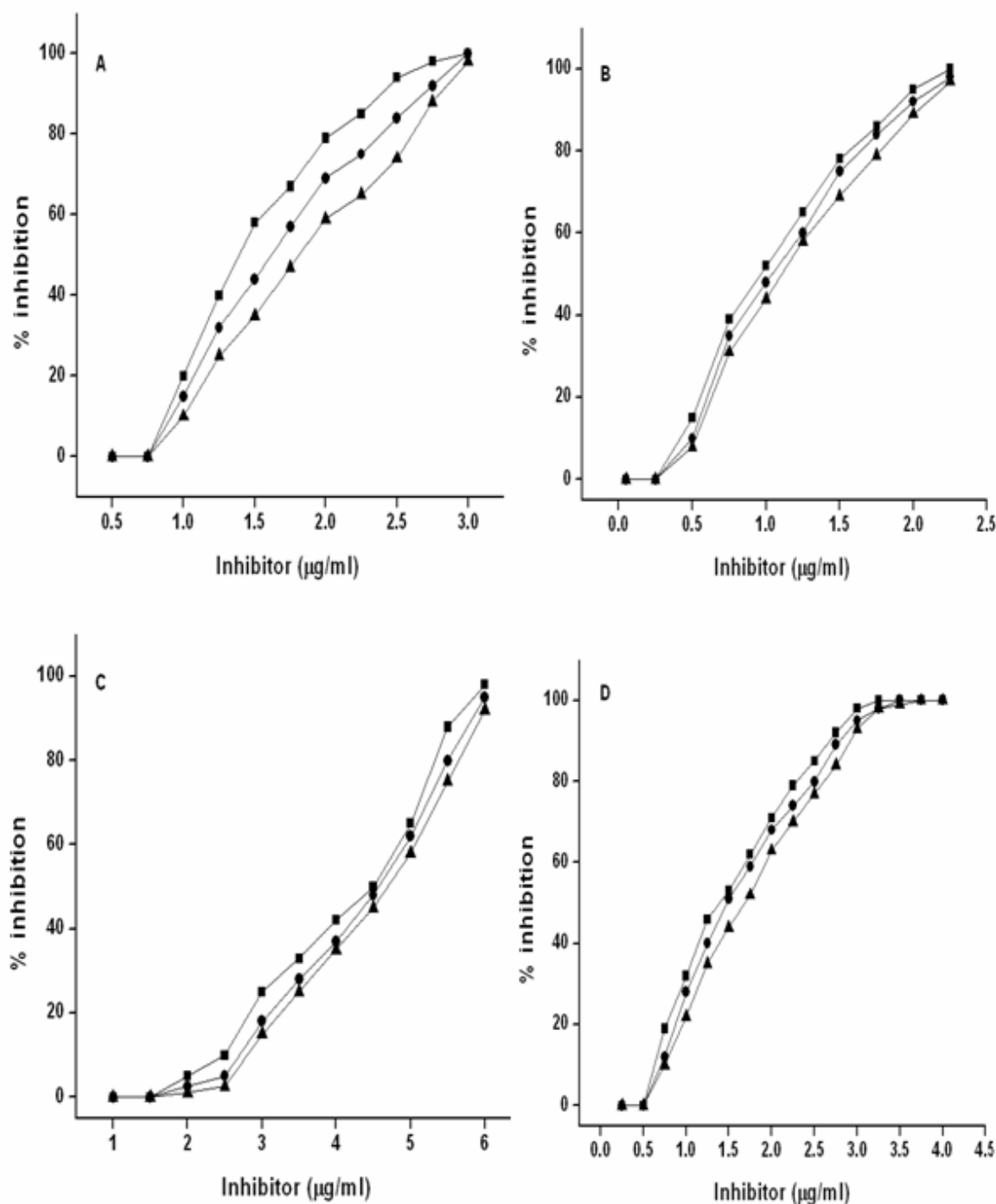
In the presence of the inhibitor, the germination of *Aspergillus* spores was delayed whereas in *F.udum* and *Rhizopus* sp, the rate of growth of the mycelia was slower. As revealed from the micrograph, there was no indication of lysis in mycelia in the presence of the inhibitor.

After 24 h, the concentration of inhibitor required for 50% inhibition ( $IC_{50}$ ) of fungal growth varied from 0.58  $\mu\text{g/ml}$  for *A. niger* to 3.21  $\mu\text{g/ml}$  for *Colletotrichum* sp, whereas the minimum inhibitory concentration (MIC) ranged from 0.30  $\mu\text{g/ml}$  for *A. niger* to 2.88  $\mu\text{g/ml}$  for *Rhizopus* sp. The time dependent dose-response curves revealed that the extent of growth inhibition tends to decrease with the increase in the incubation time (Figure 4 A & B). The time dependent decrease in potency of the inhibitor was less pronounced in *A. niger*, *F. oxysporum*, *F. udum* and *Rhizopus* sp as compared to *A. oryzae*, *A. fumigatus*, *F.solani*, and *F. moniliforme*.





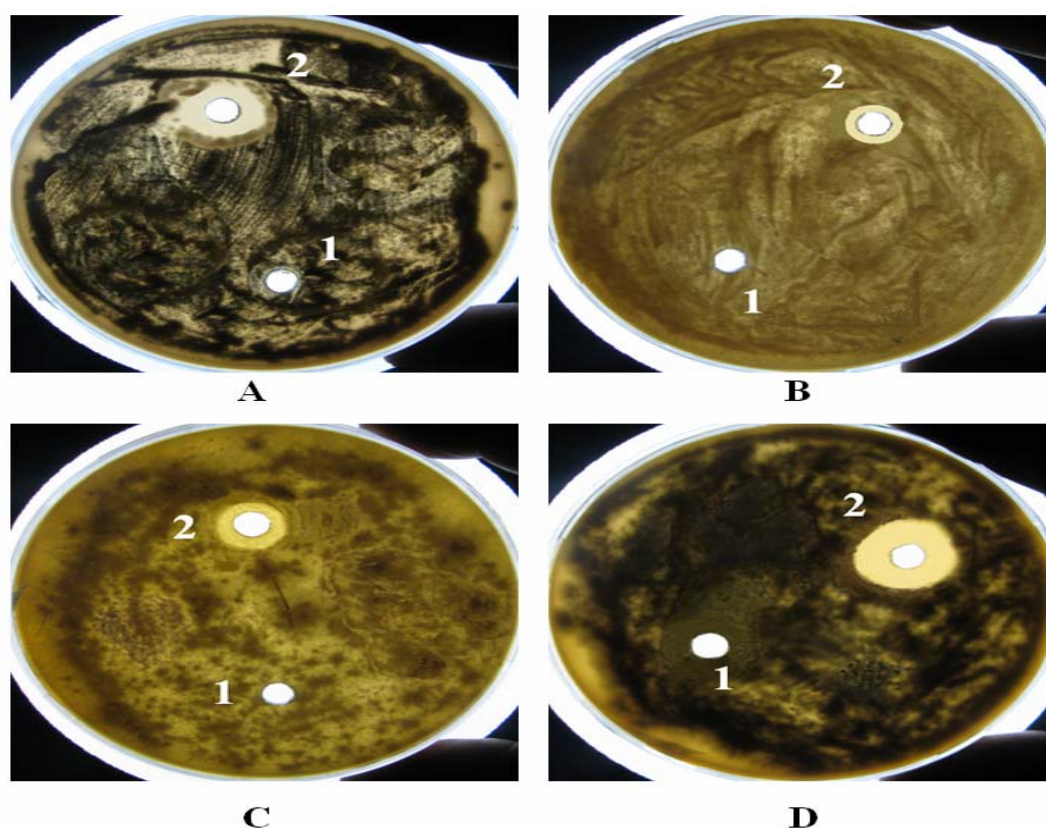
**Figure 4A** Time-dependent dose response growth inhibition curves. Growth inhibition of the fungal strains, *A. fumigatus* (A), *A. niger* (B), *A. oryzae* (C), *F. moniliforme* (D) at different concentrations of the inhibitor, was recorded after 24 h (■), 48 h (●), and 72 h (▲). To 80 µl of spore suspension ( $10^6$  spores/ml), 20 µl of test solution containing various concentrations of inhibitor was added in a micro-culture plate. Control micro-culture plate contained 20 µl of distilled water and 80 µl of spore suspension. Anti-fungal activity of the inhibitor was estimated in terms of percent inhibition and the  $IC_{50}$  values were calculated from the curves.



**Figure 4B** Time-dependent dose response growth inhibition curves. Growth inhibition of the fungal strains, *F. solani* (A), *F. udum* (B), *Rhizopus* sp (C), *F. oxysporum* (D) at different concentrations of the inhibitor, was recorded after 24 h (■), 48 h (●), and 72 h (▲). To 80 µl of spore suspension ( $10^6$  spores/ml), 20 µl of test solution containing various concentrations of inhibitor was added in a micro-culture plate. Control micro-culture plate contained 20 µl of distilled water and 80 µl of spore suspension. Anti-fungal activity of the inhibitor was estimated in terms of percent inhibition and the  $IC_{50}$  values were calculated from the curves.

### *Aspartic Protease and xyloglucanase in fungal growth inhibition*

To understand the mechanism of the fungal growth inhibition by the bifunctional inhibitor, we have investigated the role of two essential hydrolytic enzymes, xyloglucanase and aspartic protease, which are crucial for the growth of fungal strains, and thus, in their biosynthetic pathway. The production of xyloglucanase and aspartic protease is well documented in *Aspergillus* sp (Yaoi et al., 2005; Master et al., 2008; Lee and Kolattukudy 1995) and in *Fusarium* sp (Mullen and Bateman 1975; Griffen et al., 1997), hence we have evaluated the antifungal potency of the inhibitor against these two fungi by growing them on selective media. The growth of *A. fumigatus*, *A. oryzae*, *F. oxysporum* and *F. solani* on the synthetic agar medium containing xyloglucan or casein was inhibited by the inhibitor (Figure 5).

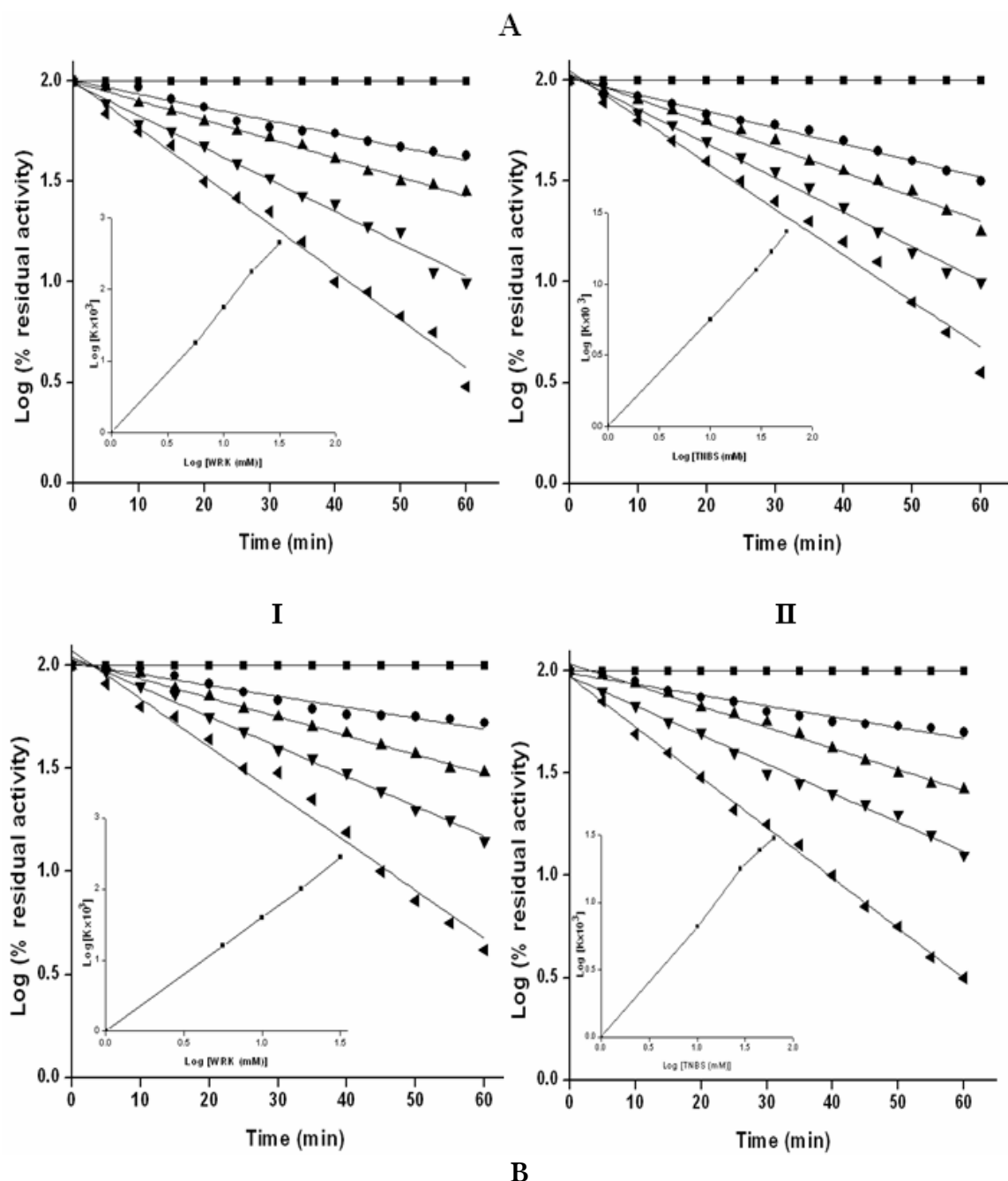


**Figure 5** Antixyloglucanolytic or antiproteolytic activities of the inhibitor. *A. fumigatus* (A), *F. oxysporum* (B), *F. solani* (C) and *A. oryzae* (D) were grown in synthetic medium containing xyloglucan or casein. Fungal spores were allowed to germinate and grow for 12 h before the test solution {0  $\mu\text{g/ml}$  (1) and 2  $\mu\text{g/ml}$  (2)} were added to the wells and the fungi were allowed to grow for 24 h.

To correlate the anti-xyloglucanolytic and anti-proteolytic activity of the inhibitor to its anti-fungal property, the fungal strains were grown in a synthetic medium in shake flasks, containing xyloglucan or soy meal as the sole carbon source and the production of xyloglucanase and aspartic protease was estimated at 96 h. In the presence of xyloglucan the fungal cultures produced considerable amount of xyloglucanase whereas the production of aspartic protease was negligible. Similarly, the selective production of aspartic protease was observed in the culture broth when soy meal was used in the growth medium. The extracellular culture filtrates showing xyloglucanase and aspartic protease activity were inhibited by the inhibitor. The retardation of fungal growth and the inhibition of xyloglucanase and aspartic protease activities by the inhibitor suggested the correlation between the inhibitions of these enzymatic activities to the fungal growth inhibition

#### *Chemical modification of the inhibitor and assessment of its antifungal activity*

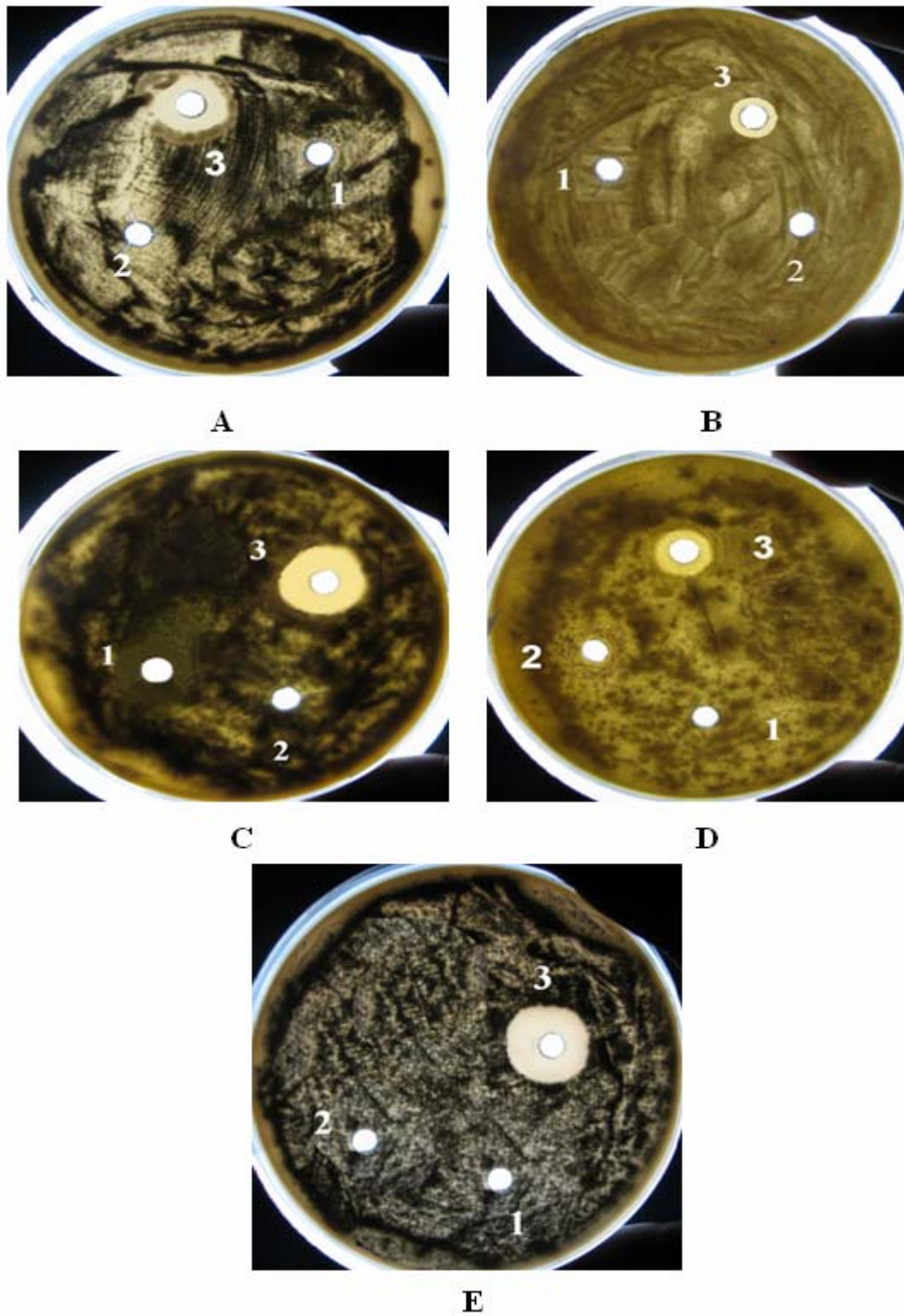
The role of functional groups for the inhibitory activity of the inhibitor was elucidated by employing chemical modifiers with specific reactivity. The amino acid composition of the inhibitor from *Penicillium* sp VM24 revealed that Lys, Asp, and Glu are the amino acids containing ionizable side chains (Chapter 3). The involvement of these groups in the mechanistic pathway was investigated using WRK, a carboxyl group modifier, and TNBS, an amine group modifier of lysine. The inhibitory activity of the WRK or TNBS modified inhibitor was determined by assaying against xyloglucanase and aspartic protease, and the residual inhibitory activity at the given time was calculated relative to the control. Xyloglucanase and aspartic protease contained carboxyl group in the active site, thus it was essential to remove the excess WRK reagent completely to avoid enzyme inactivation by the modifier itself. Semi-logarithmic plots of residual inhibitory activity against xyloglucanase (Figure 6A) and aspartic protease (Figure 6B) as a function of time were linear signifying that the inactivation process obeys pseudo-first order kinetics. Loss of inhibitory activity was dependent on time and concentration of the reagent.



**Figure 6** Differential labeling of the ionizable groups of the inhibitor with WRK and TNBS. (I) Inactivation of the inhibitor by WRK. Inhibitor (50  $\mu$ M) was treated with 0 mM (■), 5 mM (●), 10 mM (▲), 20 mM (▼), and 30 mM (◄) of WRK at 28°C for 1 h. Aliquots of the reaction mixture were removed at times indicated and the reaction was quenched with the addition of sodium acetate buffer to a final concentration of 100 mM and assayed for the inhibitory activity. (II) Effect of TNBS on the inactivation of the inhibitor. The inhibitor (50  $\mu$ M) was incubated without (■) or with 10 mM (●), 25 mM (▲), 40 mM (▼), and 50 mM (◄) of TNBS at 37°C in dark for 1 h. Aliquots at specified time intervals were removed and the reaction was stopped by adjusting the pH to 4.6. The inhibitory activity of the WRK or TNBS modified inhibitor was determined by assaying against xyloglucanase (A) and aspartic protease from *Aspergillus saitoi* (B) and the residual inhibitory activity at the given time was calculated relative to the control. The lines represent the best fit for the data obtained as the natural logarithm of percent of residual inhibitory activity versus time. Inset represents the double logarithmic plots for the pseudo first-order rate constants versus the concentration of the modifiers.

The reaction of WRK is initiated by the formation of ketoketenimine, which modifies the carboxyl groups of the inhibitor to give an enol ester. The modification of the carboxyl groups of the inhibitor was monitored by the differential absorption at 210/340 nm. Analysis of the order of reaction for xyloglucanase and aspartic protease by the method described (Levy, 1963) yielded a slope of 1.67 and 1.64, respectively (Insets of Figure 6I), suggesting the involvement of two carboxyl groups of the inhibitor in the enzyme inactivation. The participation of the amine group of the lysine residues of the inhibitor was elucidated by lysine modifier TNBS. TNBS caused time- and concentration dependent loss of the inhibitory activity of the inhibitor. A reaction order of 0.75 and 0.79 for xyloglucanase and aspartic protease respectively with respect to the modifier was determined from the slope of the double logarithmic plots (Insets of Figure 6II) indicating the involvement of a single amine group of the inhibitor in the enzyme inactivation.

In order to elucidate the mechanism of action of the inhibitor in fungal growth inhibition, the carboxyl, and amine modified inhibitor was tested for its potency towards the growth inhibition of *Aspergillus* sp and *Fusarium* sp on selective growth media. Figure 7 indicated that the TNBS or WRK modified inhibitor did not inhibit the fungal growth indicating the involvement of the amine and carboxylic groups of the Lys and Asp/Glu residues respectively. Control experiments were carried out with the chemical modifiers WRK and TNBS using the synthetic agar medium.



**Figure 7** Effect of chemically modified inhibitor on the growth inhibition of *A. fumigatus* (A), *F. solani* (B), *A. oryzae* (C), *F. oxysporum* (D) and *A. niger* (E). The test solution containing TNBS modified (1), WRK modified (2), or unmodified (3) inhibitor was applied in the wells and the fungal growth was observed after 12-24 h.

## DISCUSSION

Glycosidase and protease inhibitors play an important role in the protection of plant tissue from pest and pathogen attack by virtue of antinutritional interactions. Reports on cysteine and serine protease inhibitors, chitinases, glucanases, ribosome-inactivating proteins, and permatins as antifungal agents are well documented. Discovery of novel antifungal peptides and elucidation of their mechanism of action will expand our understanding of intrinsic host defenses and will certainly provide new approaches to antifungal chemotherapy. The present study is the report of a low molecular weight inhibitor from *Penicillium* sp VM24 exhibiting antifungal activity. It is noteworthy that many of the fungal strains inhibited by the inhibitor are plant pathogens of significant importance to agriculture. The inhibitor was found to be active against relatively a broad spectrum of filamentous fungi and its  $IC_{50}$  values indicated an exceptionally high potency. Significantly, in case of *A. niger* and *F. udum* the  $IC_{50}$  values were in nanomolar range. Our results documented that the specific activity of the inhibitor was decreased when the incubation time for the fungal growth was increased. A possible explanation for this phenomenon is that the germlings at the early stages of growth were more affected than the mycelium development at later stages. The inhibitor was found to inhibit spore germination at high concentration and at lower concentrations delayed growth of the hyphae, which subsequently exhibited abnormal morphology.

To colonize plants, fungal microorganisms have evolved strategies to invade plant tissues, to optimize growth in the plant, and to propagate. Bacteria and viruses, as well as some opportunistic fungal parasites, often depend on natural openings or wounds for invasion. In contrast, many true phytopathogenic fungi have evolved mechanisms to actively traverse the plants outer structural barriers, the cuticle, and the epidermal cell wall. To gain entrance, fungi generally secrete a cocktail of hydrolytic enzymes including cutinases, cellulases, pectinases, xylanases, xyloglucanases and proteases (Knogge 1996; Juge 2006). The role of inhibitors of chitin synthase (Chapman et al., 1992; Hori et al., 1974), glucan synthase (Beaulieu et al., 1993), xylanase (Dash et al., 2001) and proteases (Lorito et al., 1994; Dash et al.,



2001) as antifungal agents have been well established. However, there is a lacuna of literature on the inhibitors of xyloglucanase, cellulase, and aspartic protease exhibiting antifungal activity, which could provide further insight into the understanding of host-pathogen interactions. In order to examine the contribution of the inhibition of xyloglucanase and aspartic protease to the observed antifungal activity we have investigated the inhibition of these two enzymes from the culture broth of *Aspergillus* sp and *Fusarium* sp by the inhibitor. Further, to delineate the role of xyloglucanase and aspartic protease in fungal growth inhibition, we have grown *Aspergillus* sp, and *Fusarium* sp on a synthetic medium containing xyloglucan or soymeal as the sole carbon source. The inhibition of growth by the inhibitor in the presence of xyloglucan or soymeal, where the selective production of xyloglucanase and aspartic protease was observed implied the role of these enzyme activities in the fungal growth inhibition. There have been reports of bifunctional inhibitors of  $\alpha$ -amylase and trypsin (Skordalakes et al., 1998; Strobl et al., 1995), xylanase and aspartic protease (Dash et al., 2001). However, a bifunctional inhibitor of xyloglucanase and aspartic protease, which are active in distinctly different physiological conditions, is so far not reported.

The localization and characterization of the amino acids comprising the active center and the correlation between these residues with the inhibitory function are essential for understanding the mechanism of action of the inhibitor. To determine the residues involved in the antixyloglucanolytic or antiproteolytic activity, we have modified the ionizable groups of Lys, and Asp/Glu of the inhibitor. Modification of the amine group of Lys or the carboxyl group of Asp/Glu residues of the inhibitor by specific modifiers TNBS or WRK resulted in the loss of its inhibitory activity. The kinetic analysis indicated the participation of one amine and two carboxyl groups of the inhibitor in the inhibition of xyloglucanase and aspartic protease from *Aspergillus saitoi*. It is well established that the catalytic site of xyloglucanase and aspartic protease consists of two carboxyl groups and an essential lytic water molecule (Rao, et al., 1998; Gloster et al., 2007). Although both the enzymes are active in entirely different physiological conditions, the structural and kinetic studies

have revealed a similar mechanism where the enzymatic reaction follows general acid-base catalysis with the direct participation of the lytic water molecule. The probable explanation for the involvement of two carboxyl groups of the inhibitor is that they may form a network of hydrogen bonds with the catalytic water molecule and with the ionizable groups in the active site of the enzyme. The participation of the Lys residue may be explained by considering its ability to form hydrogen bonding with the catalytic carboxyl groups of the enzymes. These interactions may interfere in the native weak interactions between the carboxyl groups of the active site and the lytic water molecule leading towards the inactivation of the enzymes. Further, to decipher the role of ionizable groups of the inhibitor in fungal growth inhibition the Lys, Asp/Glu modified inhibitor was tested for its antifungal property. The modified inhibitor failed to inhibit the growth of *Aspergillus* sp and *Fusarium* sp in the presence of xyloglucan or soymeal indicating the involvement of carboxyl and amine groups in fungal growth inhibition. This can be explained by the fact that abolishing the inhibitory property of the inhibitor resulted in the recovery of the xyloglucanase and aspartic protease activity in the fungal strains. The inhibition of these enzymes by the inhibitor may circumvent host invasion and make it difficult for the phytopathogens to acquire resistance. Therefore, the direct application of the inhibitor as a biocontrol agent for the protection of plants against phytopathogenic fungi by encapsulation for surface application or by spray would be very useful.

**BIBLIOGRAPHY**

- Kulkarni A (2007) Ph D Thesis, University of Pune.
- Agrios GN (2005) Plant Pathology, Academic Press, London.
- Amsterdam D (1991) Susceptibility testing of antimicrobials in liquid media. In Lorian V (ed.), Antibiotics in laboratory medicine. Williams & Wilkins, Baltimore, Md, pp. 72–78.
- Barna B, Leiter E, Hegedus N, Biro T, Pocsi I (2008) *J Basic Microbiol* **48**, 516–520.
- Bassarello C, Lazzaroni S, Bifulco G, Lo Cantore P, Iacobellis NS, Riccio R, Gomez-Paloma L, Evidente A (2004) *J Nat Prod* **67**, 811–816.
- Beaulieu D, Tang J, Zeckner DJ, Parr TR (1993) *FEMS Microbiol Lett* **108**, 133–138.
- Bonmatin JM, Laprevote O, Peypoux F (2003) *Combinatorial Chemistry & High Throughput Screening* **6**, 541–556.
- Broekaert WF, Franky RG, Cammue BPA, Vanderleyden J (1990) *FEMS Microbiol Lett* **69**, 55–60.
- Brogden A (2005) *Nat Rev Microbiol* **3**, 238–250.
- Bulet P, Stöcklin R, Menin L (2004) *Immunol Rev* **198**, 169–184.
- Cammue BPA, DeBolle MFC, Terras FRG, Proost P, et al. (1992) *J Biol Chem* **267**, 2228–2232.
- Dash C, Ahmad A, Nath D, Rao M (2001) *Antimicrob Agents Chemother* **45**, 2008–2017.
- Chapman T, Kinsman O, Houston J (1992) *Antimicrob Agents Chemother* **36**, 1909–1914.
- Cooter PD, Hill C, Ross P (2005) *Curr Prot Pept Sci* **6**, 61–75.
- Dash C, Phadtare S, Deshpande VV, Rao M (2001) *Biochemistry* **40**, 11525–11532.
- De Lucca AJ, Walsh TJ (1999) *Antimicrob Agents Chemother* **43**, 1–11.
- Debono M, Gordee RS (1994) *Annu Rev Microbiol* **48**, 471–497.
- Degenkolb T, Berg A, Gams W, Schlegel B & Gräfe U (2003) *J Pept Sci* **9**, 666–678.
- Degenkolb T, Berg A, Gams W, Schlegel B, Gräfe U (2003) *J Pept Sci* **9**, 666–678.
- del Pozo AM, Lacadena V, Mancheno JM, Olmo N, et al. (2002) *J Biol Chem* **277**, 46179–46183.
- Fujita T, Takaishi Y, Okamura A, Fujita E, Fuji K, et al. (1981) *J Chem Soc Chem Commun* **1981**, 585–587.

- Fukushima K, Arai T, Mori Y, Tsuboi M, Suzuki M (1983) *J Antibiot* **36**, 1606–1612.
- Galvez A, Maqueda M, Martinez-Bueno M, Lebbadi M, Valdivia E (1993) *Appl Microbiol Biotechnol* **38**, 438–442.
- Galgoczy L, Papp T, Leiter E, Marx F, Pocsí I, Vagvögyi CS (2005) *J Basic Microbiol* **45**, 136–141.
- Gloster TM, Ibatullin FM, Macauley K, Eklo JM, Roberts S, Turkenburg JP, et al. (2007) *Biol Chem* **282**, 19177–19189
- Goulard C, Hlimi S, Rebuffat S, Bodo B (1995) *J Antibiot* **48**, 1248–1253.
- Griffen AM, Wiebe MG, Robson GD, Trinci APJ (1997) *Microbiology* **143**, 3007–3013.
- Hagen S, Marx F, Ram F, Meyer V (2007) *Appl Environ Microbiol* **73**, 2128–2134.
- Hancock REW (2001) *Lancet Infect Dis* **1**, 156–164.
- Holmes GJ, Eckert JW (1999) *Phytopathology* **89**, 716–721.
- Hori M, Eguchi J, Kakiki K, Misato T (1974) *J Antibiotics* **27**, 260–266.
- Ishimaru C, Klos EJ, Brubaker RR (1988) *Phytopathology* **78**, 746–750.
- Jabrane A, Sabri P, Compe`re P, Jacques I, Vandenberghe I, Van Beeumen J, Thonart P (2002) *Appl Environ Microbiol* **68**, 5704–5710.
- Juge N (2006) *Trends Plant Sci* **11**, 359–367.
- Kaiserer L, Oberparleiter C, Weiler-Görz R, Burgstaller W, Leiter E, Marx F (2003) *Arch Microbiol* **180**, 204–210.
- Knight SC, Anthony VM, Brady AM, Greenland AJ, Heaney SP, et al. (1997) *Annu Rev Phytopathol* **35**, 349–372.
- Knogge W (1996) *Plant Cell* **8**, 1711–1722.
- Lacadena J, Martinez del Pozo A, Gasset M, Campos-Olivas R, V´azquez C, Mart´inez-Ruiz A (1995) *Arch Biochem Biophys* **324**, 273–281.
- Lavermicocca P, Valerio F, Visconti A (2003) *Appl Environ Microb* **69**, 634–640.
- Lavermicocca P, Iacobellis NS, Simmaco M & Graniti A (1997) *Physiol Mol Plant Pathol* **50**, 129–140.
- Lay FT, Anderson MA (2005) *Curr Protein Pept Sci* **6**, 85–101.
- Lebbadi M, Galvez A, Maqueda M, Martinez-Bueno M, Valdivia E (1994) *J Appl Bacteriol* **77**, 49–53.
- Lee CH, Kim SH, Hyun BC, Suh JW, Yon C (1994) *J Antibiot* **47**, 1402–1405.

- Lee GD, Shin SY, Maeng CY, Jin ZZ, Kim KL, Hanm KS (1999) *Biochem Biophys Res Commun* **263**, 646–651.
- Lee JD, Kolattukudy PE (1995) *Infect Immun* **63**, 3796-3803
- Leiter E, Szappanos H, Oberparleiter C, et al. (2005) *Antimicrob Agents Chemother* **49**, 2445-2453.
- Levy HM, Leber PD, Ryan EM (1963) *J Biol Chem* **238**, 3654–3659.
- Lim Y, Suh JW, Kim S, Hyun B, Kim C, Lee CH (1994) *J Antibiot* **47**, 1406–1416.
- Lopez-Garcia B, Perez-Paya E, Marcos JF (2002) *Appl Environ Microbiol* **68**, 2453–2460.
- Lorito M, Broadway RM, Joes CMK, Woo SL, et al. (1994) *Mol. Plant-Microbe Interact* **7**, 525–527.
- Mandels M, Weber J (1969) *Adv Chem* **95**, 391-414.
- Marx F (2004) *Appl Microbiol Biotechnol* **65**, 133-142.
- Marx F, Binder U, Leiter E, Pocsi I (2008) *Cell Mol Life Sci* **65**, 445-454.
- Master ER, Zheng Y, Storms R, Tsang A, Powlowski J (2008) *Biochem J* **411**, 161-170.
- Mauch F, Mauch-Mani B, Boller T (1988) *Plant Physiol* **88**, 930–942.
- Menon V, Prakash G, Rao M (2010) *J Biotechnol* **148**, 233-239.
- Meyer V (2008) *Appl Microbiol Biotechnol* **78**, 17-28.
- Montesinos E (2007) *FEMS Microbiol Lett* **270**, 1–11.
- Moreno AB, del Pozo AM, Borja M, San Segundo B (2003) *Phytopathology* **93**, 1344-1353.
- Moreno AB, Mart´inez A, Borja M, SanSegundo B (2003) *Mol Plant-Microbe Interact* **93**, 1344–1353.
- Moreno AB, Pe˜nas G, Rufat M, Bravo J M, Estopa` M, Messeguer J, SanSegundo B (2005) *Mol Plant-Microbe Interact* **18**, 960–972.
- Mullen JM, Bateman DF (1975) *Physiol Plant Pathol* **6**, 233-246.
- Ng TB (2004) *Peptides* **25**, 1055–1073.
- Nielsen TH, Sorensen J (2003) *Appl Environ Microbiol* **69**, 861–868.
- Oita S, Horita M, Yanagi SO (1996) *Biosci Biotech Biochem* **60**, 481–483.
- Pedras MS, Ismail N, Quail JW, Boyetchko SM (2003) *Phytochemistry* **62**, 1105–1114.
- Pham HT, Riu KZ, Jang KM, Cho SK, Cho M (2004) *Appl Environ Microbiol* **70**, 4486–4490.
- Powers JS, Hancock REW (2003) *Peptides* **24**, 1681–1691.

- Raaijmakers JM, de Bruijn I, de Kock MJD (2006) *Mol Plant-Microbe Interact* **19**, 699–710.
- Radics LM, Katjar-Perady M, Casinovi CG, Rossi C, Ricci M, Tuttobelo L (1987) *J Antibiot* **40**, 714–716.
- Rao MB, Tanksale AM, Ghatge MS, Deshpande VV (1998) *Microbiol Mol Biol Rev* **62**, 597–635.
- Roberts WK, Selitrennikoff CP (1986) *Biochim Biophys Acta* **880**, 161–170.
- Rossi C, Tuttobello L, Ricci M, Casinovi CG, Radics L (1987) *J Antibiot* **40**, 130–132.
- Sato M, Beppu T, Arima K (1980) *Agric Biol Chem* **44**, 3037–3040.
- Schirmbock M, Lorito M, Wang YL, Hayes CK, Arisan-Atac I, Scala F, Harman GE, Kubicek CP (1994) *Appl Environ Microbiol* **60**, 4364–4370.
- Shai Y (1995) *TIBS* **20**, 460–464.
- Skordalakes E, Elgandy S, Goodwin CA, Green D, Scully MF (1998) *Biochemistry* **37**, 14420–14427.
- Steiner H, Andreu D, Merrifield RB (1988) *Biochim Biophys Acta* **939**, 260–266.
- Strobl S, Muehlhahn, Bernstein R, Wiltscheck R, Maskos K, et al. (1995) *Biochemistry* **34**, 8281–8293.
- Theis T, Marx F, Salvenmoser W, Stahl U, Meyer V (2005) *Res Microbiol* **156**, 47–56.
- Theis T, Wedde M, Meyer V, Stahl U (2003) *Antimicrob Agents Chemother* **47**, 588–593.
- Tincu JA, Taylor SW (2004) *Ant Agents Chem* **48**, 3645–3654.
- Toke O (2005) *Biopolymers* **80**, 717–735.
- Toniolo C, Crisma M, Formaggio F, Peggion C, Epand RF, Epand RM (2001) *Cell Mol Life Sci* **58**, 1179–1188.
- Vila L, Lacadena V, Fontanet P, Mart'inez A, SanSegundo B (2001) *Mol Plant-Microbe Interact* **14**, 1327–1331.
- Wimley WC (2010) *ACS Chem Biol* **5**, 905–917.
- Xiao-Yan S, Qing-Tao S, Shu-Tao X, Xiu-Lan C, Cai-Yun S, Yu-Zhong Z (2006) *FEMS Microbiol Lett* **260**, 119–125.
- Yaoi K, Nakai T, Hiyoshi A, Mitsuishi Y (2005) *Appl Environ Microbiol* **71**, 7670–7678.
- Zaslloff M (2002) *Nature* **415**, 389–395.

# CHAPTER 6

*'Enzymes are invented by biologist that explains things  
which otherwise require harder thinking'*

**Jerome Lettvin**

**Bifunctional role of aspartic protease inhibitor  
from *Penicillium* sp VM24: Inactivation of  
aspartic protease and xyloglucanase**



## **PART A**

### **Interactions of a protease inhibitor with an aspartic protease from *Aspergillus* sp**

## SUMMARY

Aspartic proteases from *Aspergillus* sp are significant targets for therapeutic interventions as they are reported as virulence factor in invasive aspergillosis. The present chapter describes the inactivation of an aspartic protease from *Aspergillus saitoi* by a low molecular weight peptidic inhibitor from *Penicillium* sp VM24. The steady-state kinetic interactions of the fungal aspartic protease with the inhibitor exhibited reversible, competitive, time-dependent tight binding nature of the inhibitor with  $IC_{50}$  and  $K_i$  values of 1.8  $\mu$ M and 0.85  $\mu$ M respectively. The rate constants determined for the formation and dissociation of EI were  $6.25 \times 10^{-3} \text{ s}^{-1}$  and  $11.84 \times 10^{-3} \text{ s}^{-1}$  respectively. The binding of the inhibitor with the fungal aspartic protease and the subsequent conformational changes induced were monitored by intrinsic tryptophanyl fluorescence. To investigate the effects of the inhibitor on the secondary structure of the fungal aspartic protease, we have analyzed the CD spectra of the enzyme-inhibitor complex. Interestingly, the aspartic protease-inhibitor complex and aspartic protease-pepstatin complex exhibited a similar pattern of negative ellipticity in the far-UV region. These studies deciphered that the inactivation of the enzyme is due to the binding of the inhibitor to the active site of aspartic protease. The new inhibitor will be a potential lead compound for the development of molecules to combat human fungal infections.

## INTRODUCTION

More than 100,000 species of fungi are described, but only about 400 are known to be human pathogens or to cause opportunistic infections in humans (Monod et al., 2002). Many species of human pathogenic fungi secrete proteases which are involved in fungal physiology and infection. Secreted endoproteases belong to the aspartic proteases of the pepsin family, serine proteases of the subtilisin family, and metalloproteases of two different families. In addition they include a non-pepsin-type aspartic protease from *Aspergillus niger* (Mattern et al., 1992) and a unique chymotrypsin-like protease from *Coccidioides immitis* (Cole et al., 1992). Pathogenic fungi also secrete aminopeptidases, carboxypeptidases and dipeptidyl-peptidases. Similar to many other secreted endoproteases, those from pathogenic fungi are synthesized as precursors in a preproprotein form (Von Heijne 1986). Among the several factors for fungal infection, proteases secreted by pathogenic fungi plays an important role in invasion and survival of the fungi in an infected host. The ability to destroy natural barriers to infection such as skin or airway epithelium makes fungal proteases as suitable virulence factors (Kothary et al., 1984; Rhodes et al., 1988). Fungal proteases participating in different pathological processes act directly by destroying host tissues or by eliciting/potentiating allergic and inflammatory responses. The humoral effects can be mediated by activation of the cytokine and bradykinin generating systems as well as by inactivation of complement factors and immunoglobulins. The involvement of fungal proteases in diverse pathological mechanisms makes them potential targets of therapeutic intervention and candidates for biomarkers of disease and exposure (Yike 2011).

A considerable number of *Aspergilli* species are known to produce extracellular acid proteases such as *Aspergillus niger* (Dara et al., 2001), *A. oryzae* (Tsujita and Endo 1978), *A. awamori* (Moralejo et al., 2002), *A. fumigatus* (Reichard et al., 1995) and *A. saitoi* (Tello-Solis and Hernandez-Arana 1995). *A. niger* is known to produce five different endopeptidases (Van den Hombergh et al., 1997), two carboxypeptidases (Dal Degan et al., 1992) and one aminopeptidase (Basten et al., 2001). The two major

extracellular acid proteases are called proctases A and B. Proctase A (20 kDa), a non-pepsin type protease is not inhibited by pepstatin (Takahashi et al., 1991), whereas proctase B or aspergillopepsin I (35 kDa) which is inhibited by pepstatin belonging to the A1 family of proteases (Inoue et al., 1995 & 1996). *A. fumigatus* secretes one protease called Pep1 (Reichard et al., 1995) highly similar to the Aspergillopepsin A (PepA) from *A. niger* (Berka et al., 1990) and PepO from the koji mould *A. oryzae* (Berka et al., 1993). However, a second aspartic protease was found to be present in the cell wall of *A. fumigatus* and was called *A. fumigatus* Pep2 (Reichard et al., 2000). The amino acid sequences of Pep2 and the previously characterized secreted *A. fumigatus* Pep1 are only 27% identical. *A. saitoi* produces an extracellular aspartic protease of the pepsin family. The amino acid sequence of *A. saitoi* aspartic proteinase has 70% homology to *A. fumigatus* aspartic proteinase (Lee and Kolattukudy 1995).

Among the several fungal infections, invasive aspergillosis is a major threat to the long-term survival of immunocompromised patients (Denning and Stevens 1990; Segal and Walsh 2006). Aspartic proteases from *Aspergillus* sp are reported to be a possible virulence factor in invasive aspergillosis (Lee and Kolattukudy 1995; Hogen et al., 1996). Hence approaches targeted against the aspartic protease might provide new insights for prevention and treatment of invasive aspergillosis. Considering the role of fungal aspartic protease in human infections, there is a lacuna in the studies of the mechanism of inhibition by peptidic inhibitors. The present section of the chapter envisages the kinetic and conformational studies of the inhibitor with the fungal aspartic protease. The evaluation of kinetic parameters revealed a tight-binding, reversible and competitive mechanism of inhibition of the fungal aspartic protease. The fluorescence and circular dichroism studies revealed that the binding of the inhibitor induces localized conformational changes in the fungal aspartic protease and deciphers the binding of the inhibitor to the active site of the aspartic protease. The finding of the inhibitor will potentially open the way towards the development of tight binding peptidic inhibitor against aspartic protease to combat human fungal infections.

## EXPERIMENTAL PROCEDURES

### *Materials*

Aspartic protease from *Aspergillus saitoi*, Trifluoroacetate, Hemoglobin were from Sigma-Aldrich, USA. All other chemicals used were of analytical grade.

### *Fungal aspartic protease inhibition assay*

The inhibition assay for the aspartic protease from *Aspergillus saitoi* was carried out as described in chapter 2.

### *Initial kinetic analysis for determination of $K_m$ and $K_i$*

For initial kinetic analysis, the kinetic parameters for the substrate hydrolysis were determined by measuring the initial rate of enzymatic activity. The  $IC_{50}$  value was determined by nonlinear regression of percent inhibition data by using the four parameter logistic Eq (1) where  $p$  is percent inhibition and is the relative decrease in enzymatic activity due to the inhibitor concentration  $[I]_0$  (Kulkarni and Rao 2007). The regression analysis was performed by the software Origin 8E.

$$p = p_{\min} + (p_{\max} - p_{\min}) / (1 + ([I]_0 / IC_{50})^n) \quad (1)$$

The inhibition constant  $K_i$  was determined by Dixon method (Dixon 1953) and also by the Lineweaver–Burk double reciprocal plot. For the Lineweaver–Burk analysis the aspartic protease (20  $\mu\text{M}$ ) was incubated with inhibitor concentrations of 0, 2, 4 and 6  $\mu\text{M}$  and assayed at increasing concentration of hemoglobin (75–540  $\mu\text{M}$ ) at 37°C for 30 min. The reciprocals of substrate hydrolysis ( $1/v$ ) for each inhibitor concentration were plotted against the reciprocals of the substrate concentrations. In Dixon's method, hydrolytic activity of aspartic protease (20  $\mu\text{M}$ ) was measured in the presence of 250 and 450  $\mu\text{M}$  of hemoglobin at concentrations of inhibitor ranging from 1 to 10  $\mu\text{M}$  at 37°C for 30 min. The reciprocals of substrate hydrolysis ( $1/V$ ) were plotted against the inhibitor concentration and the  $K_i$  was determined by fitting the data using Microcal Origin 8E.

### *Initial apparent inhibition constants*

Inhibition studies were performed by adding 100  $\mu\text{l}$  of the enzyme (0.05  $\mu\text{M}$ ) to 300  $\mu\text{l}$  of 250  $\mu\text{M}$  hemoglobin solution in standard buffer containing varying concentrations of the inhibitor (1–10  $\mu\text{M}$ ) at 37°C for 30 min. The product was estimated as mentioned above. Relative enzymatic activity  $R$  was computed from the ratio of product amounts obtained in the presence and absence of inhibitors as  $R = 1 - [P] / [P]_0$ . The relative inhibition was fit by non-linear least squares regression to Eq (2) where  $[I]_0$  is the total concentration of inhibitor and  $K_{app}$  the fitting parameter is the apparent inhibition constant.

$$R = [I]_0 / (K_{app} + [I]_0) \quad (2)$$

### *Substrate progress curve analysis*

The percentage of product formed,  $p$ , versus reaction time,  $t$ , was fitted to the recursive integral rate equation which is a variant of a known method for the estimation of  $K_m$  and  $V_m$  from the reaction progress. The instrumental offset parameter  $p_0$  accounts for the possible systematic error of the detection method. Other optimized parameters in the least squares regression were the specific molar instrumental response of the reaction product  $rp$ , the Michaelis constant  $K_m$ , and the maximum velocity  $V_m$ . The fixed parameters were the mixing delay time ( $t=0$ ) and the initial substrate concentration  $[S]_0$ . Auxiliary variables are defined as mentioned below:

$$Y^{(a+1)} = y^a + r_p (1 - [P]/[S]_0^{-b} / (1/[S]_0^{-b/K_M})) \quad (3)$$

$$b = ([P] - tV_m) / K_m \quad (4)$$

$$[P] = (ya - p_0) / rp \quad (5)$$

### *Inhibitor progress curve analysis*

The reaction time course in the presence of inhibitor was fitted to the equation given below, which is a modification of the standard kinetic model.

$$p = p_0 + Vst + (V_0 - V_s)[1 - \exp(-k_{app}t)]/k_{app} \quad (6)$$

The instrumental offset  $p_0$  is treated as an adjustable parameter to account for the possibility of systematic errors in measuring the product conversion degree. Each individual progress curve was fitted separately. The local fitting parameters were the initial velocity  $V_0$ , the steady state velocity  $V_s$ , the apparent first order rate constant  $K_{app}$ , and the instrumental offset  $p_0$ . These fitting parameters were analyzed to obtain approximate inhibition constants and are described in detail later. Several progress curves obtained in the presence and absence of the inhibitor at various concentrations were combined and fitted as a whole. The equation used as theoretical model is mentioned below and is applicable to a pure tight binding inhibitor.

$$v = v_0([E]_0 - [I]_0 - K_{app} + \{([E]_0 - [I]_0 - K_{app})^2 + 4[E]_0K_{app}\}^{-1/2}) \quad (7)$$

In order to fit data to this equation, the modified Marquardt–Levenberg least square fitting equation was used. The rate constants were obtained by the regression analysis of these data using the software Origin 8E. Another approach used to calculate the apparent  $K_i^*$  value for inhibitor applied the following equation:

$$IC_{50} = E_t/2 + K_i^* \quad (8)$$

$E_t$  is the total enzyme concentration and  $K_i^*$  is the apparent enzyme–inhibitor dissociation constant. For competitive inhibition, the true  $K_i$  was obtained by dividing  $K_i^*$  by  $(1 + S/K_m)$  (Dixon 1953).

### *Fluorescence analysis of enzyme-inhibitor interactions*

Fluorescence measurements were performed as described in chapter 4. For inhibitor binding studies, fungal aspartic protease (20  $\mu\text{M}$ ) was dissolved in 0.05N HCl. Titration of the enzyme with inhibitor was performed by the addition of different concentrations of the inhibitor (0, 2.5, 5 and 10  $\mu\text{M}$ ) to a fixed concentration of enzyme solution. For each inhibitor concentration on the titration curve, a new enzyme solution was used. All the data on the titration curve were corrected for dilutions, and the graphs were smoothened. Corrections for the inner filter effect

were performed as described in chapter 2. Background buffer spectra were subtracted to remove the contribution from Raman scattering.

*Secondary structural analysis of fungal aspartic protease-inhibitor complexes*

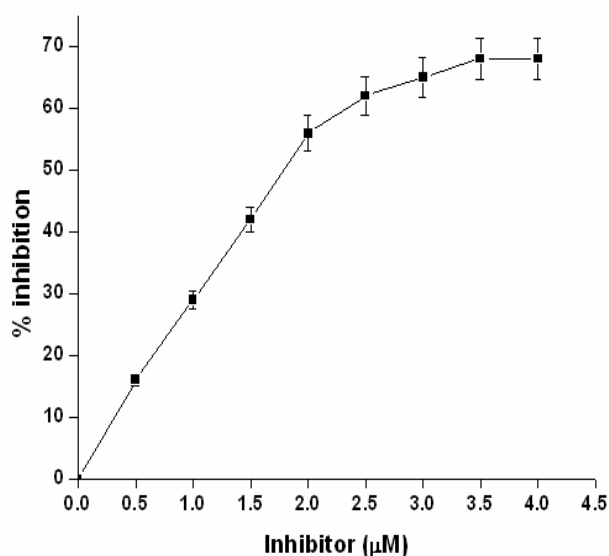
CD spectra were recorded as mentioned in chapter 4. The CD spectrum of aspartic protease (25  $\mu\text{M}$ ) was recorded in 0.05 M glycine-HCl buffer (pH 3.0) in absence/presence of inhibitor or pepstatin (5  $\mu\text{M}$  each). Secondary structure content of the aspartic protease and aspartic protease -inhibitor complex was calculated using the algorithm of the K2d program (Andrade et al., 1993; Merelo et al., 1994).



## RESULTS

### *Kinetic analysis of the inhibition of fungal aspartic protease by the inhibitor*

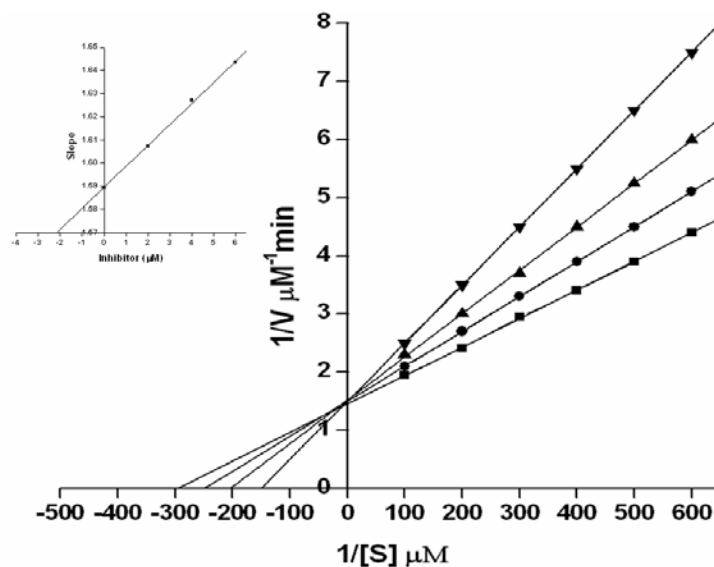
A low molecular weight aspartic protease inhibitor was purified and characterized from *Penicillium* sp VM24 (Chapter 3). The peptidic inhibitor showed inactivation of aspartic protease from *Aspergillus saitoi*. The kinetic analysis indicated an  $IC_{50}$  value of 1.82  $\mu\text{M}$  (Figure 1). The inhibition of aspartic protease followed a hyperbolic pattern with increasing concentrations of the inhibitor. However, the secondary plot (the slope of inhibition graph versus inhibitor concentration) was not linear, suggesting that the application of Michaelis–Menten inhibition kinetics was not appropriate in this study. The inhibitor showed a linear inhibitory response in the dose range of 1–10  $\mu\text{M}$ . During this course of inhibition classical competitive experiments can be performed to determine the  $K_i$  values.



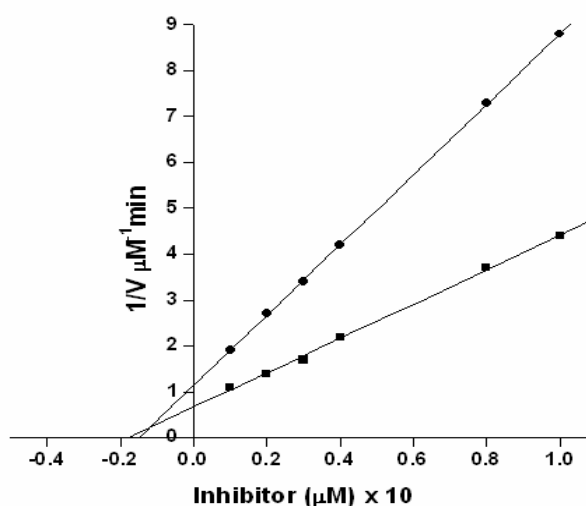
**Figure 1** The fungal aspartic protease activity (20  $\mu\text{M}$ ) was determined in the presence of increasing concentrations of inhibitor. The percent inhibition was calculated from the residual enzyme activity. The sigmoidal curve indicates the best fit for the percent inhibition data (average of triplicates) obtained, and the  $IC_{50}$  value was calculated based on the application of equation of Cha.

Initial kinetic assessments by the Lineweaver–Burk analysis revealed that the aspartic protease was competitively inhibited by inhibitor (Figure 2). The  $K_m$  value of the enzyme was 180  $\mu\text{M}$ . The secondary plot of the slope versus inhibitor concentration

gives the  $K_i$  value of 2.24  $\mu\text{M}$  (Figure 2 inset) while with the Dixon plot a  $K_i$  value of 1.2  $\mu\text{M}$  was obtained (Figure 3).



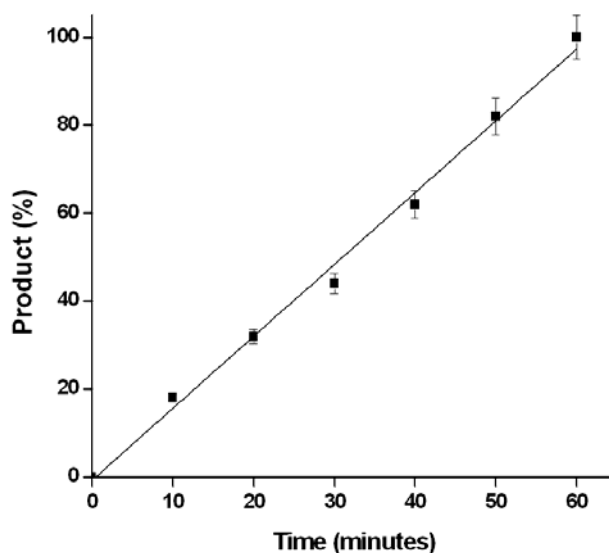
**Figure 2** Estimation of kinetic constant by Lineweaver-Burk analysis. The enzyme activity was assayed at increasing concentrations of the substrate using various inhibitor concentration, 0 (■), 2 (●), 4 (▲), 6 (▼)  $\mu\text{M}$ . The reciprocal of substrate hydrolysis ( $1/v$ ) for each inhibitor concentration were plotted against the reciprocal of the substrate concentration. The straight lines indicated the best fits for the data obtained by non-linear regression analysis and analyzed by Lineweaver-Burk's reciprocal equation for competitive type of inhibition.



**Figure 3** Enzyme activity of fungal aspartic protease (20  $\mu\text{M}$ ) was estimated using the substrate concentrations of 250 (●) and 450 (■)  $\mu\text{M}$  at different concentrations of the inhibitor. The straight line indicates the best fit of the data obtained. The inhibition constant  $K_i$  was calculated from the point of the intersection of the plots.

### Substrate kinetics

Although the  $K_m$  and  $V_m$  values are obtained from the double reciprocal plot a more comprehensive and correct understanding of these comes from the analysis of the substrate hydrolysis progress curve. Figure 4 provides the non linear least squares fit to the equations mentioned in the text previously. The initial substrate concentration was fixed at 525  $\mu\text{M}$  while the best fit values of the adjustable parameters were  $V_m = 0.548 \mu\text{M}$  per minute,  $K_m = 165 \mu\text{M}$ ,  $rp = 0.177 \text{ au } \mu\text{M}$  and  $p_0 = 0.25 \text{ au}$ . The arbitrary unit (au) of molar response is defined as percent of product formed in the reaction. From the results of fit, the maximum velocity expressed in the arbitrary units is  $0.177 \times 0.548 = 0.097\%$  of product per second, and for control the maximum conversion is  $0.177 \times 525 + 0.25 = 93.18\%$  of product.

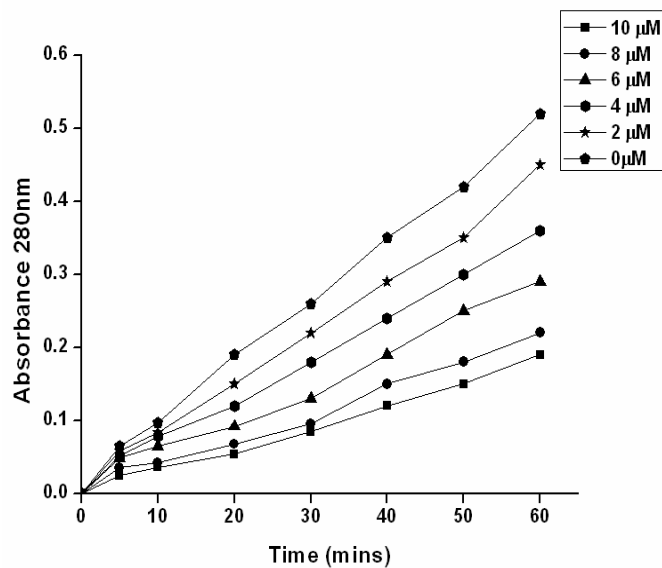


**Figure 4** Substrate curve kinetics. The least square fit of substrate progress curve to the modified integral Michaelis-Menten equation. The best fit values obtained are mentioned in the text.

### Progress curve analysis

The reaction progress was analyzed by two different methods, one based on the rapid equilibrium assumption and the other on the assumption of slow equilibrium. The results of the analysis based on the assumption of rapid equilibrium are shown in Figure 5 since the data did not fit into the other model. The progress curves obtained at 2, 4, 6, 8 and 10  $\mu\text{M}$  inhibitor were fitted individually to the equation

mentioned below. The best fit values of the individual parameters obtained are listed in Table 1.

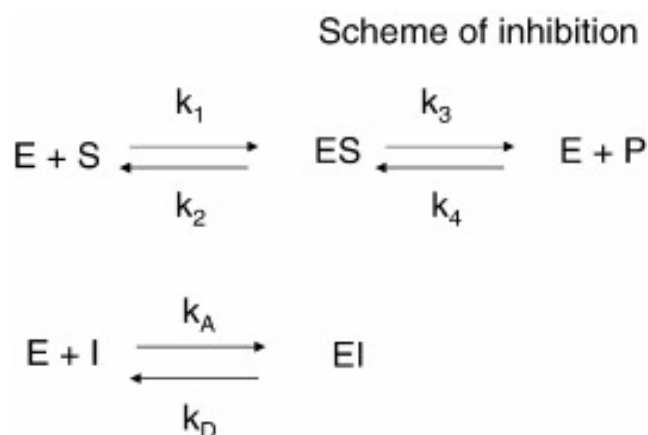


**Figure 5** Progress curve of time dependent inhibition of aspartic protease with the inhibitor. Least square fit of progress curve data of the enzyme inhibition with the inhibitor to equation mentioned in the text. The initial concentration of substrate was  $500 \mu\text{M}$ . The experimental conditions and the best fit values are mentioned in the text.

**Table 1** Kinetic rate constants by various methods

Method of analysis	Kinetic rate constant	Value obtained
Inhibitor curve analysis	$IC_{50}$	1.82 $\mu\text{M}$
Lineweaver-Burk	$K_m$	180 $\mu\text{M}$
	$K_i$	2.54 $\mu\text{M}$
	$V_m$	0.61 $\mu\text{M min}^{-1}$
Dixon plot	$K_i$	1.2 $\mu\text{M}$
Substrate kinetics	$K_m$	168 $\mu\text{M}$
	$V_m$	0.59 $\mu\text{M min}^{-1}$
Inhibitor progress curve	$K_i$	0.85 $\mu\text{M}$
	$K_i^*$	0.71 $\mu\text{M}$
	$V_m$	0.65 $\mu\text{M min}^{-1}$
	$k_A$	$6.25 \times 10^{-3} \text{ s}^{-1}$
	$k_D$	$11.84 \times 10^{-3} \text{ s}^{-1}$
Dissociation constant analysis	$K_i^*$	1.48 $\mu\text{M}$
Cha analysis	$K_i$	1.25 $\mu\text{M}$
	$K_i^*$	1.05 $\mu\text{M}$

The results corroborate with the one-step inhibition mechanism wherein the enzyme inhibitor complex is rapidly formed. The complex thus formed is stable and does not revert to another form as is the case with the slow-tight binding mechanism. The onset of inhibition is rapid and the binding indicates a tight binding mechanism. The rate constants are in agreement with the model scheme outlined in Figure 6 and rule out the possibility of a slow onset of inhibition.



**Figure 6** Model used for studying the kinetics of inhibition. E stands for the free enzyme, I is the inhibitor, EI is a rapidly forming complex.  $k_A$  and  $k_D$  stands for the association and dissociation rate constants respectively.

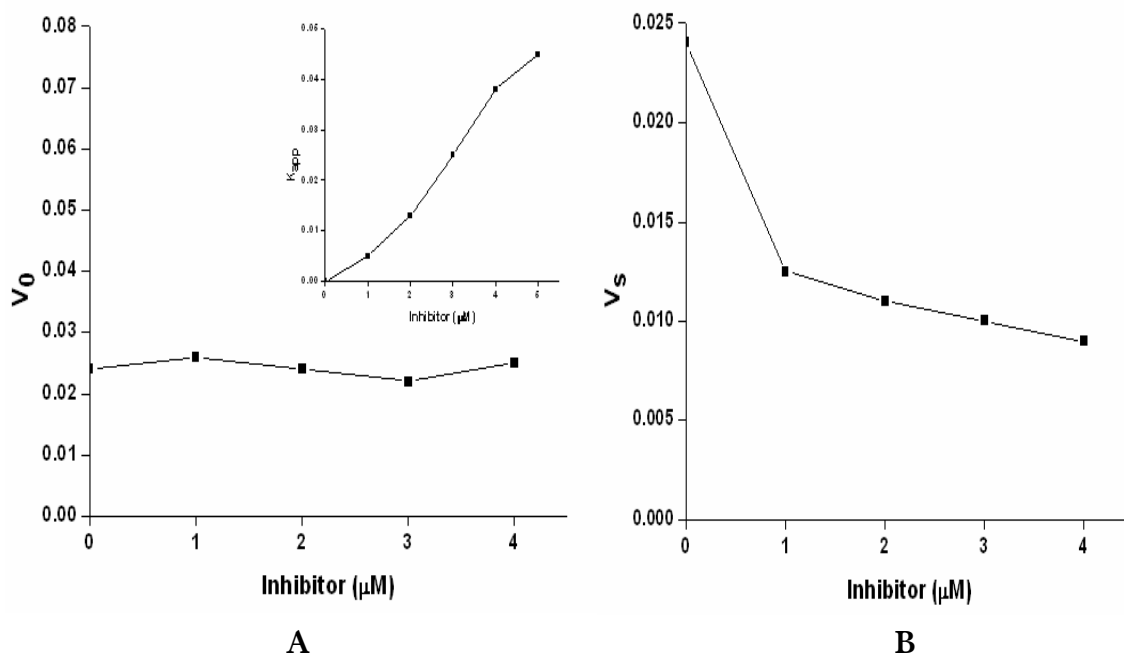
The initial velocity  $V_0$  obtained is constant and the apparent rate constant  $K_{app}$  increases linearly with the inhibitor concentration. The rate constants were obtained by fitting the data to Eq's (10)–(12).

$$V_0 = V_m[S]_0 / ([S]_0 + K_m) \quad (10)$$

$$V_s = V_m[S]_0 / \{[S]_0 + K_m(1 + [I]_0/K_i)\} \quad (11)$$

$$K_{app} = k_D + k_A[I]_0 / (1 + [S]_0/K_m) \quad (12)$$

The nonlinear least squares fit of  $V_0$ ,  $V_s$ , and  $K_{app}$  to Eq's (10)–(12) are shown in figure 7A and B. From fitting of  $V_s$  to Eq (11), the overall dissociation constant  $K_i^*$  is  $0.7271 \pm 0.005 \mu\text{M}$ ; the fitted value of  $V_{max}$  is  $0.650 \pm 0.001 \text{ au s}^{-1}$  in this case. From fitting of  $K_{app}$  to Eq (12) (Figure 7A inset), the initial inhibition constant  $K_i$  was  $0.87 \pm 0.12 \mu\text{M}$ . The isomerization rate constants were  $k_A = 6.85 \pm 0.1 \times 10^{-3} \text{ s}^{-1}$  and  $k_D = 11.84 \pm 0.06 \times 10^{-3} \text{ s}^{-1}$ , from which the total dissociation constant  $K_i^* = K_i k_D / k_A$  is  $1.5183 \mu\text{M}$ . The parameters obtained with the mechanism as explained by Cha et al (1975) corroborate well with the above mentioned mechanism yielding a  $K_i^*$  of  $1.075 \mu\text{M}$  and a  $K_i$  of  $1.1245 \mu\text{M}$ .



**Figure 7 (A)** Least square fit of steady state velocities  $V_0$  and the apparent first order rate constant  $K_{app}$  to the equation 10 & 12. The best fit values of the adjustable parameters are listed in the text. **(B)** Least square fit of steady state velocity  $V_s$  to the equation 11. The best fit values of the adjustable parameters are listed in the text.

The parameters listed in Table 2 favor the one-step mechanism, because the initial velocity does not decrease with the concentration of the inhibitor, as predicted by Eq (10). Also, the increase of the apparent rate constant with  $[I]_0$  is linear.

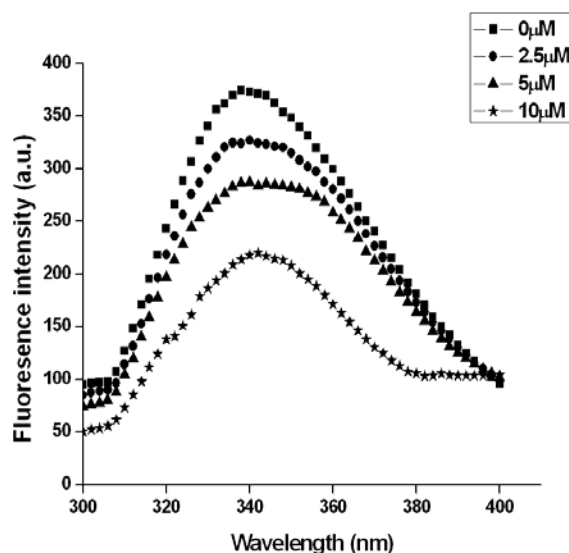
**Table 2** Best fit values of adjustable parameters, obtained in fitting the progress curves shown in figure 7 (20  $\mu\text{M}$  fungal aspartic protease, 250  $\mu\text{M}$  hemoglobin, pH 3.0, 37°C) to Eq's (10-12)

$[\text{I}]_0$ (nM)	$V_s$ (%P $\text{s}^{-1}$ )	$V_o$ (%P $\text{s}^{-1}$ )	$K_{app}$ ( $\text{s}^{-1}$ )
0	0.024	0.024	-
1	0.0125	0.026	0.005
2	0.011	0.024	0.013
3	0.010	0.022	0.025
4	0.009	0.025	0.038
5	0.007	0.026	0.045

#### *Fluoremetric analysis of aspartic protease-inhibitor interactions*

The localized changes induced in the fungal aspartic protease due to interactions with the inhibitor were investigated by fluorescence spectroscopic analysis. The conformational changes induced in the aspartic protease upon binding of inhibitor were monitored by exploiting the intrinsic fluorescence by excitation of the  $\pi$ - $\pi^*$  transition in the Trp residues. The fluorescence emission spectra of aspartic protease exhibited an emission maxima ( $\lambda_{\text{max}}$ ) at 340 nm as a result of the radiative decay of the  $\pi$ - $\pi^*$  transition from the Trp residues, confirming the hydrophilic nature of the Trp environment (Figure 8). The titration of the native enzyme with increasing concentrations of inhibitor resulted in a concentration dependent quenching of the tryptophanyl fluorescence. However, the  $\lambda_{\text{max}}$  of the fluorescence profile indicated no blue or red shift, revealing that the ligand binding caused reduction in the intrinsic protein fluorescence.



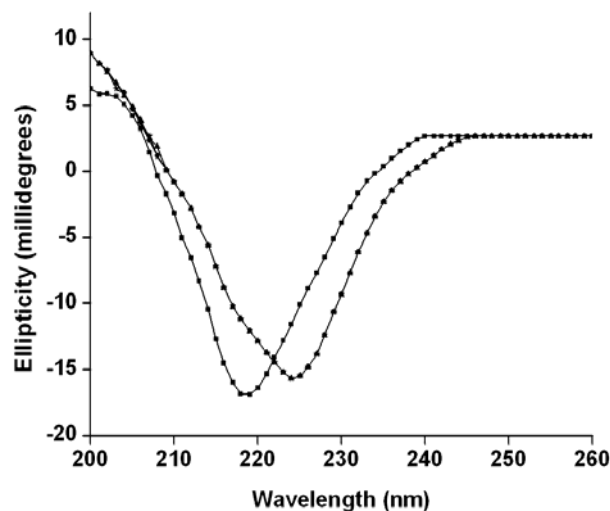


**Figure 8** Steady-state fluorescence emission spectra of aspartic protease as a function of the inhibitor. Protein fluorescence was excited at 295 nm, and emission was monitored from 300–400 nm at 25°C. Titration was performed by the addition of different concentrations of the inhibitor to a fixed concentration of enzyme.

#### *Circular dichroism analysis of aspartic protease-inhibitor complexes*

To elucidate the effects of inhibitor on the secondary structure of fungal aspartic protease, the CD spectra of enzyme-inhibitor complex was analyzed. The contents of  $\alpha$ -helix,  $\beta$ -sheet, and aperiodic structures of aspartic protease from *A. saitoi* were 2.5%, 59% and 18% respectively. The CD spectrum of the aspartic protease-inhibitor complex showed a pronounced shift in the negative band at 220 nm of the native enzyme to 227 nm (Figure 9). This shift reveals a subtle change in the secondary structure of the enzyme upon ligand binding. Further, to throw light upon the mechanism of inactivation of aspartic protease by the newly isolated inhibitor, we have analyzed the interactions of a representative competitive inhibitor, pepstatin (Richards et al., 1989) on the secondary structure of the enzyme. The binding of pepstatin to aspartic protease exhibited a similar pattern of negative ellipticity in the far-UV region indicating that the newly isolated inhibitor causes similar structural changes and were distinctly different from that of the unliganded enzyme. The comparative analysis of the CD spectra of fungal aspartic protease upon binding of the inhibitor or the known active site-based inhibitor, pepstatin was found to be

similar, suggesting that the newly isolated inhibitor binds to the active site of the enzyme and causes inactivation.



**Figure 9** Effect on the secondary structure of the fungal aspartic protease upon binding of the inhibitor. Far-UV circular dichroism spectra of the unliganded aspartic protease and its complexes with the pepstatin and inhibitor are shown. Enzyme ( $25 \mu\text{M}$ ) was dissolved in the buffer and the CD spectra were recorded in the absence (■) or in the presence of the inhibitor (●,  $5 \mu\text{M}$ ) or pepstatin (\*,  $5 \mu\text{M}$ ) from 260 to 200 nm at  $25^\circ\text{C}$ . Each spectrum represents the average of six scans.

## DISCUSSION

The data reported showed that the newly isolated inhibitor from *Penicillium* sp VM24 is a tight binding inhibitor of aspartic protease from *Aspergillus saitoi*. During initial kinetic analysis the inhibitor showed competitive inhibition against the enzyme *in vitro*. The 1:1 molar ratio of the interaction of the inhibitor with the target enzymes classified it under the “tight-binding inhibitor” group (William and Morrison 1979). The inhibitor demonstrated an  $IC_{50}$  value of 1.8  $\mu\text{M}$  and the inhibition constant  $K_i$ , determined by the different methods was found between 1 and 2.5  $\mu\text{M}$  (Table 2), which are almost equal to the  $IC_{50}$  value of the inhibitor. Characteristically the concentration of a tight binding inhibitor required to give 50% inhibition depends on the concentration of the enzyme. Therefore  $IC_{50}$  values for tight binding inhibitors become meaningless in the absence of information on the concentration of the enzyme used. A reversible tight-binding inhibitor is one that exerts its effect on an enzyme catalyzed reaction at a concentration comparable to that of the enzyme. Also several authors have pointed out the discrepancy in calculating the  $K_i$  values. As a rule when comparing  $K_i$  values for tight binding inhibitors, it is essential to examine the mathematical methods used for their estimation since different methods even when applied to the same data can yield  $K_i$  estimates differing by several orders of magnitude (Szedlacsek et al., 1991; Reich 1992). The Lineweaver–Burk reciprocal plot shows that inhibitor is a competitive inhibitor of the fungal aspartic protease. For the inhibition kinetic studies, the enzyme activity was monitored in the presence of different concentrations of inhibitor and substrate as a function of time. In the region of  $K_i$ , the  $k_A$  value is high while the  $k_D$  value is low. This signifies that inhibitor binds rapidly to the enzyme but the rate of dissociation is slow. This indicates a fast inactivation of the enzyme in the presence of the inhibitor. The tight binding inhibitors combine at the active site and rapidly cause the enzyme to lose activity. A comparative data of the kinetic parameters of the biologic inhibitors reported in literature with the newly isolated inhibitor is described in Table 3.

**Table 3** Comparison of kinetic parameters of representative biologic inhibitors against aspartic protease from *Aspergillus saitoi*

Inhibition constants (M)	Inhibitors		
	ATBI <sup>a</sup>	VrAPI <sup>b</sup>	Present work
$IC_{50}$	$5 \times 10^{-6}$	$4.6 \times 10^{-6}$	$1.8 \times 10^{-6}$
$K_i$	$3.2 \times 10^{-6}$	$9.6 \times 10^{-6}$	$0.85 \times 10^{-6}$
$K_i^*$	$5.2 \times 10^{-8}$	$1.56 \times 10^{-8}$	$1.05 \times 10^{-6}$

*Hemoglobin is used as the substrate and the assay conditions are mentioned in the experimental procedure section. a – Dash et al., 2001; b – Kulkarni A 2007*

The onset of tight-binding inhibition is caused by a normal conformational mode of the enzyme-inhibitor complex. The tight-binding inhibitors induce conformational changes that cause the enzyme to clamp down in the inhibitor, resulting in the formation of a stable enzyme-inhibitor complex. On the basis of our fluorescence studies, we propose that the rapid fluorescence loss was due to the formation of the reversible enzyme-inhibitor complex. The fluorescence quenching of the fungal aspartic protease by inhibitor revealed that the binding of inhibitor reduces the quantum yield of the Trp emission. The kinetically observable formation of enzyme-inhibitor complex does not involve a major alteration in the three-dimensional structure of the enzymes as reflected in the absence of any shift in the tryptophanyl fluorescence. As the inhibitor has no absorption in the region of 290-450 nm, we ruled out the quenching of fluorescence due to the energy transfer between the inhibitor and the tryptophan residues. The proteolytic activity of aspartic protease decreased linearly with increasing concentrations of inhibitor, yielding a stoichiometry close to 1:1. The effect of inhibitor concentration on the fluorescence quenching of the enzymes was also consistent with a 1:1 molar ratio. Irrespective of the physical explanation for the quenching process, it was apparent that the inhibitor-induced fluorescence quenching followed the formation of the

aspartic protease-inhibitor complex. These findings indicated that the polarity of the Trp environment was negligibly altered after the binding of the inhibitor, suggesting minimal conformational changes in the tertiary structure of the fungal aspartic protease. Our interpretation for the changes observed in the secondary structure of the fungal aspartic protease due to the binding of classical inhibitor, pepstatin to the active site can be correlated to the similar pattern of changes observed due to the binding of the newly isolated peptidic inhibitor. Thus, we have concluded from the fluorescence and CD studies that the peptidic inhibitor binds to the active site of the fungal aspartic protease and causes inactivation.

The results of our investigation demonstrated for the first time a low molecular weight peptidic inhibitor from *Penicillium* sp exhibiting tight binding inhibition mechanism against fungal aspartic protease. The determined kinetic data for the enzyme-inhibitor interactions were correlated with the conformational changes induced in the aspartic protease due to inhibitor binding. On the basis of our foregoing results, we propose that concomitant with the kinetic characterization, fluorescence spectroscopy will be useful for the evaluation of inhibitor kinetic constants in the absence of enzyme turnover and for the characterization of the mechanism of inhibition of aspartic proteases. The inhibitor will be significant as a lead molecule for the development of drugs targeted towards invasive aspergillosis.

## **PART B**

### **Slow-tight binding inhibition of xyloglucanase from *Thermomonospora* sp by an aspartic protease inhibitor**

## SUMMARY

This section of the chapter describes the evaluation of kinetic parameters of the inhibition of xyloglucanase by a peptidic inhibitor from *Penicillium* sp VM24. The inhibitor also inactivated an aspartic protease from *Aspergillus saitoi* (Part A) establishing the bifunctional nature of the inhibitor. Xyloglucanase was secreted by an alkalothermophilic *Thermomonospora* sp and was purified to homogeneity. The steady state kinetic interactions of xyloglucanase with the inhibitor affirmed irreversible, non-competitive, two-step inhibition mechanism with  $IC_{50}$  and  $K_i$  values of 780 nM and 500 nM respectively. CD-spectra and tryptophanyl fluorescence analysis of xyloglucanase incubated with increasing inhibitor concentrations conceded that the conformational changes in enzyme structure was due to irreversible denaturation of enzyme upon inhibitor binding. Further to elucidate the inhibition mechanism, xyloglucanase was probed with a fluorescent chemoaffinity label *o*-phthalaldehyde (OPTA), which revealed that complete inactivation occurred due to binding of one mole of OPTA to the active site of xyloglucanase. OPTA has been known to form a fluorescent isoindole derivative by crosslinking the proximal thiol and amino groups of cysteine and lysine. The chemical modification of xyloglucanase using trinitrobenzenesulphonic acid (TNBS) showed the presence of a single lysine residue in the active site of xyloglucanase. The inactivation studies of diethylpyrocarbonate (DEP)-modified xyloglucanase established the presence of an essential histidine at or near the catalytic site of xyloglucanase. The involvement of cysteine in the formation of a xyloglucanase-isoindole derivative has been negated by fluorometric and chemical modification studies on xyloglucanase with group-specific reagents. Modification of histidine and lysine residues by DEP and TNBS respectively, abolished the ability of the enzyme to form an isoindole derivative with OPTA, indicating that histidine and lysine participate in the formation of the isoindole complex. The abolished isoindole fluorescence of *o*-phthalaldehyde (OPTA)-labeled xyloglucanase revealed that the inhibitor binds to the active site of the enzyme and disrupts the native interactions between the lysine and histidine residues.

## INTRODUCTION

The vital functions of glycosidases in living systems are revealed by modifying or blocking biological processes by specific glycosidase inhibitors. Glycosidase inhibitors have many beneficial effects in agrochemicals and have varied biotechnological and pharmaceutical applications such as antifungals, insecticides, antidiabetics, antiobesities, antivirals, anticancer and as therapeutic agents for some genetic disorders (Asano 2003). A number of naturally occurring reversible glycosidase inhibitors such as nojirimycin, castanospermine, swainsonine, and acarbose have been reported (Legler G 1990). Another class of inhibitors is the synthetic analogues of sugars containing reactive groups such as epoxides, isothiocyanates,  $\alpha$ -halocarbonyls (Legler G 1990; Withers and Aerbersold 1995), triazoles (Rossi and Basu 2005) and thiasugars (Yuasa et al., 2009). There are reports of mechanism-based inhibitors such as conduritol epoxides, the quinone methide-generating glycosides, and the glycosylmethyl triazenes. To gain insight into the details of the hydrolytic mechanism of glycosidases, specific inhibitors are necessary which can act as mechanistic and structural probes and also for establishing the structures of active centers (Sorenson et al., 2004). A diverse array of extremely potent, basic, nitrogen-containing inhibitors has been developed over the years, and they have been found to be of great utility in the study of the glycosidase mechanism (Legler G 1990; Stutz 1999). Glycosidases have been studied with a clinical perspective of locating enzyme-allergens (Tarvainen and Keskinen 1991). Xyloglucanases, xylanases and cellulases have been found to cause occupational and non-occupational allergies, such as respiratory and irritant contact dermatitis. Therefore, from the biomedical point of view, inhibitors of this class of enzymes will have tremendous importance in the near future. In addition, inhibition of cellulolytic and hemicellulolytic enzymes have potential applications to prevent the degradation of wood and cloth by the action of the hydrolytic enzymes present in the gut of termites. Xyloglucanases belong to the inverting and retaining glycoside hydrolyases which constitute 113 protein families responsible for the hydrolysis and/or transglycosylation of glycosidic bonds. Xyloglucanases (3.2.1.151) represent a



class of polysaccharide degrading enzymes which can attack the backbone also at substituted glucose residues. The xyloglucan and the enzymes responsible for its modification and degradation are finding increasing prominence, reflecting the drive for diverse biotechnological applications in fruit juice clarification, textile processing, cellulose surface modification, pharmaceutical delivery, production of food thickening agents, paper and pulp industry, plant growth modulation, production of novel surfactant, synthesis of biocomposites and enzyme kinetic studies (Gloster et al., 2007; Wong et al., 2010). Xyloglucan-specific glycosidases with high substrate specificity are useful tools for analyzing the xyloglucan structure. Xyloglucanases have been used to characterize molecular alterations in plant cell-wall mutants, engineer the physical properties and biochemical composition of plant fibres and link chemically modified xylo-oligosaccharides to xyloglucan polymers that can be used to impart novel functionality to cellulose microfibrils (Master et al., 2008).

Few reports of naturally occurring proteinaceous inhibitors of xyloglucanase from tomato, tobacco, soybean, potato are available, however there are no reports on low molecular weight peptidic inhibitor of this class of enzyme from microorganisms. Low-molecular weight inhibitors released from microbial cells are different from macromolecular endogenous inhibitors. The low molecular weight inhibitors usually do not have functional roles in its cell, whereas the macromolecular endogenous inhibitors exhibit some functions in the cells. Therefore, much effort needs to be focused on the design of efficient and specific inhibitors of xyloglucanase for many potential applications such as tools for understanding the hydrolytic mechanisms and as prospective biocontrol agents. This part of the chapter describes the production and purification of xyloglucanase from the extracellular culture filtrate of an alkalothermophilic *Thermomonospora* sp. The chapter also enunciates for the first time the inhibition of xyloglucanase by an irreversible low molecular weight peptidic inhibitor from *Penicillium* sp VM24. The steady-state kinetics exhibited a two-step inhibition mechanism, and the conformational modes observed during the binding of inhibitor to the enzyme were conveniently monitored by fluorescence analysis. Chemo-affinity labeling and group-specific modification of

xyloglucanase concede the presence of lysine and histidine residues at or near the active site. The mechanism of inactivation of xyloglucanase by the inhibitor was delineated by monitoring the isoindole fluorescence of the o-phthalaldehyde (OPTA)-labeled enzyme and CD analysis.

## EXPERIMENTAL PROCEDURES

### *Materials*

Xyloglucan from tamarind seeds was a kind gift from Dr Barry McCleary, Megazyme International Ireland Ltd, Ireland. Tamarind kernel powder (TKP) was kindly provided by Mr A Agarwal, Herbex International, India. Acetonitrile was purchased from E-Merck, Germany. Ultra membranes UM-10 and UM-3, UM-0.5 was from Millipore. Trifluoroacetate, QAE Sephadex, dinitrosalicylic acid, TNBS (2,4,6-trinitrobenzenesulfonic acid, PHMB (*p*-hydroxymercuribenzoic acid), DEP (diethylpyrocarbonate), N-ethylmaleimide, Nbs<sub>2</sub> (5,5'-dithiobis(2-nitrobenzoic acid), OPTA (o-phthalaldehyde) were from Sigma-Aldrich, USA. Bio-Gel P-100 was from Bio-Rad laboratories, CA. All other chemicals used were of analytical grade.

### *Production of xyloglucanase in different media*

Alkalothermophilic *Thermomonospora* sp was maintained on Luria-Bertani wheat bran slants at pH 10.0 at 50°C according to George et al (2001a). *Thermomonospora* was grown on two different media (a) modified Reese medium (Mandels and Weber 1969) containing 1% yeast extract, 4% cellulose powder and 0.1% Tween 80 and (b) modified Reese medium with 0.5% yeast extract, 1% TKP, 1% cellulose powder and 0.1% Tween 80. The pH of the media was adjusted to 9.0 with 10% Na<sub>2</sub>CO<sub>3</sub> after autoclaving. The culture was grown at 50°C for 120 h on a rotary shaker maintained at 200 rpm. Samples were withdrawn after an interval of 24 h, centrifuged at 10000 rpm for 15 min at 4°C and the supernatant was checked for xyloglucanase activity.

### *Xyloglucanase assay*

Xyloglucanase activity was determined as mentioned in chapter 5.

### *Purification of xyloglucanase*

The culture filtrate obtained after 120 h of incubation in medium (b) was concentrated using ammonium sulphate (0-90 % saturation). All purification steps were carried out at 4°C unless otherwise stated. The precipitate was dissolved in 0.05M sodium phosphate buffer, pH 7.0, dialyzed against same buffer with several

changes for 8 h, and applied to QAE Sephadex column (3 x 20 cm) previously equilibrated with 0.05M sodium phosphate buffer, pH 7.0. The elution was carried out by a linear gradient of sodium chloride (0-0.6 M) in same buffer. The fractions having maximum specific activity were pooled and concentrated by ultrafiltration through Amicon UM-10 membrane. The concentrated sample was applied to Bio-Gel P-100 column (2 x 100 cm) previously equilibrated with 0.05M sodium phosphate buffer pH 7. Elution was carried out using the same eluent at a flow rate of 12 ml/hr. The fractions (1.5 ml each) having maximum specific activity were pooled and concentrated. The purity of the enzyme was checked by SDS-PAGE followed by silver staining (Laemmli 1970).

#### *Determination of molecular weight of the enzyme*

The molecular weight of xyloglucanase was determined by gel filtration chromatography using Sephacryl S-200 previously equilibrated with 50mM phosphate buffer, pH 7.0. The column was calibrated using the following marker proteins;  $\beta$ -amylase (Mr 205,000), alcohol dehydrogenase (Mr 97,400), bovine serum albumin (Mr 66,000), ovalbumin (Mr 43,000), carbonic anhydrase (Mr 29,000) obtained from Amersham. The void volume of the column was determined by the elution volume of blue dextran.

#### *Initial inhibition kinetic analysis*

For initial kinetic analysis, the kinetic parameters for the substrate hydrolysis were determined by measuring the initial rate of enzymatic activity. The inhibition constant ( $K_i$ ) was determined by Dixon method (Dixon 1953) and also by the Lineweaver-Burk's equation. The  $K_m$  value was also calculated from the double-reciprocal equation by fitting the data into the computer software Microcal Origin 8E. For the Lineweaver-Burk's analysis xyloglucanase (0.5 nM) was incubated with the inhibitor at (0.5  $\mu$ M) and (1  $\mu$ M) and assayed at increased concentration of xyloglucan (50-1000  $\mu$ M) at 50°C for 30 min. The reciprocals of substrate hydrolysis ( $1/v$ ) for each inhibitor concentration were plotted against the reciprocals of the substrate concentrations, and the  $K_i$  was determined by fitting the resulting data. In

Dixon's method, xyloglucanolytic activity of xyloglucanase (0.5 nM) was measured in the presence of 500 and 1000  $\mu\text{M}$  of xyloglucan, at concentrations of inhibitor ranging from 0.1 to 1  $\mu\text{M}$  at 50°C for 30 min. The reciprocals of substrate hydrolysis ( $1/v$ ) were plotted against the inhibitor concentration and the  $K_i$  was determined by fitting the data using Microcal Origin 8E. For progress curve analysis, assays were carried out in a 1 ml reaction mixture containing enzyme, substrate, and inhibitor at various concentrations. The reaction mixture contained xyloglucanase (0.5 nM) in the required buffer and varying concentrations of inhibitor (0 to 1000 nM) and 1 mM substrate (xyloglucan). Reaction was initiated by the addition of xyloglucanases at 50°C and the release of products were quantified at different time intervals by estimating the reducing sugar at 540 nm. In each slow binding inhibition experiment, five to six assays were performed with appropriate blanks. For the kinetic analysis and rate constant determinations, the assays were carried out in triplicate and the average value was considered throughout. Further details of the experiments are given in the respective figure legends.

### *Inhibitor progress curve analysis*

Lineweaver–Burk and Dixon plots ruled out the possibility of competitive, uncompetitive and mixed type of inhibition, therefore the initial rate studies were analyzed assuming reversible, pure noncompetitive kinetics as per Eq (1a) for Lineweaver–Burk plot and Eq (1b) for Dixon plot.

$$1/v = (\alpha K_M / V_{max})(1/[S]) + \alpha' / V_{max} \quad (1a)$$

$$1/v = [I] / V_{max} K_i + 1/V_{max} (1 + K_M/[S]) \quad (1b)$$

Where  $\alpha = 1 + 1/K_i$  and  $\alpha' = 1 + 1/K_i'$ .  $K_m$  is the Michaelis constant,  $V_{max}$  is the maximal catalytic rate at saturating substrate concentration [S], I is the inhibitor concentration,  $K_i = (k_4/k_3)$  and  $K_i' = (k_9/k_8)$  are the dissociation constants (inhibition constants) for the first reversible enzyme–inhibitor or enzyme–inhibitor–substrate complexes respectively. If the E and ES complex bind I with equal affinity, then

$\alpha = \alpha'$  and the apparent  $K_m$  value unchanged from the  $K_M$  for the reaction in the absence of inhibitor. In this, inhibitor would affect the  $V_{max}$  but not the  $K_m$  (Cha S 1975). The values of  $K_i$  and  $K_i'$  were estimated according to Eq (1c) and procedure suggested previously (Cha 1975; Cleland 1963).

$$\text{slope}_0 = (\text{slope}_i - \text{slope}_0) = K_i (1 + K_i' / I) / (K_i' - K_i) \quad (1c)$$

Where  $\text{slope}_0$  is the slope of the straight line on the Lineweaver–Burk plot for  $[I] = 0$  and  $\text{slope}_i$  is for  $[I] \neq 0$  (Cha 1975). The progress curves for the interactions between the inhibitor and xyloglucanase were analyzed using Eq 2 (Beith 1995; Morrison and Stone 1985),

$$[P] = v_s t + \frac{v_0 - v_s}{k} (1 - e^{-kt}) \quad (2)$$

where (P) is the product concentration at any time  $t$ ,  $v_0$  and  $v_s$  are the initial and final steady-state rates, respectively, and  $k$  is the apparent first-order rate constant for the establishment of the final steady-state equilibrium. As a prerequisite for tight binding inhibitors, corrections have been made for the reduction in the inhibitor concentration that occurs on formation of the enzyme-inhibitor (EI) complex. This is because, in the case of tight binding inhibition, the concentration of EI is not negligible in comparison to the inhibitor concentration and the free inhibitor concentration is not equal to the added concentration of the inhibitor. The corrections of the variation of the steady-state velocity with the inhibitor concentrations were made according to Eq 3 and 4 as described by Morrison and Walsh (1988),

$$v_s = \frac{k_7 S Q}{2(K_m + S)} \quad (3)$$

$$Q = [(K_i' + I_t - E_t) + 4K_i' E_t]^{1/2} - (K_i' + I_t - E_t) \quad (4)$$

where  $K_i' = K_i^* (1 + S/K_m)$ ,  $k_7$  is the rate constant for the product formation and  $I_t$  and  $E_t$  stands for total inhibitor and enzyme concentration, respectively. The relationship between the rate constant of enzymatic reaction  $k$ , and the kinetic

constants for the association and dissociation of the enzyme and inhibitor was determined as per Equation 5,

$$k = k_6 + k_5 \left( \frac{I/K_i}{1 + (S/K_m) + (I/K_i)} \right) \quad (5)$$

The progress curves were analyzed by Eq 2 and 5 using nonlinear least-square parameter minimization to determine the best-fit values with the corrections for the tight binding inhibition. The overall inhibition constant is determined as given by Eq 6 (Robert and James 1984),

$$v_s = V_{max}[S_0] / \{ \alpha' [S_0] + K_m (1 + [I_0]/K_i^*) \} \quad (6)$$

For the time-dependent inhibition, there exists a time range in the progress curves wherein formation of EI\* is small. Within this time range, it is possible to directly measure the effect of the inhibitor on  $v_0$ , i.e. to measure  $K_i$  directly. Values for  $K_i$  were obtained from Dixon analysis at a constant substrate concentration as described in Eq 7,

$$v_0 = V_{max}[S_0] / (\alpha' [S_0] + \alpha K_M) \quad (7)$$

The rate constant  $k_6$ , for the dissociation of the second enzyme inhibitor complex was measured directly from the time-dependent inhibition. Concentrated xyloglucanase and inhibitor were incubated in a reaction mixture to reach equilibrium, followed by large dilutions in assay mixtures containing near-saturating substrate. Xyloglucanase (500 nM) was preincubated with equimolar concentrations of the inhibitor for 30 and 60 min in 0.05 M phosphate buffer, pH 7.0. 5  $\mu$ l of the preincubated sample was removed, diluted 5000-fold in the same buffer, and assayed at 50°C using xyloglucan at different time intervals.

### *Fluorescence analysis of enzyme-inhibitor interactions*

Fluorescence measurements were carried out as mentioned in chapter 4. For inhibitor binding studies, xyloglucanase (5 nM) was dissolved in 0.05 M phosphate buffer, pH 7.0. Titration of xyloglucanase with the inhibitor was performed by the addition of different concentrations of inhibitor to the enzyme solution. The

magnitude of the rapid fluorescence decrease ( $F_0 - F$ ) was calculated as described in chapter 4. The first-order rate constants for the slow loss of fluorescence  $K_{obs}$ , at each inhibitor concentration  $[I]$  were calculated as mentioned in chapter 4 for the determination of  $k_s$ .

#### *Secondary structural analysis of xyloglucanase-xyloglucan-inhibitor complexes*

Secondary structural changes were recorded as mentioned in chapter 4. The CD spectrum of xyloglucanase (50 nM) was recorded in 0.05N HCl in the absence/presence of xyloglucan (10  $\mu$ M) or inhibitor (100-500 nM) at 4°C. Secondary structure content of xyloglucanase and the complexes were calculated as described in chapter 4.

#### *Chemical modification of xyloglucanase and the effect of inhibitor on the isoindole fluorescence of OPTA-labeled xyloglucanase*

Fresh OPTA solution was prepared in methanol for each experiment. The modification was carried out by incubating xyloglucanase (2  $\mu$ M) in 1 ml of 0.05 M sodium phosphate buffer, pH 7, with different concentrations of OPTA at 25°C. Methanol had no effect on the activity of the enzyme and was always less than 2% (v/v). At different time intervals, an aliquot was withdrawn from the reaction mixture and the residual activity was measured on termination of the reaction by adding 5  $\mu$ L of 10 mM cysteine. The formation of xyloglucanase-isoindole derivative was followed spectrofluorometrically by monitoring the increase in fluorescence with the excitation wavelength fixed at 338 nm (George et al., 2001b). Xyloglucanase (2  $\mu$ M) was incubated with varying concentrations of 2,4,6-trinitrobenzenesulfonic acid (4-10 mM) in the presence of 0.25 ml 4% sodium carbonate at 25°C. Aliquots were withdrawn at suitable time intervals and the reaction was terminated by adjusting the pH to 4.5. Xyloglucanase (2  $\mu$ M) was incubated with high concentrations of PHMB (10 - 50 mM) in 0.05 M phosphate buffer, pH 7.0 at 25°C. Samples were removed at different time intervals and assayed for residual xyloglucanase activity. Control tubes having only enzyme or only inhibitor were



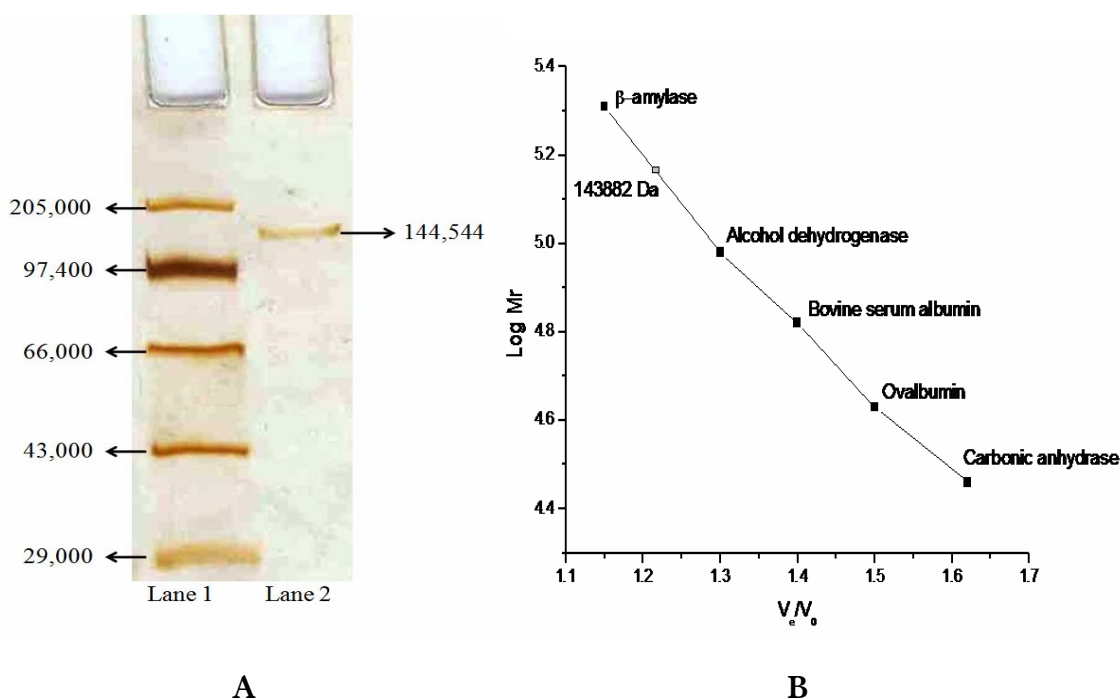
incubated under identical conditions. Similar experiments were performed in the presence of N-ethylmaleimide. Xyloglucanase was titrated with Nbs<sub>2</sub> according to the method of Ellman (1959) to assess the number of free thiol groups present. A 1mL sample of xyloglucanase (10 μM) in 8 m urea/0.05 M Tris buffer, pH 8.0, was added to a quartz cuvette with 2 mM Nbs<sub>2</sub>. The change in absorbance at 412 nm was continuously monitored at 25°C for 60 min, and the number of cysteine residues was estimated spectrophotometrically at 412 nm by using a molar absorption coefficient of  $1.36 \times 10^4 \text{ M}^{-1}\text{cm}^{-1}$  for the release of 5-mercapto-2- nitrobenzoic acid (Ellman 1959). Xyloglucanase (5 μM) in 2 ml of sodium phosphate buffer, 0.05 M, at pH 7 was incubated with varying concentrations of DEP (2-10 mM) at 25°C. Freshly prepared DEP in absolute ethanol was used. Samples were removed at different time intervals and the reaction was arrested by the addition of 50 μL of imidazole buffer, 10 mM, pH 7.5. The number of cysteine and histidine residues was determined as described by Geroge and Rao (2001). Control tubes with only enzyme, only inhibitor were incubated under identical conditions.

To monitor the effect of inhibitor on the isoindole fluorescence of xyloglucanase, the enzyme was preincubated with inhibitor (100 nM) for 20 min, and then OPTA was added and the formation of isoindole derivative was monitored as described above.

## RESULTS

### *Purification of xyloglucanase*

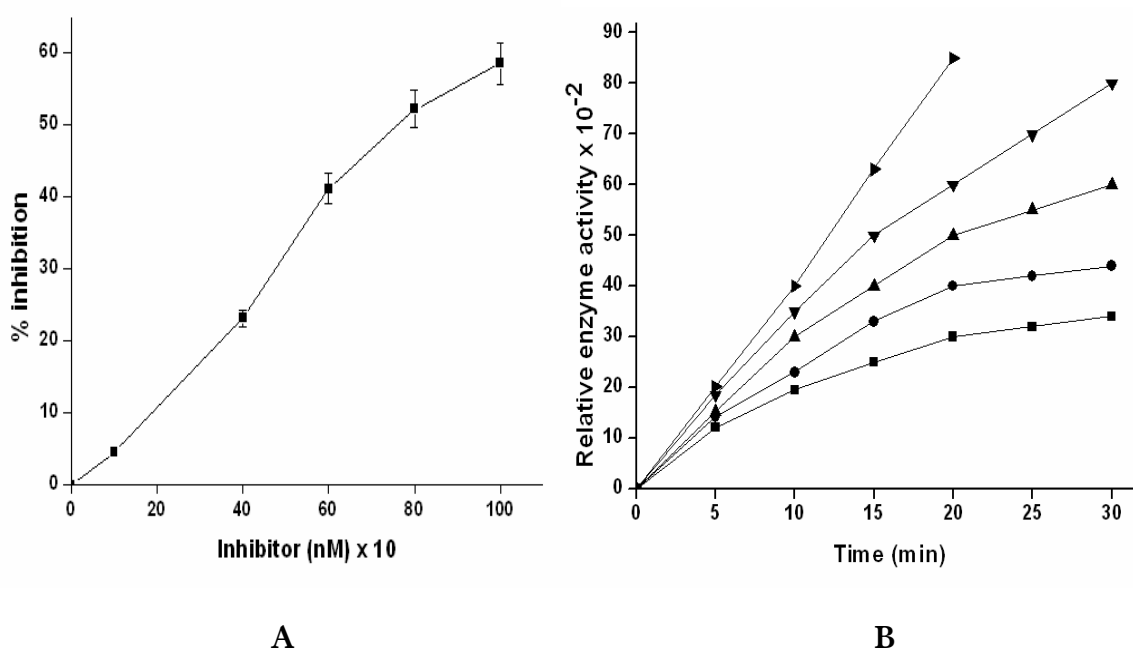
The purification of xyloglucanase from the extracellular culture filtrate of an alkalothermophilic *Thermomonospora* sp was carried out by ammonium sulphate precipitation (0-90% saturation) followed by chromatography on QAE Sephadex ion exchange column and Bio-Gel P-100 gel filtration column. Xyloglucanase from *Thermomonospora* sp was purified to homogeneity with 10 fold purification, specific activity of 121 U/mg and percent recovery of 7.46 (Pol et al., 2012). SDS PAGE revealed a single homogeneous band of pure protein with a molecular mass of 144 KDa (Figure 10A). A sharp peak of an average molecular mass of 144 KDa was obtained by gel permeation chromatography (Figure 10B). This is the first report of a high molecular weight xyloglucanase from an alkalothermophilic *Thermomonospora* sp (Pol et al., 2012).



**Figure 10** Mr determination of xyloglucanase (A) 10% SDS-PAGE visualized by silver staining: lane 1, standard molecular marker proteins and lane 2, purified xyloglucanase (B) Gel filtration chromatography by Sephacryl S 200

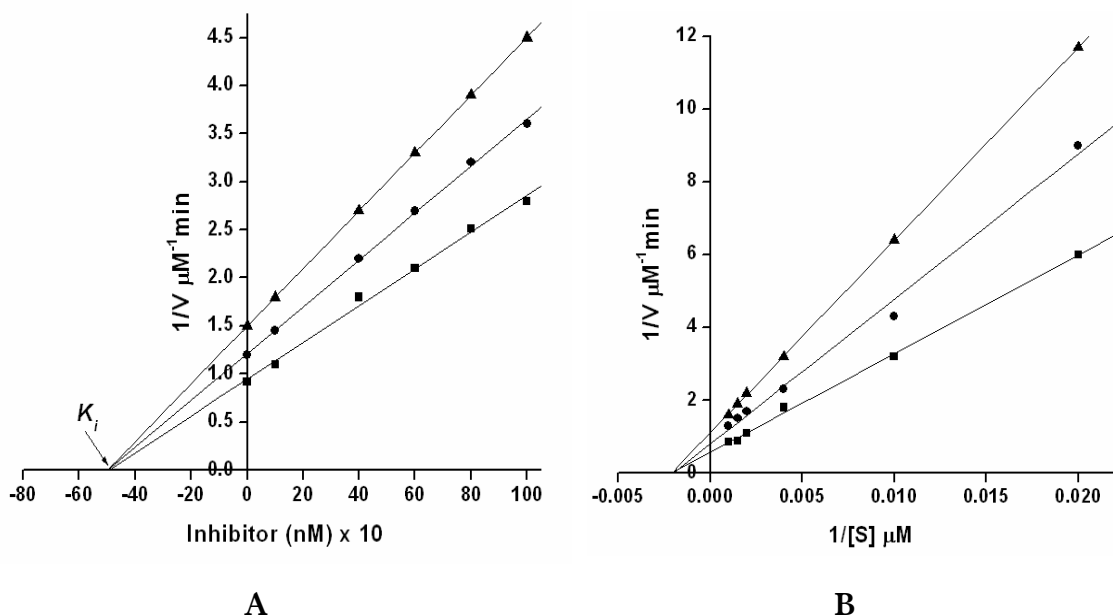
### Kinetic analysis of the inhibition of xyloglucanase

The aspartic protease inhibitor was produced extracellularly from a *Penicillium* sp VM24 and was characterized for its inhibitory activity toward aspartic protease in part A. The bifunctional nature of the inhibitor was established by inactivation toward xyloglucanase. Initial kinetic assessments of the inhibitor with xyloglucanase revealed a pure non-competitive inhibition of xyloglucanase with an  $IC_{50}$  value of 780 nM (Figure 11A). The steady-state rate of catalytic activity of xyloglucanase was reached rapidly in the absence of the inhibitor, whereas, in its presence a time-dependent decrease in the rate as a function of the inhibitor concentration was observed. Evaluation of the progress curves revealed a time range where the initial rate of the reaction did not deviate from linearity (Figure 11B) and the conversion of EI to EI\* was minimal.



**Figure 11 (A)** The activity of the xyloglucanase was determined with increasing concentrations of the inhibitor. The percent inhibition was calculated from the residual enzyme activity. The sigmoidal curve indicates the best fit for the percent inhibition data obtained, and the  $IC_{50}$  value was calculated from the graph. **(B)** Time-dependent inhibition of xyloglucanase as a function of inhibitor concentration. The reaction mixture contained xyloglucanase (0.5 nM) in 0.05 M phosphate buffer (pH 7.0) and various concentrations of inhibitor and 1 mM xyloglucan. The points represent the product released as a function of time and the lines are the best fits of data obtained from Eqs. (2) and (5), with the corrections made as per the Eqs. (3) and (4). Concentrations of inhibitor were: 0 (▲), 200 (▼), 400 (▲), 600 (●) and 1000 nM (■).

This time range was 5 min for a low concentration of the inhibitor, within which all the noncompetitive inhibition experiments were used to determine the  $K_i$  values (Eq 5). The inhibition constant  $K_i$  associated with the formation of the reversible EI was 492 nM and 530 nM as determined from the Dixon plot and double-reciprocal plot respectively (Figure 12 A & B). The  $K_i$  and  $K_i'$  values determined from the Equation 1c were found to be 550 nM and 580 nM respectively. The mode of inhibition was also studied by plotting  $1/(k-k_0)$ , from the Eq 5 as a function of  $[S]$  and was found to be independent of the substrate concentration (data not shown). The concentration of xyloglucan was set to a value below the Michaelis constant ( $K_m$ ) 500  $\mu\text{M}$ , to make reactions approximately first-order.



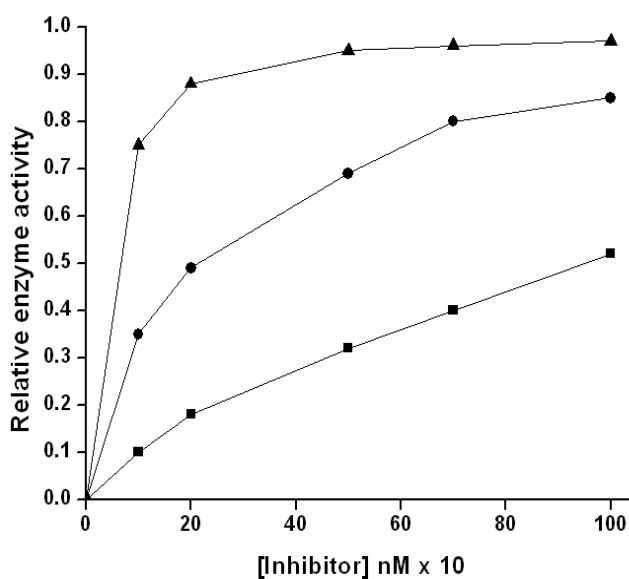
**Figure 12** Initial rate of catalytic activity of xyloglucanase in the presence of inhibitor. Enzymatic activity of xyloglucanase was estimated in 0.05 M phosphate buffer (pH 7.0) and the reducing sugar released was estimated spectrophotometrically at 540 nm. (A) Xyloglucanase (0.5 nM) was assayed using xyloglucan at 0.5 mM (▲), 0.75 mM (●) and 1 mM (■) at different inhibitor concentrations (0.1–1.0  $\mu\text{M}$ ) at 50°C for 30 min. The reciprocal of reaction velocity ( $1/v$ ) was plotted against the reciprocal of the inhibitor concentration. (B) Xyloglucanase (0.5 nM) was incubated without (■) or with the inhibitor at 0.5  $\mu\text{M}$  (●) and 1  $\mu\text{M}$  (▲) and assayed at increasing concentration of xyloglucan (50–1000  $\mu\text{M}$ ) at 50°C for 30 min. The reciprocal of reaction velocity ( $1/v$ ) for each inhibitor concentration was plotted against the reciprocal of the substrate concentration. The straight lines indicate the best fits for the data obtained by non-linear regression analysis and analyzed by the Dixon method (A) and Lineweaver–Burk reciprocal equation (B), respectively.

The results from the preincubation experiments with the inhibitor are presented in Table 4. The apparent inhibition constants decreased 41 fold over a 30 min period (Figure 13).

**Table 4** Apparent inhibition constant with or without preincubation of the inhibitor (100-1000 nM) with xyloglucanase (0.5 nM)

$K_{app}$ ( $\mu\text{M}$ )		
t = 0 min	t = 15 min	t = 30 min
$949.5 \pm 0.18$	$185 \pm 0.2$	$21.7 \pm 0.13$

*Xyloglucanase was preincubated with varying concentrations of inhibitor for 0, 15 or 30 min before the assay. Residual enzyme activity was measured as mentioned in the text.*



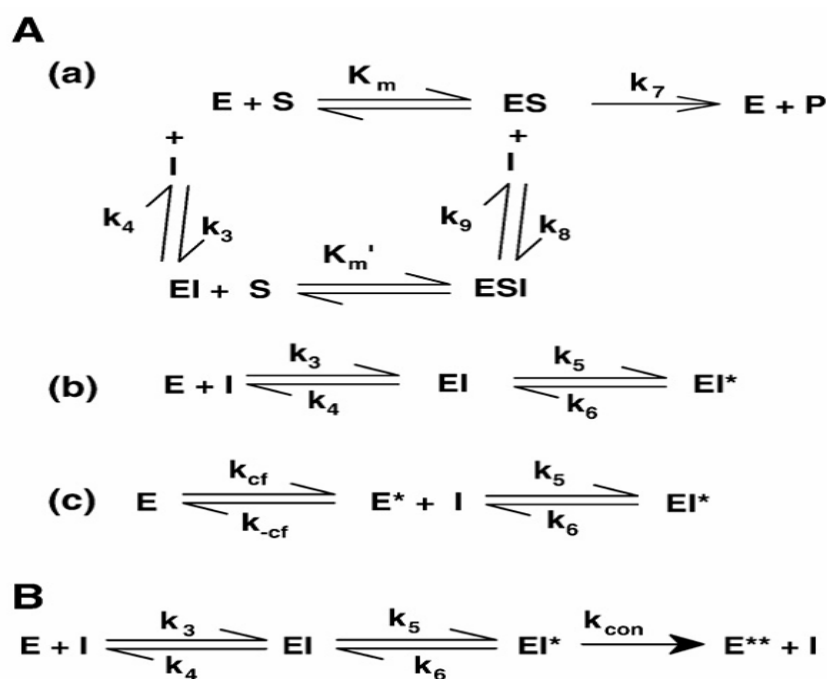
**Figure 13** The preincubation kinetic studies. Apparent inhibition constant with or without preincubation of the inhibitor (100-1000 nM) with xyloglucanases (0.5 nM) was estimated for 30 min (■), 15 min (●) and 0 min (▲). Results are described in Table 4.

The results of a preliminary analysis based on the assumption of rapid equilibrium are shown in Figure 11B. The progress curves obtained at 0, 100, 200, 400, 600 and 1000 nM of the inhibitor were fitted individually to Eq 2. The best-fit values of adjustable parameters, for each concentration of the inhibitor are listed in Table 5.

**Table 5** Best fit values of adjustable parameters obtained in fitting the progress curves shown in figure 5 (0.5 nM xyloglucanase, 1 mM xyloglucan, 50°C, pH 7.0)

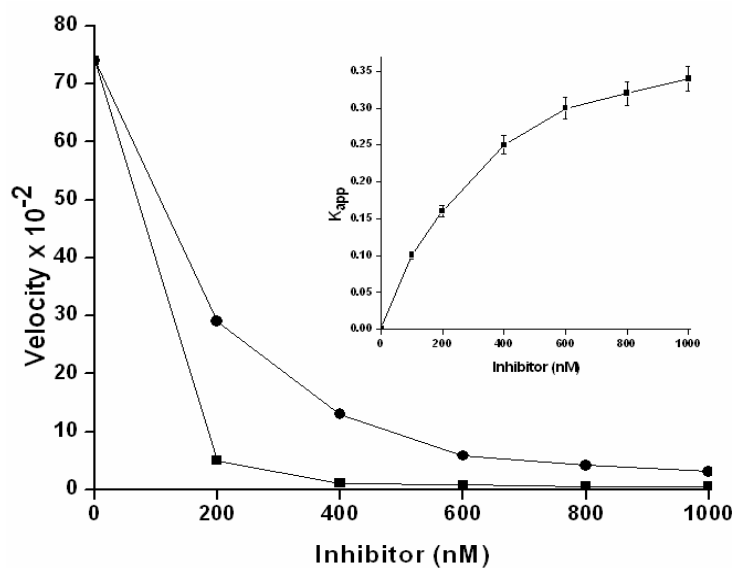
$[I]_0$ (nM)	$v_s \times 10^{-2}$ (%P s <sup>-1</sup> )	$v_o \times 10^{-2}$ (%P s <sup>-1</sup> )	$K_{app}$ (s <sup>-1</sup> )
0	74.00	74.00	0.00
100	13.91	49.88	0.11
200	5.21	29.26	0.16
400	1.1	13.01	0.25
600	0.8	5.8	0.30
800	0.6	4.2	0.32
1000	0.5	3.1	0.34

For a one-step inhibition mechanism (Scheme 1A,a), without an intermediate enzyme-inhibitor complex, the initial velocity  $v_o$  should be constant, and the apparent rate constant  $K_{app}$  should increase linearly with the inhibitor concentration  $[I]_0$ . On the other hand, for a two-step inhibition mechanism (Scheme 1A,b), the initial velocity should decrease with the inhibitor concentration followed by a typical binding curve, and the apparent rate constant should depend on  $[I]_0$  as a biphasic hyperbola.



**Scheme I** Scheme I (A and B) E stands for free enzyme, I is free inhibitor, EI is a rapidly forming pre-equilibrium complex, EI\* is the final enzyme–inhibitor complex and E\*\*+I is the irreversibly denatured state of enzyme upon binding of the inhibitor. Alternately, E may undergo interconversion into another form E\*, which binds to the inhibitor by a fast step, where  $k_{cf}$  and  $k_{-cf}$  stand for the rate constants for forward and backward reaction, respectively, for the conversion of the enzyme. Rate constant  $k_{con}$  is associated with the irreversible denatured conformational change in the EI\* to E\*\*+I.  $K_m$  is the Michaelis constant for reaction of substrate with enzyme and  $K_{m'}$  is the Michaelis constant for the reaction of substrate with enzyme–inhibitor complex.  $k_3$ ,  $k_4$ ,  $k_5$ ,  $k_6$ ,  $k_8$  and  $k_9$  are the rate constants and described in the text.  $k_7$  is the rate constant for the formation of product from ES complex.

The parameters listed in Table 5 favor the two-step inhibition mechanism, because the initial velocity does decrease with the concentration of the inhibitor, as predicted by Eq 7. Also, the increase of the apparent rate constant with  $[I]_0$  is hyperbolic, instead of linear. The non-linear least squares fit of  $K_{app}$ ,  $v_s$ , and  $v_0$  to Eq 5–7 respectively are shown in Figure 14. From fitting of  $K_{app}$  to Eq 5 (Figure 14 inset), the initial inhibition constant  $K_i$  was 585 nM. The isomerization rate constants were  $k_5 = 8.7 \pm 0.1 \times 10^{-3} \text{ s}^{-1}$  and  $k_6 = 7.3 \pm 0.6 \times 10^{-5} \text{ s}^{-1}$ , from which the total dissociation constant  $K_i^* = K_i k_6 / k_5$  was 4.5 nM. From fitting of  $v_s$  to Eq 6, the overall dissociation constant  $K_i^*$  was  $5 \pm 0.2 \text{ nM}$ . From fitting of  $v_0$  to Eq 7, the dissociation constant  $K_i$  of the initial complex was 530 nM.

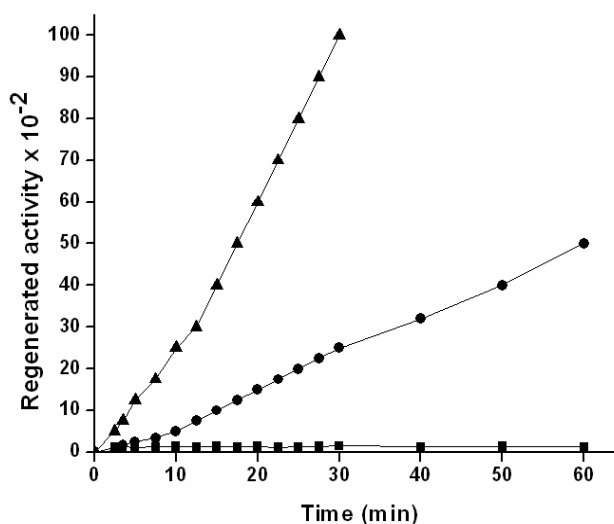


**Figure 14** Least-squares fit of the steady-state velocity  $v_s$  (■), initial velocity  $v_0$  (●) and apparent first-order rate constant  $K_{app}$  (inset) from the data provided in Table 1. The steady-state velocity ( $v_s$ ), initial velocity ( $v_0$ ) and the apparent first-order rate constant ( $K_{app}$ ) curves were fitted to eq (5-7) respectively to get the values for  $K_i$  and  $K_i^*$ ,  $k_5$  and  $k_6$ . The solid line indicates the best fit of the data obtained.

In an alternative method, the rate constant  $k_6$ , for the conversion of  $EI^*$  to  $EI$ , was determined by preincubating high concentrations of enzyme and inhibitor for sufficient time to allow the system to reach equilibrium. Dilution of the enzyme-inhibitor complex into a relatively large volume of assay mixture containing saturating substrate concentration causes dissociation of the enzyme-inhibitor complex and thus regeneration of enzymatic activity. Under these conditions,  $v_0$  and the effective inhibitor concentration can be considered approximately equal to zero and the rate of activity regeneration will provide the  $k_6$  value. After preincubating xyloglucanases with the inhibitor, the enzyme-inhibitor mixture was diluted 5000-fold into the assay mixture containing the substrate at saturating concentrations. By least squares minimization of Eq 2 to the data for recovery of enzymatic activity, the determined  $k_6$  value was  $7.3 \pm 0.6 \times 10^{-5} \text{ s}^{-1}$  (Figure 15), which clearly indicated a very slow dissociation of  $EI^*$ . The final steady-state rate  $v_s$ , was determined from the control that was preincubated without the inhibitor. The value of the rate constant  $k_5$ , associated with the isomerization of  $EI$  to  $EI^*$ , was  $7 \pm 0.1 \times 10^{-3} \text{ s}^{-1}$  as obtained from fits of Eq 5 to the onset of inhibition data using the experimentally determined



values of  $K_i$  and  $k_6$ . The overall inhibition constant  $K_i^*$  (5.1 nM) is a function of  $k_6/(k_5+k_6)$  and is equal to the product of  $K_i$  and this function. The  $k_6$  value indicated a slower rate of dissociation of  $EI^*$  and the half-life ( $t_{1/2}$ ) for the reactivation of  $EI^*$  determined from the  $k_6$  value was 2.6 h, suggesting high binding affinity of the inhibitor toward xyloglucanase. When the incubation time was more than 60 min, there was a negligible recovery in the enzymatic activity (Figure 15). This observation can be attributed to irreversible denaturation of xyloglucanase upon binding of the inhibitor.

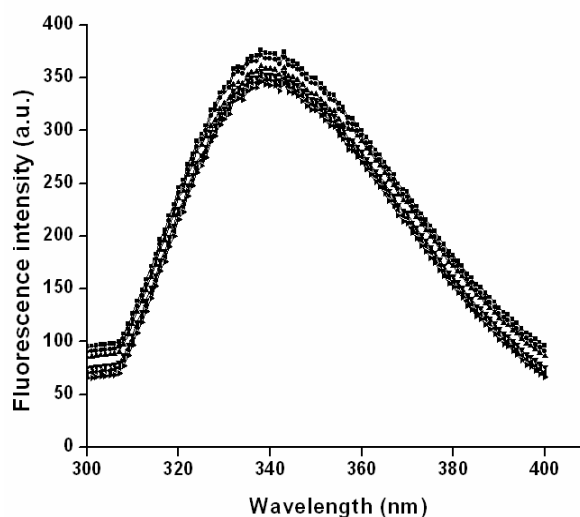


**Figure 15** Dissociation rate constant ( $k_6$ ) for the xyloglucanase–inhibitor complex. Xyloglucanase (500 nM) was pre-incubated without (▲) or with inhibitor (500  $\mu$ M) for 30 (●) or 60 (■) min in 0.05 M phosphate buffer, (pH 7.0), at 50°C. At the specified times indicated by the points, 5  $\mu$ l of the pre-incubated sample was removed, diluted 5000-fold in the same buffer, and assayed for the catalytic activity using xyloglucan (1 mM). The rate constant associated with the regeneration of activity ( $k_6$ ) was determined by estimating the absorption of the released products as described in the text.

### *Fluorescence studies on enzyme-inhibitor interactions*

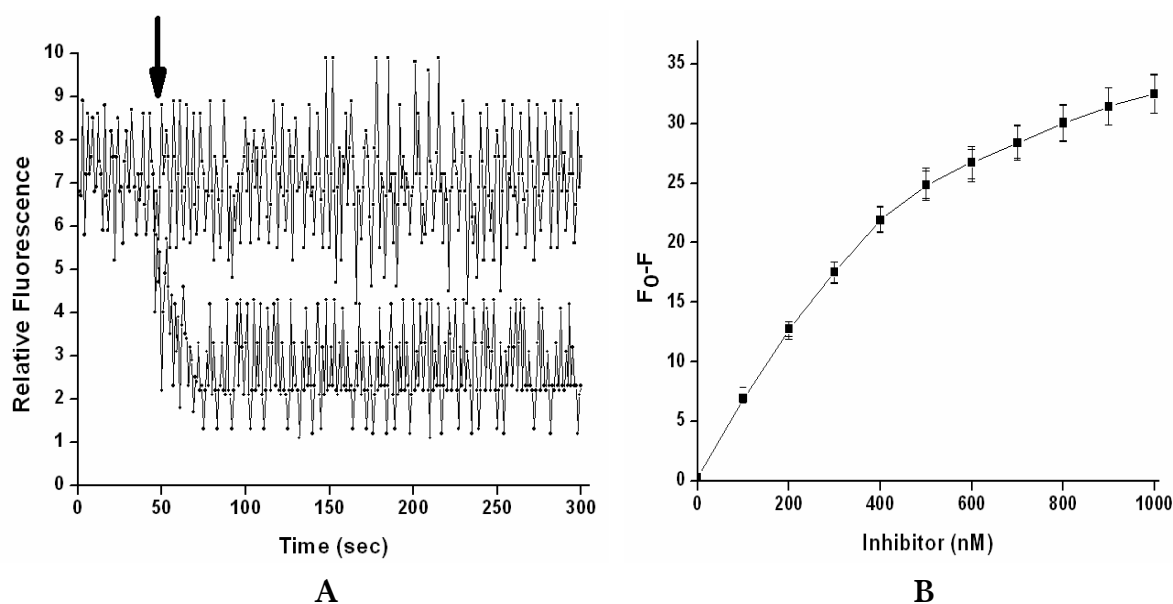
The kinetic analysis revealed a two-step inhibition mechanism, where the EI complex isomerizes to a tightly bound, slow dissociating  $EI^*$  complex. This isomerization is a consequence of the conformational changes induced in xyloglucanase due to the binding of the inhibitor. The localized conformational changes induced in xyloglucanase due to interactions with the inhibitor were investigated by exploiting the intrinsic fluorescence by excitation of the  $\pi-\pi^*$

transition in the Trp residues. The fluorescence emission spectra of xyloglucanase exhibited an emission maxima ( $\lambda_{\max}$ ) at 340 nm as a result of the radiative decay of the  $\pi$ - $\pi^*$  transition from the Trp residues, confirming the hydrophilic nature of the Trp environment (Figure 16). The titration of the native enzyme with increasing concentrations of inhibitor resulted in a concentration dependent quenching of the tryptophanyl fluorescence. However, the  $\lambda_{\max}$  of the fluorescence profile indicated no blue or red shift, revealing that the ligand binding caused reduction in the intrinsic protein fluorescence. The subtle conformational changes induced during the isomerization of EI to EI\* was monitored by analyzing the tryptophanyl fluorescence of the complexes as a function of time.



**Figure 16** Fluorescence analysis of interaction between xyloglucanase and the inhibitor. Protein fluorescence was excited at 295 nm and emission was monitored from 300 to 400 nm at 25°C. Titration was performed by the addition of different concentrations of the inhibitor to a fixed concentration of enzyme. Xyloglucanase (5 nM) was dissolved in 0.05 M phosphate buffer (pH 7.0) and the concentrations of inhibitor used were: 0 (■), 200(●), 400(▲), 600(▼), 800(◄), 1000(►) nM.

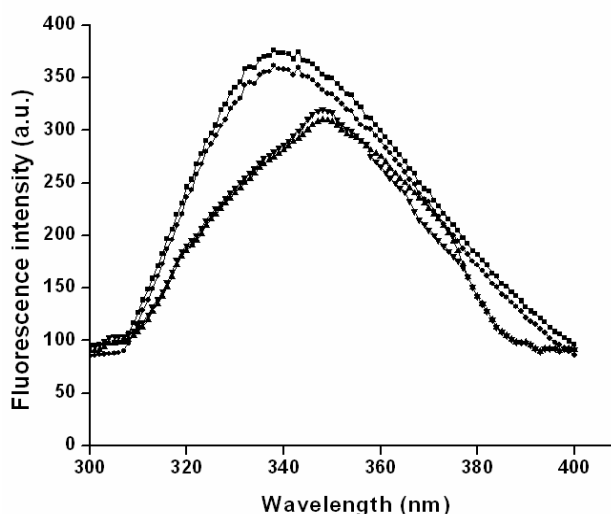
Binding of the inhibitor resulted in an exponential decay of the fluorescence intensity as indicated by a sharp decrease in the quantum yield of fluorescence followed by a slower decline to a stable value (Figure 17A). Furthermore, the titration of the inhibitor against xyloglucanase revealed that the magnitude of the initial rapid fluorescence loss ( $F_0 - F$ ) increased in a saturation-type manner (Figure 17B), which corroborated the two-step slow-tight binding inhibition of the enzyme by the inhibitor.



**Figure 17** (A) Time-dependent effect of inhibitor on the intrinsic fluorescence of xyloglucanase. Inhibitor was added to xyloglucanase (5 nM) at the specified time (indicated by the arrow) and the fluorescence emission was monitored for 300s, at a data acquisition time of 0.1 s. The excitation and emission wavelengths were fixed at 295 and 335 nm, respectively. The data were the average of five scans with the correction for buffer and dilutions. The concentrations of inhibitor used were: 0 (■) and 200 nM (●). (B) Effect of inhibitor concentration on the tryptophanyl fluorescence of xyloglucanase. A specified concentration of enzyme (5 nM) was treated with increasing concentrations of inhibitor. The fluorescence was measured at 25°C (excitation 295 nm and emission 335 nm). Each measurement was repeated five times and the average values of the fluorescence intensity were recorded. Control experiments with the buffer and inhibitor were performed under identical conditions. The fluorescence changes ( $F_0 - F$ ) were plotted against the inhibitor concentrations. The resulting hyperbola curve was fitted to the equation  $(F_0 - F) = \Delta F_{\max} / (1 + (K_i/[I]))$  to give the calculated value of  $K_i$ .

From the data in figure 17B, the magnitude of the rapid fluorescence decrease at a specific inhibitor concentration was found to be close to the total fluorescence quenching observed in figure 16, indicating that the EI and EI\* complexes have the same intrinsic fluorescence. The value of  $K_i$  determined by fitting the data for the magnitude of the rapid fluorescence decrease ( $F_0 - F$ ) was 505 nM, and the  $k_5$  value determined from the data derived from the slow decrease in fluorescence was  $7.5 \pm 0.5 \times 10^{-3} \text{ s}^{-1}$ . These rate constants are in good agreement with that obtained from the kinetic analysis, therefore, the initial rapid fluorescence decrease can be correlated to the formation of the reversible complex EI, whereas the slow, time-dependent decrease reflected the accumulation of the tight bound slow dissociating complex

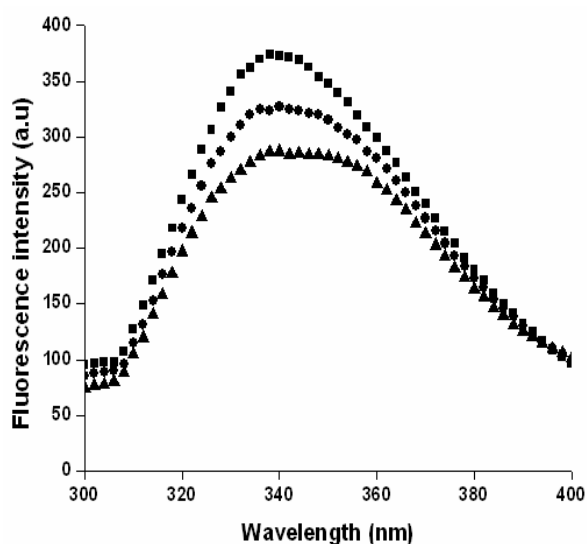
EI\*. The conformational modes observed in the EI\* complex were found to be time dependent. After 60 min the fluorescence spectra of EI\* revealed a shift in  $\lambda_{\max}$  indicating induction of gross conformational changes in the enzyme (Figure 18). To examine whether the inhibitor can be released from the EI\* after 60 min, the complex was allowed to dissociate. However, it failed to release the inhibitor, which revealed that the complex undergoes irreversible conformational changes induced by the interaction of the inhibitor. These observations revealed that the slow tight binding EI\* complex can release the inhibitor only when the complex has undergone the subtle conformational changes, however, once the inhibitor is incubated with the enzyme for a longer time, the enzyme may change to irreversible denatured state ( $E^{**} + I$ ). It may be due to weakening of some crucial interactions within the enzyme structure leading to a slow irreversible unfolding.



**Figure 18** Time-dependent conformational changes in the enzyme–inhibitor complex. Xyloglucanase and the inhibitor were incubated for 60 min and the changes in the conformational states were monitored by fluorescence. Tryptophanyl fluorescence of xyloglucanase (■) was quenched upon addition of inhibitor (●) without any shift, however, when the incubation time is above 60 min (▲) there was a shift in the emission maximum by 8 nm, indicating induction of gross conformational changes in the enzyme–inhibitor complex. There was no change in the emission spectra once these conformational changes are induced after 120 (▼) min indicating the irreversible nature of the changes in the enzyme–inhibitor complex.

Further, to conclude the mechanism of inactivation of the enzyme by the inhibitor, the interaction of xyloglucan and xyloglucanase by steady-state intrinsic fluorescence

measurements were performed. A progressive quenching in the fluorescence of xyloglucanase at 340 nm was observed concomitant to the binding of xyloglucan (Figure 19). The comparative analysis of the intensity changes in the fluorescence spectra of xyloglucanase upon binding of the substrate was found to be similar to that of inhibitor, suggesting that the inhibitor binds to the active site of the enzyme.

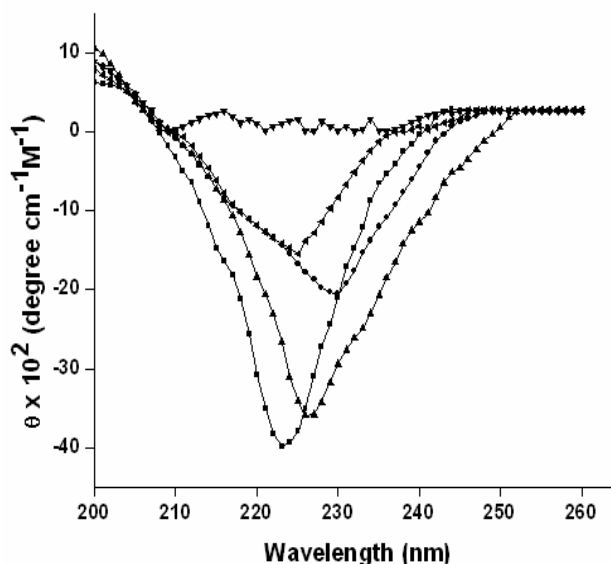


**Figure 19** Fluorescence spectra of xyloglucanase in the absence (■) or presence of xyloglucan at concentrations, 50  $\mu\text{M}$  (●) and 100  $\mu\text{M}$  (▲).

### *Circular dichroism analysis of enzyme-substrate-inhibitor complexes*

To evaluate the effects of inhibitor on the secondary structure of the enzyme, the CD spectra of xyloglucanase–inhibitor complex were analyzed. The estimated secondary structure contents from the CD analysis are 52%  $\alpha$ -helix, 28%  $\beta$ -sheet, and 16% aperiodic structure. The CD spectrum of xyloglucanase–inhibitor complex shows a pronounced shift in the negative band at 225 nm of the native enzyme to 230 nm at 250 nM inhibitor concentration. The shift in negative band reveals gross conformational changes in the secondary structure of xyloglucanase upon inhibitor binding at 500 nM concentration. A comparison of the changes in the secondary structure of xyloglucanase–inhibitor complex with that of xyloglucanase–substrate complex (experiments were performed at 4°C to avoid the hydrolysis of substrate by

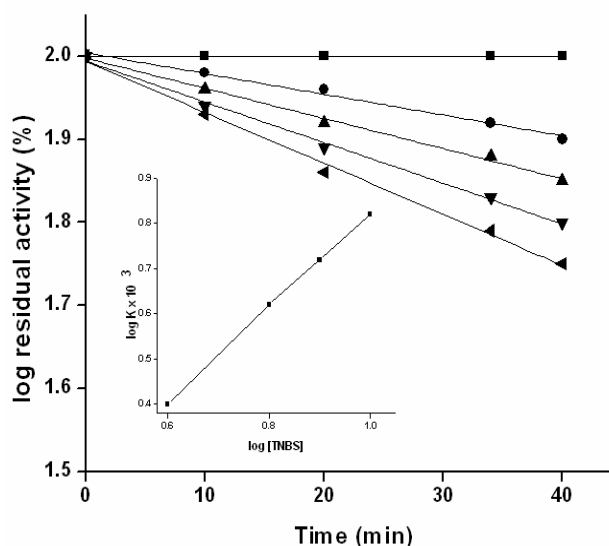
enzyme) was studied (Figure 20). Interestingly, xyloglucanase–inhibitor and xyloglucanase–substrate complexes exhibit a similar pattern of negative ellipticity in the far-UV region.



**Figure 20** Effect on the secondary structure of xyloglucanase upon binding of the inhibitor and xyloglucan. Far-UV circular dichroism spectra of the unliganded xyloglucanase and its complexes with the inhibitor are shown. The xyloglucanase (50 nM) dissolved in 0.05 N HCl (as described under “Experimental procedures”) and the CD spectra were recorded in the absence (■) or in the presence of xyloglucan 100 μM (▲) or inhibitor 100 nM (▲), 250 nM (●) and 500 nM (▼) from 200 to 260 nm at 4°C. Each spectrum represents the average of five scans.

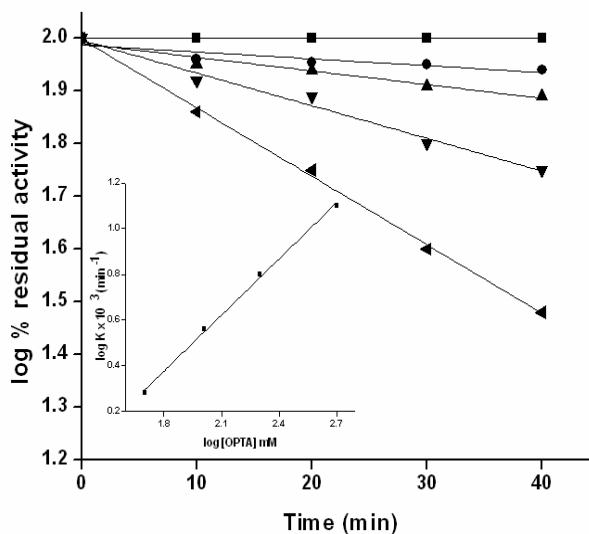
### *Inactivation of xyloglucanase by TNBS, PHMB and DEP*

Incubation of xyloglucanase (2 μM) with different concentrations of TNBS resulted in a time and concentration dependent loss of enzyme activity (Figure 21). The reaction followed pseudo first order kinetics. The pseudo first order rate constants (K) were linearly related to the concentrations of the reagent, suggesting that no reversible complex was formed during the inactivation process. Furthermore a reaction order of 0.86 with respect to the modifier was determined from the slope of the double logarithmic plots (Figure 21 inset), indicating that 1 mol of TNBS inactivated 1 mol of enzyme.



**Figure 21** Kinetics of inactivation of xyloglucanase by TNBS. Pseudo first order plots for the inactivation of xyloglucanase by TNBS. Xyloglucanase (2  $\mu$ M) was incubated with 0 ( $\blacksquare$ ), 4 ( $\bullet$ ), 6 ( $\blacktriangle$ ), 8 ( $\blacktriangledown$ ), and 10 ( $\blacktriangleleft$ ) mM TNBS at 25°C. Aliquots were removed at indicated time intervals and the reaction terminated by adjusting the pH to 4.5. Inset- Double logarithmic plots of pseudo first order rate constants as a function of TNBS concentration.

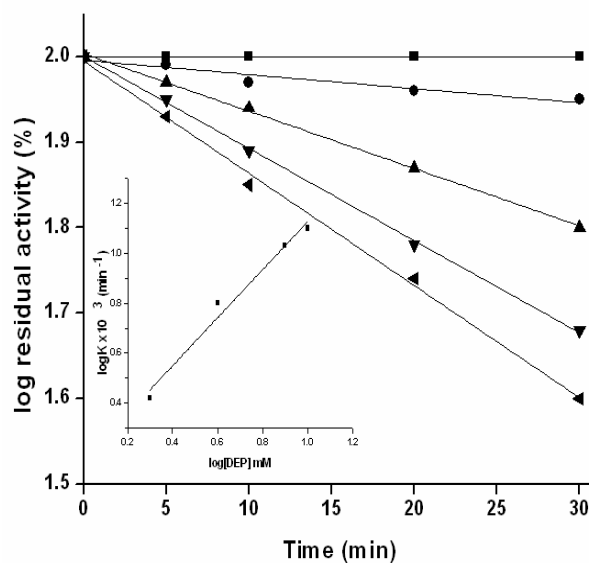
The participation of cysteine groups in the mechanism of catalysis was investigated using cysteine-specific reagents such as PHMB and N-ethylmaleimide. It was observed that xyloglucanase was not inactivated in the presence of high concentrations of PHMB and N-ethylmaleimide (50 mM) and retained complete activity. Titration of xyloglucanase with Nbs<sub>2</sub> (2 mM) in urea (8 M) at pH 8, over an extended time period did not result in the release of 5-mercapto-2-nitrobenzoic acid, suggesting that no free thiol groups exist in xyloglucanase. The inactivation of xyloglucanase with increasing concentrations of OPTA (0.05-0.5 mM) resulted in a time-dependent decrease in enzyme activity. The pseudo first-order rate constants for different concentrations of OPTA were calculated and the slope of the plots of log K against log [OPTA] produced a value of 0.82, indicating that one molecule of OPTA binds to one molecule of enzyme at the active site (Figure 22).



**Figure 22** Kinetics of inactivation of xyloglucanase by OPTA. Pseudo first order plots for the inactivation of xyloglucanase by OPTA. Xyloglucanase (2  $\mu$ M) was incubated with 0 ( $\blacksquare$ ), 0.05 ( $\bullet$ ), 0.1 ( $\blacktriangle$ ), 0.2 ( $\blacktriangledown$ ) and 0.5 ( $\blacktriangleleft$ ) mM OPTA at 25°C. Aliquots were removed at indicated time intervals and the reaction terminated by 10 mM of cysteine. Inset- second order plots of pseudo first order rate constants as a function of log OPTA concentration.

Reaction of xyloglucanase with DEP resulted in a progressive loss of activity. DEP is specific for histidine at neutral pH, but it also reacts to a lesser extent with tyrosine, cysteine and lysine (Miles 1977). The modification of tyrosine residues by DEP was excluded, as there was no decrease in the absorbance of the modified protein at 278 nm. Moreover, there was no loss in activity on treating the purified enzyme with N-acetyl imidazole, which is a tyrosine-specific reagent. The modification of cysteine could be ruled out as xyloglucanase does not contain any cysteine residues as revealed by the inactivation studies using PHMB. The recovery of total activity in the presence of hydroxylamine further proved the involvement of DEP in histidine modification and negated the modification of lysine by DEP. Carboxylation of the enzyme at pH 7.0 for 30 min resulted in 60% loss of its initial activity. The inactivation was dependent on the concentration of DEP. The pseudo first-order rate constants for different concentrations of DEP (2-10 mM) were calculated and the slope of the plots of log K against log [DEP] produced a value of 0.94 (Figure 23). These results showed that the loss in activity was due to the modification of a single histidine residue.





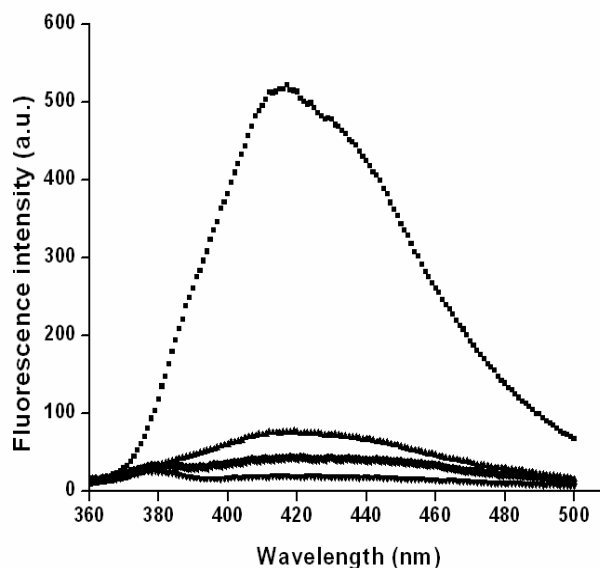
**Figure 23** Time course of inactivation of xyloglucanase by DPE. Each incubation mixture contained 5  $\mu$ M xyloglucanase in 0.05 M sodium phosphate buffer, pH 7.0 and 0 (■), 2 (●), 4 (▲), 8 (▼) and 10 (◄) mM DEP. Inset- second order plots of pseudo first order rate constants as a function of log DEP concentration.

#### *Effect of inhibitor on the isoindole fluorescence of xyloglucanase by OPTA*

Inactivation of xyloglucanase by OPTA resulted in the formation of an isoindole derivative, which is characterized by excitation and emission maxima at 338 nm and 415 nm respectively (Figure 24). OPTA is a bifunctional agent that forms fluorescent isoindole derivative by crosslinking the proximal thiol and amino groups of cysteine and lysine residues. The involvement of a lysine residue in the formation of an isoindole ring was confirmed by the inability of TNBS-modified xyloglucanase to form a xyloglucanase-isoindole derivative with OPTA. The prior modification of a lysine residue by TNBS makes lysine unavailable for further reaction with OPTA. Similar experiments were performed by modifying histidine residues in xyloglucanase by diethylpyrocarbonate. DEP-modified xyloglucanase was also unable to form an isoindole derivative with OPTA (Figure 24). However, xyloglucanase pretreated with PHMB and N-ethylmaleimide was unable to abolish the formation of the isoindole peak at 420 nm with OPTA (excitation wavelength, 338 nm). These results indicated the involvement of lysine and histidine residues in

the formation of an isoindole derivative and the involvement of these residues in the active site of xyloglucanase.

To investigate the binding of the inhibitor to the active site and changes in the native intermolecular interactions, the changes in the interaction of lysine and histidine residue due to inhibitor binding, and their influence on the isoindole fluorescence of xyloglucanase was monitored (Figure 24). The unbound enzyme did not show fluorescence when excited at 338 nm, however on incubation with OPTA resulted in an increase in the fluorescence with a  $\lambda_{\max}$  at 420 nm due to the formation of the isoindole derivative. The inhibitor-preincubated xyloglucanase failed to react with OPTA as revealed by the total loss of isoindole fluorescence, which not only confirmed the binding of the inhibitor to the active site of xyloglucanase but also further revealed that the binding of inhibitor resulted in the formation of a new set of hydrogen bonding and other non-ionic interactions. These altered weak interactions cause disruption of the native hydrogen bonding network of the histidine and lysine residues, which are essential for the formation of isoindole derivative.



**Figure 24** Effects of inhibitor binding on the OPTA fluorescence of xyloglucanase. Xyloglucanase (5 nM) was treated without or with the inhibitor (100 nM) at 25°C for 20 min and then further incubated with a fresh solution of OPTA (25  $\mu$ M). The isoindole fluorescence of the xyloglucanase-bound OPTA was measured with excitation at 338 nm. The lines represent the isoindole fluorescence of xyloglucanase ( $\blacktriangle$ ), xyloglucanases + OPTA ( $\blacksquare$ ), and xyloglucanase (pre-incubated with inhibitor) + OPTA ( $\blacktriangledown$ ), xyloglucanase (modified with DEP) + OPTA ( $\bullet$ ) and xyloglucanase (modified with TNBS) + OPTA ( $\blacktriangleleft$ ) and are the average of six scans with corrections from buffer and respective controls.

## DISCUSSION

Glycosidase inhibitors have been extensively studied concerning their synthesis and evaluation of biological properties. Although a plethora of synthetic inhibitors have been reported, there is lacuna of peptidic inhibitors of glycosidases from microbial origin. Fungal aspartic protease and xyloglucanase catalyze hydrolytic cleavage of two different substrates made of peptide bond and glycosidic bond, respectively. Fungal aspartic protease, didnot show any activity on xyloglucan, a sugar polymer made of glycosidic bond and xyloglucanase did not show any activity against protein substrates, such as hemoglobin and casein, made of peptide bond, indicating that these enzymes are absolutely specific toward their natural substrates. We present here the first report of a low molecular weight peptidic inhibitor from *Penicillium* sp VM24 exhibiting slow tight binding inhibition against xyloglucanase. The bifunctionality of the inhibitor was revealed as it was found to inhibit fungal aspartic protease. The inhibitor showed exceptionally high potency against thermostable xyloglucanase from *Thermomonospora* sp., and its 1:1 molar ratio of interaction with the enzyme indicated its “tight binding” nature. The two-step inhibition mechanism was corroborated by the equilibrium binding studies of the enzyme and inhibitor and the correlation of the kinetic data with the conformational changes induced in the enzyme-inhibitor complexes.

The pure noncompetitive nature of the inhibitor may be addressed due to the equal binding affinity of the inhibitor to enzyme and enzyme-substrate. The double-reciprocal plot shows that inhibitor is affecting the  $V_{max}$  but not the  $K_m$ . Therefore the inhibition constant values obtained from the double-reciprocal plot and Dixon plot were the result of correct models. The values of  $K_i$  and  $K_i^*$  estimated according to Eq. (1c) were found to be nearby same which further supported the data in favor of pure noncompetitive inhibition. Thus, the enzyme and enzyme-substrate complex binding I with equal affinity, then  $\alpha = \alpha'$  and hence  $K_i = K_i' = k_4/k_3 = k_9/k_8$ . The reciprocal noncompetitive equation by Dixon also define the noncompetitive inhibition in the conditions when  $\alpha = \alpha'$  (Dixon 1953; Cha 1975). The plot of  $1/(k-k_6)$  as a function of [S] also can be accessed the mode of inhibition where a straight

line with a positive slope obtained (Morrison and Walsh 1988). If the inhibition is mixed,  $1/(k-k_0)$  bear a hyperbolic relation to  $[S]$  and become independent of  $[S]$  for pure noncompetitive inhibition. The results showed that the slope was independent of  $[S]$ . Some enzymatic reactions display a slow onset of inhibition in the presence of inhibitors, such type of inhibition is called slow-binding inhibition, and the inhibitors are called slow-binding inhibitors. Kinetically, the slow tight binding inhibition mechanism can be illustrated by three mechanisms (Scheme 1A). When an inhibitor has a low  $K_i$  value and the concentration of I varies in the region of  $K_i$ , both  $k_3I$  and  $k_4$  values would be low. Thus, a simple second order interaction between E and I, and low rates of association and dissociation would lead to slow-binding inhibition (Scheme 1A,a). The Scheme 1A,a also suggests that I bind to ES complex to form ESI complex which dissociate to give EI and S. The dissociation constant  $K_i'$  for ESI to EI and S is equal to  $K_i$  when E and ES complex have equal binding affinity with I. Alternatively, a two-step model depicts the rapid formation of an initial collisional complex EI, which slowly isomerizes to form a tightly bound slow dissociating complex EI\* (Scheme 1A,b). Slow-binding inhibition can also arise because of an initial slow inter-conversion of the enzyme E, into another form E\*, which binds to the inhibitor by a fast step (Scheme 1A,c). Kinetically, these mechanisms can be differentiated by investigating the behavior of the enzyme-inhibitor system at varying concentrations of the inhibitor. Scheme 1A,a would predict that in the presence of substrate, the initial rate of substrate hydrolysis will be independent of inhibitor concentrations because the concentration of EI would be significantly low. However, in Scheme 1A,b (slow tight binding inhibition), the inhibitor will inhibit the enzyme competitively or noncompetitively at the onset of the reaction, and at increasing concentrations of inhibitor, the initial rate of substrate hydrolysis will decrease hyperbolically as a function of time. In tight binding inhibition, corrections have to be made for the reduction in the inhibitor concentration that occurs on formation of the EI complex, because the concentration of EI is not negligible in comparison to the inhibitor concentration and the free inhibitor concentration is not equal to the added concentration of the

inhibitor. An understanding of the basis of the isomerization of the EI complex to EI\* complex could lead to the design of structures that allow titration of the lifetime of an EI\* complex. The future development of tight binding inhibitors will undoubtedly depend on application of kinetic techniques that yield quantitative information about the behavior of the inhibitors.

The kinetic analysis of xyloglucanase inhibition provides a unique opportunity for the quantitative determination of these rates and affinities, which can be extended to other slow tight binding inhibition systems. Scheme 1A also describes two alternative models for the time-dependent inhibition. The mechanism of binding of the inhibitor to the enzyme according to Scheme 1A,a is slow, tight and occurs in a single step. This mechanism can be eliminated based on the data from Table 5, because the inhibitor has a measurable effect on the initial rates before the onset of slow tight binding inhibition of xyloglucanase. Scheme 1A,c represents the inhibition model where the inhibitor binds only to the free enzyme that has slowly adopted the transition state configuration that can also be eliminated by the observed rates of onset of inhibition. As in most ground state inhibitors, formation of the EI complex between enzyme and inhibitor was too rapid to be measured at steady-state kinetics and was likely to be near diffusion control. However, the isomerization of EI to the second tightly bound enzyme inhibitor complex, EI\*, was too slow and relatively independent of the stability of the EI. The  $k_6$  values revealed very slow dissociation of the EI\* complex indicating a highly stable, non-dissociative nature of the second complex. Therefore, for slow tight binding inhibition the major variable is  $k_6$ , the first-order rate constant associated with the conversion of EI\* to EI, and the apparent inhibitor constant  $K_i^*$  depends on the ability of the inhibitor to stabilize the EI\*. The half-life as derived from the  $k_6$  value indicated a long half life of the EI\*, which is an essential parameter for an inhibitor to have biotechnological applications. The results for the inactivation of xyloglucanase are consistent with the slow tight binding mechanism as described in Scheme 1A,b. However, the time-dependent non-dissociative nature of the EI\* complex and the formation of an irreversible denatured enzyme state  $E^{**} + I$  revealed the mechanism of inhibition. As

a function of time; it acts like an irreversible suicidal type inhibitor (Scheme 1B) essentially because of the conformational modes attended by the enzyme–inhibitor complex. These conformational changes are mainly induced because of extended secondary interactions between the inhibitor and xyloglucanase. Scheme 1B describes the kinetics and conformational modes of the proposed mechanism of inhibition of xyloglucanase by the inhibitor, where the rate constant  $k_{con}$  is associated with the irreversible denatured conformational change in the EI\*.

The characteristic feature of slow binding inhibition is the induction of conformational changes in the enzyme-inhibitor complex, resulting in the clamping down of the enzyme to the inhibitor, thus, the formation of a stable enzyme-inhibitor complex. The two-step inhibition mechanism of xyloglucanase by the inhibitor was reflected in the quenching pattern of the fluorescence of the enzyme-inhibitor complexes. The rate constants derived from the fluorescence analysis of the complexes corroborated the values derived from the kinetic analysis. Therefore, the initial rapid fluorescence loss reflected the formation of the reversible complex EI, whereas the subsequent slower decrease was correlated to the accumulation of the tightly bound complex EI\*. Any major alteration in the three-dimensional structure of xyloglucanase due to the binding of the inhibitor can be ruled out, since there was no shift in the tryptophanyl fluorescence of the complexes. However, because the inhibitor has no absorption in the region of 290–450 nm, the fluorescence quenching due to the energy transfer between the inhibitor and the tryptophan residues of xyloglucanase has been neglected. From the physical explanation for the quenching process it was apparent that the inhibitor induced fluorescence quenching followed by the formation of both the complexes. The agreement of the rate constants concomitant with the fluorescence changes observed during the time-dependent inhibition led us to correlate the localized conformational changes in the enzyme-inhibitor complex to the isomerization of the EI to EI\*. The shift in the emission maxima as a function of time in the EI\* indicated induction of gross conformational changes in the complex because of the secondary interactions within protein and the inhibitor. These interactions are strong enough to form an irreversible complex of

the enzyme–inhibitor from which the inhibitor failed to dissociate. This is the first report of a peptidic slow tight binding inhibitor behaving as an irreversible suicidal type inhibitor of xyloglucanase as a function of time.

Conformational integrity of the active site of an enzyme is essential for its catalysis, and investigations on the molecular orientation of the functional groups of the active site as well as their microenvironment are areas of growing scientific interest. Chemo-affinity labeling is a powerful technique to assign the binding sites of ligand-macromolecule complexes, which combines some of the advantages of both the photoactivated and electrophilic affinity labeling (Simson and Johnson 1978). Catalytic site of xyloglucanase consists of two carboxyl groups and an essential lytic water molecule and follows a general acid-base catalytic mechanism (Rao et al., 1998). OPTA is a bifunctional, fluorescent chemoaffinity label, which is known to have absolute specificity for amino and thiol groups for the formation of an isoindole derivative (Palczewski et al., 1983). Fluorescence chemo-affinity labeling with OPTA and chemical modification studies using group specific reagents revealed the involvement of histidine and lysine residues in the formation of isoindole derivative and presence of these residues in the active site of xyloglucanase. OPTA contains two aldehyde groups, one of which reacts with the primary amine of lysine while the second group reacts with the secondary amine of the imidazole ring of histidine, resulting in the formation of the isoindole derivative (George and Rao 2001). The foregoing results revealed that, when xyloglucanase was preincubated with the inhibitor, OPTA failed to form the isoindole derivative, as reflected by the loss of fluorescence. The inability of OPTA to form the isoindole derivative with the enzyme-inhibitor complex could be attributed to the interaction of the inhibitor with the histidine and lysine residues, thereby changing the native molecular interactions of these residues. The amino acid composition of the inhibitor showed the presence of Asp, Glu and Lys residues with charges side chain (Chapter 3). We propose that the carboxyl group of the Asp residues of the inhibitor can form hydrogen bonding with the amines of His and Lys residues of xyloglucanase, thereby preventing the binding of OPTA. This, however, does not exclude the

possible role of steric hindrance exerted by the bound inhibitor in preventing the binding of OPTA to the active site. The existing experimental evidence suggested that the charged side chains of the amino acids, the amide nitrogens, and the carbonyl oxygen groups of the inhibitor could form many intermolecular hydrogen bonds and other weak interactions (van der Waals, ionic, etc.) with the residues present in or near the active site of xyloglucanase. The tight binding and non-competitive nature of the inhibitor in conjunction with the multiple nonbonded interactions may be sufficient to interfere in the native weak interactions between the carboxyl groups, the lytic water molecule, and the essential histidine residue of the active site, leading toward the inactivation of xyloglucanase. However, the crystal structure of the enzyme-inhibitor complex will aid in understanding the mechanism of inactivation of xyloglucanase in depth and will further shed light on the molecular interactions between the enzyme and inhibitor.

The formation of a tight complex between the enzyme and inhibitor can be attributed to the secondary interactions between the inhibitor and xyloglucanase as analyzed by the CD-spectra analysis. CD-spectra analysis has revealed the presence of  $\beta$ -sheet structures in the inhibitor (Chapter 3).  $\beta$ -sheet structures are known to play a critical role during secondary contacts between the other reported inhibitors and enzymes. These secondary  $\beta$ -sheet interactions along with the network of hydrogen bonding, non-ionic and other weak interactions between the proximal active site and reactive site residues probably are sufficient for  $EI^*$  complex leading toward the formation of the irreversible  $E^{**}+I$  complex. Interpretation for the changes observed in the secondary structure of xyloglucanase due to the binding of the substrate to the active site can be correlated to the similar pattern of changes observed due to the binding of the peptidic inhibitor. Fluorescence and CD studies revealed that the peptidic inhibitor binds to the active site of xyloglucanase and causes inactivation.

The kinetic analysis demonstrated that the inhibition of xyloglucanase by the inhibitor followed slow-tight binding mechanism. Chemo-affinity labeling of the



enzyme active site has demonstrated that the inactivation of xyloglucanase was due to the interference in the electronic microenvironment and disruption of the hydrogen bonding network between the essential histidine and lysine involved in catalysis. Being a bifunctional inhibitor of xyloglucanase and aspartic protease, the inhibitor may have significant potential as a biocontrol agent against phytopathogenic fungi. The bifunctional inhibitors may have application as 'two-in-one' affinity ligands for the purification of aspartic proteases and xyloglucanases.

**BIBLIOGRAPHY**

Andrade MA, Chacon P, Merelo JJ, Moran F (1993) *Protein. Eng.* **6**, 383-390.

Asano N (2003) *Glycobiology.* **13**, 93-104.

Basten DEJW, Visser J, Schaap PJ (2001) *Microbiology,* **147**, 2045-2050.

Beith JG (1995) *Methods Enzymol.* **248**, 59-84.

Berka RM, Carmona CL, Hayenga KJ, Thompson SA, Ward M (1993) *Gene* **125**, 195-198.

Berka RM, Ward M, Wilson LJ, Hayenga KJ, Kodama KH, Carlomango LP, Thompson SA (1990) *Gene* **86**, 153-162.

Cha S, Agarwal RR, Parks RE (1975) *Biochem. Pharmacol.* **24**, 2187-2197.

Cleland WW (1963) *Biochim. Biophys. Acta.* **67**, 173-187.

Cole, GT, Zhu SW, Hsu LL, Kruse D, Seshan KR, Wang F (1992) *Infect. Immun.* **60**, 416-427.

Dal Degan F, Ribadeau-Dumas B, Breddam K (1992) *Appl. Environ. Microbiol.* **58**, 2144-2152.

Dara OD, Wang L, Xu J, Darin R, Gu T, Murray MY (2001) *Biochem. Eng. J.* **8**, 187-193.

Dash C, Phadtare S, Desphande VV, Rao M (2001) *Biochemistry* **40**, 11525-11532.

Denning DW, Stevens DA (1990) *Rev. Infect. Dis.* **12**, 1147-1201.

Dixon M (1953) *Biochem. J.* **55**, 170-171.

Ellan GL (1959) *Arch. Biochem. Biophys.* **82**, 70-77.

George SP, Ahmad A, Rao M (2001a) *Bioresour Technol* **77**, 171-175.

George SP, Ahmad A, Rao M (2001b) *Biochem. Bioph. Res. Co.* **282**, 48-54.

George SP, Rao M (2001) *Eur. J. Biochem.* **268**, 2881-2888.

Gloster TM, Ibatullin FM, Macauley K, Eklo JM, et al. (2007) *J. Biol. Chem.* **282**, 19177-19189.

Hogan LH, Klein BS, Levitz SM (1996) *Clin. Microbiol. Rev.* **9**, 469-488.

Inoue H, Hayashi T, Huang XP, Lu J, Athanda SBP, Kong K, Yamagata H, Ukada S, Takahashi K (1996) *Eur. J. Biochem.* **237**, 719-725.

Inoue H, Lu JF, Athauda SBP, Kong KH, Hayashi T, Kimura T, Makabe O, Takahashi K (1995). *Adv. Exp. Med. Biol.* **362**, 581-587.

Kothary, MH, Chase Jr T, Macmillan JD (1984) *Infect. Immun.* **43**, 320-325.

Kulkarni A (2007) PhD Thesis, University of Pune.

Kulkarni A, Rao M (2007) *Biochim. Biophys. Acta.* **1774**, 619-627.

Laemmli UK (1970) *Nature* **227**, 680-685

Lee JD, Kolattukudy PE (1995) *Infect. Immun.* **63**, 3796-3803.

Legler G (1990) *Adv. Carbohydrate. Chem. Biochem.* **48**, 319-385.

Mandels M, Weber J (1969) *Adv. Chem.* **95**, 391-414.

Master ER, Zheng Y, Storms R, Tsang A, Powlowski J (2008) *Biochem J.* **411**, 161-170

Mattern IE, van Noort JM, van den Berg P, Archer DB, Roberts IN, van der Hondel CA (1992) *Mol. Gen. Genet.* **234**, 332-336.

Merele JJ, Andrade MA, Prieto A, Moran F (1994) *Neurocomputing.* **6**, 443-454.

Miles EW (1977) *Methods. Enzymol.* **47**, 431-442.

Monod M, Capoccia S, Lechenne B, Zaugg C, Holdom M, Jousson O (2002) *Int. J. Med. Microbiol.* **292**, 405-419.

- Moralejo FJ, Cardoza RE, Gutierrez S, Lombraña M, Fierro F, Martin JF (2002) *Appl Environ Microbiol.* **68**, 3550-3559.
- Morrison JF, Stone SR (1985) *Comments. Mol. Cell. Biophys.* **2**, 347-368.
- Morrison JF, Walsh CT (1988) *Adv. Enzymol. Relat. Areas. Mol. Biol.* **61**, 201-302.
- Palczewski K, Hargrave PA, Kochman M (1983) *Eur. J. Biochem.* **137**, 429-435.
- Pol D, Menon V, Rao M (2012) *Extremophiles* **16**,135-146.
- Rao MB, Tanksale AM, Ghatge MS, Deshpande VV (1998) *Microbiol Mol Biol Rev* **62**, 597-635.
- Reich JG (1992) *Curve Fitting and Modelling for Scientists and Engineers*, McGraw-Hill, New York.
- Reichard U, Cole GT, Rachel R, Monod M (2000) *Int. J. Med. Microbiol.* **290**, 85-96.
- Reichard U, Monod M, Ruechel R (1995) *FEMS. Microbiol. Lett.* **130**, 69-674.
- Rhodes JC, Bode RR, McCuan-Kirsch CM (1988) *Diagn. Microbiol. Infect. Dis.* **10**, 165-170.
- Robert S, James RF (1984) *Biochemistry* **23**, 5225-5233.
- Rossi LL, Basu A (2005) *Bioorgan.Med. Chem.* **15**, 3596-3599.
- Segal BH, Walsh TJ (2006) *Am. J. Resp. Crit. Care.* **173**, 707-717.
- Simons Jr SS, Johnson DF (1978) *Anal. Biochem.* **90**, 705-725.
- Sørensen JF, Kragh KM, Sibbesen O, Delcour J, et al. (2004) *Biochim Biophys Acta.* **1696**, 275-287.
- Stutz AE (1999) *Immunosugars as glycosidase inhibitors: Nojirimycin and beyond*, Wiley-VCH, Weinheim.
- Szedlacsek SE, Duggleby RE, Vlad MO (1991) *Biochem. J.* **279**, 855-861.

Takahashi K, Inoue H, Sakai K, Kohama T, Kitahara S, Takashima K, Tanji M, Athauda SBP, Takahashi T, Akanuma H, Mamiya G, Yamasaki M (1991) *J Biol Chem.* **266**, 19480-19483.

Tarvainen K, Keskinen H (1991) *Clin. Exp. Allergy* **21**, 609-615.

Tello-Solis SR, Hernandez-Arana A (1995) *Biochem. J.* **311**, 969-974.

Tsujita Y, Endo A (1978) *Eur. J. Biochem.* **15**, 347-353.

Van den Hombergh JP, Van de Vondervoort PJI, Fraissinet-Tachet L, Visser J (1997) *Trends Biotechnol.* **15**, 256-263.

Von Heijne G (1986) *Nucleic Acids Res.* **14**, 4683-4690.

Williams JW, Morrison JF (1979) *Methods Enzymol.* **63**, 437-467.

Withers SG, Aebersold R (1995) *Protein. Sci.* **4**, 361-372.

Wong DDWS, Chan VJ, McCormack AA, Batt SB (2010) *Appl. Microbiol. Biotechnol.* **86**, 1463-1471.

Yike I (2011) *Mycopathologia* **171**, 299-323.

Yuasa H, Izumi M, Hashimoto H (2009) *Curr Top Med Chem.* **9**, 76-86.

# CHAPTER 7

*‘Most enzymes start off with a promiscuous function.  
These promiscuous enzymes can do many different  
things’*

**Yasuo Yoshikuni**

**Functional aspects of hydrolases**

## SUMMARY

Glycosyl hydrolases are a widespread group of enzymes that hydrolyse the glycosidic bond between two or more carbohydrates, or between a carbohydrate and a non-carbohydrate moiety. They are increasingly being utilized for the bioconversion of lignocellulose for potential application in biofuel sector. Lignocellulose consists of cellulose, hemicellulose and lignin. The effective utilization of hemicellulose would play a significant role in the economic viability of second generation biofuel. The present chapter reports the hydrolysis and ethanol production from tamarind kernel powder, a rich source of galactoxyloglucan using xyloglucanase and thermotolerant *Debaromyces hansenii*. The acid hydrolysis of tamarind kernel powder with 2 N H<sub>2</sub>SO<sub>4</sub> yielded an overall saccharification of 94% based on the total available carbohydrate content and further fermentation at 40°C with thermotolerant *D hansenii* produced an ethanol yield of 0.35 g/g. A maximum hydrolysis of 55% and 78% for galactoxyloglucan was obtained in 48 h at 50°C using *Thermomonospora* xyloglucanase and a commercial enzyme, Accellerase™1000 respectively. The synergistic effect of β-galactosidase and xyloglucanase was demonstrated by the exogenous addition of β-galactosidase to *Thermomonospora* xyloglucanase which improved the overall hydrolysis of galactoxyloglucan by 30%. The rate of hydrolysis of galactoxyloglucan with xyloglucanase and accellerase was increased by 15-20% in the presence of chemical surfactants (tween 80 and toluene) or protein additive (BSA). The fermentation of enzymatic hydrolysates of galactoxyloglucan by xyloglucanase or accellerase with *D hansenii* at 40°C produced an ethanol yield of 0.39 g/g and 0.41 g/g respectively. The enzymatic hydrolysates of galactoxyloglucan by xyloglucanase or accellerase when fermented with Ca-alginate immobilized *D. hansenii* produced an ethanol yield of 0.45 g/g and 0.43 g/g respectively with theoretical conversion efficiencies of 78% - 88%. The immobilized yeast cells were reused six cycles at 40°C with 100% fermentation efficiency.



## INTRODUCTION

Glycosidases, the enzymes responsible in nature for the catabolism of carbohydrates are well-studied catalysts with varied industrial and biotechnological applications. Glycosidases play a significant role in anti-bacterial defense strategies (e.g., lysozyme), in pathogenesis mechanisms (e.g., viral neuraminidases), in normal cellular function (e.g., trimming mannosidases involved in N-linked glycoprotein biosynthesis) and in degradation of biomass such as cellulose and hemicellulose (Henrissat and Davies 2000; Minic 2008). Lignocellulose is a major structural component of woody and non-woody plants and consists of cellulose, hemicellulose and lignin. Various agricultural residues contain about 20-30% hemicellulose, the second most abundant biopolymer found in nature. They are heterogeneous polymer of pentoses (xylose and arabinose), hexoses (mannose, glucose and galactose) and sugar acids (Kulkarni et al., 1999). In recent years, bioconversion of hemicellulose has received much attention because of its practical applications in various agro-industrial processes, for the production of fuels and chemicals, delignification of paper pulp, digestibility enhancement of animal feedstock, clarification of juices, and improvement in the consistency of beer (Saha 2003). Xyloglucan (XG), a predominant hemicellulose found in the primary cell wall of dicots and several monocots, consists of a  $\beta$ -(1 $\rightarrow$ 4) - linked  $\beta$ -D-Glcp ( $\beta$ -D-glucopyranose) backbone having up to 75% of the  $\beta$ -D-Glcp residues covalently linked to  $\alpha$ -D-Xylp ( $\alpha$ -D-xylopyranose) at the O-6 position. While the extent of xylose substitution varies considerably, the glucose backbone structure is typically substituted by 50% or 75% xylose (Powlowski et al., 2009). Xylose can be further substituted by galactose or arabinose and the galactose may be fucosylated. In addition, xyloglucans can contain O-linked acetyl groups (Maruyama et al., 1996; Sims et al., 1996). The glucose, xylose and galactose residues are present in the ratio of 2.8: 2.25:1.0. XG is also a storage polymer in the seed endosperm of many plants. Xyloglucans interact with cellulose microfibrils by the formation of hydrogen bonds, thus contributing to the structural integrity of the cellulose network (Carpita and Gibeaut 1993; De Vries and Visser 2001). Tamarind kernel powder (TKP) an

opulent source of hemicellulose galactoxyloglucan (GXG), is a crude extract derived from the seeds of *Tamarindus indica* Linn., an abundantly grown tree of Southeast Asia, India, Mexico, and Costa Rica (Goyal et al., 2007).

Without a profitable use of the hemicellulose fraction, bioethanol is too expensive to compete in commercial markets (Wyman 1999). Therefore to foster the commercial production of lignocellulosic ethanol, bioconversion of the hemicelluloses into fermentable sugars is essential. The hydrolysis of XG is catalyzed by specific xyloglucanases or xyloglucan specific endoglucanases which represents a new class of polysaccharide degrading enzymes which can attack the backbone at substituted glucose residues. The action of xyloglucanases enhances the hydrolysis of lignocellulose by making the cellulose more accessible to cellulase enzymes and also improves the economics of biomass conversion. The complete hydrolysis of galactoxyloglucan requires an accessory enzyme,  $\beta$ -galactosidase which cleaves the galactose residue attached to the branched xylose moiety in the  $\beta$ -D-glucopyranose backbone (Benko et al., 2008). The present chapter describes for the first time the possibility of galactoxyloglucan (GXG) predominant hemicellulose from TKP as a source of fermentable sugars for the production of ethanol using xyloglucanase from an alkalothermophilic *Thermomonospora* sp and a thermotolerant *Debaromyces hansenii*. Comparative studies with a commercial enzyme Accellerase<sup>TM</sup> 1000 from *Trichoderma reesei* and further fermentation to ethanol were pursued. The effect of chemical surfactants and protein additives on the hydrolysis of GXG was also studied. The potency of the enzymes in hydrolysis and the thermotolerant yeast in fermentation were evaluated in separate hydrolysis and fermentation (SHF) models.

## EXPERIMENTAL PROCEDURES

### *Materials*

Tamarind Kernel Powder (TKP) was a kind gift from Herbex International Ltd, Mumbai, India. Accellerase™ 1000 was a kind gift from Danisco US Inc. Genencor Division, USA. 3, 5-dinitrosalysilic acid (DNS) and  $\beta$ -galactosidase from *Escherichia coli* were obtained from Sigma-Aldrich Co. St Louis, MO USA. Ethanol was purchased from Les Alcools De Commerce Inc, Brampton, Ontario. All other chemicals were of analytical grade.

### *Hemicellulose hydrolysate preparation*

#### *a. Acid hydrolysis*

Tamarind kernel powder (TKP) was used as the raw material. Particles in the size range from 50 -100 mesh were used in experiments. The biomass at a solid loading of 10% (w/v) was mixed with varying concentration of sulphuric acid (1 – 5 N) at different temperatures (50, 100 and 120°C) and residence time (15, 30, 45 and 60 min). The liquid fraction was neutralized with NaOH and centrifuged to remove the solid residues. The acid hydrolysate was overlimed at room temperature by adding dried lime till the pH reached 10.0 with constant stirring for 30 min. After overliming, the hydrolysate was neutralized with concentrated H<sub>2</sub>SO<sub>4</sub> and centrifuged at 10,000 g for 20 min to remove the precipitate. The overlimed hydrolysate was further detoxified by treating with activated charcoal (1% w/v) with constant stirring at room temperature for 20 min and the sugar concentrate was recovered by filtration.

#### *b. Isolation of galactoxyloglucan (GXG) from TKP*

The slurry was prepared by mixing 10 g of TKP with 100 ml of ice-cold distilled water. The slurry was poured to 400 ml of boiling distilled water and is boiled for 20 min at constant stirring. The solution is left overnight at room temperature and is centrifuged at 10,000 g for 20 min to separate the supernatant. The supernatant solution is added to absolute alcohol with constant stirring at room temperature.

The white precipitate formed is centrifuged to obtain pellets (Rao et al., 1946). The galactoxyloglucan (GXG) pellets is washed with ethanol and dried under vacuum. The pellet is suspended at 10 g of xyloglucan /L in 50 mM phosphate buffer, pH 6.8 / 50 mM acetate buffer, pH 4.8.

### *Microorganisms and cultivation conditions*

Alkalothermophilic *Thermomonospora* sp. was maintained on Luria Bertani wheat bran slants at pH 10.0 and 50°C as mentioned in chapter 6.

### *Debaromyces hansenii*

*D. hansenii* (Prakash et al., 2011) was grown in a medium containing (g/L): xylose, 40.0; malt extract, 3.0; yeast extract, 3.0; peptone, 5.0; agar, 20.0; at pH  $6.0 \pm 0.2$  on a rotary shaker at 180 rpm for 48 h at 40°C. After 48h the inoculum was centrifuged at 10,000 rpm for 20 min and the supernatant was discarded. The cells were washed twice with sterile 0.9% NaCl solution and centrifuged again. The supernatant was removed and the cells were weighed and used for fermentation studies.

### *Enzyme assays*

#### *a. Xyloglucanase assay*

Xyloglucanase activity was determined as mentioned in chapter 6.

#### *b. $\beta$ -galactosidase assay*

$\beta$ -galactosidase was measured according to the standard procedure recommended by Commission on Biotechnology, IUPAC (Ghose and Bisaria., 1987). One unit of enzyme activity is defined as the amount of enzyme required to liberate 1  $\mu$ mol of p-nitrophenol per min from PNP-Gal under the assay conditions.

### *Enzymes*

Xyloglucanase was obtained from the extracellular culture broth of *Thermomonospora* sp as described in chapter 6. The supernatant was concentrated using ammonium sulphate (0-90%) and was the source of enzyme. The preparation contained 140 U/ml and 0.5 U/ml of xyloglucanase and  $\beta$ -galactosidase respectively.

The commercial enzyme Accellerase™ 1000 was a kind gift from Dr Raj Lad and Dr Surendra Bade, Danisco US Inc. Genencor Division, USA. The enzyme showed 3200 U/ml of xyloglucanase and 3.57 U/ml of  $\beta$ -galactosidase.

#### *Immobilization of Debaryomyces in Ca-alginate beads*

*D. hansenii* cells were harvested after 48 h of growth at 40°C by centrifugation at 10,000 rpm for 20 min, washed and 1 g (wet cell weight) was added to 10 ml of 2%(w/v) sodium alginate as described by Keirstan and Bucke (1977). The suspension was then extruded dropwise through a 5 ml syringe into a gently stirred cold solution of CaCl<sub>2</sub> and hardened at 4°C for 1 h in this solution. Particle integrity and absence of microbial contamination were ensured by means of optical microscopy. The beads (mean diameter of 2 mm) were washed with distilled water and used for fermentation.

#### *Hydrolysis of GXG*

The hydrolysis of GXG was carried out at two substrate concentrations (10 g/L and 25 g/L) with varying concentrations of *Thermomonospora* xyloglucanase and commercial enzyme Accellerase™1000 at 50°C. The hydrolysis of GXG with varying concentrations of *Thermomonospora* xyloglucanase was also carried out at 40, 60 and 70°C. The hydrolysis was carried out in a stoppered flask in 25 ml reaction volume containing appropriate concentrations of substrates in 50 mM phosphate buffer, pH 7.0 for *Thermomonospora* xyloglucanase and 50 mM acetate buffer, pH 4.8 for accellerase under static condition. Hydrolysis was terminated by boiling at 100°C for 5 min at the end of stipulated time intervals, filtered and the filtrate was assayed for reducing sugar by dinitrosalicylic method (Mandel and Weber., 1969). Appropriate substrate and enzyme controls were performed.

To determine the synergistic effect of xyloglucanase and  $\beta$ -galactosidase, the hydrolysis was performed with 10 g/L of GXG using a xyloglucanase dosage of 20 U/ml from *Thermomonospora* sp and a  $\beta$ -galactosidase dosage of 1 U/ml from *Escherichia coli*.

Various surfactants (1% w/v) including nonionic surfactants (Tween 80, Triton X-100, Toluene), Polyethylene glycol, ionic surfactants {sodium dodecyl sulphate (SDS)} and protein additives {bovine serum albumin (BSA) and gelatin} were used for studying their effect in improving enzymatic saccharification of GXG.

### *Ethanol fermentation*

The ethanol production from the hydrolysates obtained after acid hydrolysis of TKP and enzymatic saccharification of GXG by free and immobilized *D. hansenii* was investigated. The acid and enzymatic hydrolysates were filtered and supplemented with nutrients (g/L); Urea; 5., MgSO<sub>4</sub>·7H<sub>2</sub>O; 5., K<sub>2</sub>HPO<sub>4</sub>; 2 and inoculated with 10% free and immobilized yeast and fermentation was carried out at 40°C at static condition. Aliquots were withdrawn, sugar and ethanol were determined.

### *Reuse of Immobilized yeast*

The hydrolysates obtained in SHF were used to investigate the ability of thermotolerant *Debaryomyces* for reprocessing. The Ca-alginate immobilized cells (10%) were added to hydrolysates supplemented with nutrients and fermentation was performed at 40°C for 48 h. After which the Ca-alginate beads were retrieved and reused repeatedly with fresh charge of hydrolysates and the ethanol formed was assayed at the end of each cycle of operation.

### *Analytical methods*

The hydrolysates were analyzed by high performance liquid chromatography (HPLC) (Waters) for the presence of carbohydrates using Waters Sugar Pack Column 6.5x300 mm. The mobile phase used was Milli Q water with 100 µM EDTA and 200 µM CaCl<sub>2</sub>. The flow rate was maintained at 0.4 ml/minute keeping the oven temperature at 70°C. The sugars were detected by Waters 2410 refractive index detector. Ethanol was estimated by gas chromatography (Master DANI) with a BP1 (fused silica bonded phase) column (30.0m x 0.32 mm) at oven temperature of 85°C and flame ionization detector (FID) at 200°C. The ethanol standards were prepared using commercial ethanol. Nitrogen with a flow rate of 0.5 ml/min was used as carrier gas.

## RESULTS AND DISCUSSION

### *Acid hydrolysis of TKP*

The hydrolysis of TKP with increasing concentrations of H<sub>2</sub>SO<sub>4</sub> at 50°C, 100°C and 120°C, showed increase in release of reducing sugar with an acid concentration upto 2 N H<sub>2</sub>SO<sub>4</sub> and thereafter it declined. The maximum sugars (582 mg/g) were released when the substrate was treated with 2 N H<sub>2</sub>SO<sub>4</sub> at 120°C for 30 min corresponding to a sugar yield of 94% based on the total available carbohydrate from TKP. The proximate composition of TKP is set out in Table 1. There was negligible difference in sugar release when the hydrolysis was carried out either for 45 min or 60 min (Table 2). The acid hydrolysate contained 45 g/L of reducing sugar.

**Table 1** Proximate composition of TKP

Constituents	Chemical composition (% dry matter)
Galactoxyloglucan	55-65
Proteins	18-20
Lipids	6-10
Minor constituents*	-

*includes fibres, minerals and sugars etc.*

**Table 2** Release of reducing sugar during the sulphuric acid hydrolysis of tamarind kernel powder at different temperature

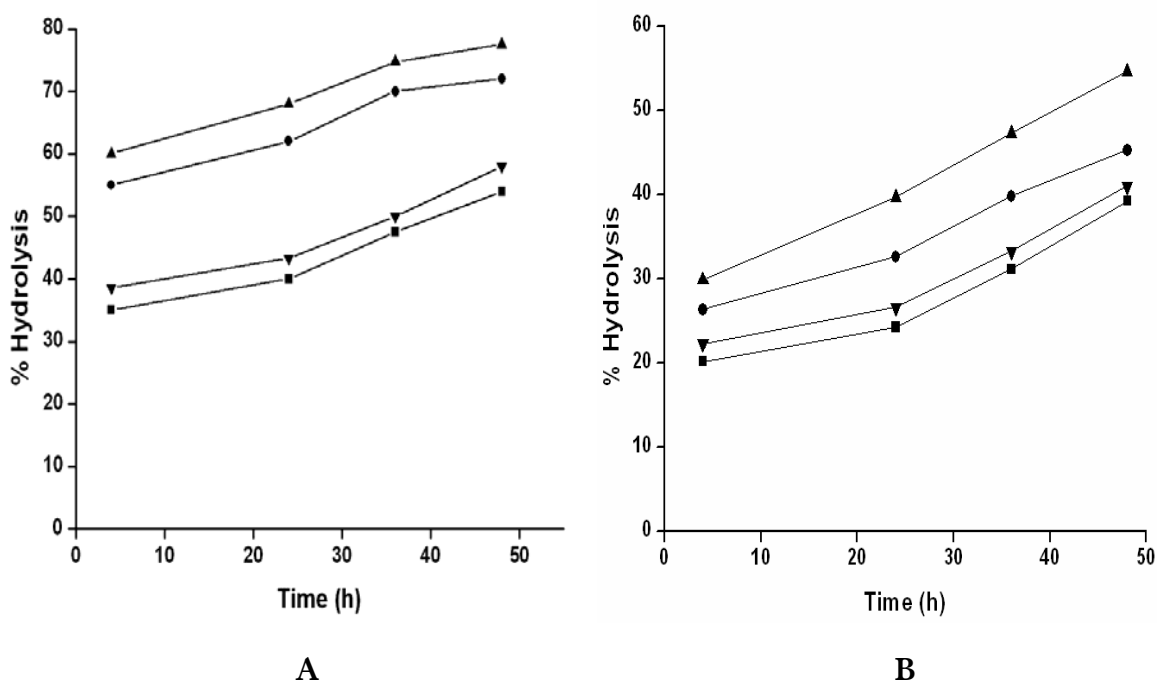
Temperature (°C)	50			100			120					
	15	30	45	60	15	30	45	60	15	30	45	60
Time (min)												
Acid Conc (N)												
	<b>Reducing sugar ( mg/g)</b>											
1	85 (13.70)*	118 (19.03)	152 (24.52)	92 (14.84)	121 (19.25)	253 (40.81)	195 (31.45)	217 (35)	161 (25.96)	389 (62.74)	248 (40)	306 (49.35)
2	107 (17.25)	142 (22.90)	127 (20.48)	82 (13.23)	252 (40.65)	268 (43.23)	413 (66.61)	303 (48.87)	142 (22.90)	582 (93.87)	326 (52.58)	491 (79.19)
3	79 (12.74)	104 (16.77)	119 (19.19)	93 (15)	110 (17.74)	190 (30.65)	130 (20.96)	168 (27.09)	303 (48.87)	288 (46.45)	207 (33.38)	245 (39.52)
4	82 (13.23)	94 (15.16)	80 (12.90)	65 (10.48)	102 (16.45)	122 (19.68)	109 (17.58)	142 (22.90)	121 (19.52)	211 (34.03)	210 (33.87)	178 (28.71)
5	78 (12.58)	89 (14.35)	74 (11.94)	58 (9.35)	96 (15.48)	101 (16.29)	91 (14.68)	94 (15.61)	103 (16.61)	142 (22.90)	157 (25.32)	121 (19.52)

*The tamarind kernel powder was hydrolyzed with different concentrations of acid at varying temperature and time intervals. \* Values in parenthesis are sugar yield with respect to total carbohydrate content of tamarind kernel powder.*



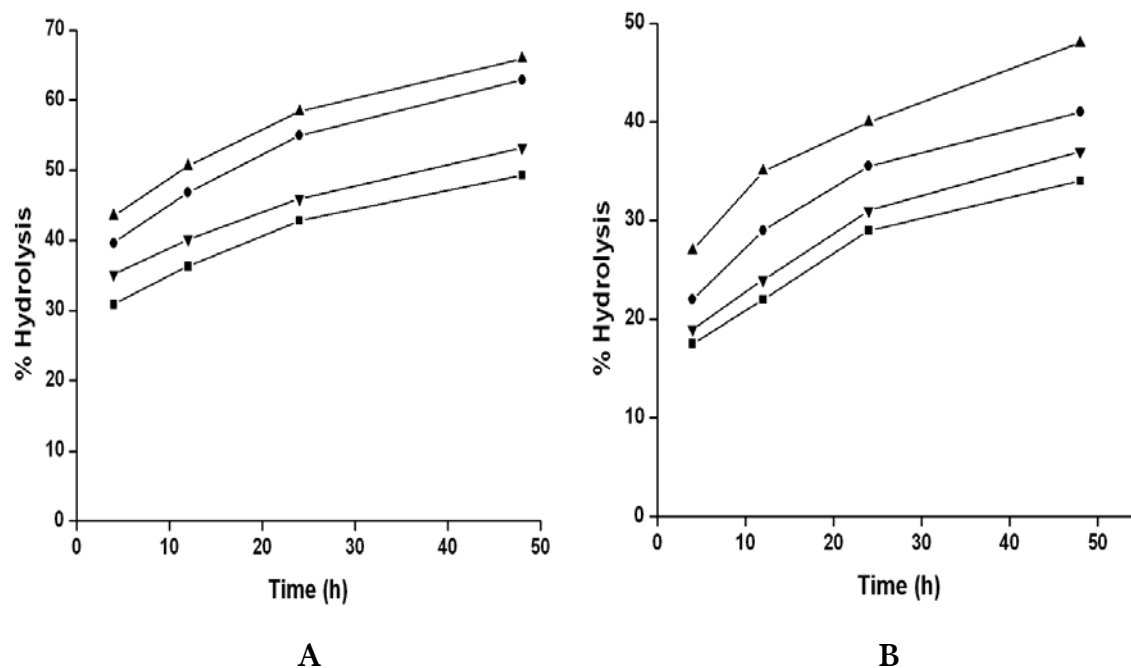
*Enzymatic hydrolysis*

Saccharifications of GXG from TKP with *Thermomomospora* xyloglucanase and accellerase with respect to varying enzyme and substrate concentrations were pursued. Increasing enzyme concentrations showed higher percentage of hydrolysis for both the enzymes (Figure 1). A maximum hydrolysis of 55% and 78% was obtained in 48 h with 10 g/L of GXG at 50°C using cognate enzyme dosage (40 U/ml) of xyloglucanase and accellerase respectively.



**Figure 1** Enzymatic hydrolysis of galactoxyloglucan at a substrate loading of 10 g/L with varying concentrations of Accellerase™1000 (A) and *Thermomomospora* xyloglucanase (B). Enzyme concentrations were 10 (■), 20 (▼), 30 (●) and 40 (▲) U/ml.

A maximum hydrolysis of 49% and 65% was obtained in 48 h with 25 g/L of GXG at 50°C using cognate enzyme dosage (40 U/ml) of xyloglucanase and accellerase respectively (Figure 2). Accellerase consistently showed increase in saccharification as compared to *Thermomomospora* xyloglucanase.



**Figure 2** Enzymatic hydrolysis of galactoxyloglucan at a substrate loading of 25 g/L with varying concentrations of accellerase™1000 (A) and *Thermomonospora xyloglucanase* (B). Enzyme concentrations were 10 (■), 20 (▼), 30 (●) and 40 (▲) U/ml.

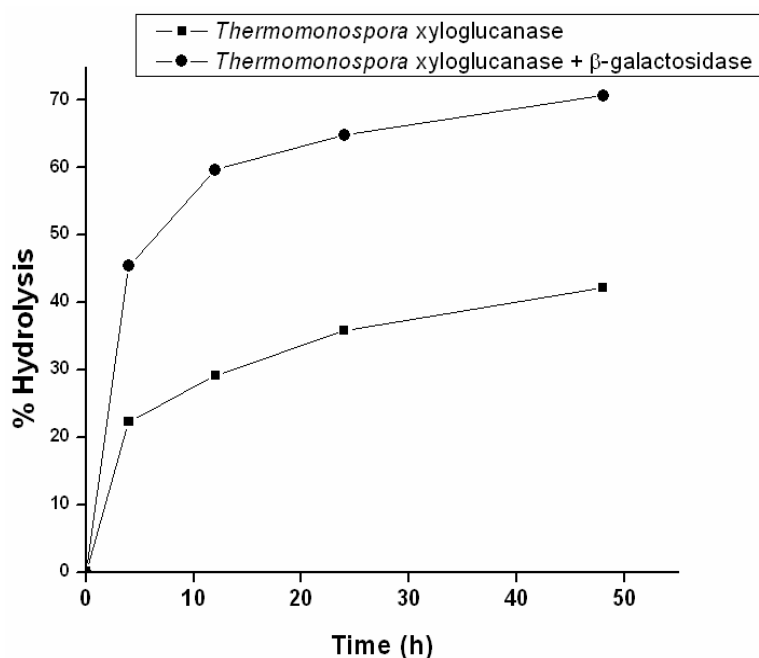
Saccharification of GXG with thermostable xyloglucanase with respect to varying enzyme and substrate concentrations at different temperatures were also pursued. A maximum hydrolysis of 57% was obtained in 6 and 12 h at 70°C and 60°C respectively using thermostable xyloglucanase with an enzyme dosage of 40 U/ml and a substrate loading of 10g/L (Table 3). At higher substrate concentration (25 g/L), a hydrolysis of 50% was obtained in 6 h at 70°C with an enzyme dosage of 20 U/ml as compared to 50°C wherein the same percentage of hydrolysis was achieved with 40 U/ml in 48h. The hydrolysis at higher temperature favors a reduction in process time and enzyme dosage. The role of thermostable xylanase in the hydrolysis of hemicellulosic substrates, favoring a reduction in process time and enzyme dosage was reported by Menon et al (2010).

**Table 3** Enzymatic hydrolysis of GXG at 10 g/L and 25 g/L substrate concentrations with *Thermomonospora xyloglucanase* at different temperatures

Temperature (°C)	40			60			70					
	10	20	25	10	20	25	10	20	25			
Substrate concentration (g/L)												
Enzyme dosage (U/ml)	20	40	40	40	20	40	40	20	40			
Time (h)	<b>Percent hydrolysis</b>											
3	10.20	12.09	8.69	10.35	28.69	34.67	25.23	30.25	38.47	42.84	29.20	35.96
6	12.50	18.69	10.66	15.92	40.59	42.81	37.25	41.69	55.21	57.41	49.85	51.33
12	19.36	26.38	15.28	23.58	55.24	57.89	48.65	50.36	55.39	57.33	50.05	52.54
24	22.64	32.25	20.67	28.34	55.50	57.25	49.25	52.67	55.58	57.68	50.58	52.12
48	28.92	40.66	24.69	33.69	55.89	57.66	49.81	52.33	55.97	57.92	50.66	52.85

The different hydrolysis patterns exhibited by similar dosage of *Thermomonospora* and accellerase xyloglucanase may be due to the varying levels of  $\beta$ -galactosidase activities. Accellerase had higher ratio of xyloglucanase to  $\beta$ -galactosidase as opposed to *Thermomonospora*. Xyloglucanase act on the backbone of GXG even at the branched glucose residues. The complete hydrolysis of galactoxyxyloglucan requires an accessory enzyme,  $\beta$ -galactosidase which cleaves the galactose residue attached to the branched xylose moiety in the  $\beta$ -D-glucopyranose backbone.

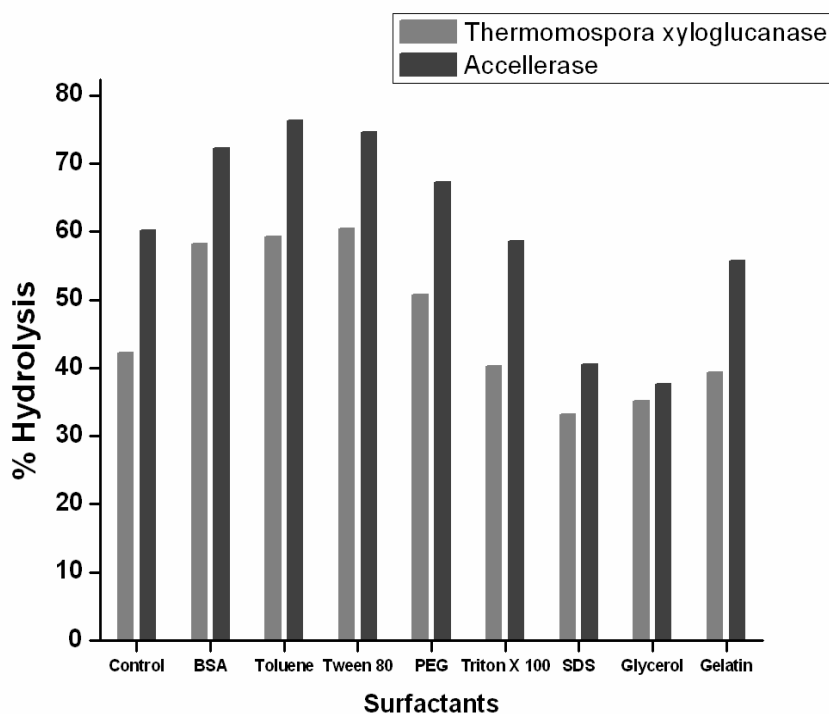
An experiment was designed to determine the synergistic effect of  $\beta$ -galactosidase and xyloglucanase which is crucial for the overall hydrolysis of GXG. This was confirmed by the exogenous addition of  $\beta$ -galactosidase to *Thermomonospora* xyloglucanase thereby increasing the hydrolysis from 42% to 71% (Figure 3). Similar synergistic effects of  $\beta$ -glucosidase and  $\beta$ -xylosidase are also reported in the overall hydrolysis of cellulose and hemicellulose. (Kotaka et al., 2008; Fujita et al., 2004; Hashimoto et al., 2003)



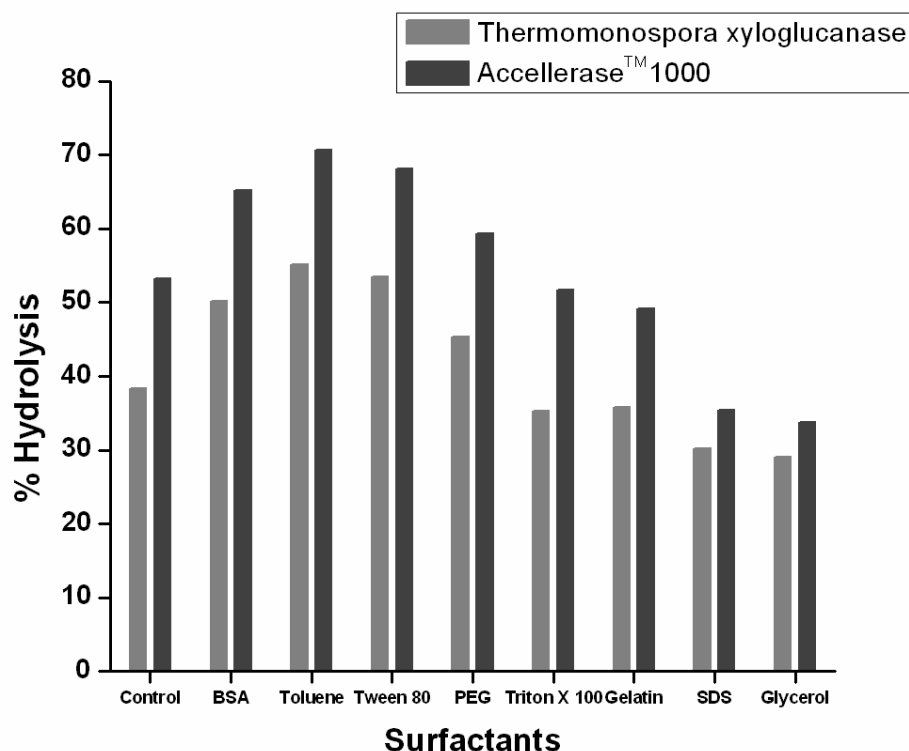
**Figure 3** Synergistic effect of *Thermomonospora* xyloglucanase and  $\beta$ -galactosidase from *E.coli* at an enzyme loading of 20 U/ml and 1 U/ml respectively in the hydrolysis of galactoxyxyloglucan at 10 g/L level.

### *Effect of surfactants on GXG hydrolysis*

Effect of various surfactants and protein additives were studied on the hydrolysis of GXG with xyloglucanase and accellerase. The rate of hydrolysis in presence of tween 80 and toluene with xyloglucanase and accellerase were increased by 15 and 18% respectively. The enzyme dosage (40 U/ml) required to achieve a maximum hydrolysis of 78% for GXG at 10 g/L level using accellerase was reduced to half in the presence of surface active additives. In case of protein additives BSA was found to be superior and increased the hydrolysis by 20% (Figure 4 & 5).



**Figure 4** Effect of surfactants and protein additives on the enzymatic hydrolysis of galactoxyloglucan at 10 g/L using *Thermomonospora xyloglucanase* and accellerase loading of 20 U/ml.



**Figure 5** Effect of surfactants and protein additives on the enzymatic hydrolysis of galactoxyloglucan at 25 g/L using *Thermomonospora xyloglucanase* and accellerase loading of 20 U/ml.

### *Fermentation of acid and enzymatic hydrolysates*

Separate hydrolysis and subsequent fermentation was carried out using free cells of *D. hansenii* at 40°C. The fermentation of hemicellulosic hydrolysates from the acid hydrolysis of TKP produced 14 g/L of ethanol with a yield of 0.31 g/g and volumetric productivity of 0.29 g/L/h. The hemicellulosic hydrolysates from the enzymatic saccharification of GXG using xyloglucanase at 25 g/L substrate loading contained 13 g/L of reducing sugars and produced 5.18 g/L of ethanol with yield of 0.39 g/g and volumetric productivity of 0.14 g/L/h wherein the hydrolysates from saccharification of GXG using accellerase contained 17 g/L of reducing sugars and produced 7 g/L of ethanol with yield of 0.41 g/g and volumetric productivity of 0.19 g/L/h. (Table 4)

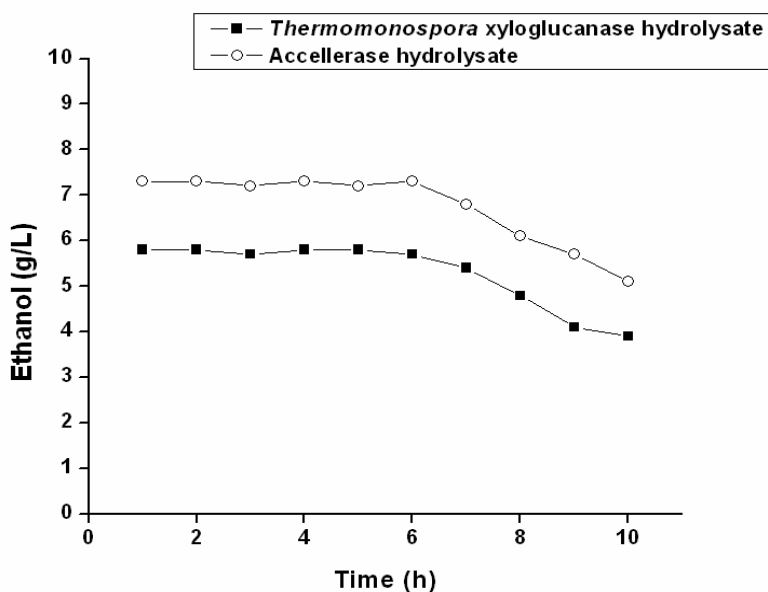
**Table 4** Ethanol production from acid and enzymatic hydrolysates by free and immobilized *Debaryomyces hansenii* in separate hydrolysis and fermentation system at 40°C

Hydrolysis	Time (h)	Sugar (g/L)	Ethanol (g/L)		Ethanol Yield (g/g)		Ethanol productivity (g/L/h)	
			Free	Immobilized	Free	Immobilized	Free	Immobilized
Acid hydrolysis	0	45	-	-	-	-	-	-
	4	39	5	7	0.11	0.16	1.25	1.75
	12	31	9	10	0.20	0.22	0.75	0.83
	24	26	12	14	0.27	0.31	0.5	0.58
	36	20	16	19	0.35	0.42	0.44	0.53
	48	15	14	17	0.31	0.38	0.29	0.35
	72	6	13	15	0.28	0.33	0.18	0.21
Enzymatic hydrolysis with <i>Thermomonospora xyloglucanase</i>	0	13	-	-	-	-	-	-
	4	11	1.24	2.43	0.09	0.19	0.31	0.61
	12	9	2.53	3.92	0.19	0.30	0.21	0.33
	24	5	3.92	5.30	0.30	0.41	0.16	0.22
	36	1	5.18	5.81	0.39	0.45	0.14	0.16
	48	0.9	4.33	5.44	0.33	0.42	0.09	0.11
	0	17	-	-	-	-	-	-
Enzymatic hydrolysis with accelerase	4	13	2.52	3.41	0.15	0.2	0.63	0.85
	12	10	3.81	4.82	0.22	0.28	0.32	0.4
	24	6	5.93	6.13	0.35	0.36	0.25	0.25
	36	1	7	7.34	0.41	0.43	0.19	0.21
	48	0.8	6.14	6.55	0.36	0.38	0.13	0.14

The tamarind kernel powder (TKP) was hydrolyzed with 2N H<sub>2</sub>SO<sub>4</sub> at 120°C for 30min and was detoxified and further fermented with free and immobilized *D hansenii* at 40°C. Galactoxyloglucan from TKP is hydrolyzed with *Thermomonospora xyloglucanase* and accelerase at a substrate loading of 250/1. and the hydrolysates were fermented with free and immobilized *D hansenii* at 40°C.

*Immobilization and reuse of D hansenii*

*D. hansenii* cells were immobilized in Ca-alginate matrix as described in experimental procedures. The fermentation of enzymatic hydrolysate at 25 g level of GXG using *Thermomonospora xyloglucanase* and accellerase released 13 g/L and 17g/L of reducing sugars and fermentation with immobilized cells produced 5.81 g/L and 7.34 g/L of ethanol with a yield of 0.45 g/g and 0.43 g/g respectively (Table 4). Immobilized cells showed a significant increase in ethanol yield as compared to free cells. The immobilized yeast was reprocessed for 10 cycles using a batch mode at 40 °C. The system was reused six times with 100% fermentation efficiency and with final conversion efficiency of 60% in the 10<sup>th</sup> cycle (Figure 6).



**Figure 6** Reuse of calcium alginate immobilized *Debaryomyces* in hemicellulosic hydrolysates of galactoxyloglucan at 40°C.



## DISCUSSION

A logical approach is to develop processes for ethanol production using alternative feedstocks while waiting for the lignocellulosic biomass ethanol technology to be ready for commercialization. A hemicellulose based feedstock such as tamarind kernel powder which can be readily hydrolyzed to value added products is foreseen to be significant from this aspect. In the current work TKP was hydrolyzed using various concentrations of sulphuric acid to obtain maximum reducing sugar with minimum adverse conditions. The optimum acid hydrolysis condition of 2 N H<sub>2</sub>SO<sub>4</sub> at 120°C for 30mins released the maximum reducing sugars (582 mg/g). Acid hydrolysis of TKP yielded a saccharification of 94% and further fermentation produced an ethanol yield of 0.35 g/g.

Enzymatic hydrolysis offers a cleaner process than acid hydrolysis however the rate of saccharification is less due to the need of various accessory enzymes. The hydrolysis of GXG from TKP with *Thermomonospora* xyloglucanase and accellerase produced glucose, xylose and galactose. The effect of chemical surfactants has also been observed during the hydrolysis of various pure and lignocellulosic substrates (Helle et al., 1993; Kristensen et al., 2007). Unlike previous studies, which have focused on materials with little hemicellulose content, the present investigation reveals the positive pronounced effect of chemical surfactants (Tween 80 and Toluene) and protein additives (BSA) addition on the increased hydrolysis of GXG from TKP by 15-20%. The fermentation of enzymatic hydrolysates produced ethanol with higher yields and theoretical conversion efficiency of 78-88% as compared to 65% from acid hydrolysate. The higher conversion efficiencies are due to the absence of inhibitory compounds. The complete conversion of enzymatic hydrolysates to ethanol is not achieved as the galactose is not fermented by *D. hansenii* from the sugar mixtures.

The chapter enunciates for the first time the hydrolysis and ethanol production from a rich hemicellulosic substrate TKP, an agro-industrial by-product abundantly available in India and Southeast Asia. The experimental results demonstrated the synergistic role of

xyloglucanase and  $\beta$ -galactosidase in the overall hydrolysis of GXG and thereby improving the saccharification efficiency. The thermotolerant yeast was able to ferment both glucose and xylose efficiently from the acid hydrolysate of TKP and enzymatic hydrolysate of GXG to ethanol in SHF system at 40°C. The immobilized yeast was reused for six cycles with 100% fermentation efficiency.

**BIBLIOGRAPHY**

- Benko Z, Siika-aho M, Viikari L, Reczey K (2008) *Enzyme Microb. Technol.* **43**, 109–114.
- Carpita NC, Gibeaut DM (1993) *Plant J* **3**, 1-30.
- De Vries RP, Visser J (2001) *Microbiol. Mol. Biol Rev* **65**, 497.
- Fujita Y, Ito J, Ueda M, Fukuda H, Kondo A (2004) *Appl. Environ. Microbiol.* **70**, 1207–1212.
- Ghose TK, Bisaria VS (1987) *Pure Appl. Chem.* **59**, 1739–1752.
- Goyal P, Kumar V Sharma P (2007) *Carbohydr Polym* **69**, 251-255.
- Hashimoto T, Nataka Y (2003) *J. Biosci. Bioeng.* **95**, 164–169.
- Helle SS, Duff SJB, Copper DG (1993) *Biotechnol. Bioeng.* **42**, 611–617.
- Henrissat B, Davies GJ (2000) *Plant Physiology* **124**, 1515-1519.
- Kierstan M, Bucke C (1977) *Biotech. Bioeng* **19**, 387-397.
- Kotaka A, Bando H, Kaya M, Kato-Murai M, Kuroda K, Sahara H, Hata Y, Kondo A, Ueda M (2008) *J Biosci Bioeng.* **105**, 622-627.
- Kristensen JB, Borjesson J, Bruun MH, Tjerneld F, Jorgensen H (2007) *Enzyme Microb. Technol.* **40**, 888–895.
- Kulkarni N, Shendye A, Rao M (1999) *FEMS Microbiol. Rev.* **23**, 411–456.
- Mandels M, Weber J (1969) *Adv. Chem.* **95**, 391–414.
- Maruyama K, Goto C, Numata M, Suzuki T, Nakagawa Y, Hoshino T, Uchiyama T (1996) *Phytochemistry* **41**, 1309-1314.

Menon V, Prakash G, Prabhune A, Rao M (2010) *Bioresource Technology* **101**, 5366–5373.

Minic Z (2008) *Planta* **227**, 723-40.

Powlowski J, Mahajan S, Schapira M, Master ER (2009) *Carbohydr Res.* **344**, 1175-1179.

Prakash G, AJ Varma, Prabhune A, Shouche Y, Rao M (2011) *Bioresource Technology* **102**, 3304–3308.

Rao PS, Gosh TP, Krishna S (1946) *J. Sci. Ind. Res. (India)* **4**, 705.

Saha BC (2003) *J Ind Microbiol Biotechnol* **30**, 279-291.

Sims IM, Munro SLA, Currie G, Craik D, Bacic A (1996) *Carbohydr. Res* **293**, 147-172.

Wyman E (1999) *Annu.Rev.Energy.Environ* **24**, 189-226.

*Remember ~ time takes away everything from us  
Be good & do good to everybody in the World  
Because skin, face & personality will never stay  
But our work and name will always be there .....*